CONTRACTOR REPORT

SAND94–2870/1
Unlimited Release
UC–1243

A Study of Production/Injection Data From Slim Holes and Production Wells at the Oguni Geothermal Field, Japan

Sabodh K. Garg
S-Cubed
3398 Carmel Mountain Road
San Diego, CA 92121-1095

Jim Combs
Geo-Hills Associates
27790 Edgerton Road
Los Altos Hills, CA 94022

M. Abe
Electric Power Development Co. Ltd.
15-1, Ginza 6-chome
Chuo-Ku, Tokyo 104
Japan

Prepared by
Sandia National Laboratories
Albuquerque, New Mexico 87185 and Livermore, California 94550
for the United States Department of Energy
under Contract DE-AC04-94AL85000

Printed March 1995

Issued by Sandia National Laboratories, operated for the United States Department of Energy by Sandia Corporation.

Available to DOE and DOE contractors from
Office of Scientific and Technical Information
PO Box 62
Oak Ridge, TN 37831

Prices available from (615) 576-8401, FTS 626-8401

Available to the public from
National Technical Information Service
US Department of Commerce
5285 Port Royal RD
Springfield, VA 22161

NTIS price codes
Printed copy: A09
Microfiche copy: A01

SAND94-2870/1 Distribution Category
Unlimited Release UC-1243
Printed March 1995

A STUDY OF PRODUCTION/INJECTION DATA FROM SLIM HOLES AND PRODUCTION WELLS AT THE OGUNI GEOTHERMAL FIELD, JAPAN

CONTRACTOR REPORT
This work performed under Sandia contract AG-4388

S. K. Garg
S-Cubed

J. Combs
Geo Hills Associates

M. Abe
Electric Power Development Company, Ltd.

ABSTRACT

Production and injection data from slim holes and large-diameter wells at the Oguni Geothermal Field, Japan, were examined in an effort to establish relationships (1) between productivity of large-diameter wells and slim holes, (2) between injectivity and productivity indices and (3) between productivity index and borehole diameter. The production data from Oguni boreholes imply that the mass production from large-diameter wells may be estimated based on data from slim holes. Test data from both large- and small-diameter boreholes indicate that to first order the productivity and the injectivity indices are equal. Somewhat surprisingly, the productivity index was found to be a strong function of borehole diameter; the cause for this phenomenon is not understood at this time.

This work was supported by the US Department of Energy at Sandia National Laboratories under contract DE-AC04-94AL85000

Abstract

Production and injection data from slim holes and large-diameter wells at the Oguni Geothermal Field, Japan, were examined in an effort to establish relationships (1) between productivity of large-diameter wells and slim holes, (2) between injectivity and productivity indices and (3) between productivity index and borehole diameter. The production data from Oguni boreholes imply that the mass production from large-diameter wells may be estimated based on data from slim holes. Test data from both large- and small-diameter boreholes indicate that to first order the productivity and the injectivity indices are equal. Somewhat surprisingly, the productivity index was found to be a strong function of borehole diameter; the cause for this phenomenon is not understood at this time.

Acknowledgment

We express our sincere appreciation to the Electric Power Development Company, Tokyo, Japan (EPDC) for their kind cooperation in making their proprietary data for the Oguni Geothermal Field available for the present study.

NOTICE

Appendices B and C, which contain data proprietary to Electric Power Development Company, have been intentionally omitted from this report. Appendix B has drilling and completions details for the wells discussed in this report, while Appendix C has tabular listings for pressure-temperature data taken in the wells while discharging.

These appendices have been included with the reports distributed internally to Sandia and DOE, and must be protected as proprietary data. If you receive a copy of the appendices and do not wish to safeguard it, please return that report to the Geothermal Research Department, Organization 6111. Copies of the appendices will be available to others, on a limited basis, until December 31, 1996. If you wish to receive a copy, please complete the Nondisclosure Agreement on the following pages and submit it, referencing this report, to:

Director
Geothermal Engineering Division
Electric Power Development Co., Ltd
15-1, Ginza 6-Chome
Chuo-Ku
Tokyo, 104 Japan

Phone: 81-3-3546-2211
Fax: 81-3-3546-1685

After their approval, EPDC will forward the Nondisclosure Agreement to Sandia, and the report will be sent to you. If there are any questions, you may contact the Geothermal Research Department at Sandia.

Jim Dunn — phone (505) 844-4715
OR
John Finger — phone (505) 844-8089
Geothermal Research Department
Sandia National Laboratories
Albuquerque, NM 87185-1033

Table of Contents

SECTION 1

Introduction

Since a major impediment to the exploration for and assessment of new geothermal areas worldwide is the high cost of conventional rotary drilling, it would be desirable to be able to utilize low-cost slim holes (≤ 15 cm diameter) for geothermal exploration and definitive reservoir assessment. Garg and Combs (1993) presented a review of the publicly available Japanese data regarding slim holes. Slim holes have been successfully used in Japan (Garg and Combs, 1993) for (1) obtaining core for geological studies and delineating the subsurface stratigraphic structure, (2) characterizing the geothermal reservoir fluid state, and (3) as shutin observation boreholes in pressure interference tests. In order to establish the utility of slim holes for definitive reservoir assessment, it is also necessary to be able to predict the discharge characteristics of large-diameter wells based on injection/discharge tests on small-diameter slim holes. At present, there do not exist sufficient published data, either in Japan or elsewhere, to establish a statistically meaningful relationship between the injectivity/productivity of small-diameter slim holes and of large-diameter production and/or injection wells.

The U.S. Department of Energy (DOE) through Sandia National Laboratories (Sandia) has initiated a research effort to demonstrate that slim holes can be used (1) to provide reliable geothermal reservoir parameter estimates comparable to those obtained from large-diameter wells, and (2) to predict the discharge behavior of large-diameter wells (Combs and Dunn, 1992). As part of its research program, DOE/Sandia plans to drill and test pairs of small-diameter slim holes with existing large-diameter production wells in several geothermal fields in the western United States; the first of these tests was recently completed in mid-1993 at the Steamboat Hills Geothermal Field, Nevada (Finger *et al.*, 1994). Because of fiscal constraints, it is unlikely that sufficient U.S. data will become available in the near future. Fortunately, the Japanese geothermal industry has had extensive experience in the use of slim holes for geothermal exploration and reservoir assessment. Most of the Japanese slim hole data are proprietary. However, assuming that data ownership issues can be resolved, the existing Japanese data in conjunction with planned field tests in the United States should help in establishing a statistically valid relationship between the injectivity/productivity of slim holes and of large-diameter wells.

During the past year, S-Cubed—under a contract with Sandia National Laboratories—approached several Japanese geothermal developers for release of their proprietary data for use in DOE/Sandia's slim-hole program. As a result of these negotiations, S-Cubed was fortunate to obtain permission from Electric Power Development Company (EPDC) for use of pertinent data from

the Oguni Geothermal Field. The Oguni Geothermal Field, Kumamoto Prefecture, Kyushu, Japan, is a particularly good candidate for a case history on the use of slim holes in geothermal exploration and reservoir assessment. Since 1983, EPDC has carried out an extensive exploration and reservoir assessment program in the area. As of mid-1993, EPDC had drilled and tested more than twenty boreholes ranging in depth from 500 to 2000 meters. EPDC has utilized slim holes not only for selecting large-diameter well locations, but also for predicting the production capacity of the large-diameter wells being drilled. The article by M. Abe of EPDC, reproduced in Appendix A of this report, explains in some detail EPDC's approach towards the use of slim holes in geothermal exploration and reservoir assessment.

In the present report, we examine data from eleven slim holes and ten large-diameter wells at the Oguni Geothermal Field. A brief overview of the Oguni Geothermal Field is presented in Section 2. The drilling information and downhole pressure, temperature and spinner surveys are analyzed in Section 3 to determine feedzone locations, pressures, and temperatures, *etc.* Injectivity indices and estimates of reservoir permeability-thickness product (kh) obtained from injection and fall-off data are discussed in Section 4. The discharge test data, productivity indices, and estimates of kh product given by pressure buildup data are presented in Section 5. In Section 6, we discuss the (1) variation of discharge rate, productivity index, and injectivity index with borehole diameter, (2) relationship between productivity and injectivity indices, and (3) kh determined from short-term injection and longer-term discharge tests. Our recommendations for future work are also outlined in Section 6.

SECTION 2

An Overview of Oguni Geothermal Field

2.1 Introduction

The Oguni and the Sugawara Geothermal Fields together comprise the northwestern Hohi geothermal region, Kumamoto and Oita Prefectures, Kyushu, Japan (see Figure 2.1. In this report, we use the Central Kyushu Co-ordinate System (CKCS). The origin of CKCS is located at 33° 0′ north latitude and 131°0′ east longitude.). An area of numerous hot springs, it is approximately 40 km southwest of the coastal resort of Beppu, and some 20 km north of Mt. Aso, an active caldera. The New Energy and Industrial Technology Development Organization (NEDO) carried out a regional (200 km^2 area) exploration program in the Hohi area during the years 1979–1985; this work resulted in the identification of a high permeability geothermal area in the northwestern Hohi area. EPDC initiated a geothermal exploration program in the Oguni area in 1983. The Oguni field is located at the northeast end of Kumamoto Prefecture; Oita Prefecture is to the north and northeast of the Oguni area. The Sugawara field, to the north of the Oguni area, is being surveyed by NEDO as a possible site for the demonstration of a binary power plant. Although the northern Hohi area has been subdivided into two separate geothermal fields (Oguni, Sugawara), the area constitutes a single hydrological unit.

The topography of the Oguni field is dominated by Mt. Waita (Figure 2.1), which rises to an elevation of about 1500 m ASL (meters above sea level) to the southeast of the field. Many of the boreholes are located on the flanks of Mt. Waita. The Oguni boreholes are in Kumamoto Prefecture. Striking WNW-ESE is the valley containing the hot spring areas (and towns) of Takenoyu and Hagenoyu. To the north of the valley is the Sugawara plateau (in Oita Prefecture) where NEDO has drilled a number of boreholes (BS series, Figure 2.1) for a binary power plant. The Takenoyu/Hagenoyu valley forms a natural division of the field into two parts, north and south of the valley.

2.2 Subsurface Stratigraphic Structure

The subsurface stratigraphic structure in the northern Hohi area is shown in Figures 2.2 to 2.4. The granitic basement (not shown in Figures 2.2 to 2.4) was encountered in only two boreholes (DW-7 and DY-2) at about –960 m ASL in the Oguni area, and drops off steeply to the northeast in the Sugawara area. The stratigraphic sequence above the basement consists of the Pliocene Taio formation, the late Pliocene/early Pleistocene Shishimuta formation (pre-Kusu group), the lower to middle Pleistocene Hohi and Kusu formations, and the upper Pleistocene Kuju formation. The Nogami mudstones (part of the Kusu

Continued on page 2-6

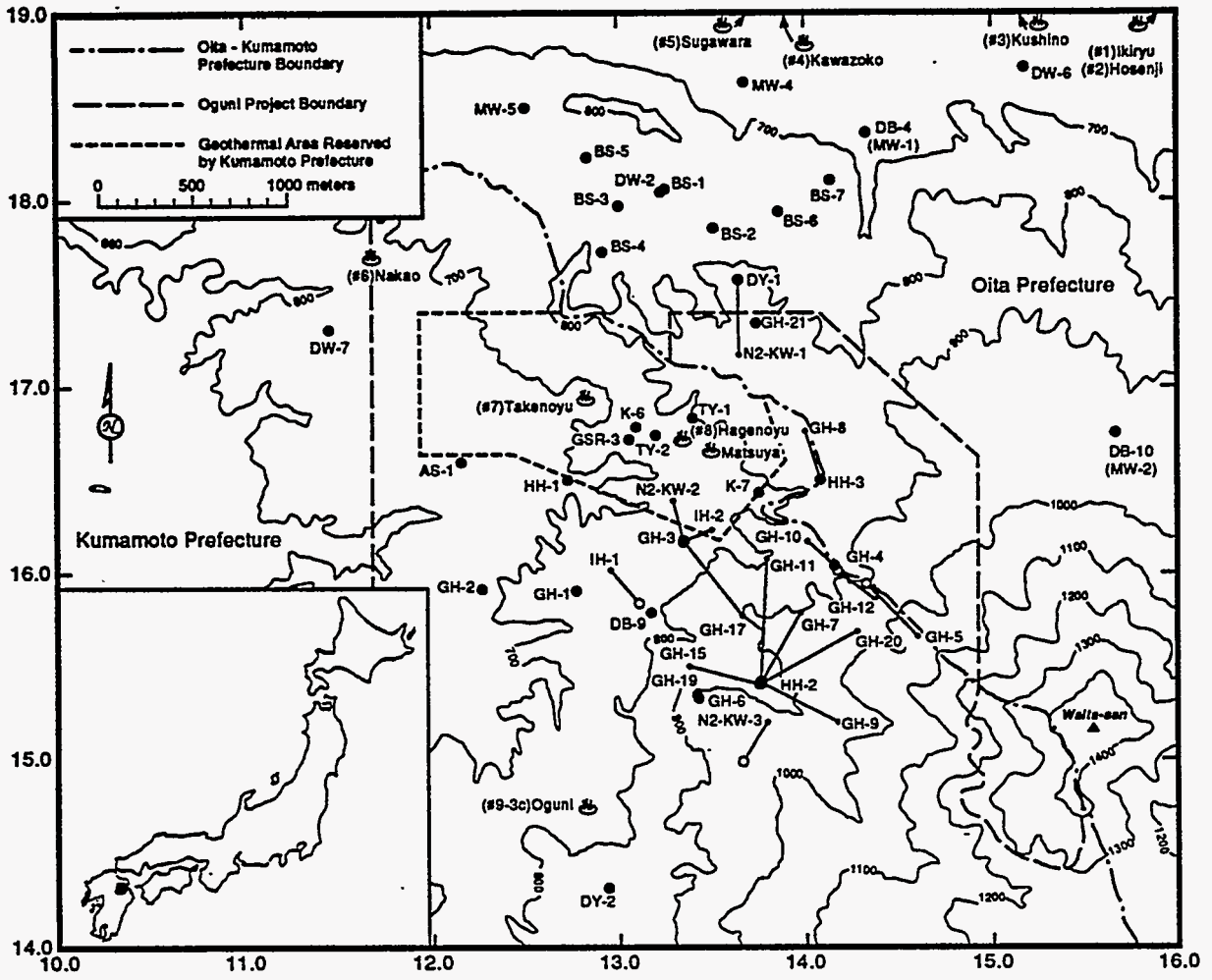

Figure 2.1. The northern Hohi geothermal area, Kyushu, Japan. The inset map of Japan (lower left hand corner) shows the location of the Hohi geothermal area (dark rectangle).

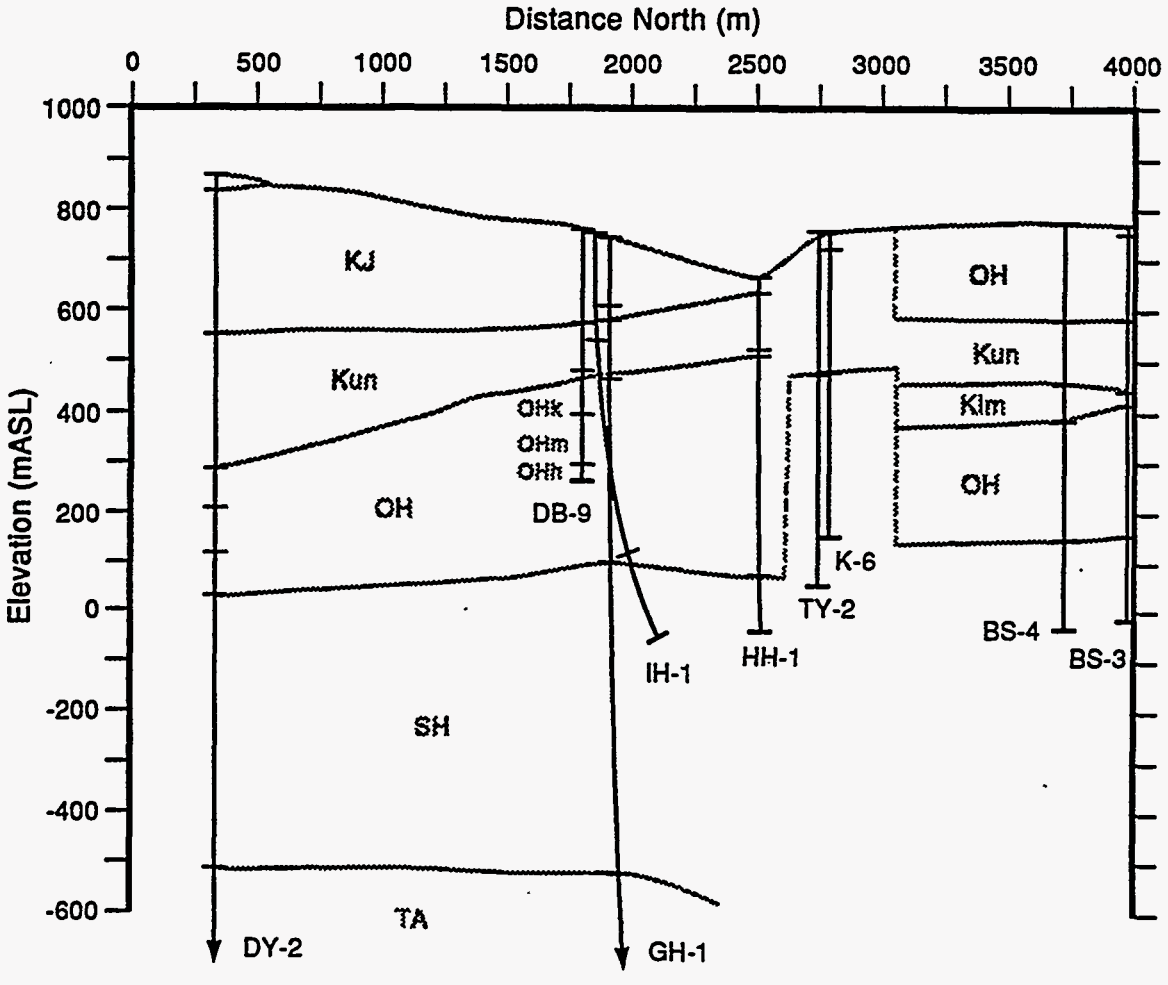

Figure 2.2. Stratigraphic cross section striking north along east-west CKCS co-ordinate 13. The ordinate is meters north from north-south CKCS co-ordinate 14. The following abbreviations are used for formation names: KJ (Kusu); Kun (Kusu/Nogami mudstone); Klm (Kusu/Machida lava); OH (Hohi); OHk (Hohi/Kotobakiyama lava); OHm (Hohi/Nambira lava); OHh (Hohi/Hatchobaru lava); SH (Shishimuta); TA (Taio).

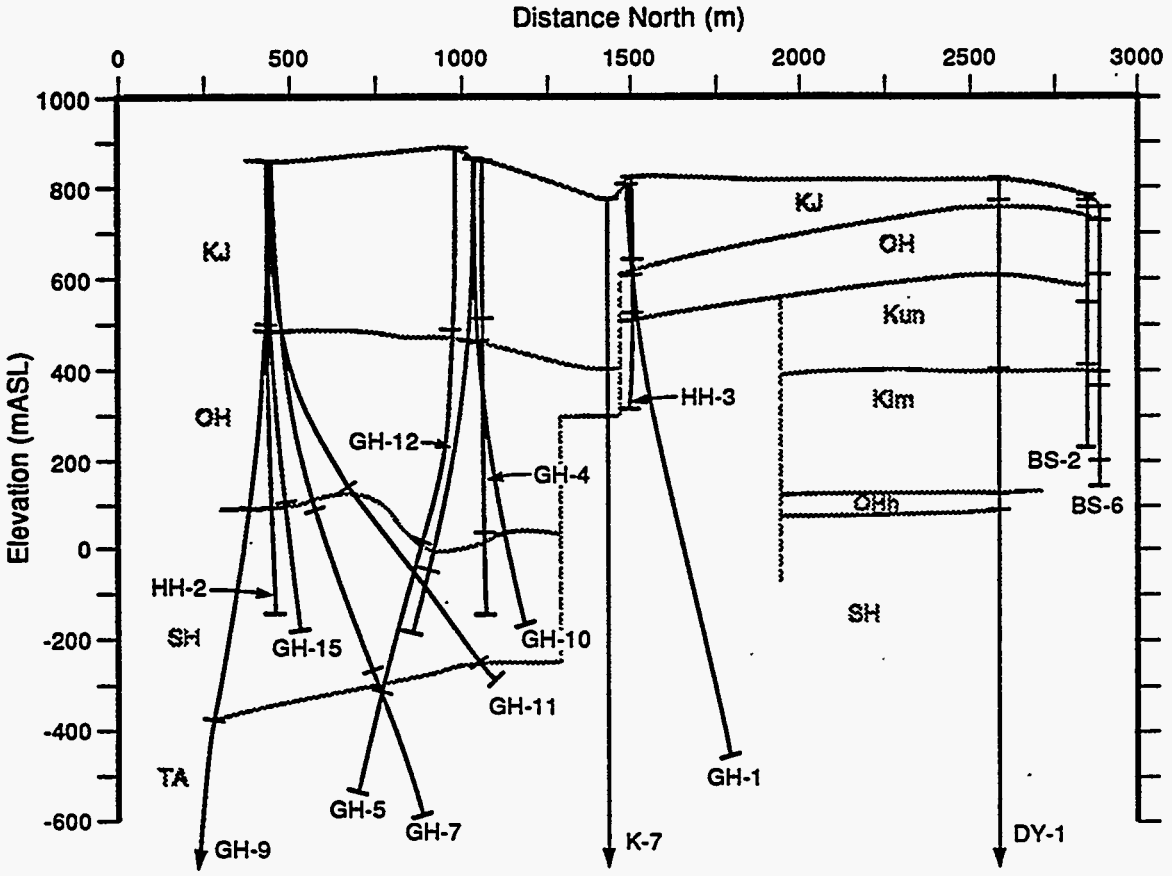

Figure 2.3. Stratigraphic cross section striking north along east-west CKCS co-ordinate 14. The ordinate is meters north from north-south CKCS co-ordinate 15. The following abbreviations are used for formation names: KJ (Kusu); Kun (Kusu/Nogami mudstone); Klm (Kusu/Machida lava); OH (Hohi); OHh (Hohi/Hatchobaru lava); SH (Shishimuta); TA (Taio).

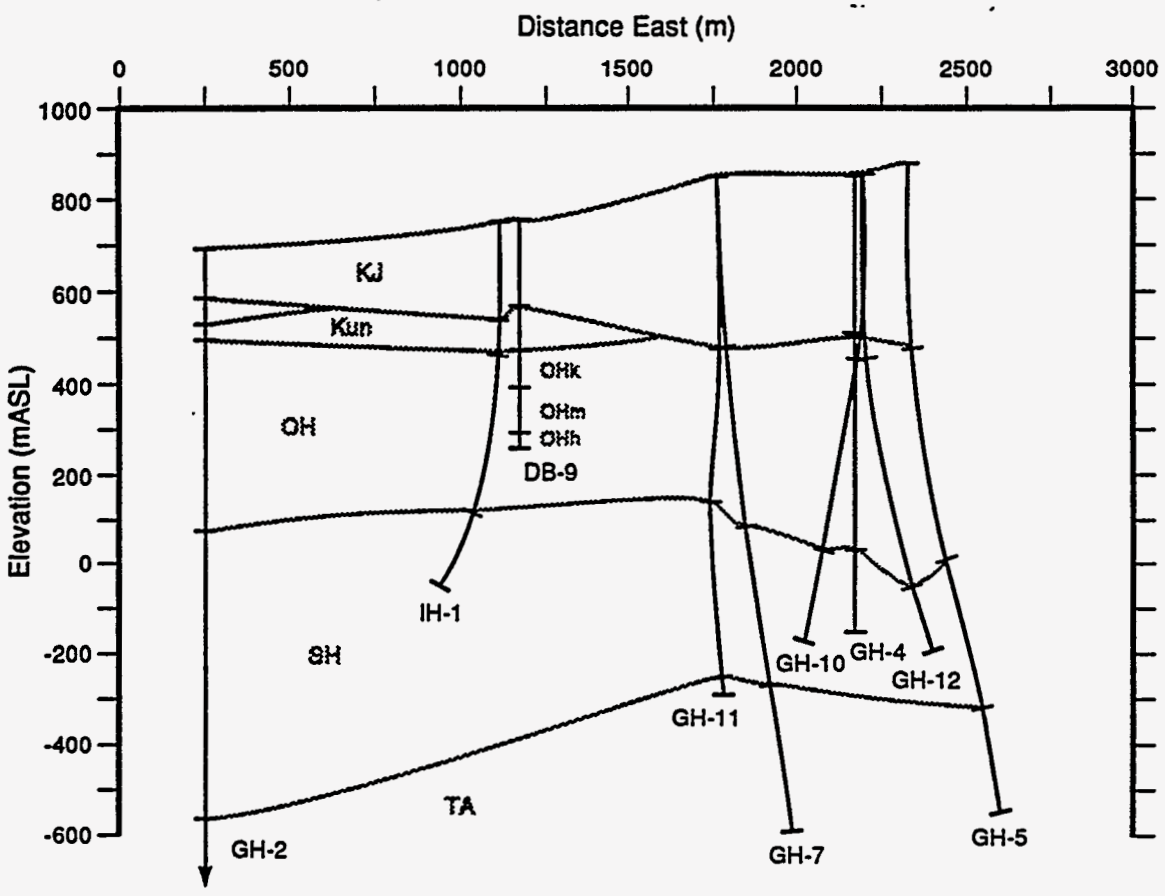

Figure 2.4. Stratigraphic cross section striking east along north-south CKCS co-ordinate 16. The ordinate is meters east from east-west CKCS co-ordinate 12. The following abbreviations are used for formation names: KJ (Kuju); Kun (Kusu/Nogami mudstone); OH (Hohi); OHk (Hohi/Kotobakiyama lava); OHm (Hohi/Nambira lava); OHh (Hohi/Hatchobaru lava); SH (Shishimuta); TA (Taio).

group) and the Kuju volcanics appear to function as a caprock for the geothermal system. Based upon feedpoint locations, it appears that the Hohi formation and the upper part of the Shishimuta formation constitute the principal geothermal aquifers.

The upper interface of the Taio formation (*i.e.*, the contact between Taio and Shishimuta formations) is found in the Oguni area at elevations between –200 and –400 m ASL. In the northern part of the field (*i.e.*, Sugawara area), this interface was encountered in boreholes DY-1 and DW-7 at much deeper elevations (–1320 and –825 m ASL, respectively).

The elevation of the top of the Shishimuta formation varies between about 50 and 150 m ASL except in the Takenoyu-Hagenoyu area. In this area, penetrated by boreholes GH-8, HH-3, K-6, TY-1 and TY-2, the top of the Shishimuta formation has a much higher elevation (about 500 m ASL). This local rise in the formation is interpreted to be a small upthrown block.

The Hohi and Kusu formations are interfingered in a complicated manner. Both of these groups are interrupted in the vicinity of the uplift of the Shishimuta rocks in the Takenoyu-Hagenoyu area.

2.3 Fluid State

2.3.1 Reservoir Pressures

Garg, *et al.* (1993) have analyzed drilling information, and downhole pressure, temperature, and spinner surveys for 45 boreholes in the northern Hohi area in an effort to deduce feedzone depths and pressures. The feedzone pressures imply that the northern Hohi region consists of two pressure zones (a high pressure zone in the area of boreholes GH-15, GH-19, GH-6, HH-2, N2-KW-3 and DY-2 in the southern part of the Oguni field; a low pressure zone in the central and northern parts of the area shown in Figure 2.1). At present, the reasons for the existence of two pressure regions in close proximity to each other (within at most a few hundred meters) are poorly understood.

The feedzone pressures for the "low-pressure zone" boreholes can be fit by the following correlation:

$$P = 56.0888 - 0.08531 z^*$$
$$z^* = z + 7.619(x_N - 15)$$

where P is in bars (absolute), z^* and z are in m ASL, and x_N is the distance in kilometers from the origin of the Central Kyushu Co-ordinate System. As can be seen from Figure 2.5, the pressure correlation agrees closely with all the pressure measurements for low-pressure zone boreholes. The pressures for "high-pressure zone" boreholes (GH-6, GH-15, GH-19, HH-2, DY-2, N2-KW-3) do, however, lie considerably above the straight line in Figure 2.5, as do those from the shallow boreholes (MW-5, DB-9, DB-10) which do not penetrate the deep reservoir.

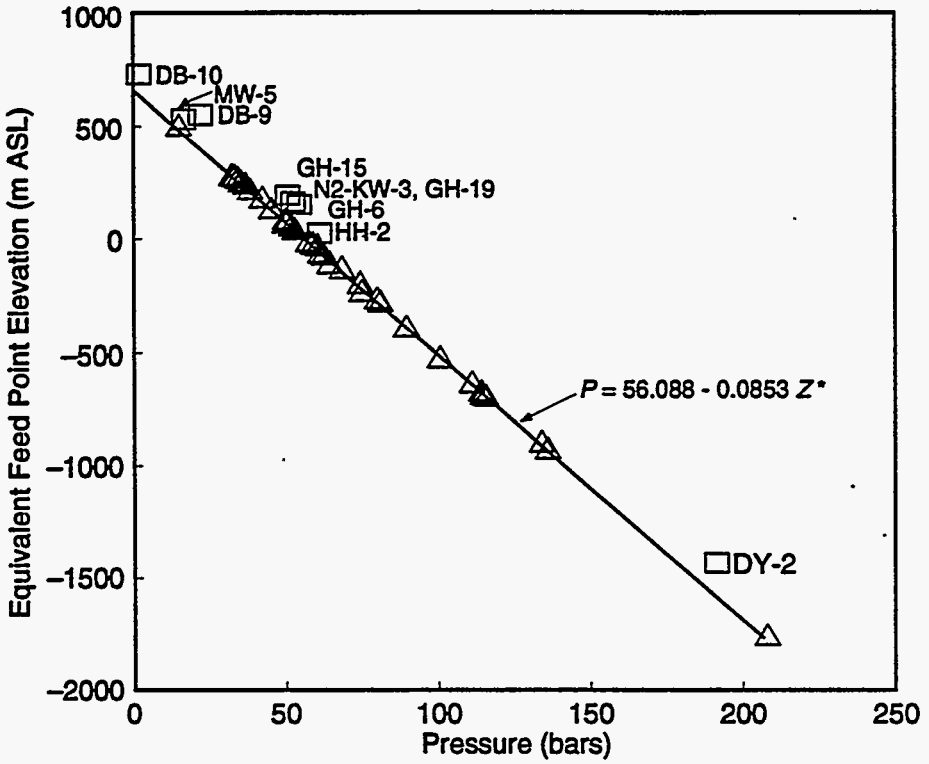

Figure 2.5. Correlation of pressure with equivalent feedpoint elevation of low-pressure zone boreholes (Δ). Also shown as □ are boreholes (DB-10, MW-5, DB-9, GH-15, N2-KW-3, GH-19, GH-6, HH-2, DY-2) not included in the pressure correlation.

The vertical pressure gradient in the Oguni/Sugawara area is 8.531 kPa/m and corresponds to a hydrostatic gradient at ~ 195°C. This implies fluid upflow in regions of the reservoir where temperature exceeds 195°C. The pressure correlation also implies that pressures decrease to the north; the pressure gradient is ~ 0.65 bars/km. Thus, in the natural state there exists a regional flow (to the north) in the northern Hohi area.

2.3.2 Reservoir Temperatures

The stable preproduction temperature measurements in the Oguni/Sugawara boreholes were used to estimate the natural subsurface temperature distribution in the area. The inferred temperature distribution along a north-south vertical plane is shown in Figure 2.6. The temperature contours in Figure 2.6 were drawn by interpolating and extrapolating between the measurements. The temperatures undergo a steep decline to the south of boreholes HH-2, GH-7 and GH-6. Furthermore, the temperatures exhibit a gradual decline to the north of GH-series boreholes.

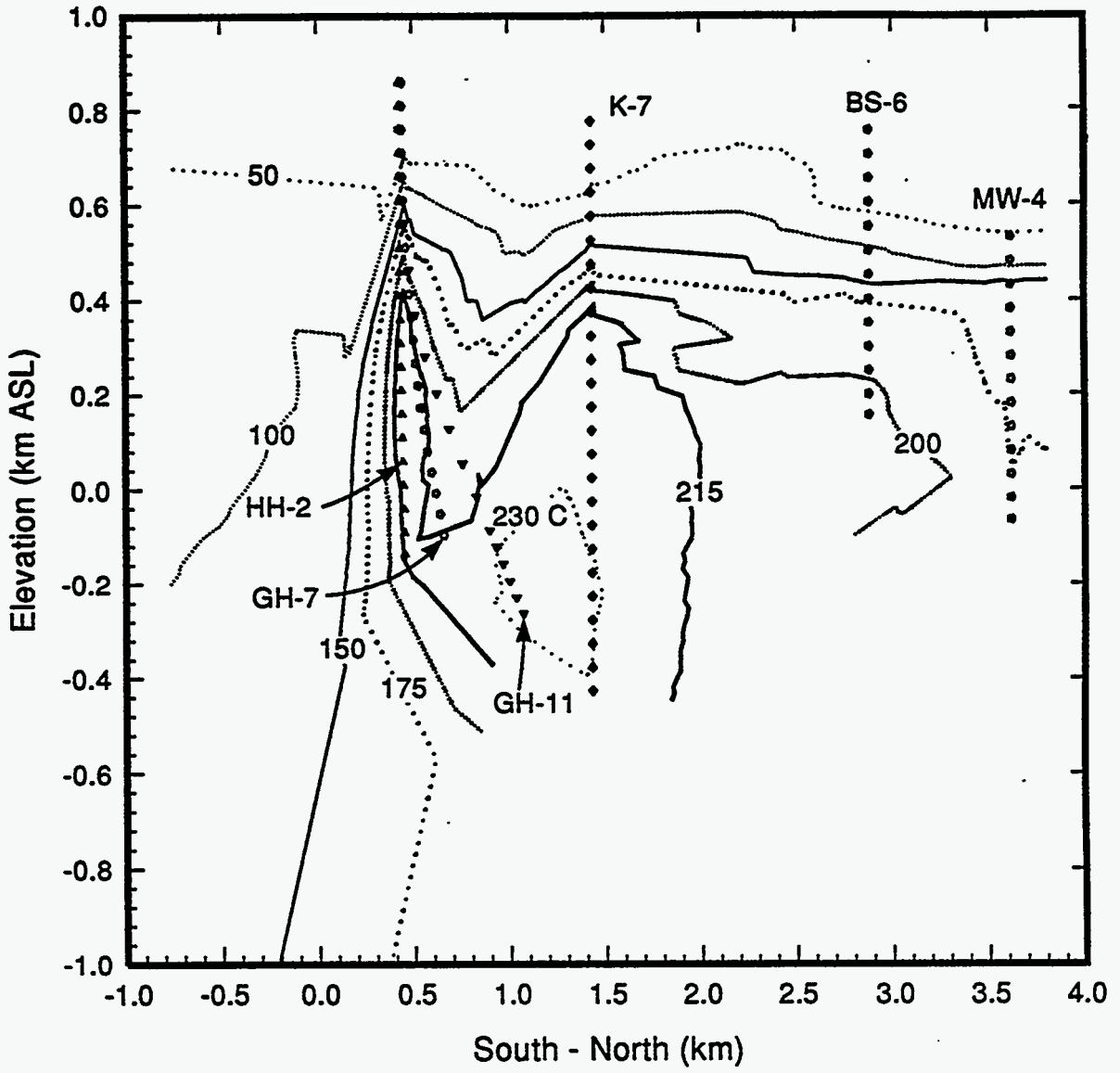

Figure 2.6. Subsurface temperature distribution along a south-north vertical plane in the northern Hohi area.

The temperature distribution along an east-west plane in the Oguni area is shown in Figure 2.7. The temperature decline rapidly to the east and west of Oguni boreholes GH-4, GH-10, GH-11 and GH-12. The maximum temperature (~ 240°C) in the area occurs near Oguni boreholes GH-4, GH-10, GH-11, and Kumamoto Prefecture well K-7.

2.3.3 Fluid Salinity and Gas Content

The Oguni reservoir fluid appears to be a relatively homogenous sodium-chloride brine of moderate salinity (average chloride concentration ~ 1100 ± 100 mg/l). Carbon-dioxide constitutes the bulk of non-condensable gases in the reservoir fluid. The average carbon-dioxide content is about 700 mg/l, which is equivalent to a partial pressure of CO_2 of about 1.65 bars. Thus, for practical reservoir engineering purposes, the Oguni reservoir fluid may be treated as pure water.

The Oguni reservoir fluid is single-phase liquid. The geothermal boreholes do not provide any direct evidence of a two-phase zone at depths greater than 300 meters in the Oguni area. (The feedzones for all of the Oguni boreholes are deeper than 400 meters.) The presence of boiling at shallow depths (*i.e.*, depths less than 300 meters) is, however, suggested by the occurrence of warm and boiling steam-heated sulfate and bicarbonate spring waters in the Takenoyu and Hagenoyu areas.

2.4 Reservoir Permeability

EPDC has performed numerous pressure transient tests to define the detailed permeability structure in the Oguni/Sugawara area. The available data set includes (1) cold fluid injection and fall-off tests in single boreholes, (2) pressure drawdown (*i.e.*, production tests) and buildup tests in single boreholes, and (3) pressure interference tests involving multiple boreholes. The injection and production test data from single boreholes will be discussed in detail in Sections 4 and 5, respectively, of this report. A detailed consideration of pressure interference data is, however, outside the scope of this report. Analyses of pressure interference data from the low-pressure zone boreholes imply that the northern Hohi reservoir has a transmissivity of about 100–250 darcy-meters (Garg, *et al.*, 1993). In contrast to the high transmissivity obtained in the low-pressure zone, the high pressure zone has only a modest transmissivity (~ 15 darcy-meters).

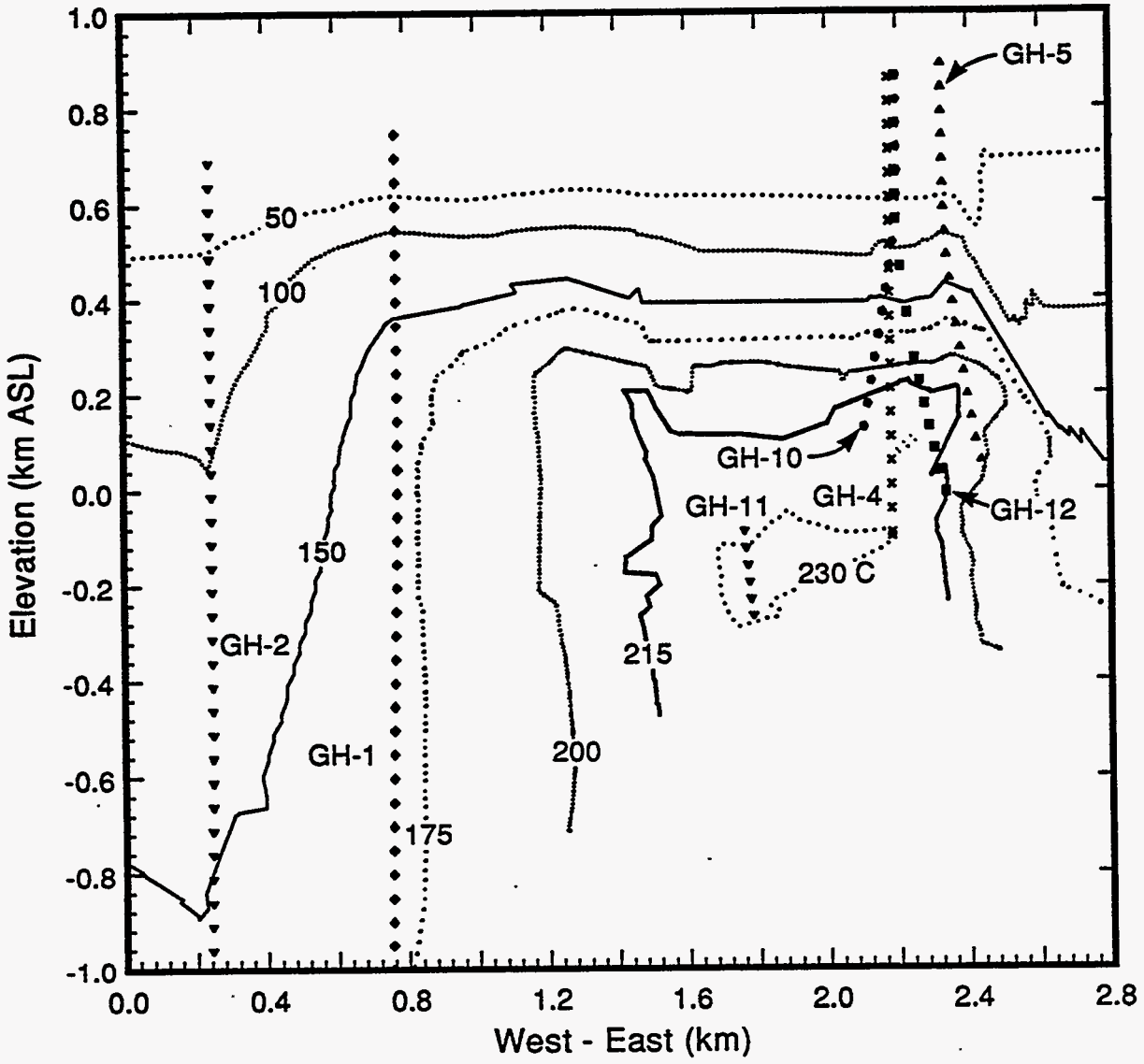

Figure 2.7. Temperature distribution along a west-east vertical plane in the northern Hohi area.

SECTION 3

Analysis of Downhole Data

As part of its drilling and testing program, EPDC has drilled both small-diameter core holes (9 GH-series and 3 HH-series) and large-diameter production size wells (8 GH and 2 IH-series). In addition, NEDO has drilled three small-diameter core holes (N2-KW-1, N2-KW-2 and N2-KW-3) in the Oguni area. With the exception of four core holes (GH-1, GH-2, HH-1 and HH-3), some production and/or injection data are available for all of the Oguni boreholes. In this section, we will analyze available drilling (circulation loss, borehole completion and geologic data) and downhole PTS (*i.e.*, pressure, temperature and spinner) surveys to obtain feedzone depths, pressures and temperatures for the 21 boreholes listed in Table 3.1. The essential drilling and completion data, required in the interpretations, are given in Appendix B. Since most of the Oguni boreholes were deviation drilled, measured depths along the wellbore (MD) must be corrected to obtain true vertical depths (TVD). In this report, depths are also sometimes given in terms of elevations (meters) above sea level (meters ASL). Thus, –800 m ASL denotes a location 800 meters below sea level. Casing, liner and wellbore dimensions are given in mm for slim holes (borehole diameter < 100 mm) and in inches for large-diameter (borehole diameter > 100 mm) wells.

Table 3.1. List of Oguni boreholes with production or injection data.

Borehole Name	Measured Depth (meters)	Vertical Depth (m TVD)	Feedzone Depth (m TVD)	Final Diameter (mm)	Downhole Flowing Temp (°C)	Production/ Injection Data
A. Low-Pressure Reservoir						
GH-3	1500	1498	1030	79	214	P
GH-4	1001	1001	900	76	235	P
GH-5	1501	1421	1100	76	187	P
GH-7	1547	1442	980/1400	98	220	P
GH-8	1300	1255	1220	78	212	P,I
GH-10	1063	1027	1010	159	241	P,I
GH-11	1381	1143	1140	216	237	P,I
GH-12	1100	1045	750	216	232	P,I
GH-17	1505	1354	760	216	—	I
GH-20	1790	1576	1560	216	241	P,I
GH-21	810	810	650	216	—	I
IH-1	900	810	590	159	—	I
IH-2	650	616	550	216	226	P,I
N2-KW-1	1000	898	860	76	—	I
N2-KW-2	1000	978	860	76	—	I
B. High-Pressure Reservoir						
GH-6	1003	1003	770	76	215	P
GH-9	1600	1481	?	78	—	I
GH-15	1190	1048	680	216	Two-Phase	P,I
GH-19	773	773	750	216	—	I
HH-2	1000	999	850	76	Two-Phase	P
N2-KW-3	1350	1317	810	76	227	P,I

3.1 Slim Hole GH-3

Heatup surveys (profiles 1, 2, 3 and 6, Figure 3.1) for slim hole GH-3 show (1) extremely rapid temperature recovery at ~ 570 m TVD, and (2) persistent temperature depressions at ~ 610 m TVD and ~ 1050 m TVD. Interestingly, major circulation losses were encountered near all of these horizons. Temperature profile 9, taken during a production test, has an isothermal zone over the depth interval ~ 500–1030 m TVD. It is, therefore, likely that the major feedzone for GH-3 is located at ~ 1030 m TVD. Temperature survey 8, taken after a long shutin interval, shows a clear temperature inversion; maximum temperature (~ 224°C) occurs at ~ 560 m TVD. The flowing temperature at the main feedzone (1030 m TVD) is 214°C.

Pressure profiles, computed from water level and temperature data, form a pivot at ~ 1020–1040 m TVD (Figure 3.2); the pressure at 1030 m TVD (~ –249 m ASL) is ~ 75 bars. The latter estimate for feedpoint pressure is virtually identical with that recorded by a downhole gauge on January 29, 1987 (Figure 3.3).

3.2 Slim Hole GH-4

Heatup surveys for slim hole GH-4 (profiles 1, 3, 5 and 6, Figure 3.4) show either a large change in temperature gradient or a temperature depression at ~ 900 m TVD; this denotes the major feedpoint for slim hole GH-4. Flowing temperature survey 8 (Figure 3.4) is consistent with a liquid entry (temperature ~ 235°C) at 900 m TVD.

Static pressure profiles, computed from water level and temperature data, form a pivot at 850–900 m TVD (Figure 3.5); the pressure at 900 m TVD (~ –40 m ASL) is ~ 59 bars. The latter pressure value is in good agreement with that (~ 58.5 bars) recorded by a downhole survey on February 7, 1986 (Figure 3.6).

3.3 Slim Hole GH-5

Heatup surveys (profiles 1, 3, and 5, Figure 3.7) for slim hole GH-5 show a rapid temperature recovery at ~ 980 m TVD (*i.e.*, just below the 4-inch casing shoe at ~ 964 m TVD). This indicates the presence of a feedzone at this depth. A large change in temperature gradient at ~ 1270 m TVD implies that little or no permeability is present below this depth. All the temperature profiles (see *e.g.*, profile 9, Figure 3.7) recorded under flowing conditions display a change in temperature gradient at ~ 1100 m TVD and an isothermal zone from ~ 500 m TVD to ~ 1100 m TVD; these observations suggest that the major feedpoint for GH-5 is located at ~ 1100 m TVD. The long time shutin temperature survey 11 (Figure 3.7) indicates a clear temperature inversion; the maximum temperature (~ 215°C) was recorded at ~ 700 m TVD. The flowing temperature at the major feedzone (1100 m TVD) is 187°C.

Continued on page 3-10

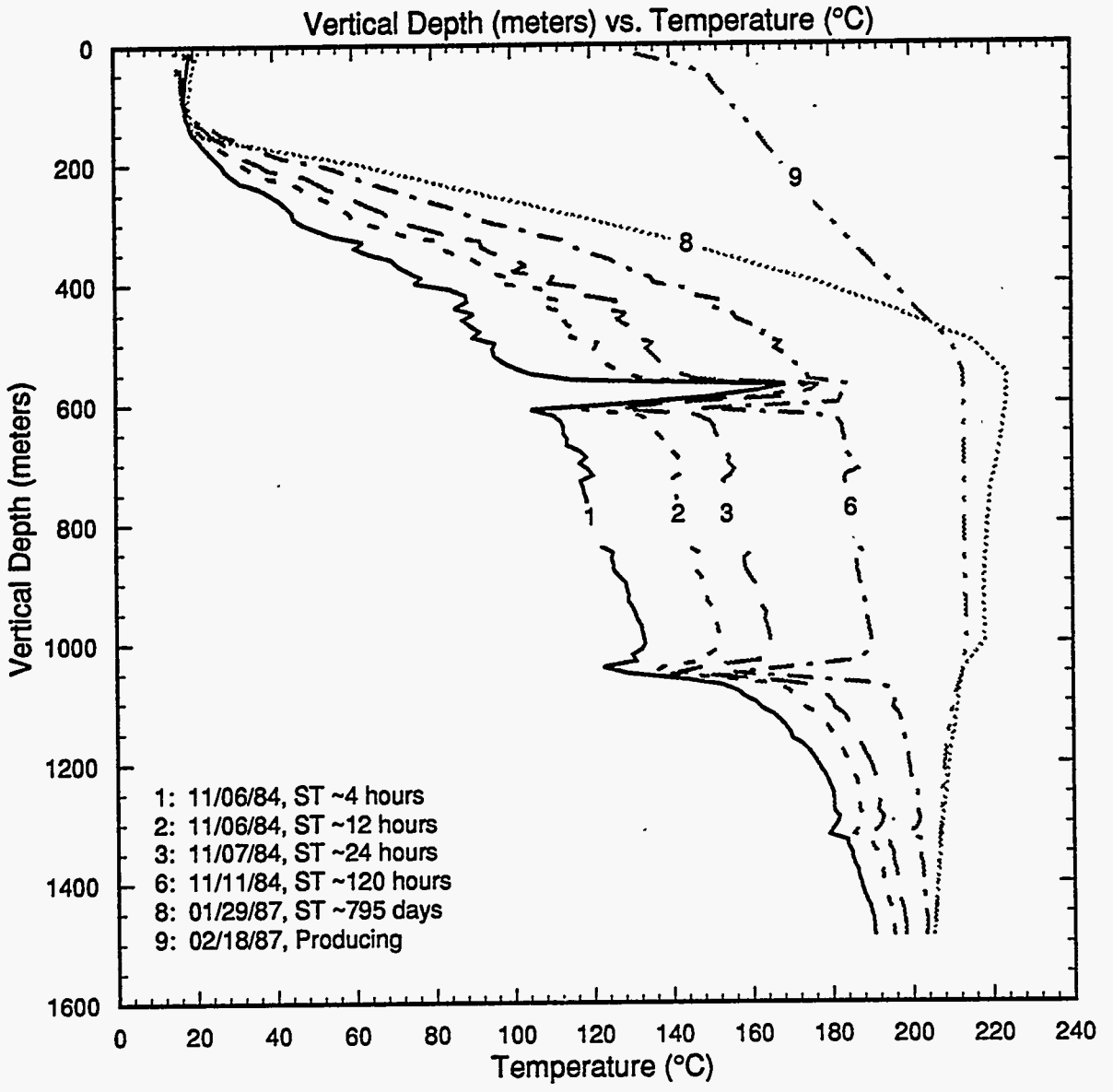

Figure 3.1. Selected temperature profiles for slim hole GH-3.

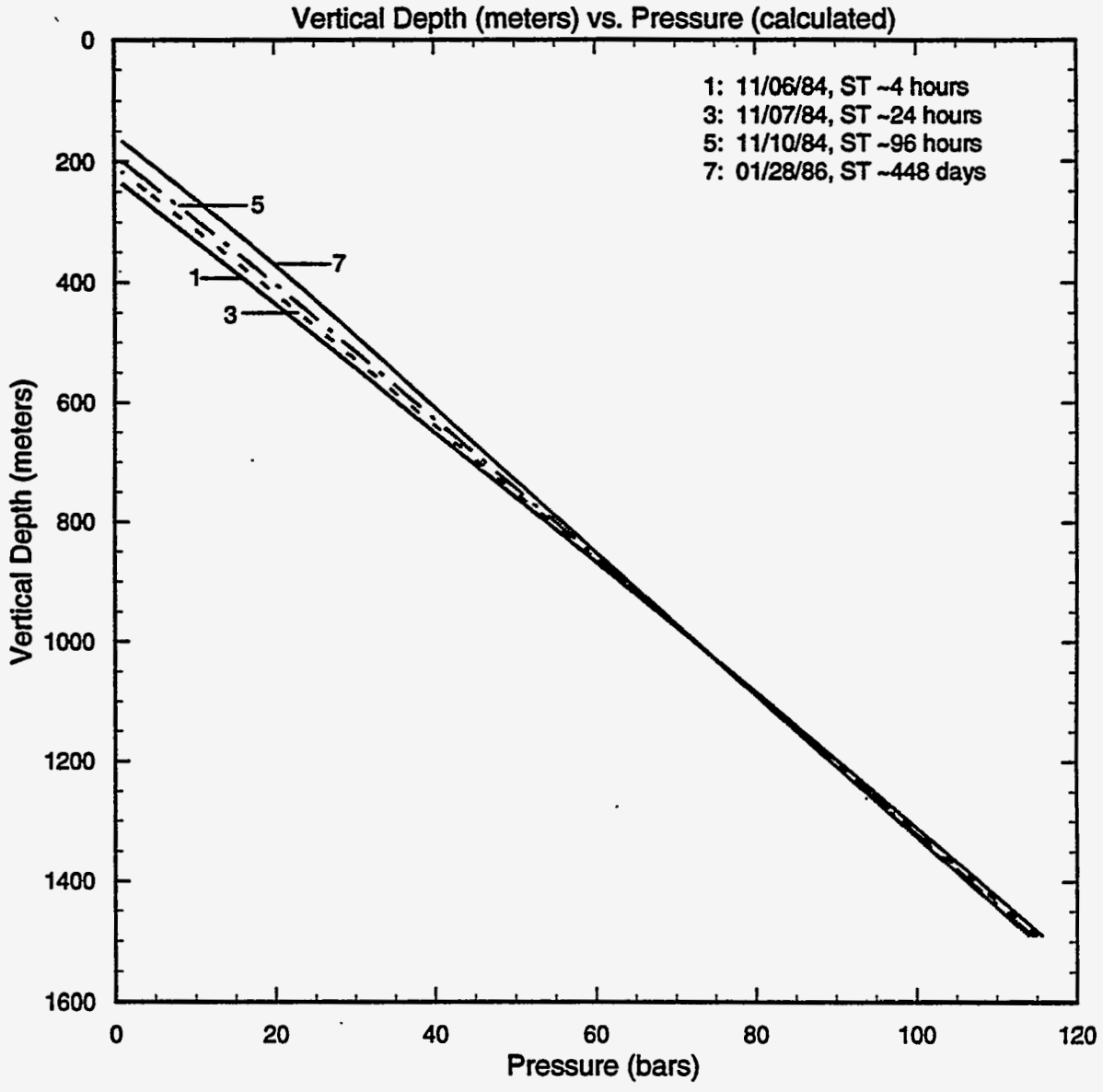

Figure 3.2. Pressure profiles, computed from water level and temperature data, for slim hole GH-3.

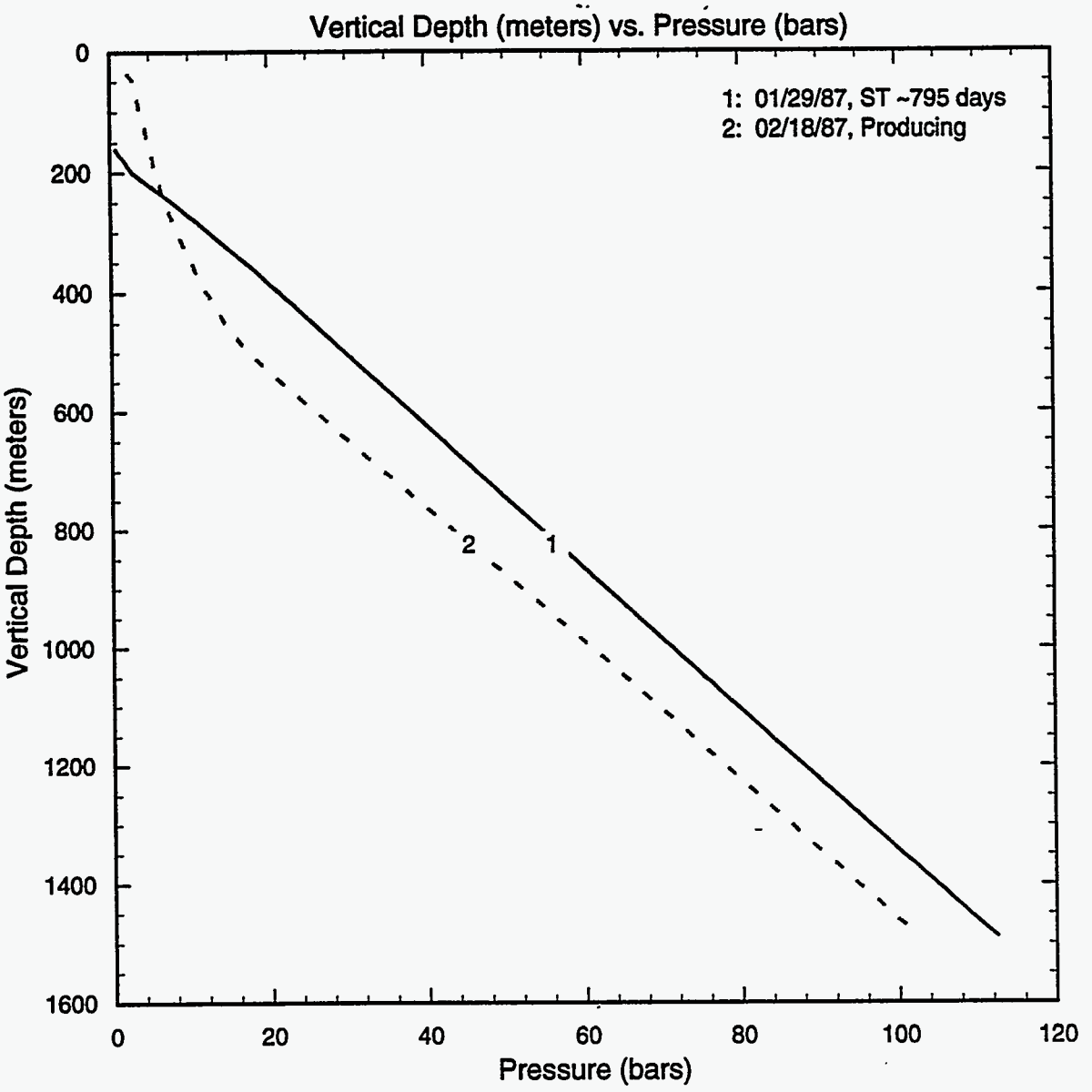

Figure 3.3. Pressures (bars, gauge) recorded by downhole gauges in slim hole GH-3.

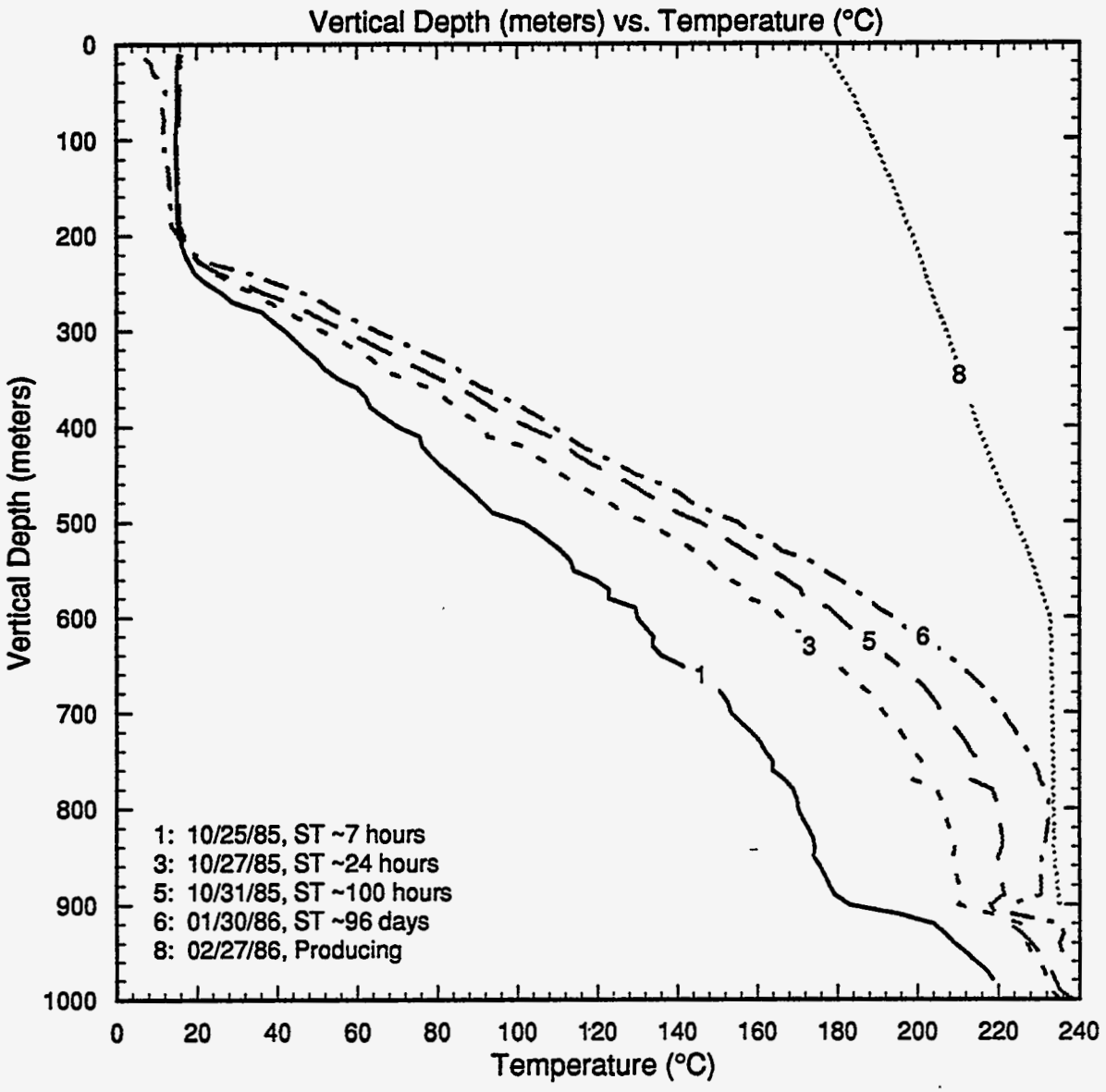

Figure 3.4. Selected temperature profiles for slim hole GH-4.

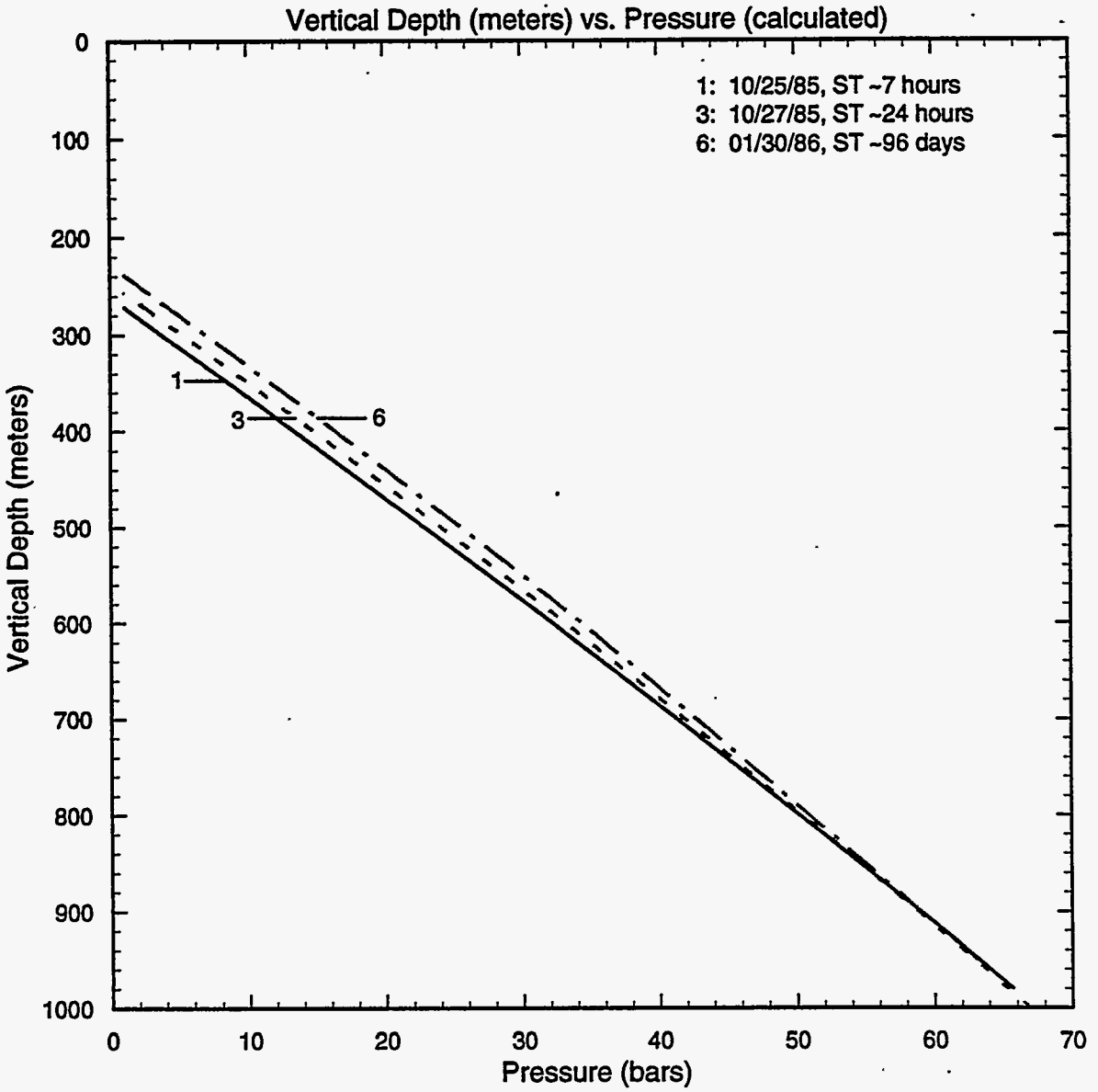

Figure 3.5. Pressure profiles, computed from water level and temperature data, for slim hole GH-4.

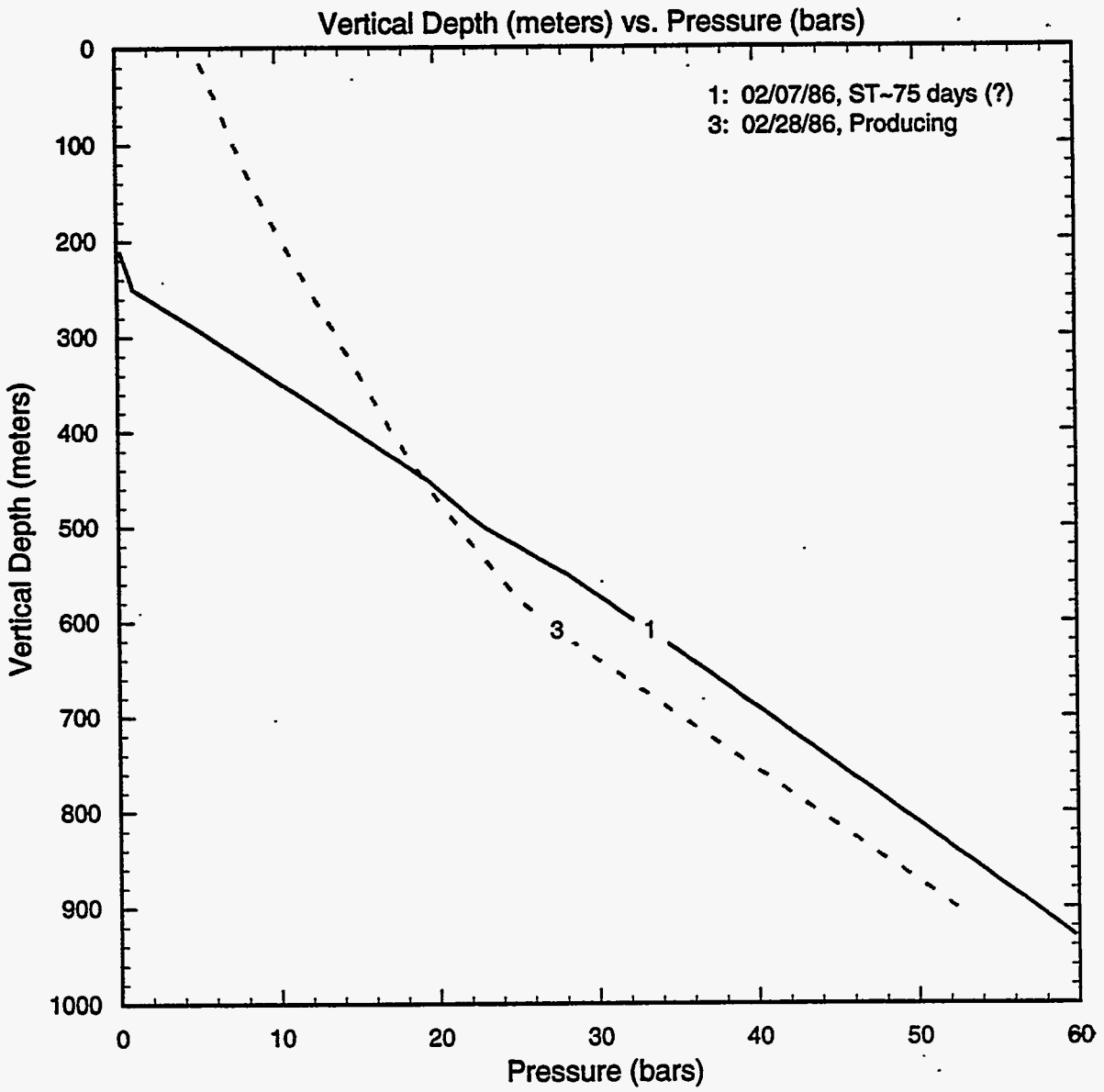

Figure 3.6. Measured pressure (bars, gauge) profiles in slim hole GH-4.

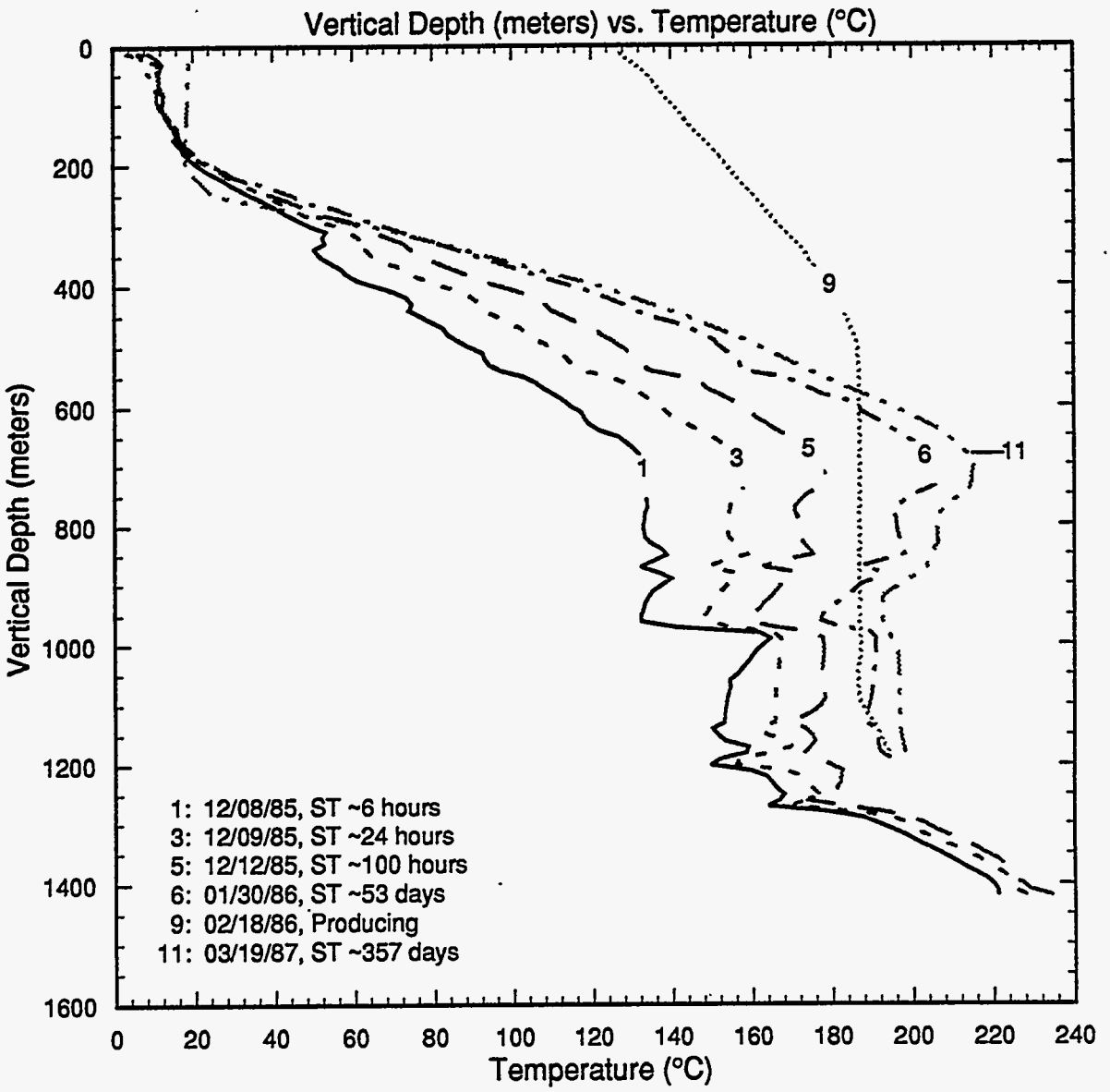

Figure 3.7. Selected temperature surveys for slim hole GH-5.

Pressure profiles, computed from water level and temperature data, are plotted in Figure 3.8; the pressure at 1100 m TVD (~ –210 m ASL) is ~ 74.5 bars. The latter pressure value is in good agreement with that (~ 74 bars) recorded by a downhole gauge in March 1987 (see profile 5, Figure 3.9). The pressure profile recorded in February 1986 (profile 1, Figure 3.9) gave, however, a substantially lower pressure value (~ 71.5 bars) at 1100 m TVD; this lower pressure value is most likely the result of an error in gauge calibration.

3.4 Slim Hole GH-6

Heatup surveys taken shortly after cold water circulation/injection (surveys 1, 2, 3, and 5 in Figure 3.10) in slim hole GH-6 all show a rapid temperature recovery at 760–780 m TVD; this denotes the major feedpoint for this slim hole. An essentially isothermal temperature profile below ~ 780 m TVD in temperature surveys 1, 2, and 3 implies some liquid downflow in the slim hole and the possible presence of a minor feedzone towards the bottom of the slim hole. Temperature survey 10, taken during a production test extends to only ~ 770 m TVD, and supports the location of the major feedzone for GH-6 at ~ 770 m TVD (temperature ~ 215°C). Long time shutin survey 6 shows a temperature inversion in GH-6; the maximum temperature (~ 220°C) occurs at about 500 m TVD.

Pressure profiles, computed from water level and temperature data, are shown in Figure 3.11; the pressure at 770 m TVD (134 m ASL) is 54 bars. The latter pressure value is in good agreement with that (~ 53 bars) recorded by a downhole gauge (profile 1, Figure 3.12) in GH-6.

3.5 Slim Hole GH-7

Short shutin time heatup surveys for slim hole GH-7 (profiles 3, 5, 7, and 8, Figure 3.13) show a rapid temperature recovery at ~ 990 m TVD; this indicates the presence of a major feedzone at about this depth. Persistent low temperatures at and below ~ 1370 m TVD (survey 3, 5, and 7, Figure 3.13) imply the location of another feedzone at this depth. A more definitive identification of feedzone locations is provided by the flowing temperature surveys (see *e.g.*, survey 12, Figure 3.13); these surveys show that the major feedzones for slim hole GH-7 are located at 960–1000 m TVD and at ~ 1400 m TVD. The temperature at the deeper feedzone (1400 m TVD) is ~ 230°C. The long shutin time temperature survey 9 (Figure 3.13) indicates that the shutin temperature at 1400 m TVD is substantially lower than that indicated by the flowing surveys (~ 230°C). It is likely that the shutin temperatures in the depth interval below 1000 m TVD are affected by internal flow in the wellbore (downflow from 1000 m TVD). The flowing temperature above the upper feedzone (980 m TVD) is ~ 220°C.

Continued on page 3-17

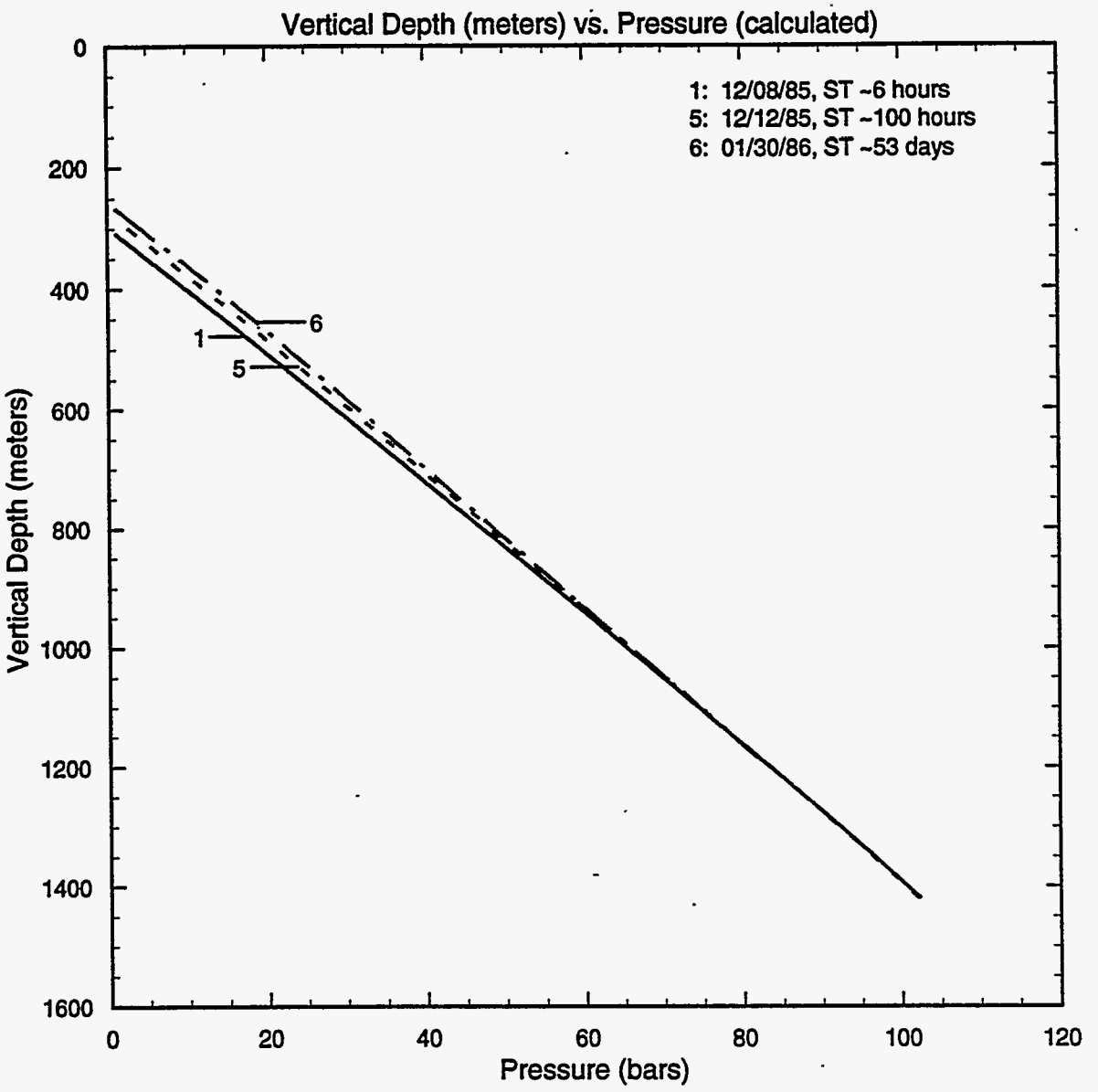

Figure 3.8. Pressure profiles, computed from water level and temperature data, for slim hole GH-5.

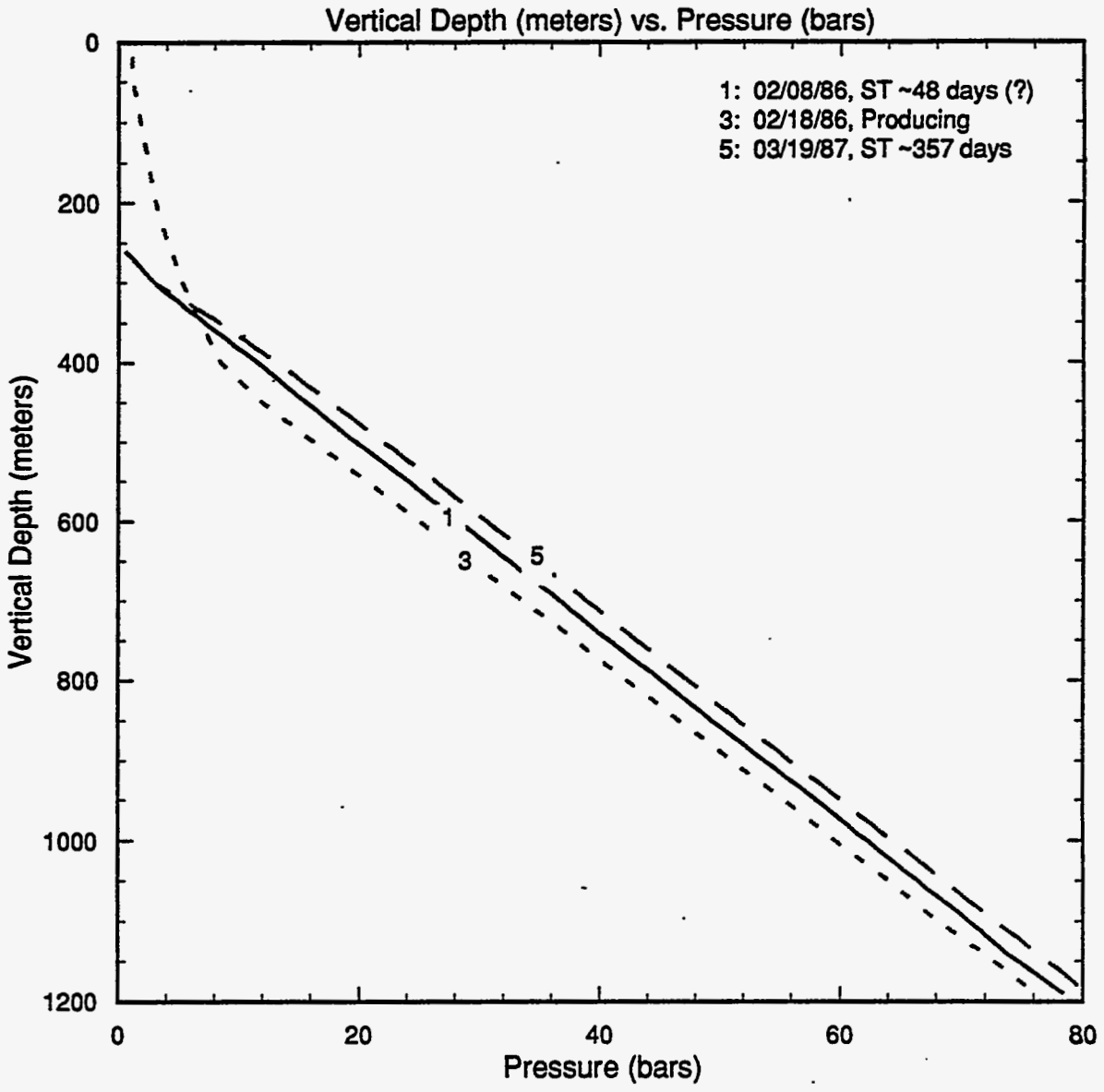

Figure 3.9. Selected measured pressure (bars, gauge) profiles in slim hole GH-5.

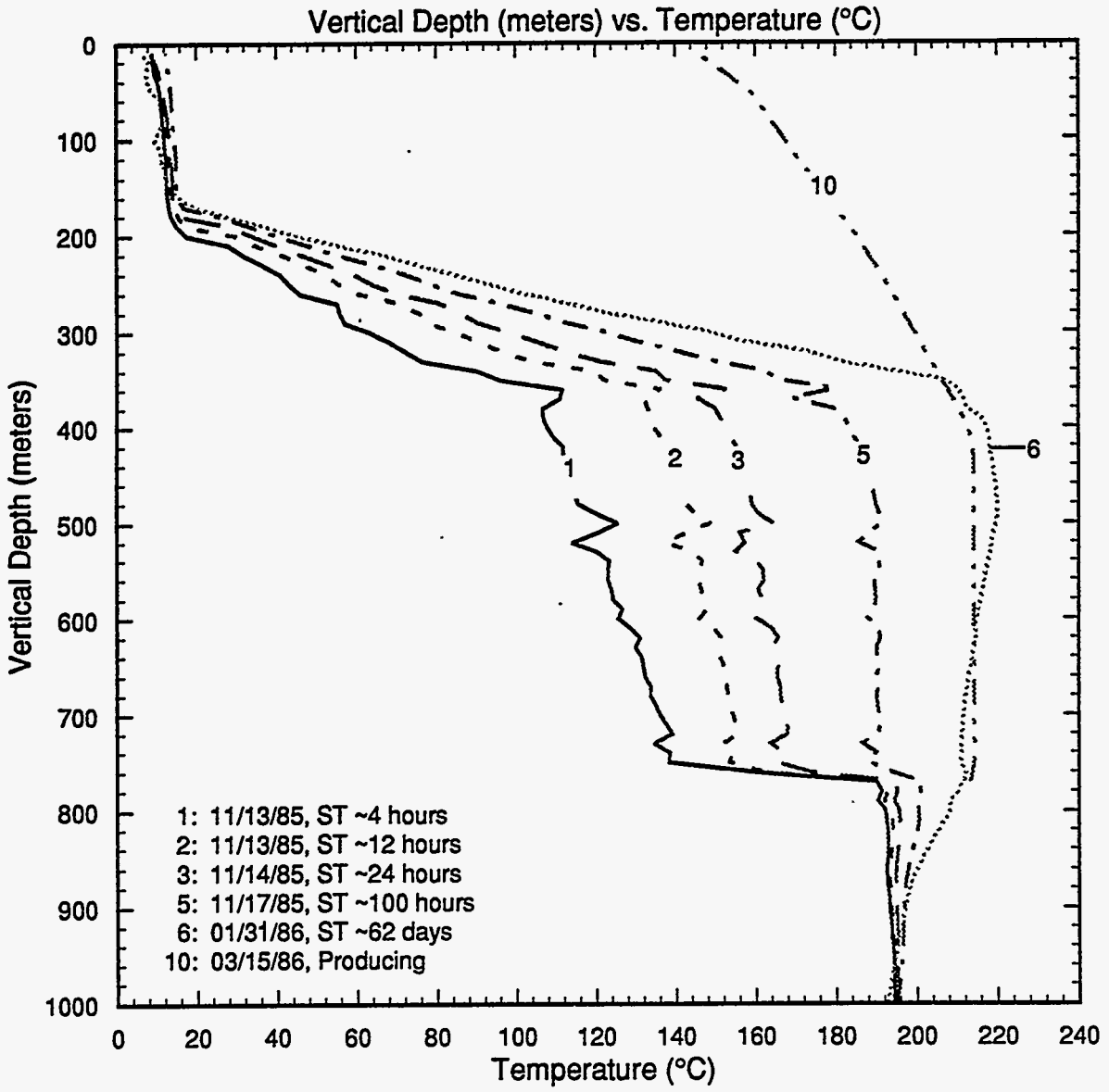

Figure 3.10. Selected temperature surveys for slim hole GH-6.

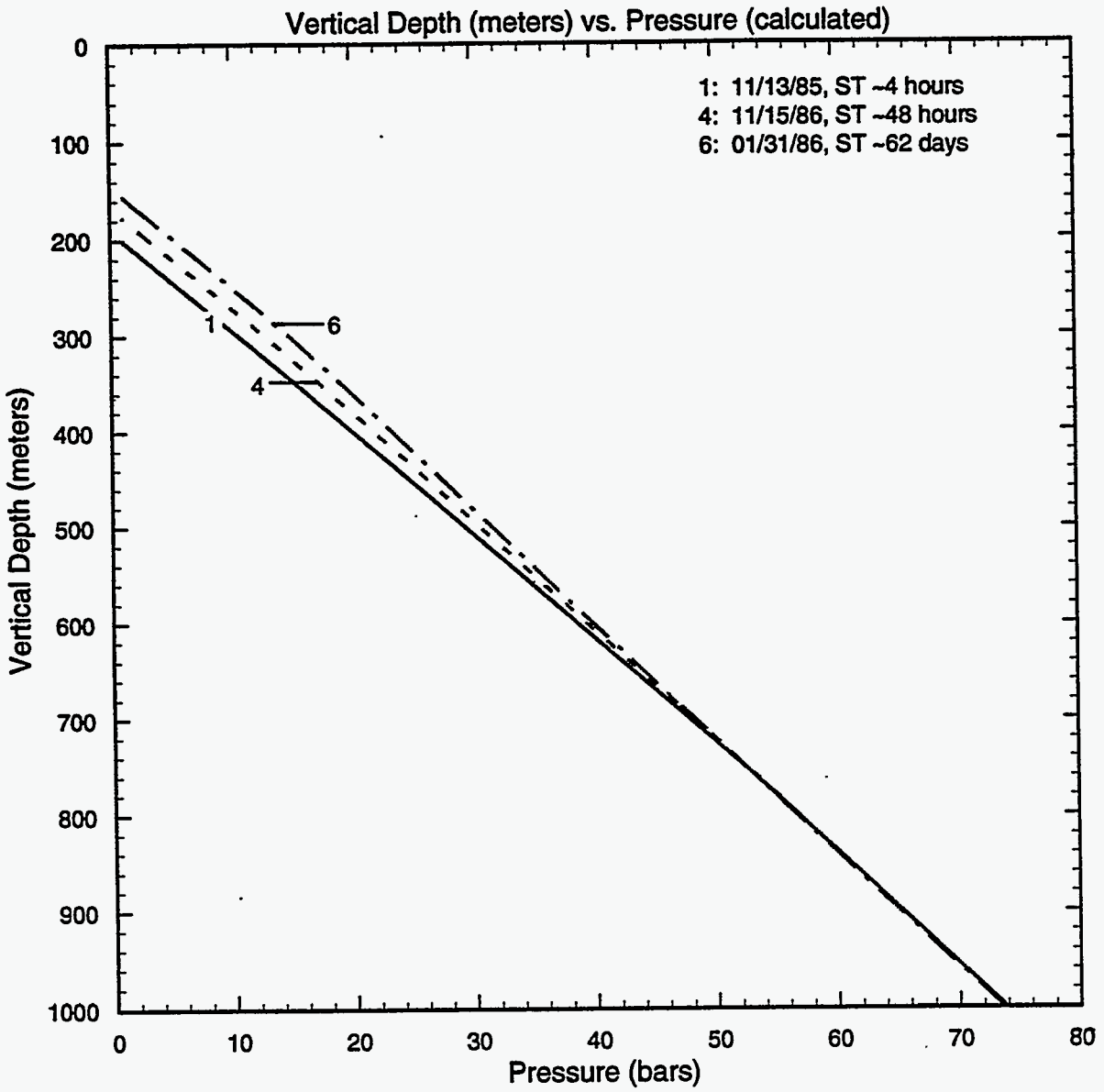

Figure 3.11. Pressure profiles, computed from water level and temperature data, for slim hole GH-6.

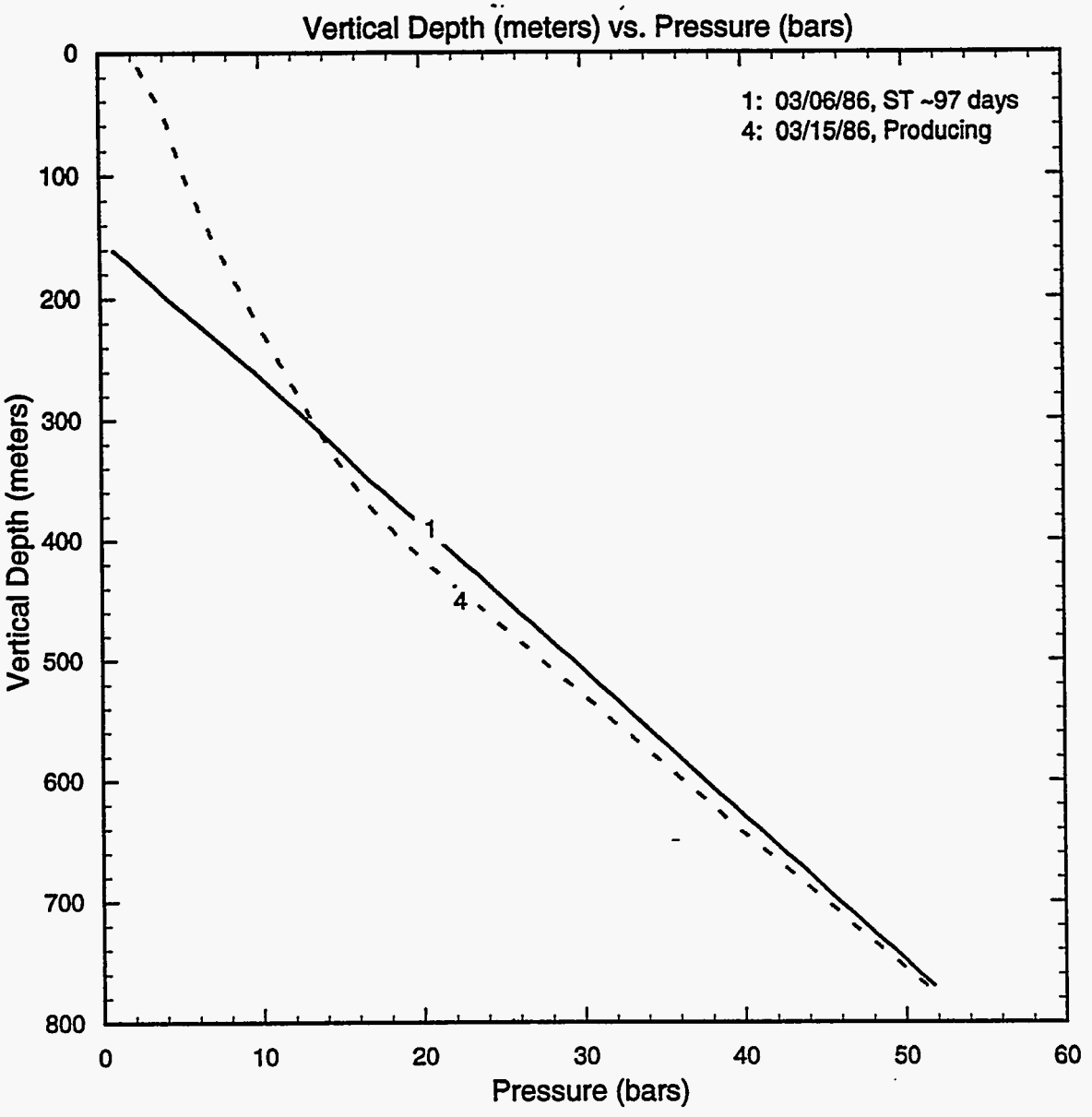

Figure 3.12. Measured pressure (bars, gauge) profiles for slim hole GH-6.

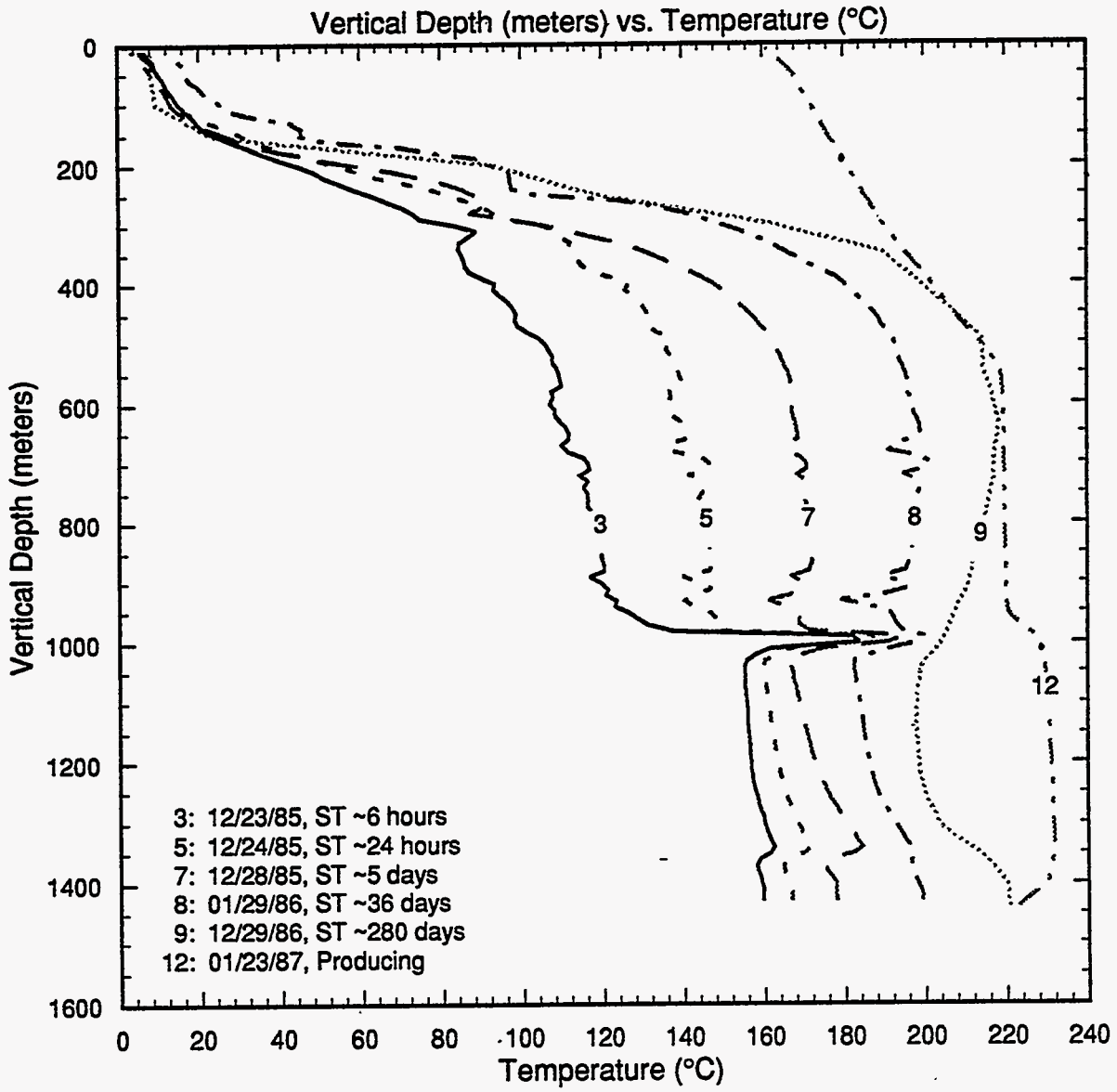

Figure 3.13. Selected temperature profiles for slim hole GH-7.

Pressure profiles, computed from water level and temperature data, are illustrated in Figure 3.14. The pressure at 980 m TVD (–121.5 m ASL) is ~ 64.5 bars, and the pressure at 1400 m TVD (–541.5 m ASL) is ~ 101 bars. These estimated feedzone pressures are in good agreement with those (~ 64 and ~ 100 bars) given by a downhole survey taken in December 1986 (survey 1, Figure 3.15). The downhole pressure survey recorded on July 9, 1990 (survey 5, Figure 3.15) is, however, in substantial disagreement with the December 1986 pressure data; this discrepancy is most likely the result of an error in gauge calibration.

3.6 Slim Hole GH-8

Heatup surveys 1, 3 and 5 (Figure 3.16) for slim hole GH-8, taken shortly after circulation/injection of cold water, show rapid temperature recovery at ~ 1220 m TVD; this implies the location of a fluid entry at this depth. Temperature survey 9 (Figure 3.16), recorded during a production test, supports the conclusion that the major feedpoint for GH-8 is located at about 1220 m TVD. Long shutin time temperature survey 6 shows a temperature inversion in GH-8; the maximum temperature (~ 223°C) occurs around 800 m TVD. The feedzone temperature is ~ 212°C.

Pressure profiles, computed from water level and temperature data, are plotted in Figure 3.17; the pressure at 1220 m TVD (–412.5 m ASL) is estimated to be 89.5 bars. The latter pressure value is virtually identical with that (89.3 bars) recorded by a downhole survey (profile 1, Figure 3.18) in August 1987.

3.7 Slim Hole GH-9

The heatup surveys for slim hole GH-9 (Figure 3.19) provide no indication of permeability below the bottom of the 4-inch casing at ~ 950 m TVD. Significantly, no circulation losses were recorded while drilling below ~ 598 m MD. The maximum temperature (~ 243°C) in GH-9 was observed towards the bottom of the slim hole.

3.8 Well GH-10

Short shutin time heatup surveys 2 and 4 (Figure 3.20) for well GH-10 exhibit a negative temperature gradient in the depth interval 800–1010 m TVD; major circulation losses were recorded while drilling through this depth interval. A sharp break in temperature gradient is present in temperature survey 5 at ~ 1010 m TVD. Flowing temperature survey 7 is consistent with the hypothesis that the major entry for GH-10 is located at about 1010 m TVD. The feedzone temperature is ~ 241°C.

Continued on page 3-25

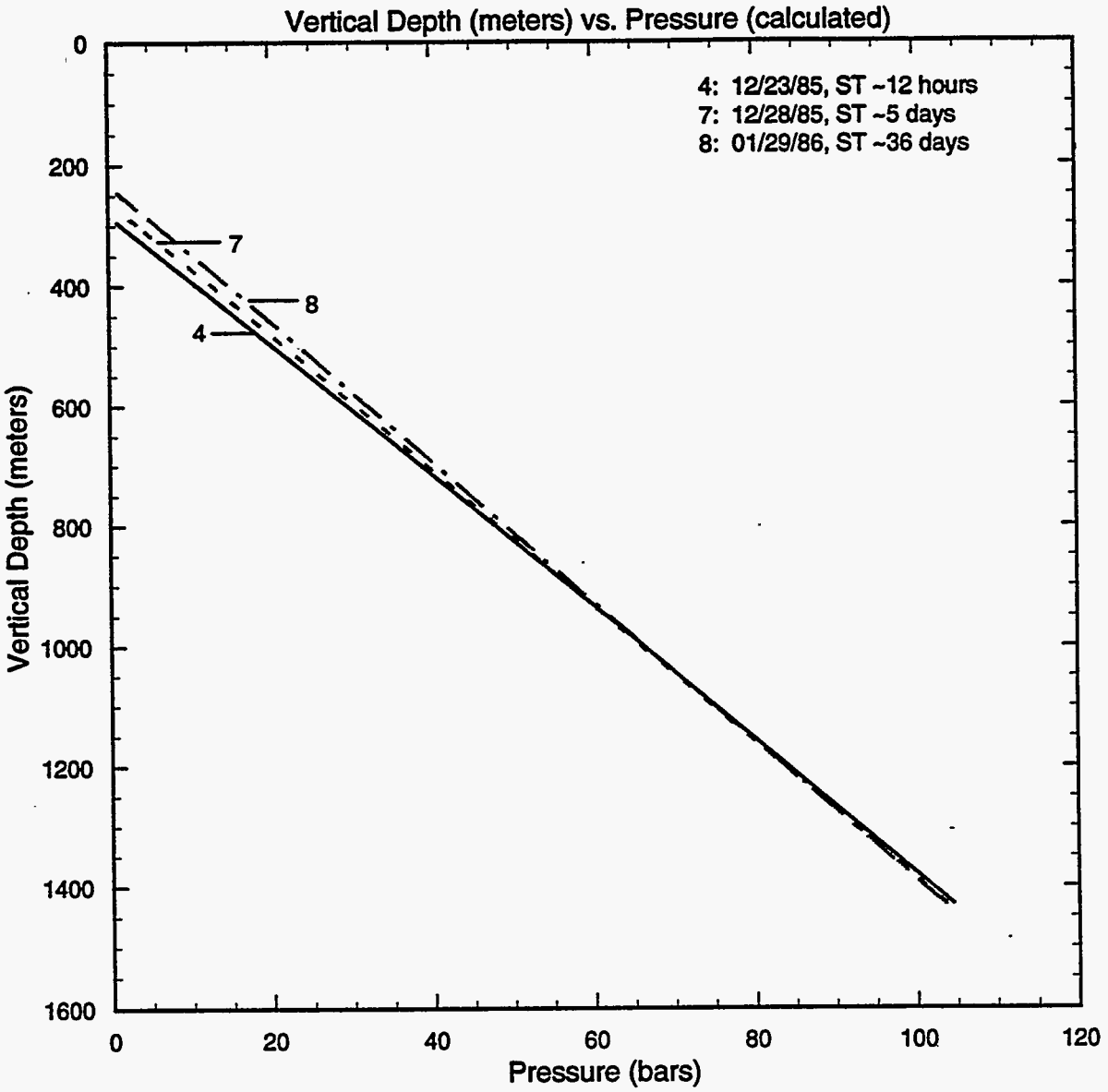

Figure 3.14. Pressure profiles, computed from water level and temperature data, for slim hole GH-7.

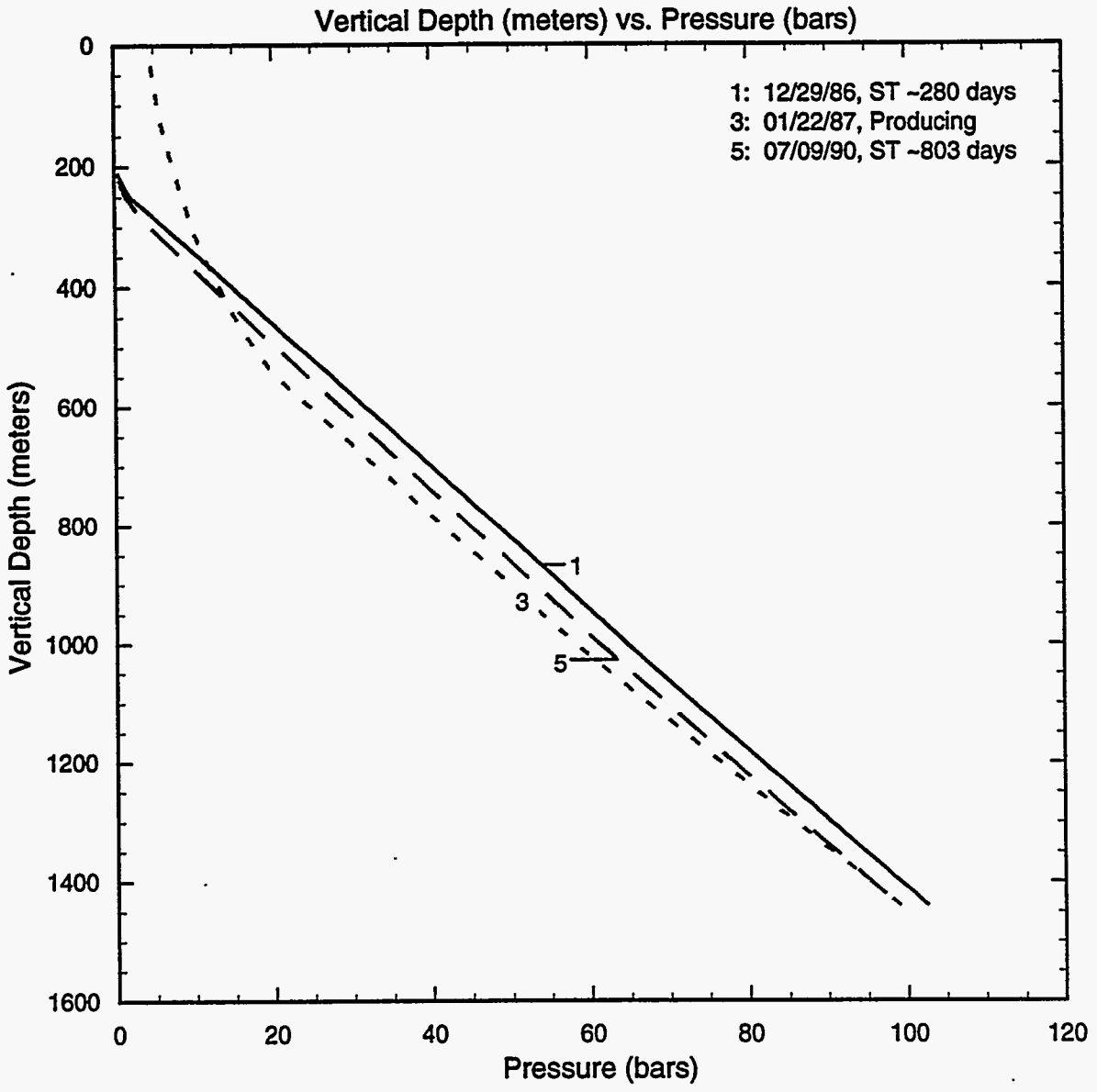

Figure 3.15. Measured pressure (bars, gauge) profiles for slim hole GH-7.

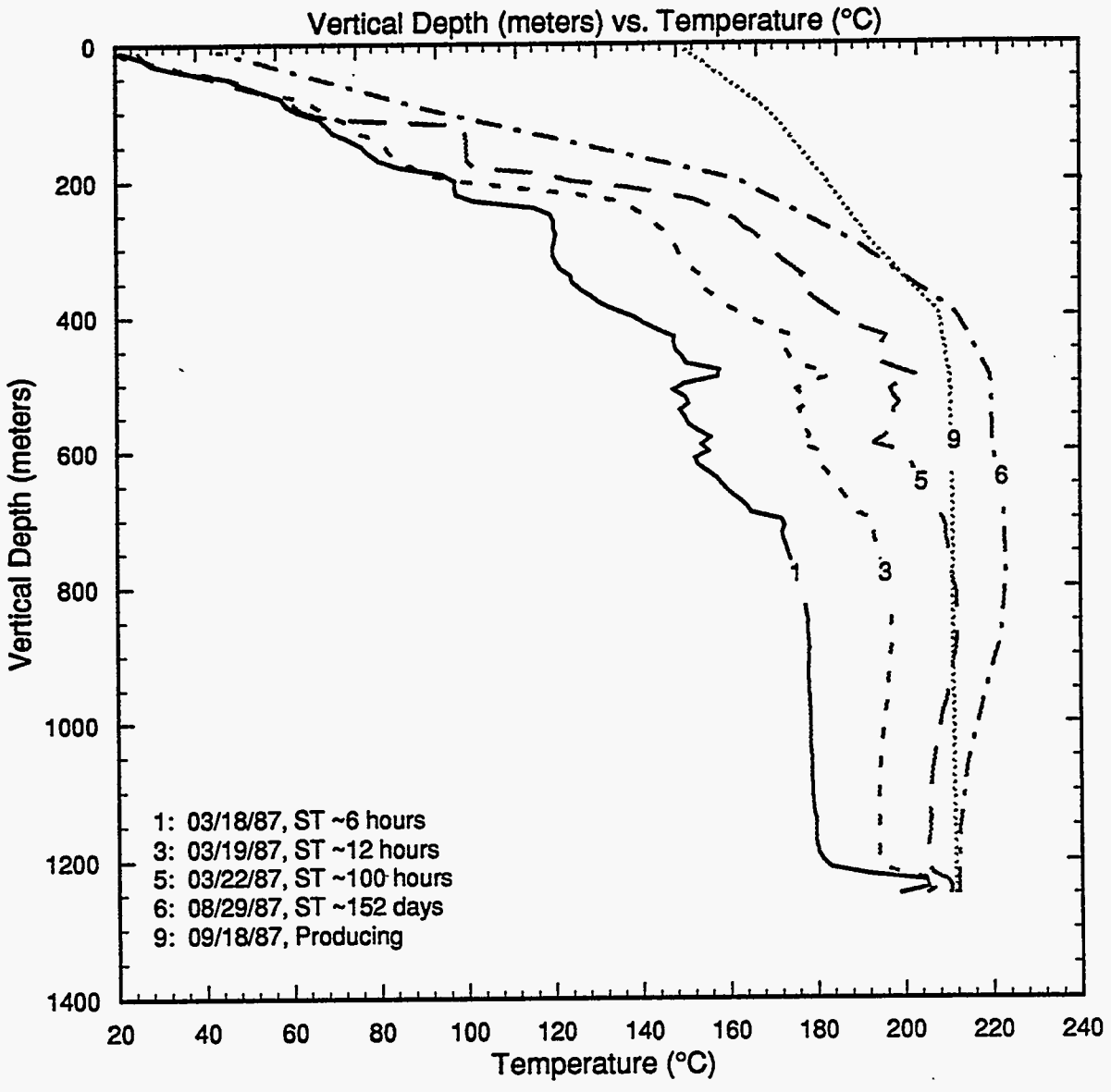

Figure 3.16. Selected temperature surveys for slim hole GH-8.

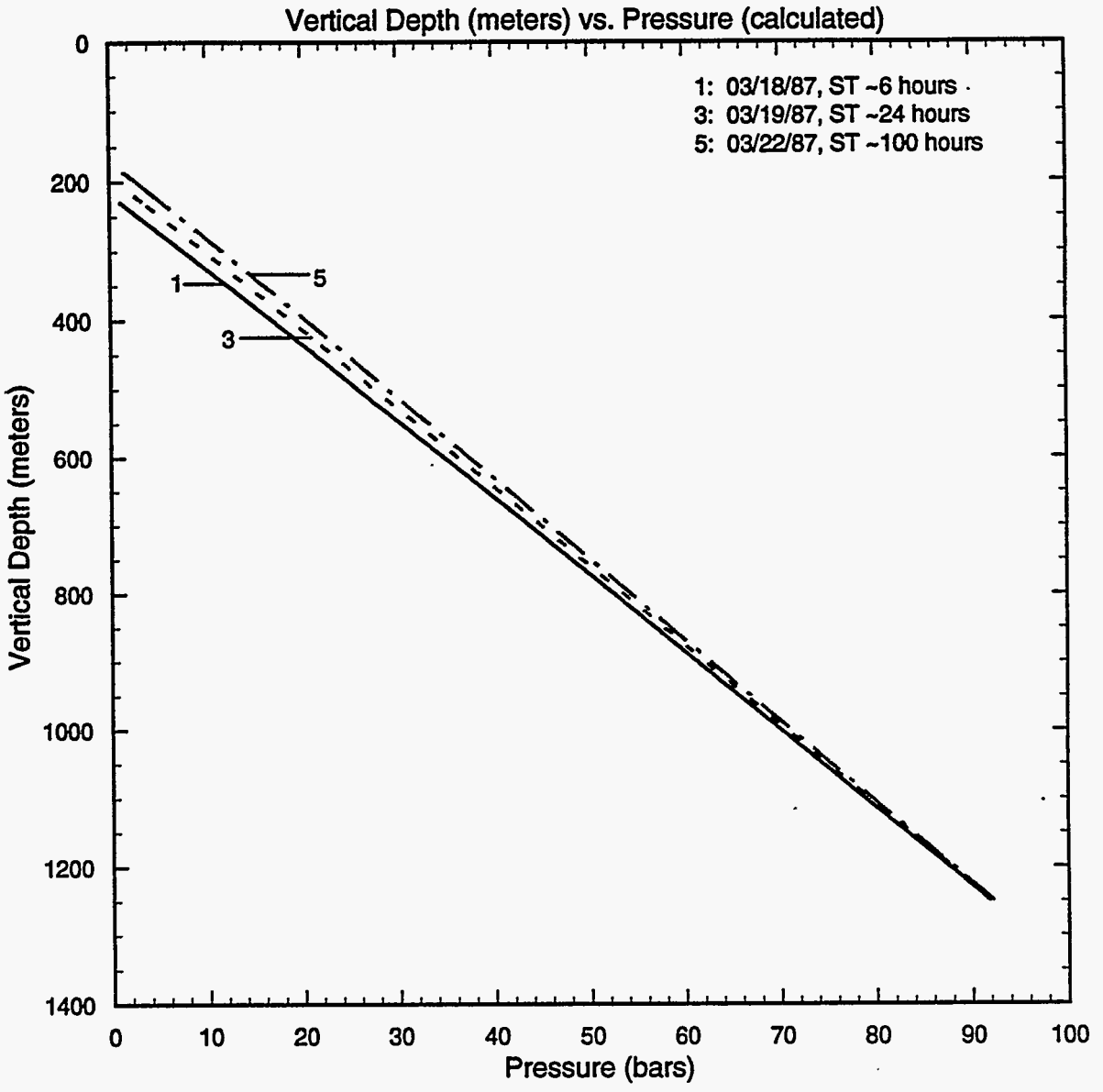

Figure 3.17. Pressure profiles, computed from water level and temperature data, for slim hole GH-8.

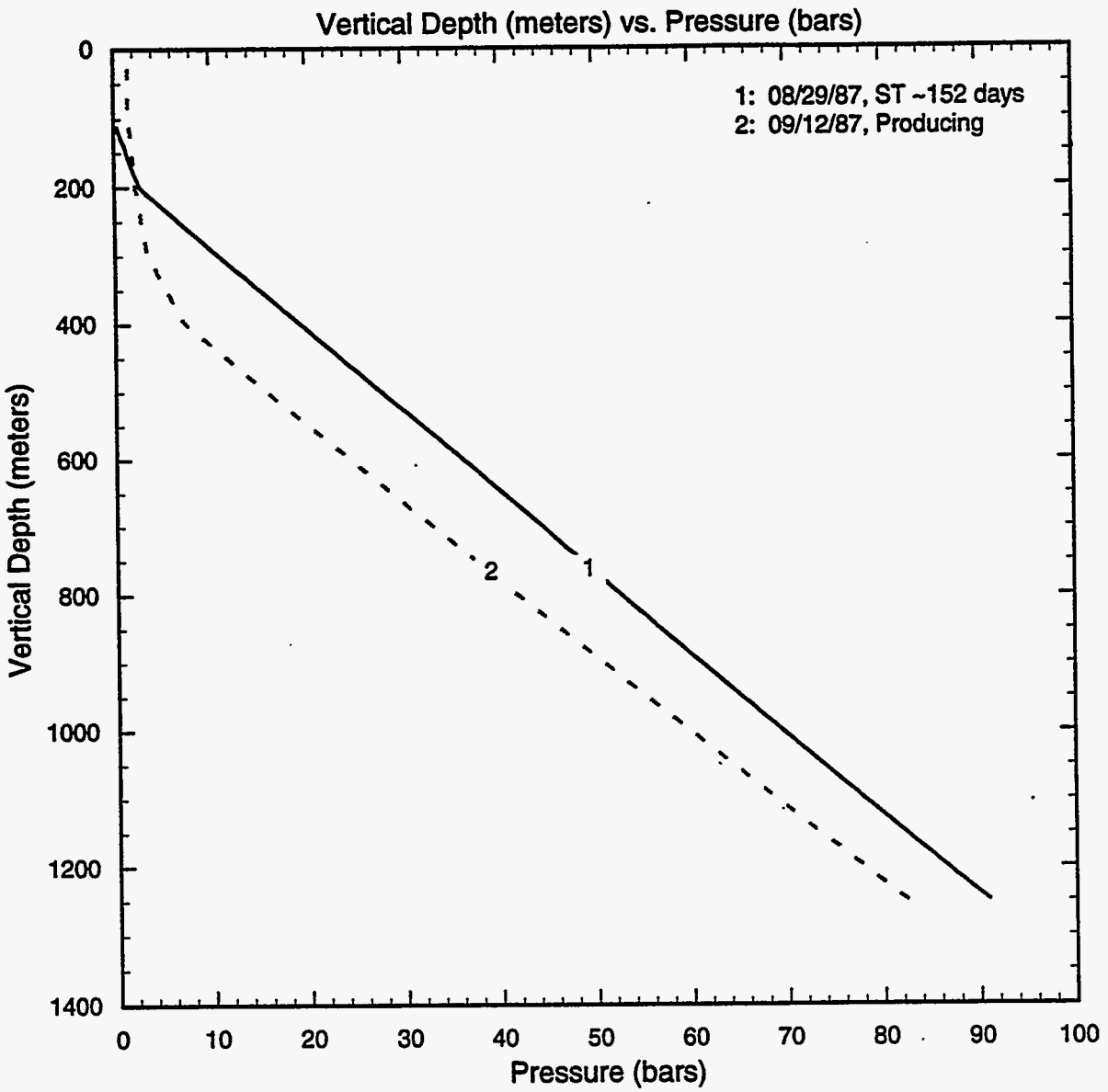

Figure 3.18. Measured pressure (bars, gauge) profiles for slim hole GH-8.

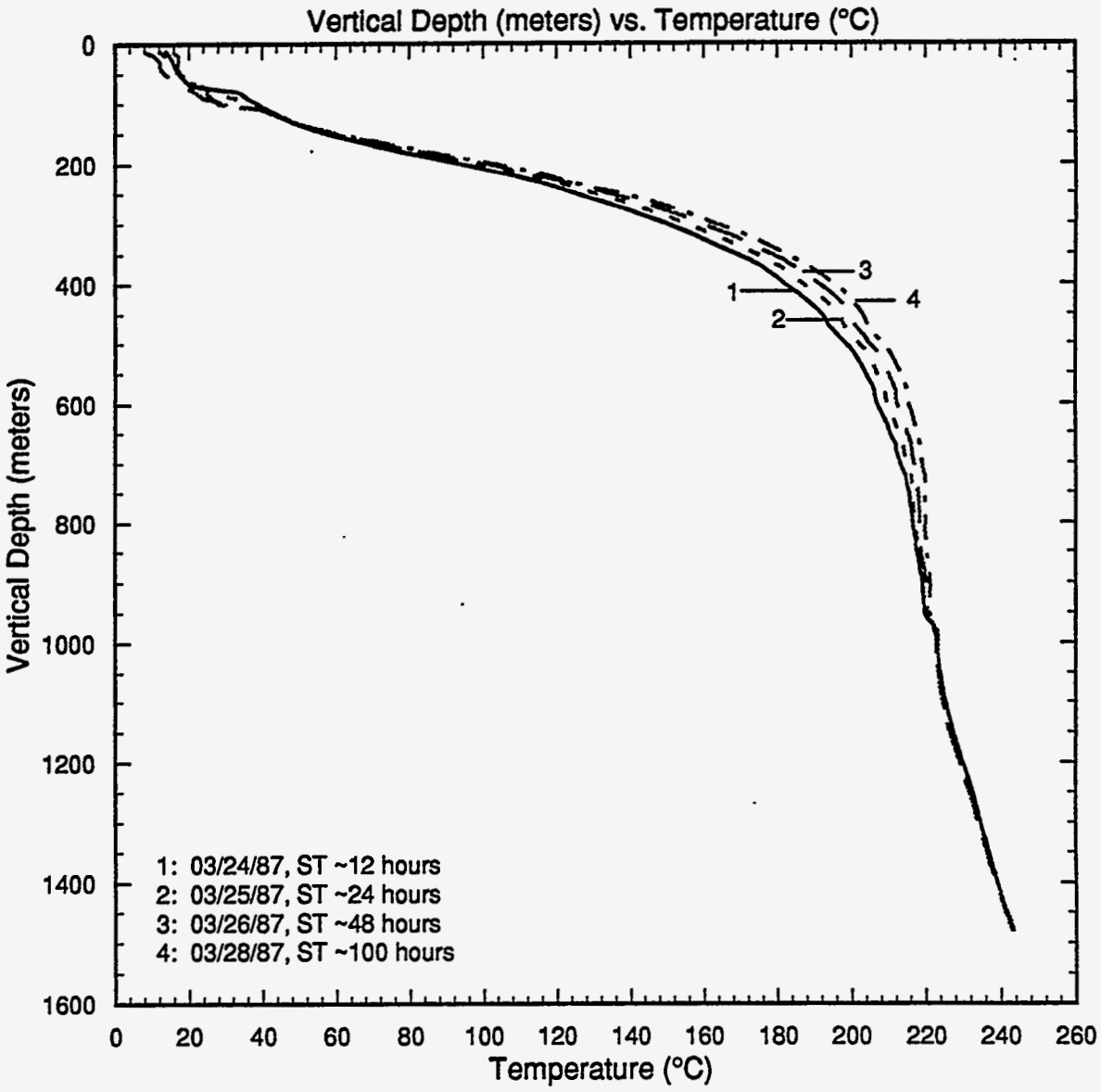

Figure 3.19. Available temperature surveys for slim hole GH-9.

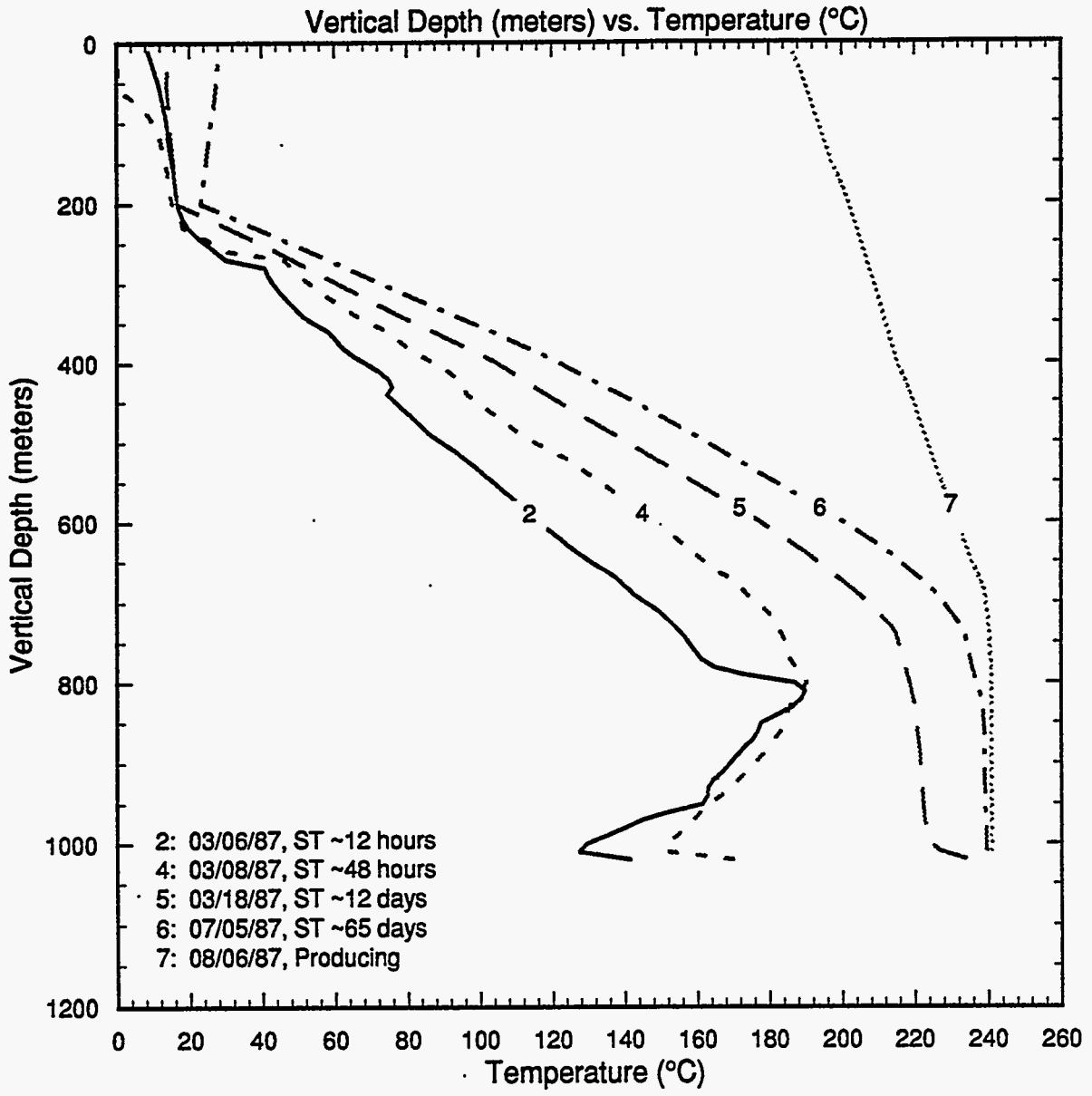

Figure 3.20. Selected temperature profiles for well GH-10

Pressure profiles, computed from water level and temperature data, are plotted in Figure 3.21; the estimated pressure at 1010 m TVD (–145 m ASL) is ~ 68.5 bars. The latter pressure value is in good agreement with downhole pressure (68.6 ± 0.3 bars) measurements (profiles 1 and 2, Figure 3.22).

3.9 Well GH-11

Heatup surveys 1, 2, and 4 (Figure 3.23) for well GH-11 show a persistent temperature depression at ~ 1120 m TVD. The available PTS surveys (Figure 3.23, temperature profile 7; Figure 3.24, pressure profile 3; Figure 3.25, spinner profiles 1 and 2) indicate the presence of a liquid entry (temperature ~ 237°C) at about 1140 m TVD. A circulation loss zone was recorded nearby at ~ 1137 m TVD. We conclude that the major permeable zone for well GH-11 is located at 1140 m TVD. The long shutin time temperature survey 5 (Figure 3.23) exhibits an isothermal profile below ~ 1020 m TVD; this indicates internal flow (upflow?) in the wellbore between the feedzone at 1140 m TVD and another (possibly minor) permeable horizon at ~ 1020 m TVD. The latter permeable horizon is most likely associated with a minor circulation loss zone at ~ 1029 m TVD.

Pressure profiles, computed from water level and temperature data, are plotted in Figure 3.26; the pressure at 1140 m TVD (–282 m ASL) is ~ 80 bars. The latter pressure value is in good accord with that (~ 80 bars) recorded by a downhole gauge in January 1990 (Figure 3.24).

3.10 Well GH-12

Heatup surveys 1, 2 and 4 (Figure 3.27) for well GH-12, taken shortly after cold water injection/circulation, show a persistent temperature depression at ~ 750 m TVD; a major circulation loss zone was encountered nearby at ~ 744 m TVD. Temperature surveys recorded during a production test in 1991 (profiles 6 and 7, Figure 3.27) show an isothermal temperature profile between ~ 750 m TVD and 960 m TVD; an isothermal profile implies permeability at both its end points. The corresponding spinner surveys (Figure 3.28) do not, however, give any indication of a significant fluid entry at 960 m TVD. We, therefore, conclude that the principal feedzone for GH-12 is located at 750 m TVD. The liquid entering the wellbore at 750 m TVD is at a temperature of ~ 232°C. The long shutin time temperature survey 5 (Figure 3.27) exhibits a temperature inversion; the maximum temperature occurs at about 730 m TVD.

Pressure profiles, computed from water level and temperature data, are displayed in Figure 3.29; the feedzone (750 m TVD ≈ 114 m ASL) pressure is ~ 46 bars. A downhole pressure survey taken in January 1990 (Figure 3.30) indicates that the feedzone pressure may be slightly lower (~ 45 bars).

Continued on page 3-36

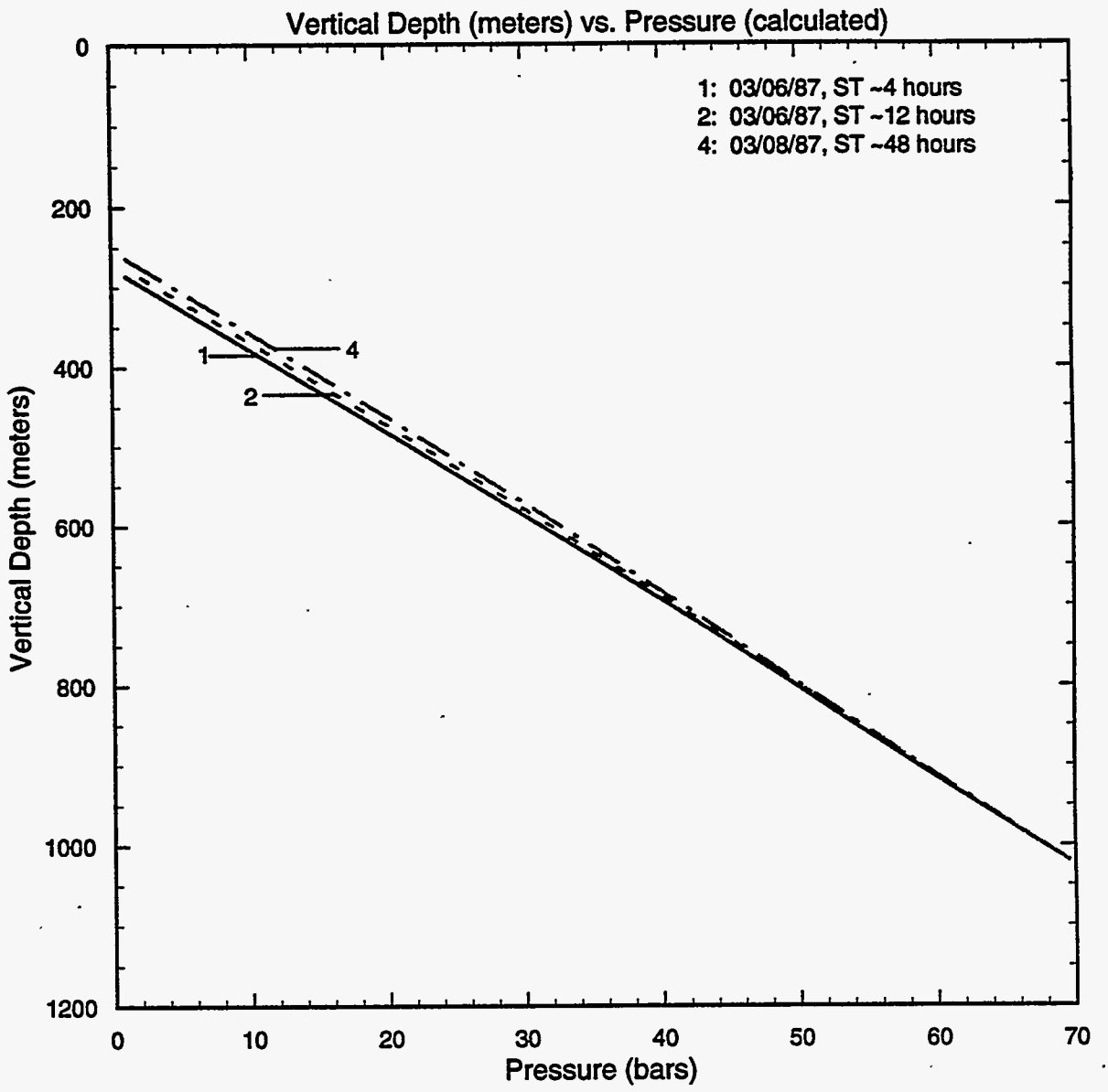

Figure 3.21. Pressure profiles, computed from water level and temperature data, for well GH-10.

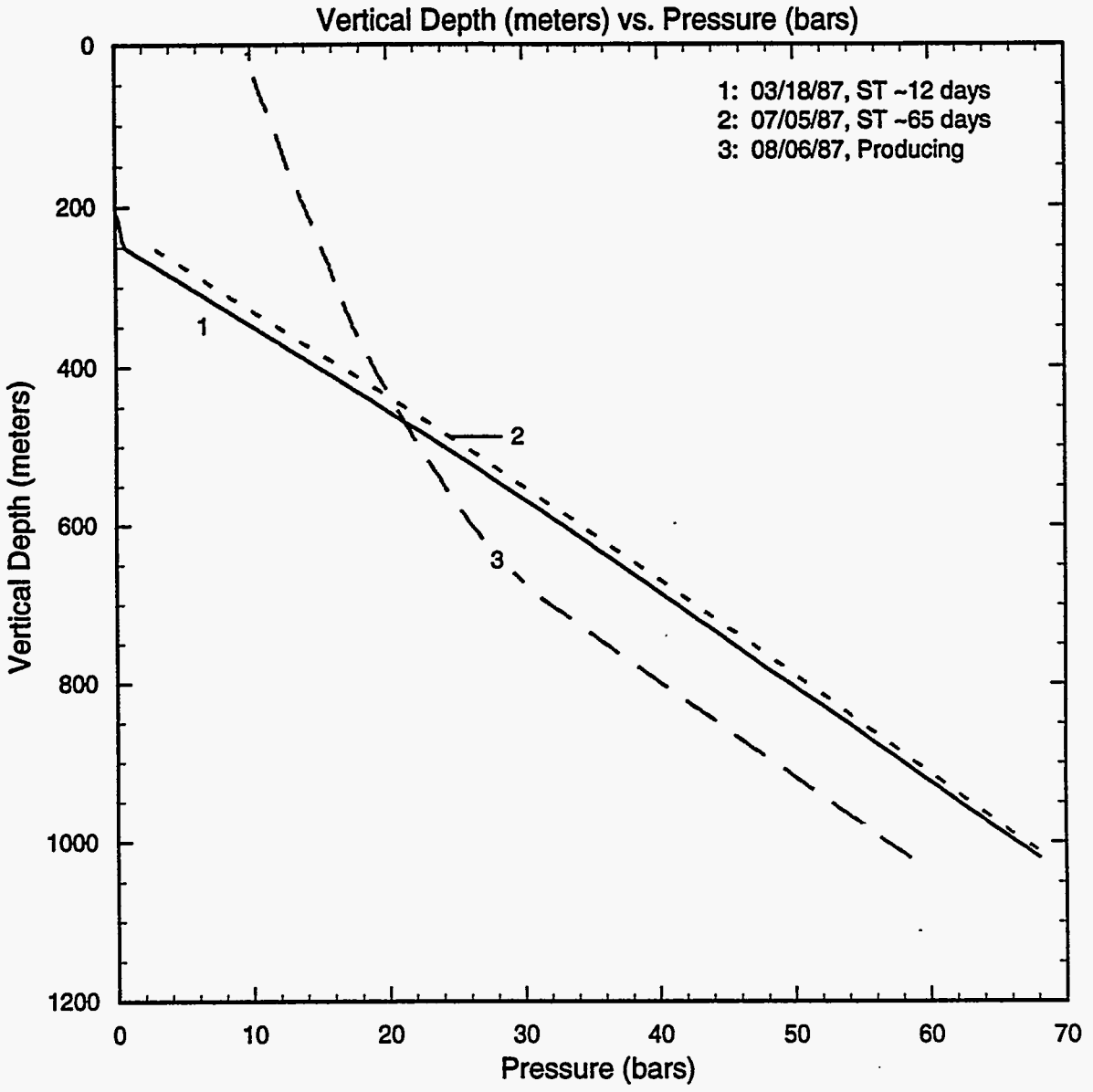

Figure 3.22. Measured pressure (bars, gauge) profiles for well GH-10.

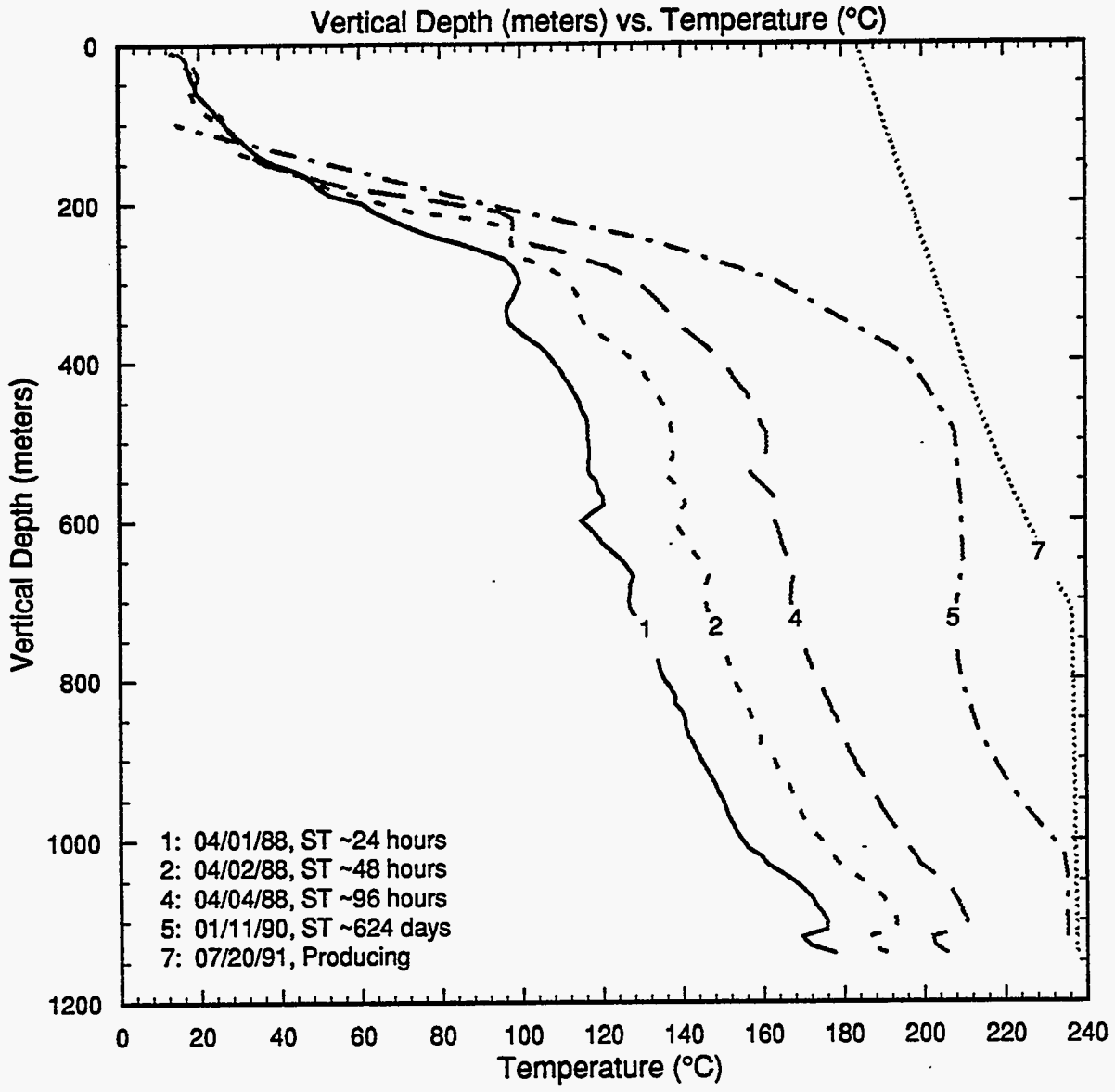

Figure 3.23. Selected temperature surveys for well GH-11.

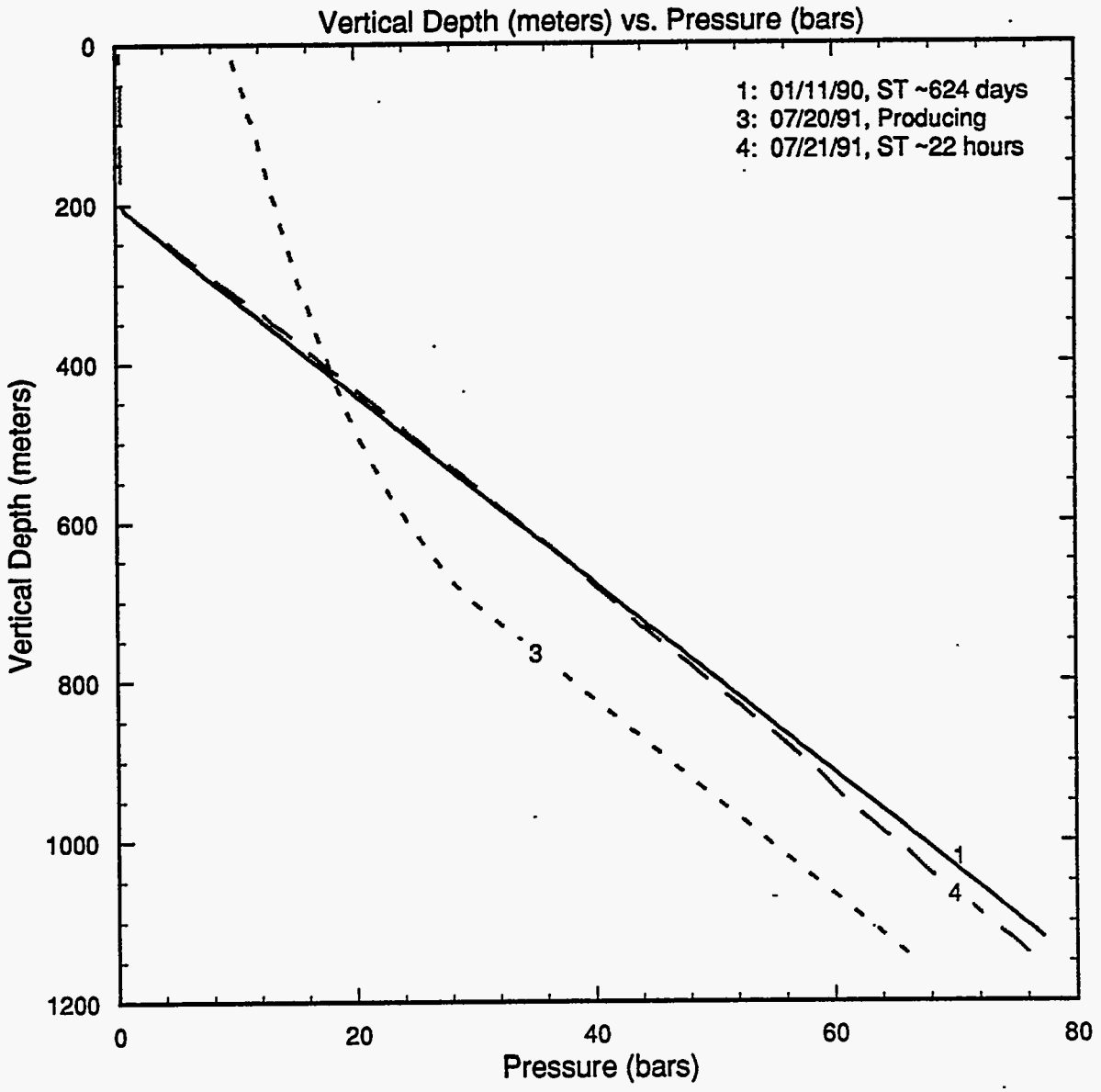

Figure 3.24. Selected pressure (bars, gauge) surveys taken in well GH-11.

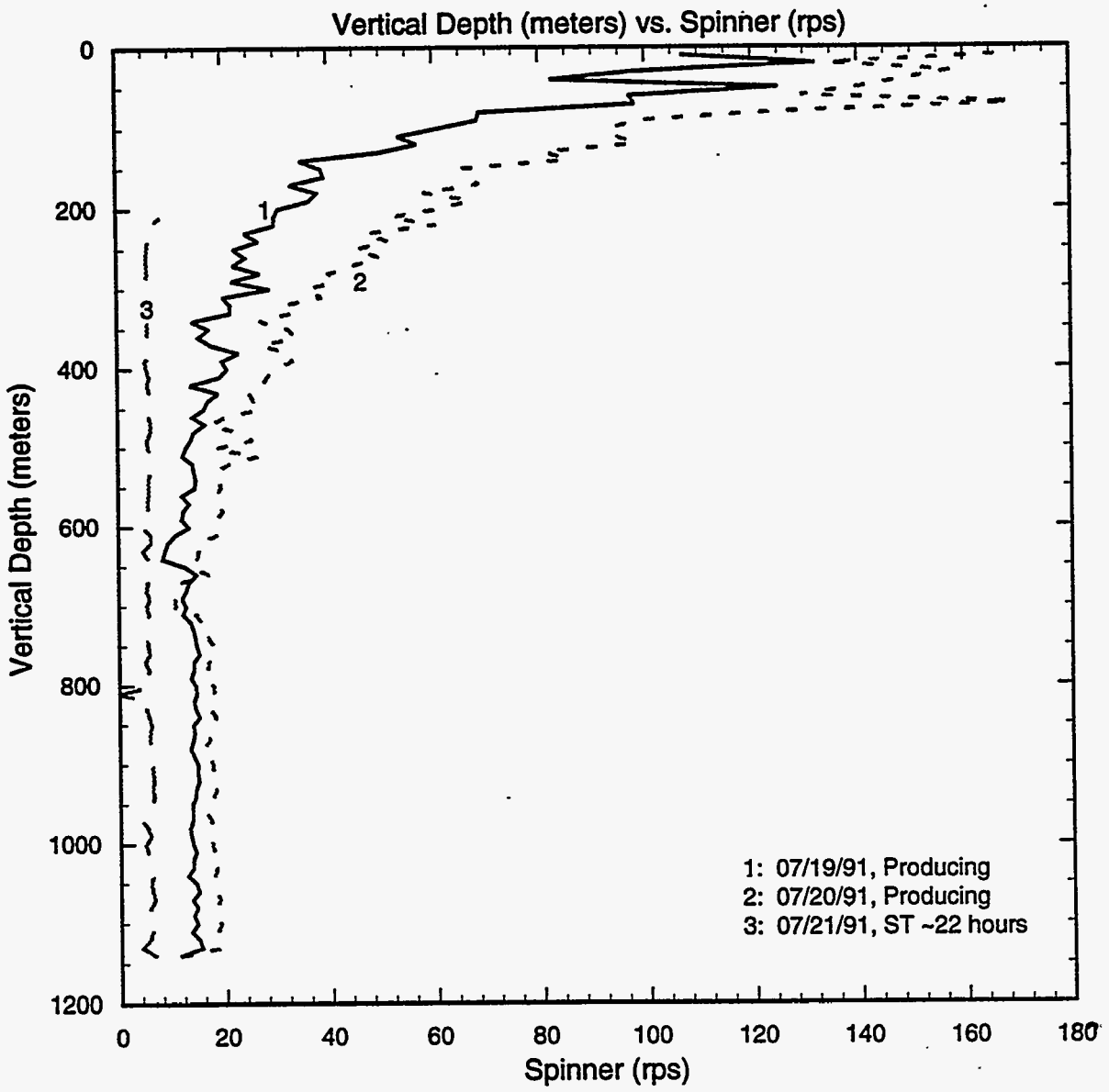

Figure 3.25. Spinner surveys recorded in well GH-11.

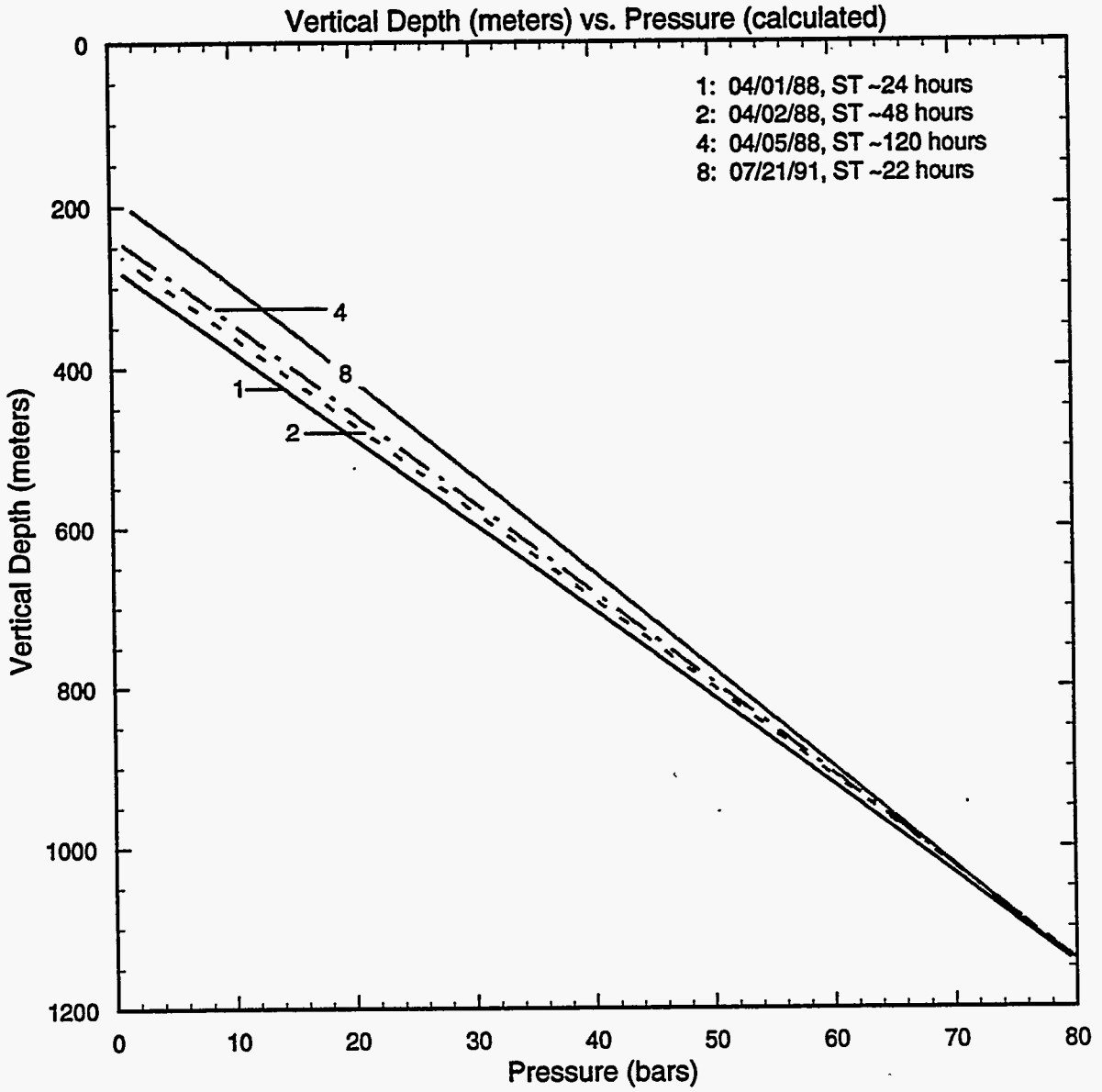

Figure 3.26. Pressure profiles, computed from water level and temperature data, for well GH-11.

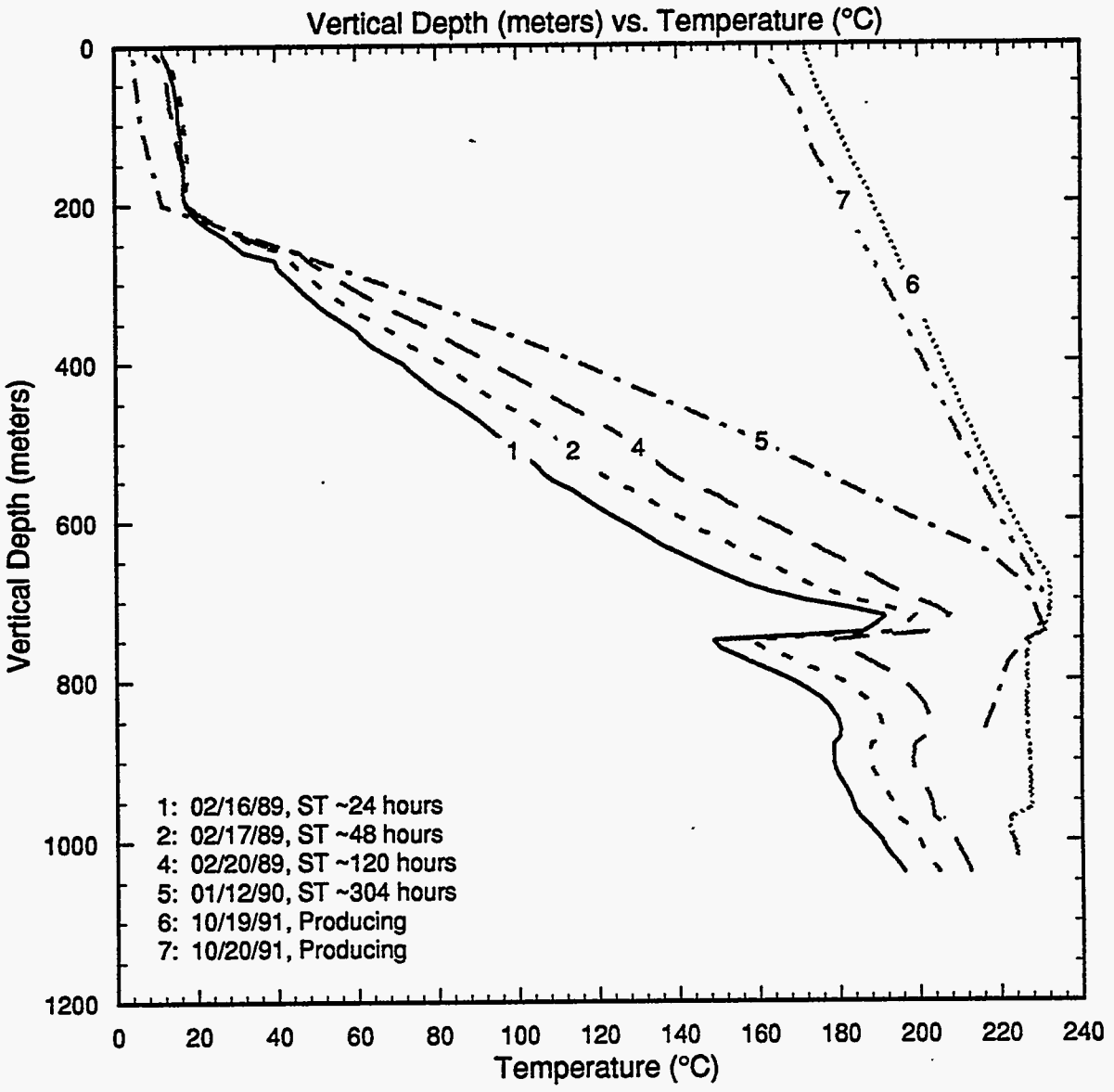

Figure 3.27. Selected temperature profiles for well GH-12.

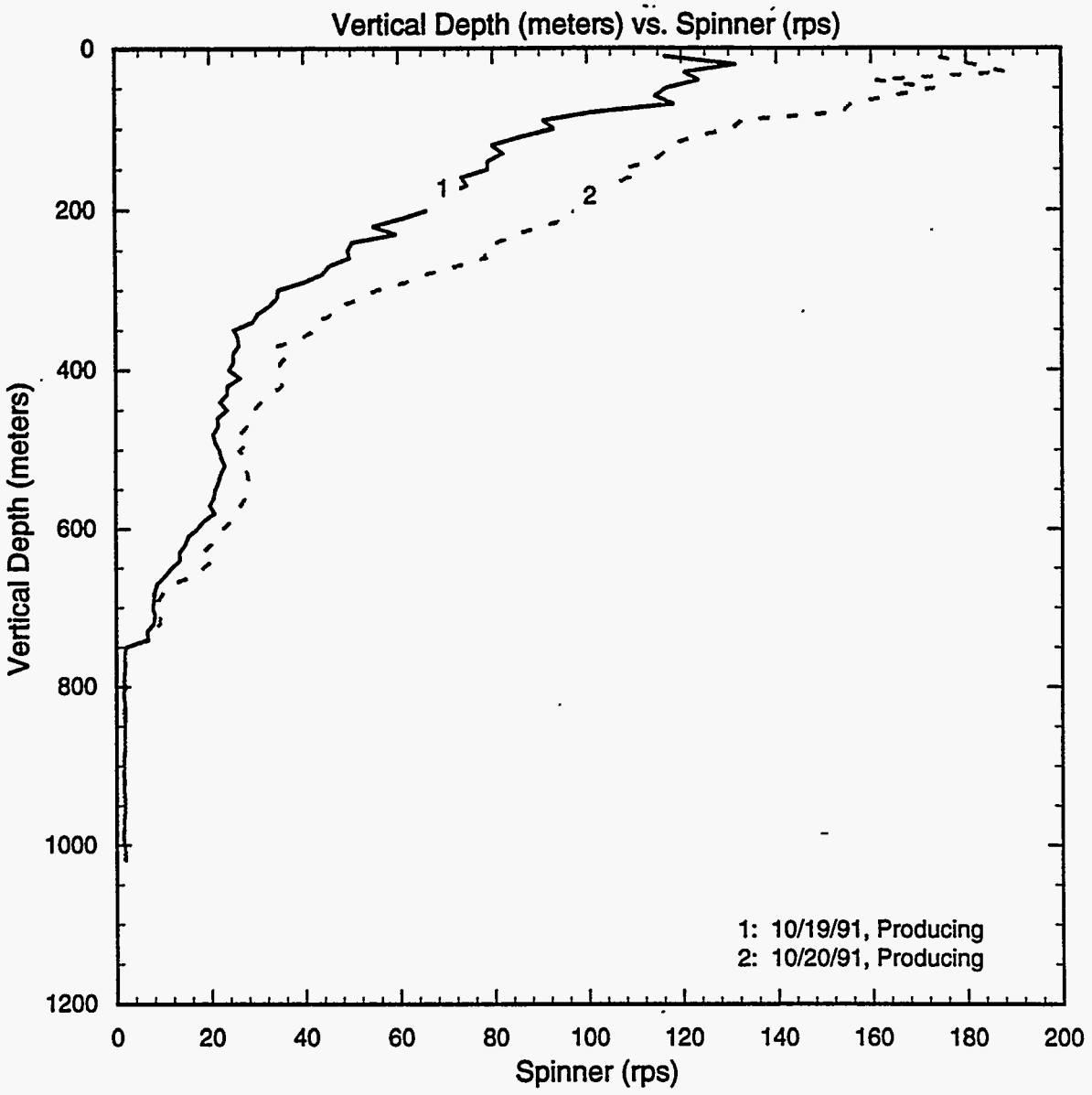

Figure 3.28. Spinner surveys taken during a production test in well GH-12.

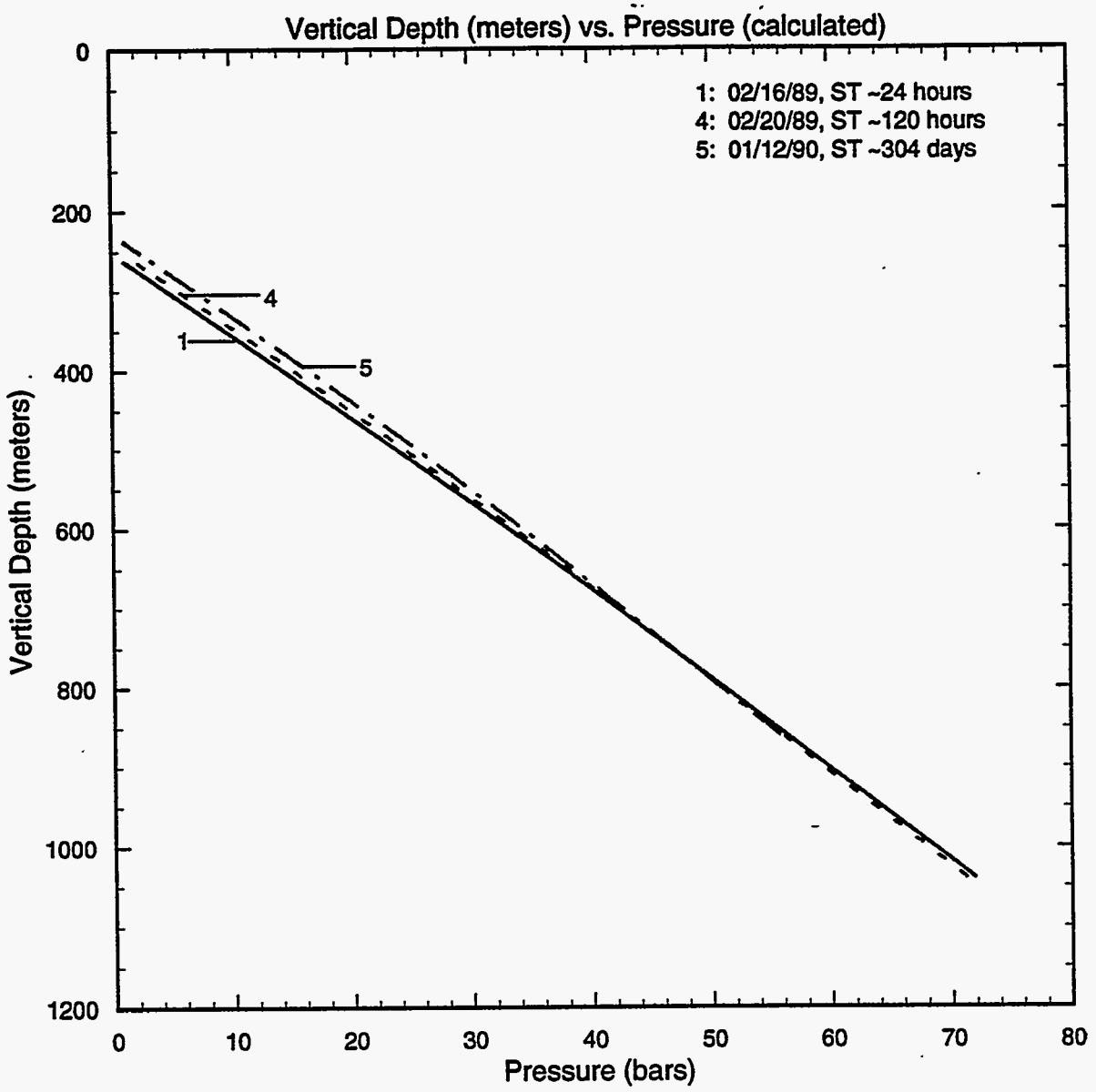

Figure 3.29. Pressure profiles, computed from water level and temperature data, for well GH-12.

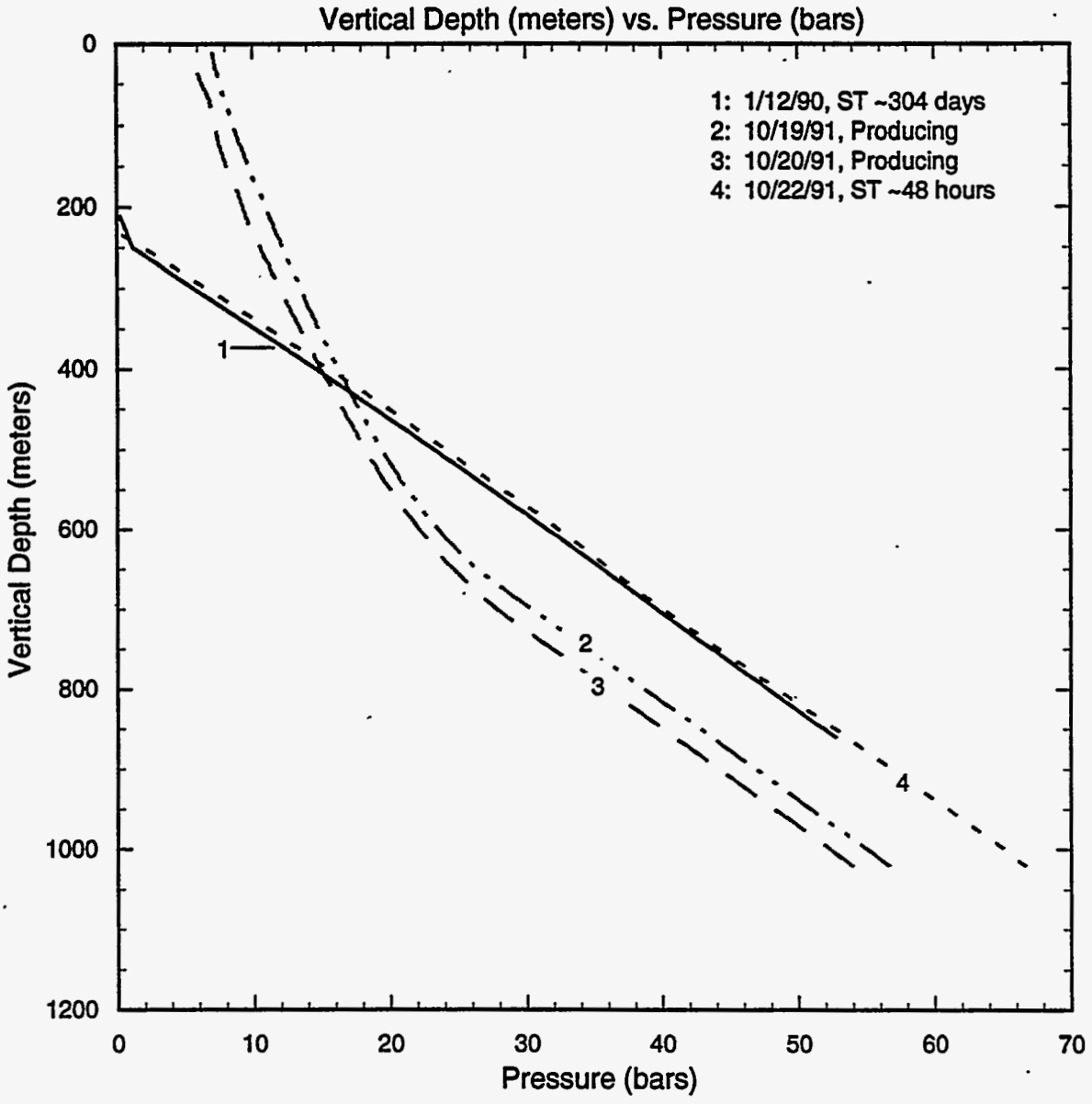

Figure 3.30. Available pressure (bars, gauge) surveys for well GH-12.

3.11 Well GH-15

Heatup surveys 1, 2 and 4 (Figure 3.31) for well GH-15, taken shortly after well completion, exhibit (1) a temperature depression at ~ 560 m TVD, (2) an isothermal zone from ~ 610 m TVD to ~ 680 m TVD, and (3) a change in temperature gradient at ~ 690 m TVD. Temperature and pressure surveys (Figures 3.32 and 3.33) recorded during a production test indicate the presence of a two-phase entry at ~ 680 m TVD. On shutin, a rapid temperature recovery is observed in the depth interval ~ 560–680 m TVD (profile 7, Figure 3.32). A study of pressure and temperature profiles taken during the production test (Figures 3.32 and 3.33) shows the existence of single-phase (liquid) conditions below ~ 700 m TVD. The latter fact taken together with non-isothermal conditions below 680 m TVD would tend to argue against the presence of any fluid entries deeper than ~ 700 m TVD. Temperature surveys 8 and 9 (Figure 3.31), taken during an injection test, imply that the injected fluid is lost in the depth interval 680–700 m TVD. We, therefore, suggest that the principal feedpoint for GH-15 is located at 680 m TVD.

Pressure profiles, computed from water level and temperature data, are displayed in Figure 3.34; the pressure at 680 m TVD (178 m ASL) is ~ 50.5 bars. The latter pressure value is in substantial disagreement with that (~ 46.5 bars) recorded by a downhole pressure gauge on November 16, 1990 (profile 3, Figure 3.33). We suggest that the pressure value recorded on November 16, 1990 is too low and does not represent the reservoir pressure in the vicinity of well GH-15; insufficient buildup time after the production test and/or an error in gauge calibration may be responsible.

3.12 Well GH-17

Heatup surveys 1–4 (Figure 3.35) in well GH-17, recorded shortly after well completion, show a persistent temperature depression at ~ 760 m TVD. A total circulation loss zone was encountered at 753 m TVD, and blind drilling was used below the latter depth. Therefore, it appears that the principal feedzone for well GH-17 is located at 760 m TVD.

Pressure profiles, computed from water level and temperature data, are plotted in Figure 3.36; the pressure at 760 m TVD (25 m ASL) is about 53 bars.

3.13 Well GH-19

Heatup surveys 1, 2 and 4 (Figure 3.37) in well GH-19, taken shortly after well completion, show fast temperature recovery at ~ 760 m TVD. Temperature survey 6, recorded during an injection test, indicates fluid losses at 746 m TVD and at 758 m TVD. We, therefore, conclude that the principal fluid entry for well GH-19 is at 750 (±10) m TVD.

Continued on page 3-44

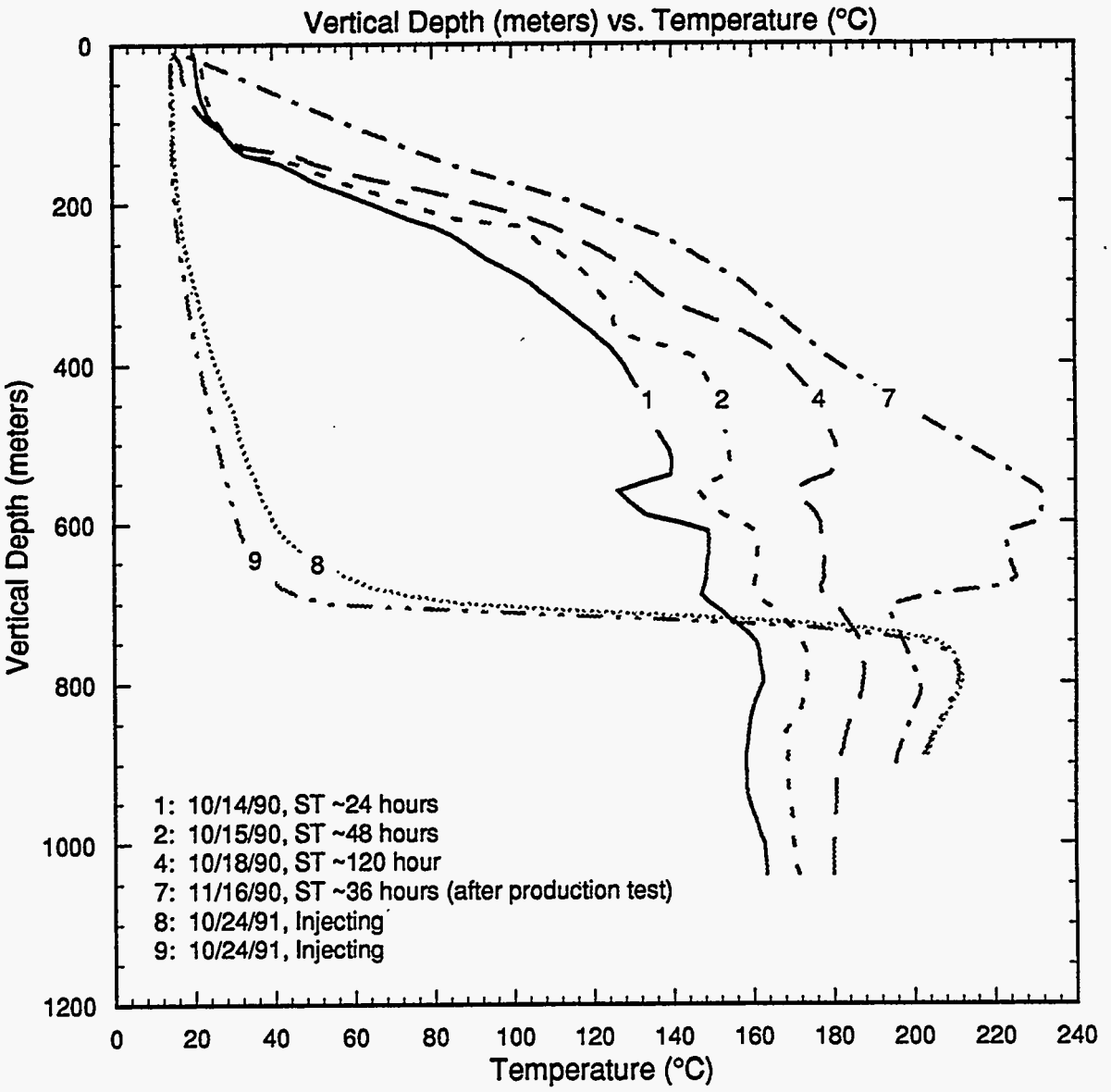

Figure 3.31. Selected heatup surveys for well GH-15.

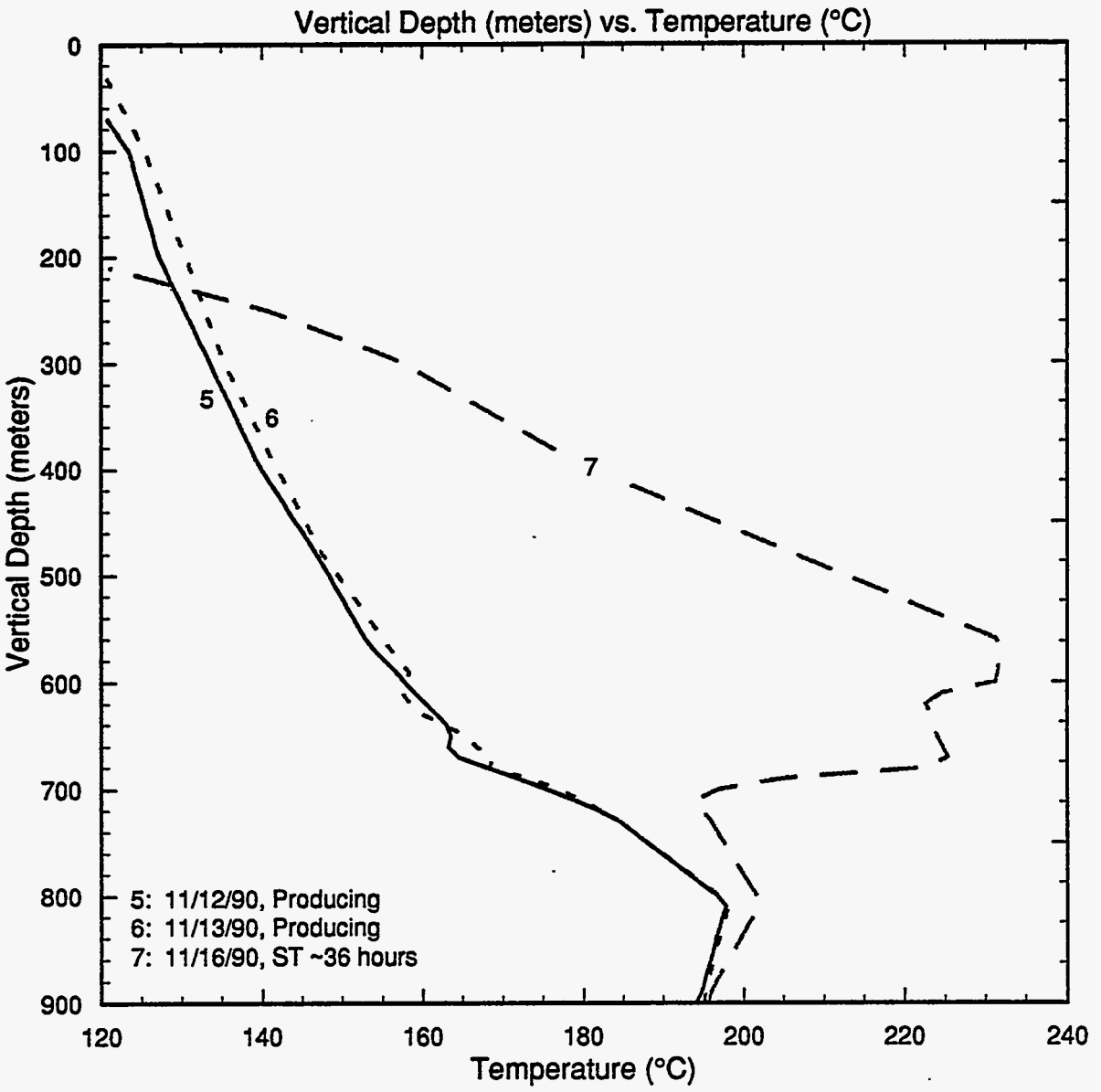

Figure 3.32. Selected temperature profiles for well GH-15.

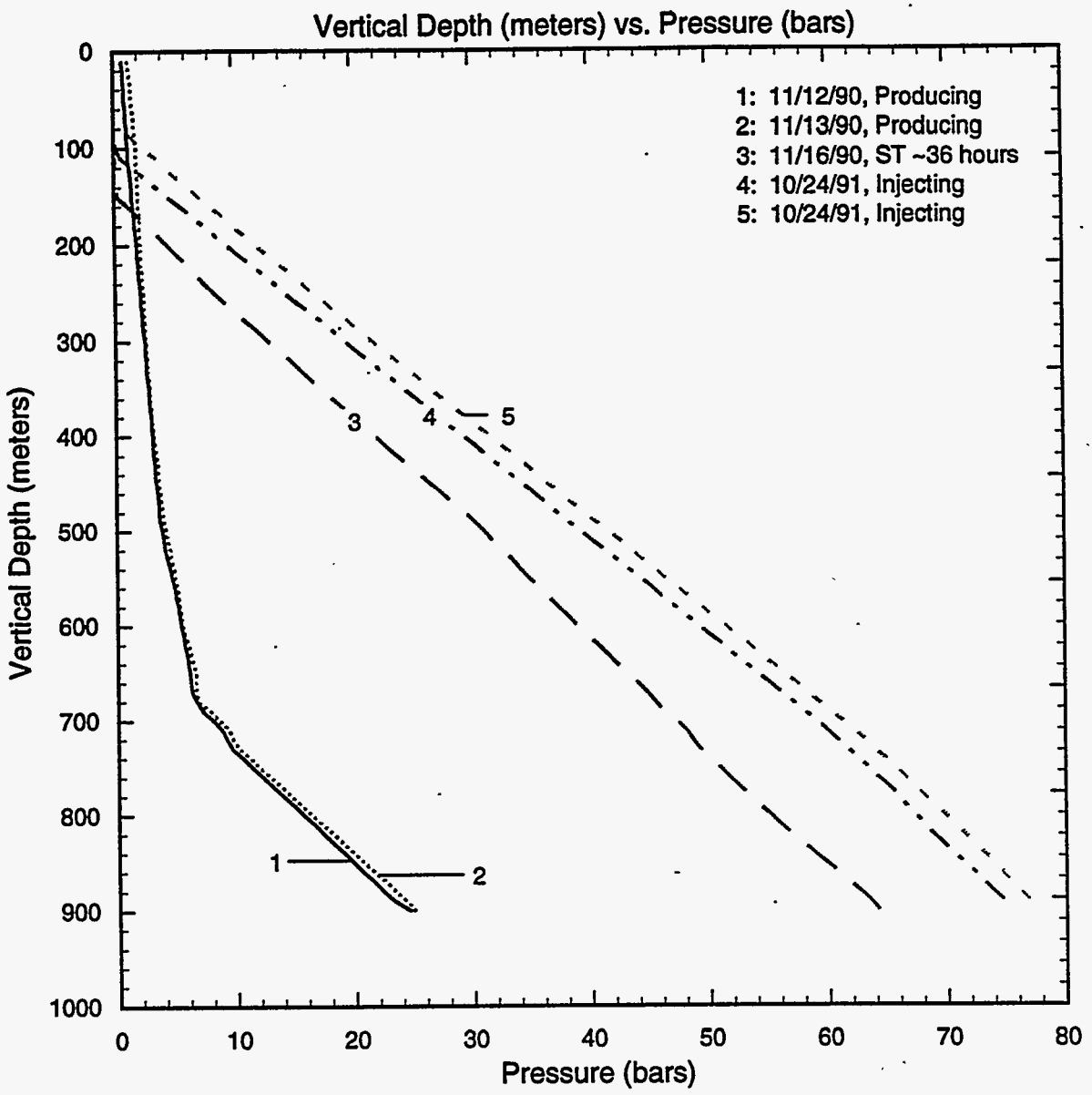

Figure 3.33. Selected pressure (bars, gauge) surveys recorded for well GH-15.

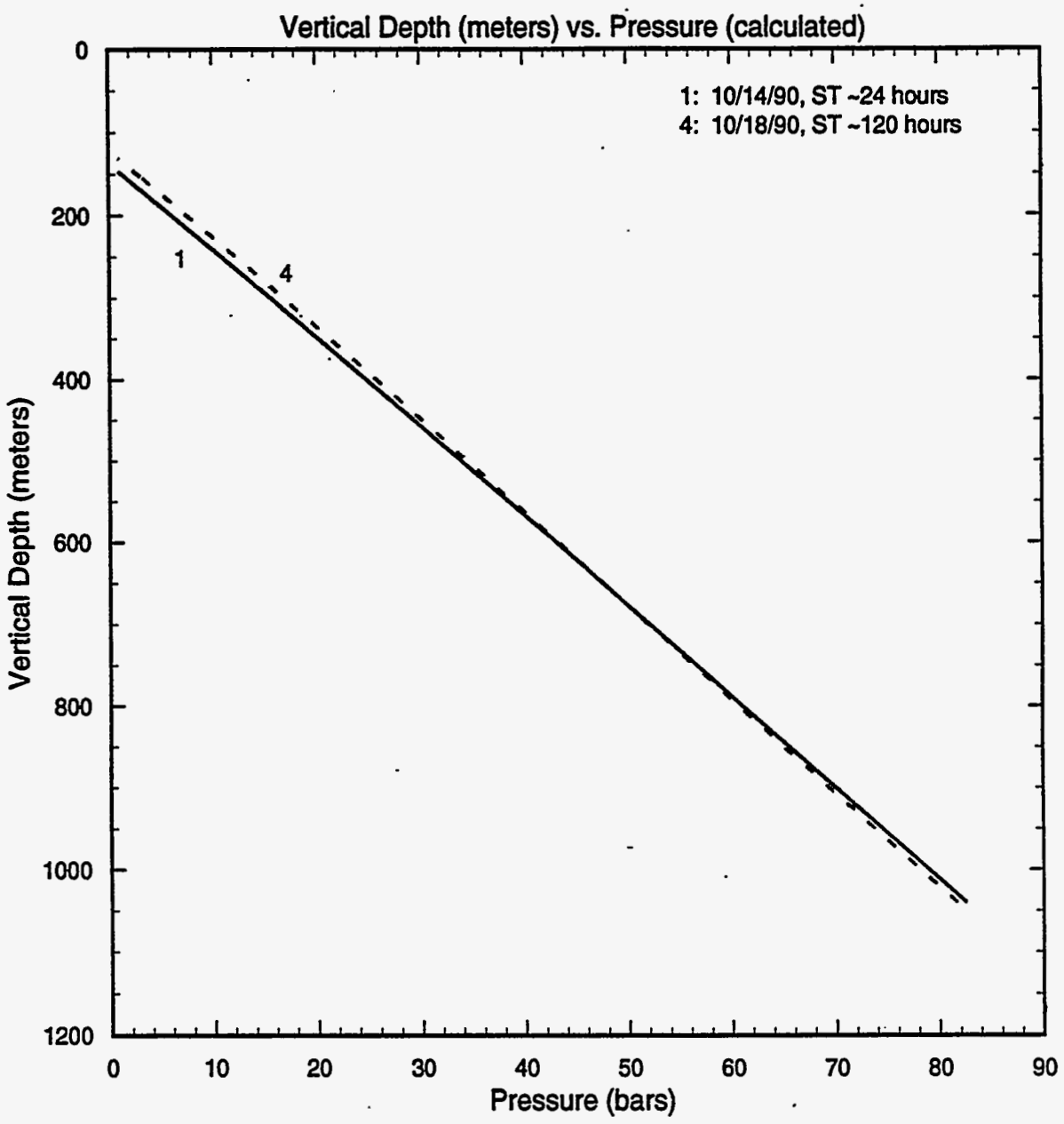

Figure 3.34. Pressure profiles, computed from water level and temperature data, for well GH-15.

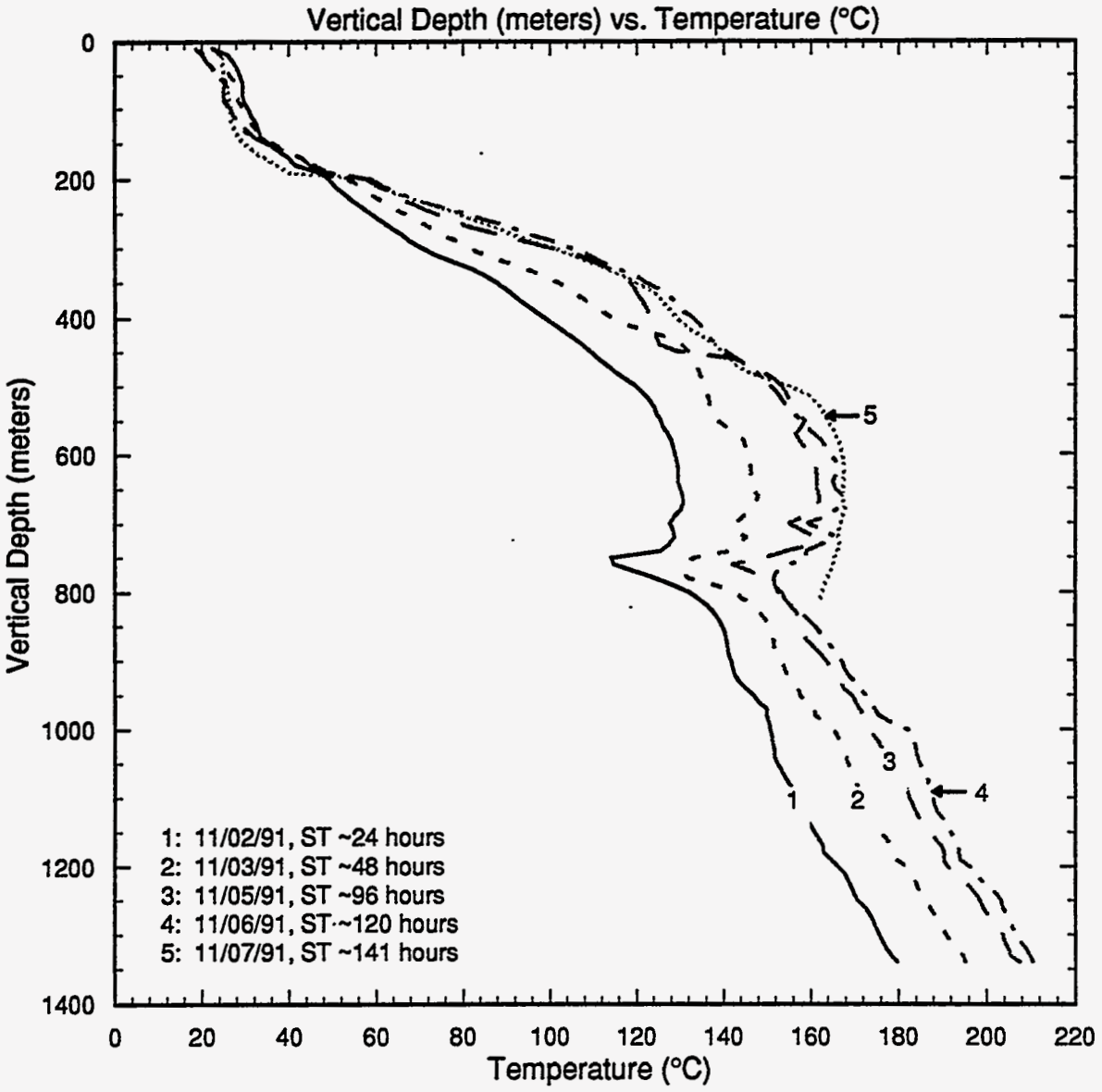

Figure 3.35. Selected heatup surveys for well GH-17.

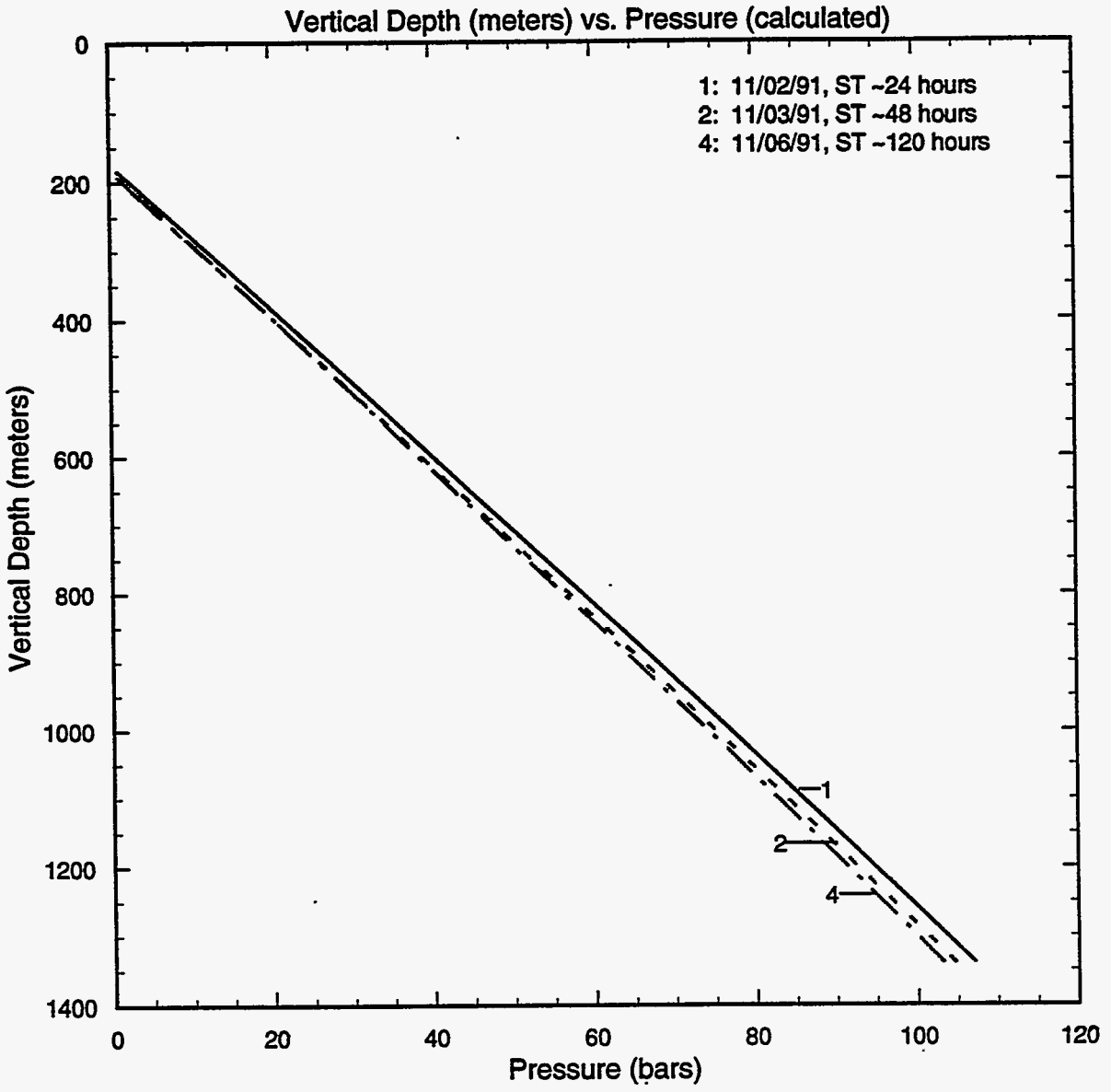

Figure 3.36. Selected pressure profiles, computed from water level and temperature data, for well GH-17.

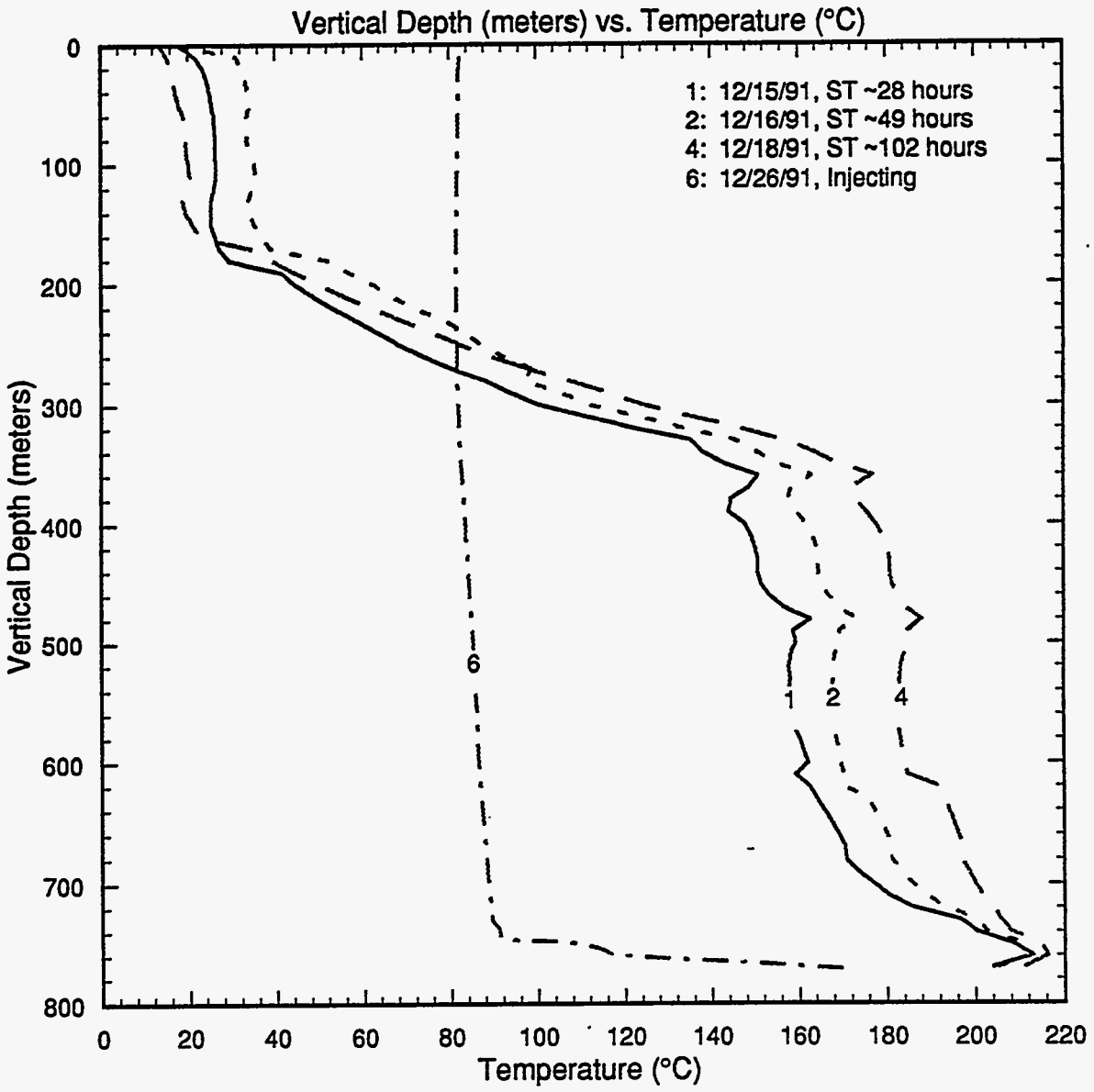

Figure 3.37. Selected temperature surveys recorded in well GH-19.

Pressure profiles, computed from water level and temperature data, are displayed in Figure 3.38; the pressure at 750 m TVD (154 m ASL) is ~ 52.5 bars. The latter pressure value is in good agreement with that recorded by a downhole gauge (52 bars) on December 25, 1991 (Figure 3.39).

3.14 Well GH-20

Heatup surveys 3 and 6 (Figure 3.40) in well GH-20, recorded shortly after well completion, show rapid temperature recovery at ~ 980 m TVD and at 1440–1560 m TVD. Temperature surveys 8 and 9, taken during a production test, have an isothermal profile above 1560 m TVD; this implies that the major feedzone for well GH-20 is located at 1560 m TVD. The feedzone temperature is about 241°C. Pressure surveys 3 and 5 (Figure 3.41), recorded concurrently with temperature surveys 8 and 9 (Figure 3.40) indicate that the fluid entering the wellbore at 1560 m TVD is single-phase liquid.

Pressure profiles, computed from water level and temperature data, are displayed in Figure 3.42; the pressure at 1560 m TVD (–702 m ASL) is about 114.5 bars. The latter pressure value is in good agreement with that (~ 114 bars) recorded by a downhole gauge on April 28, 1991 (profile 6, Figure 3.41).

3.15 Well GH-21

Temperature survey 1 (Figure 3.43) taken while injecting cold fluid on November 16, 1992 in well GH-21, shows large changes in temperature gradient at ~ 650 m TVD and at ~ 780 m TVD; apparently, cold fluid is being injected in the depth interval from 650 m TVD to ~ 780 m TVD. The injection of cold fluids is most likely responsible for the depressed temperatures seen in profile 2 (Figure 3.43) in the depth interval 650–780 m TVD. A slightly negative temperature gradient below 650 m TVD in profile 10 (Figure 3.43) suggests downflow of hot fluid between 650 m TVD and 780 m TVD. It, therefore, appears that the major feedzone for GH-21 is located at about 650 m TVD.

Pressure profiles, computed from water level and temperature data, are plotted in Figure 3.44. The pressure at 650 m TVD is estimated to be ~ 38.5 bars.

3.16 Slim Hole HH-2

Slim hole HH-2 was initially drilled (November 1984) to a total depth of 700 meters. It was subsequently deepened to 1000 meters in October 1986. Temperature profiles in the original hole (see *e.g.*, profile 1, Figure 3.45) provide no clues regarding permeability. The water level (and computed pressures) in the 700 meter hole continued to decline (see profiles 5 and 6, Figure 3.46) for a long period of time after shutin; this indicates poor formation permeability.

Continued on page 3-54

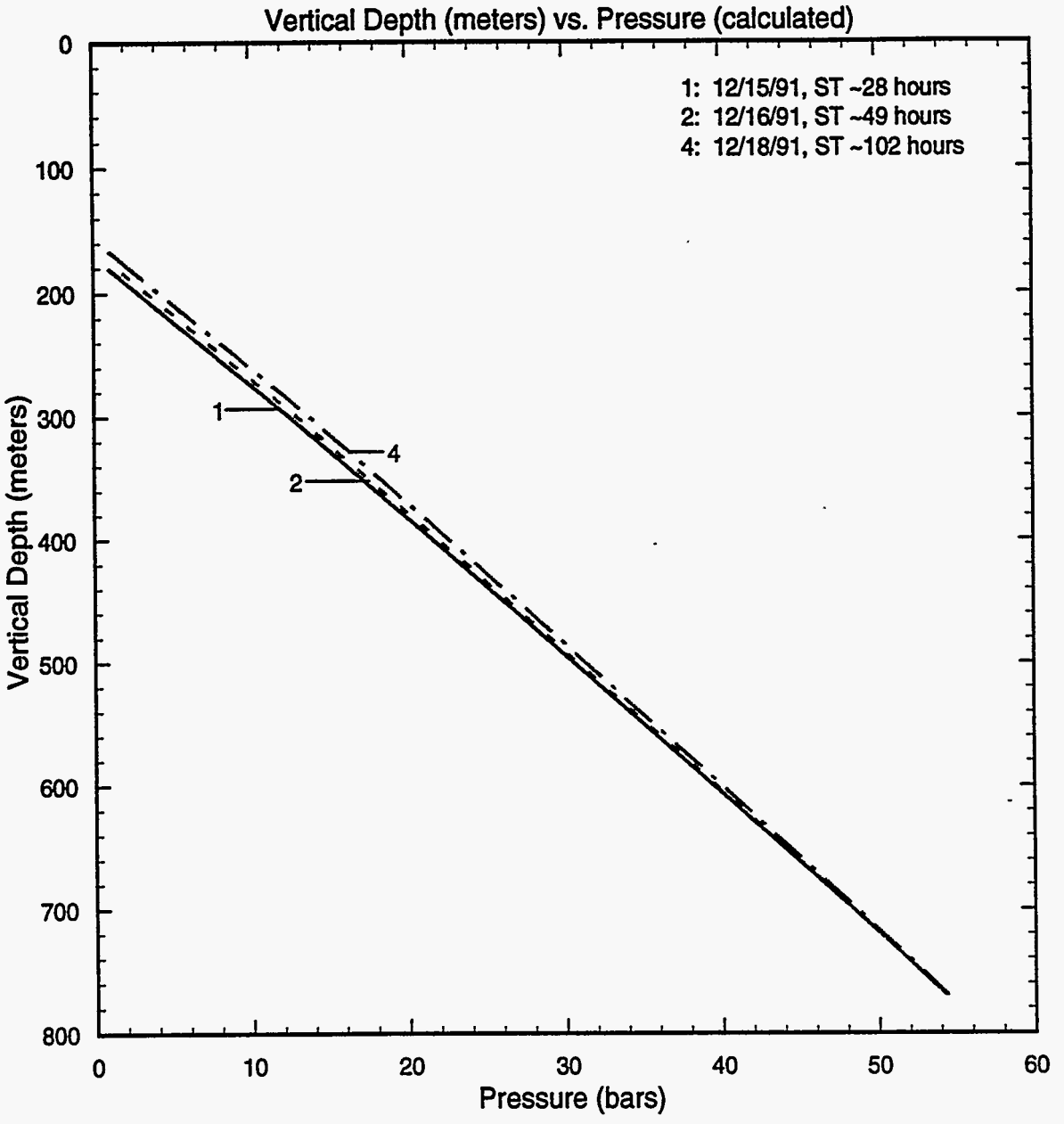

Figure 3.38. Pressure profiles, computed from water level and temperature data, for well GH-19.

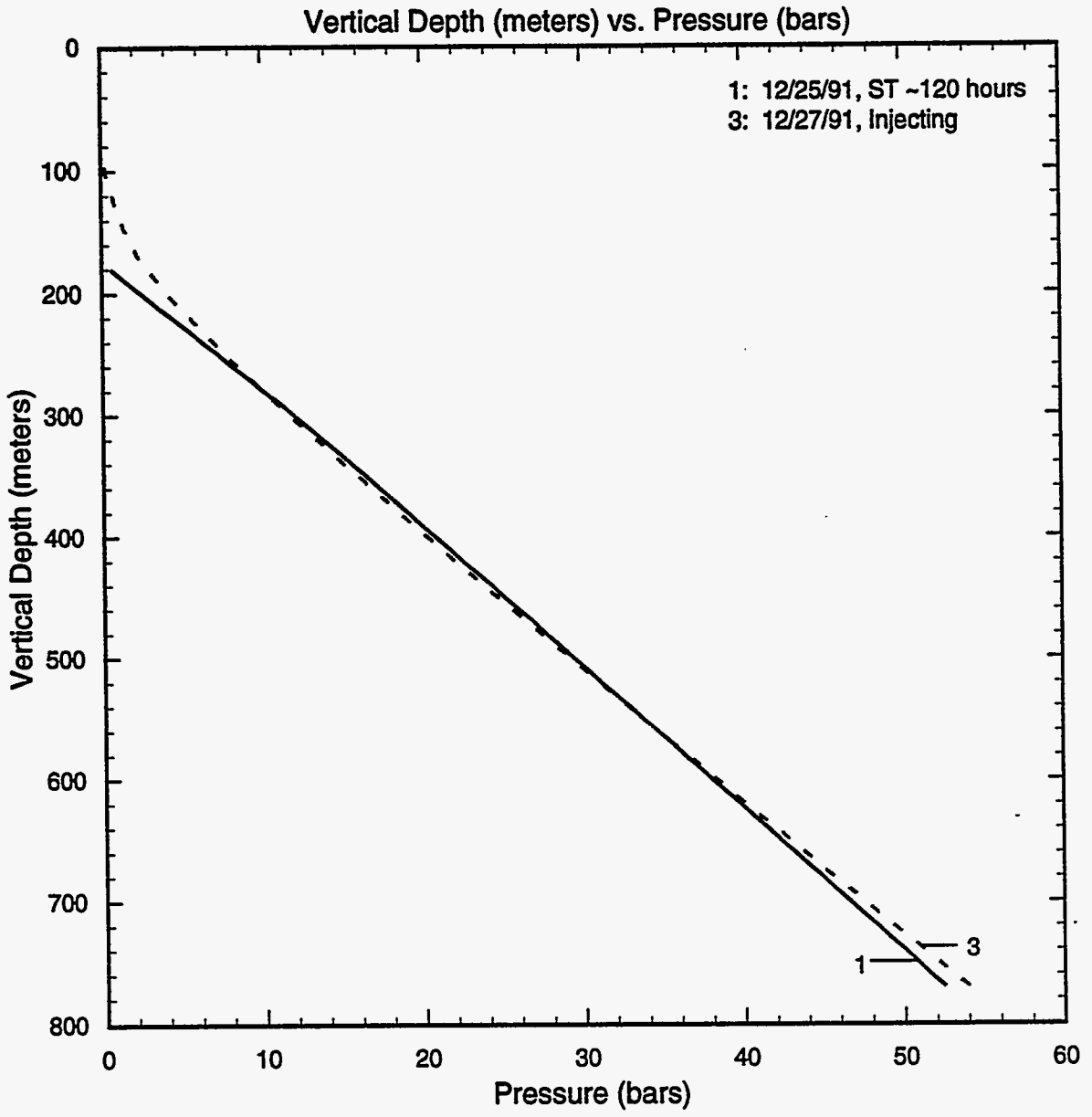

Figure 3.39. Selected pressure (bars, gauge) surveys for well GH-19.

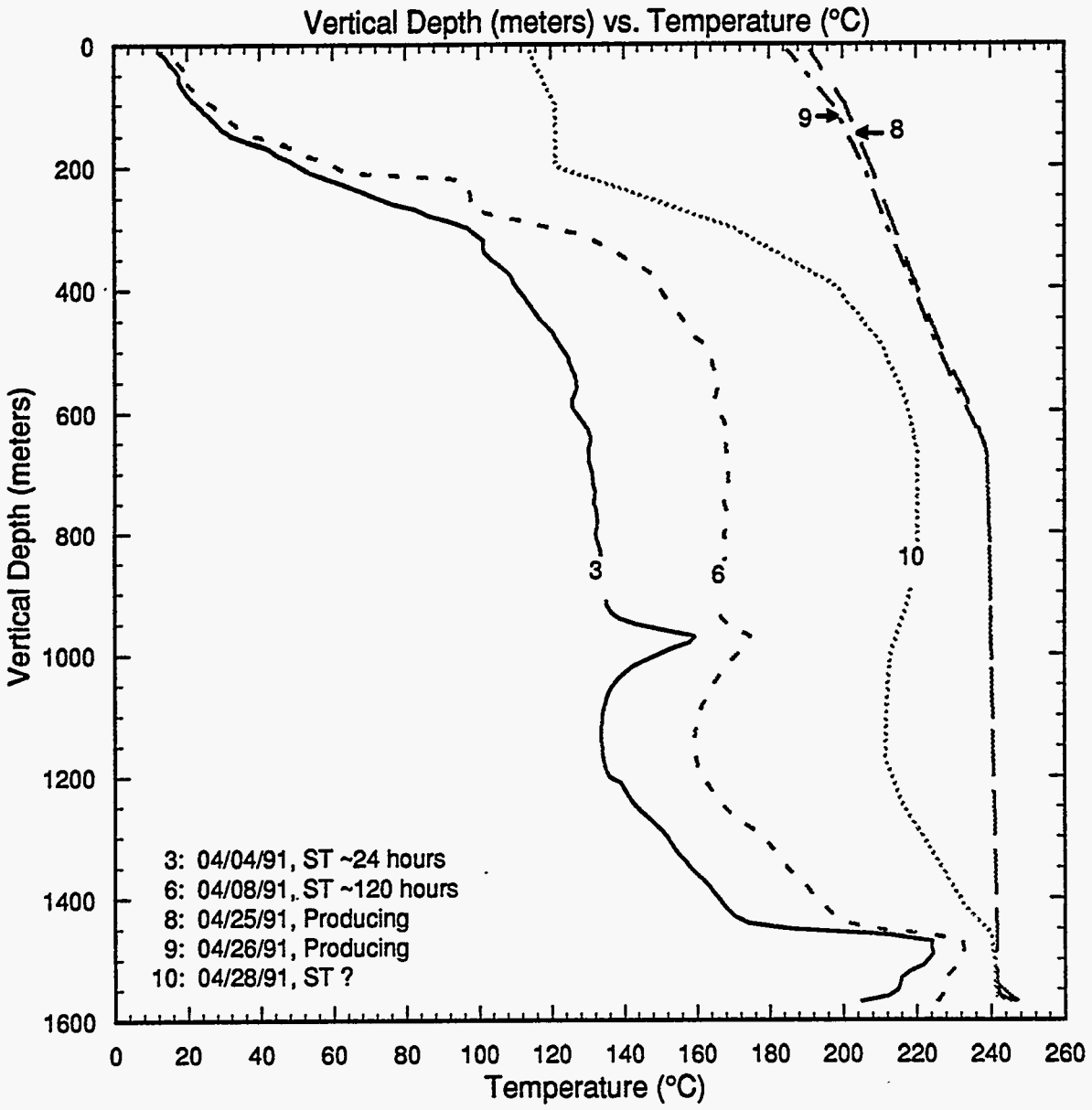

Figure 3.40. Selected temperature surveys recorded in well GH-20.

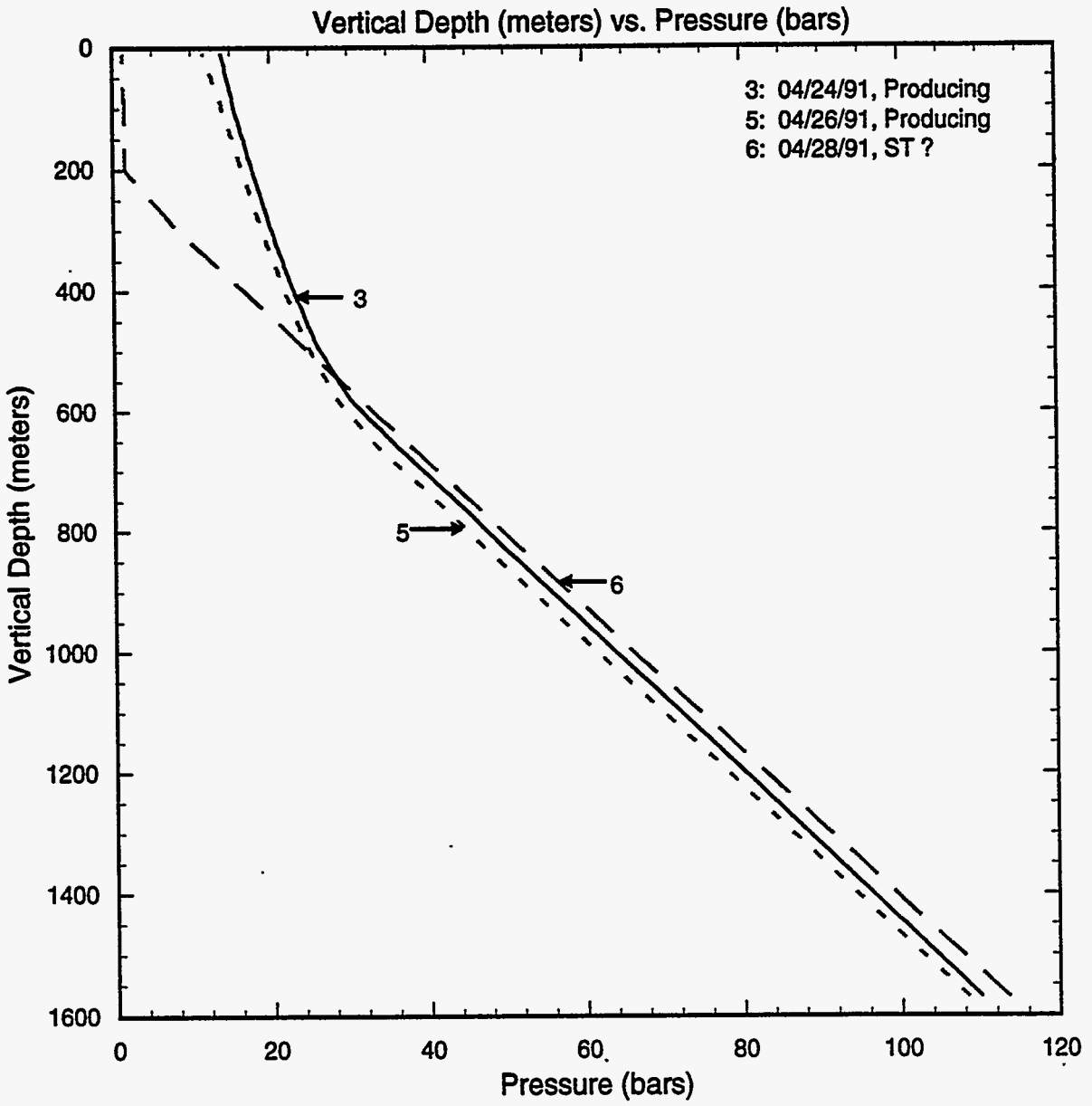

Figure 3.41. Selected pressure (bars, gauge) surveys recorded in well GH-20.

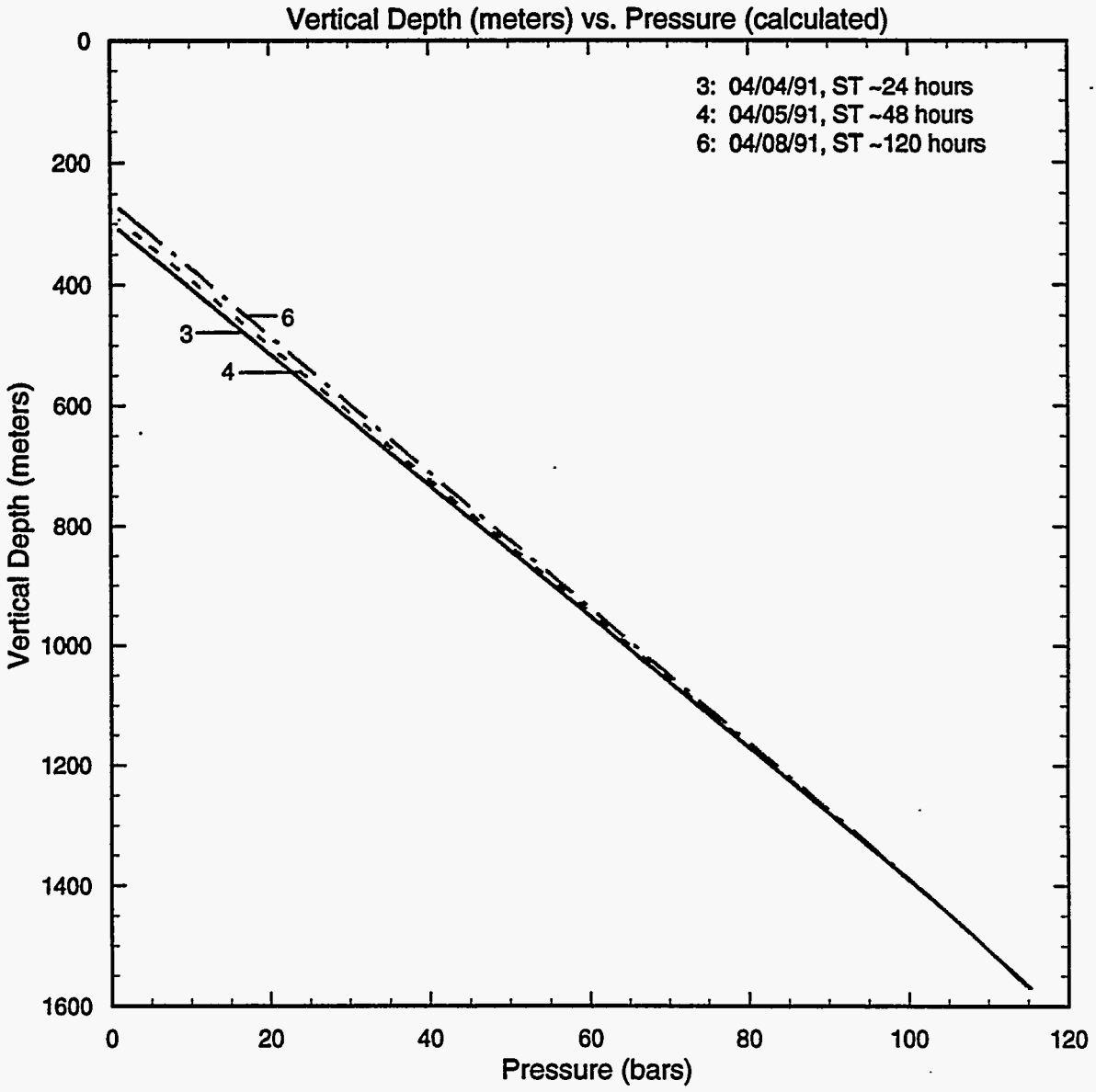

Figure 3.42. Pressure profiles, computed from water level and temperature data, for well GH-20.

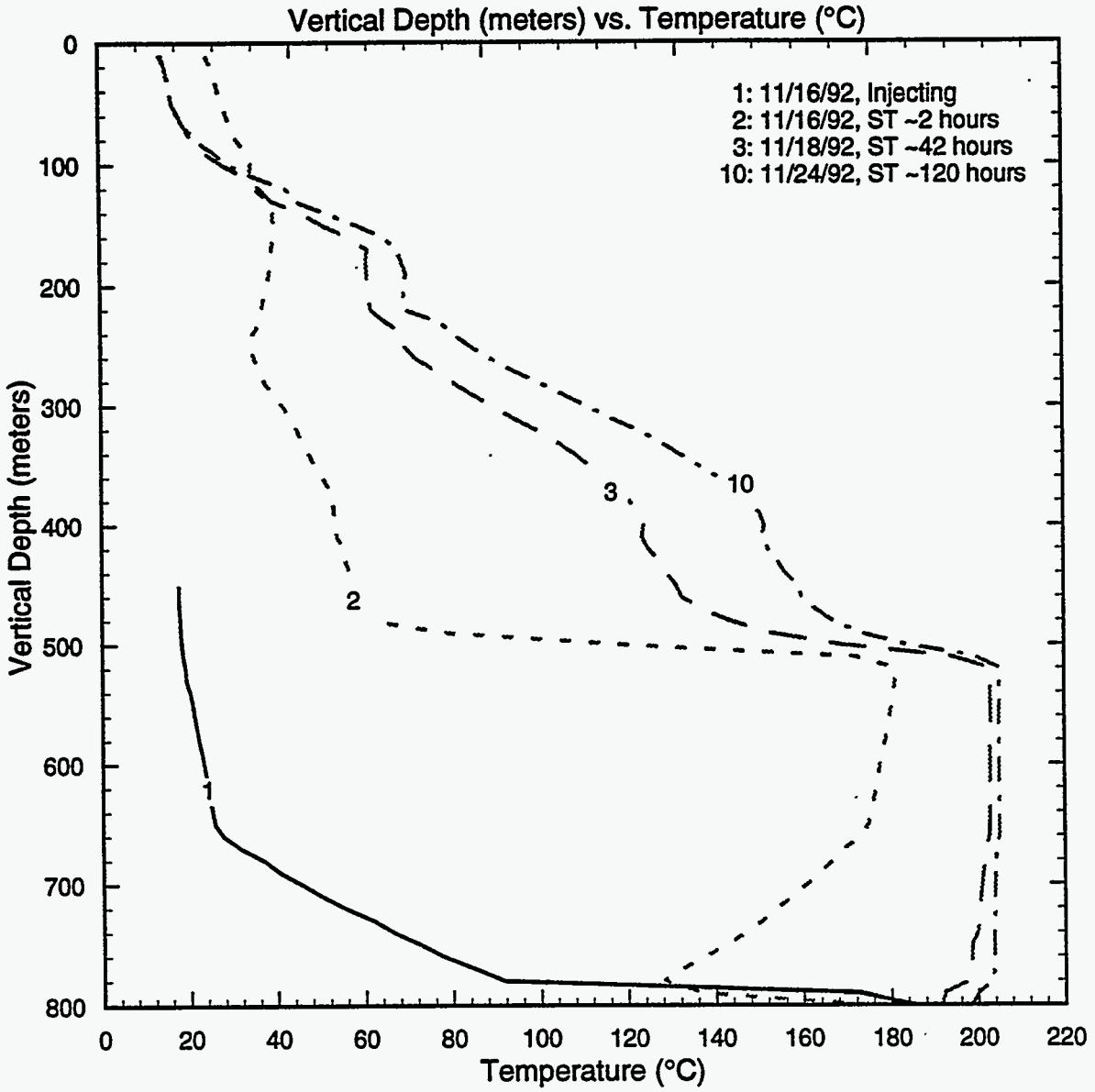

Figure 3.43. Selected temperature surveys for well GH-21.

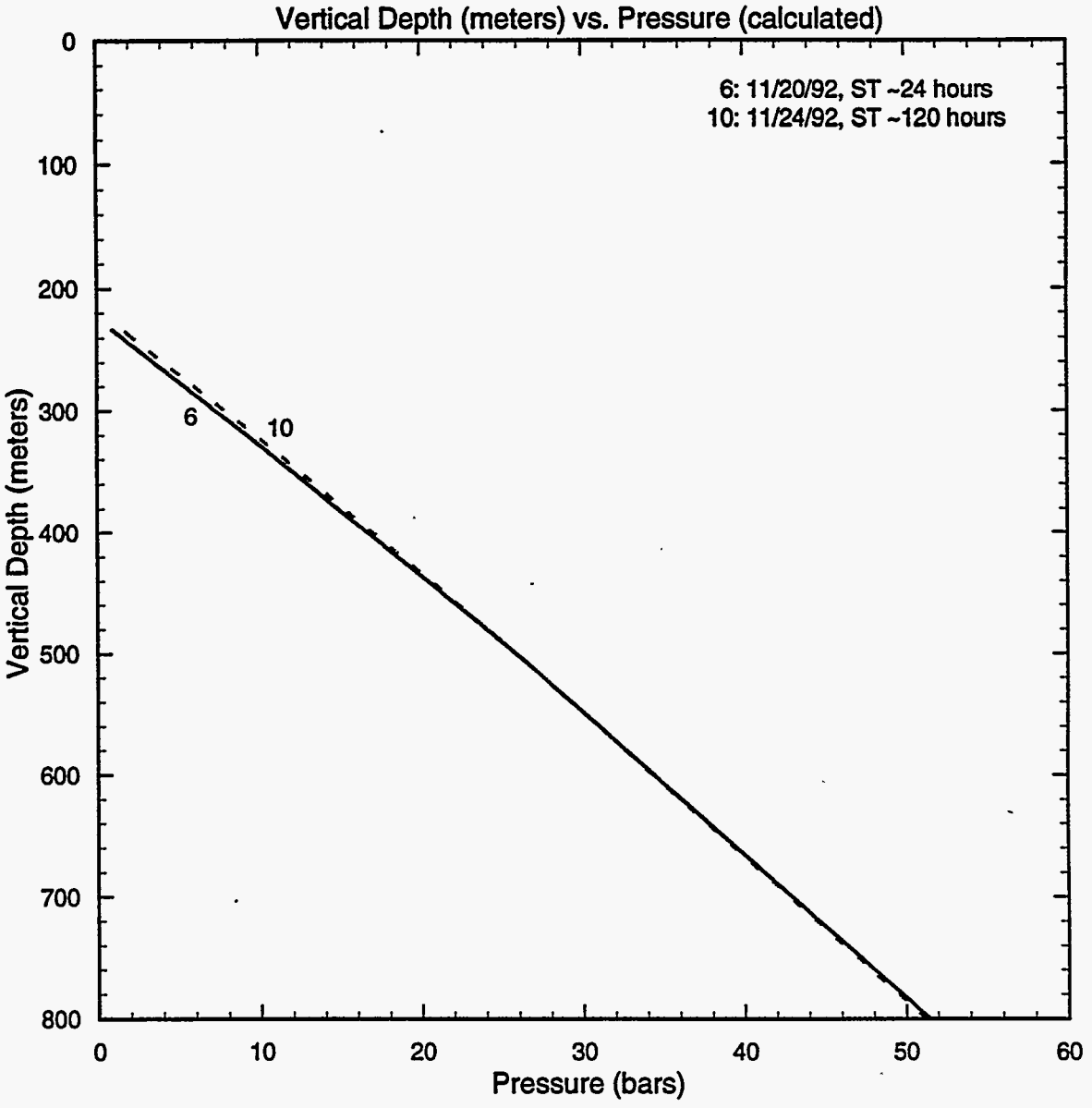

Figure 3.44. Pressure profiles, computed from water level and temperature data, for well GH-21.

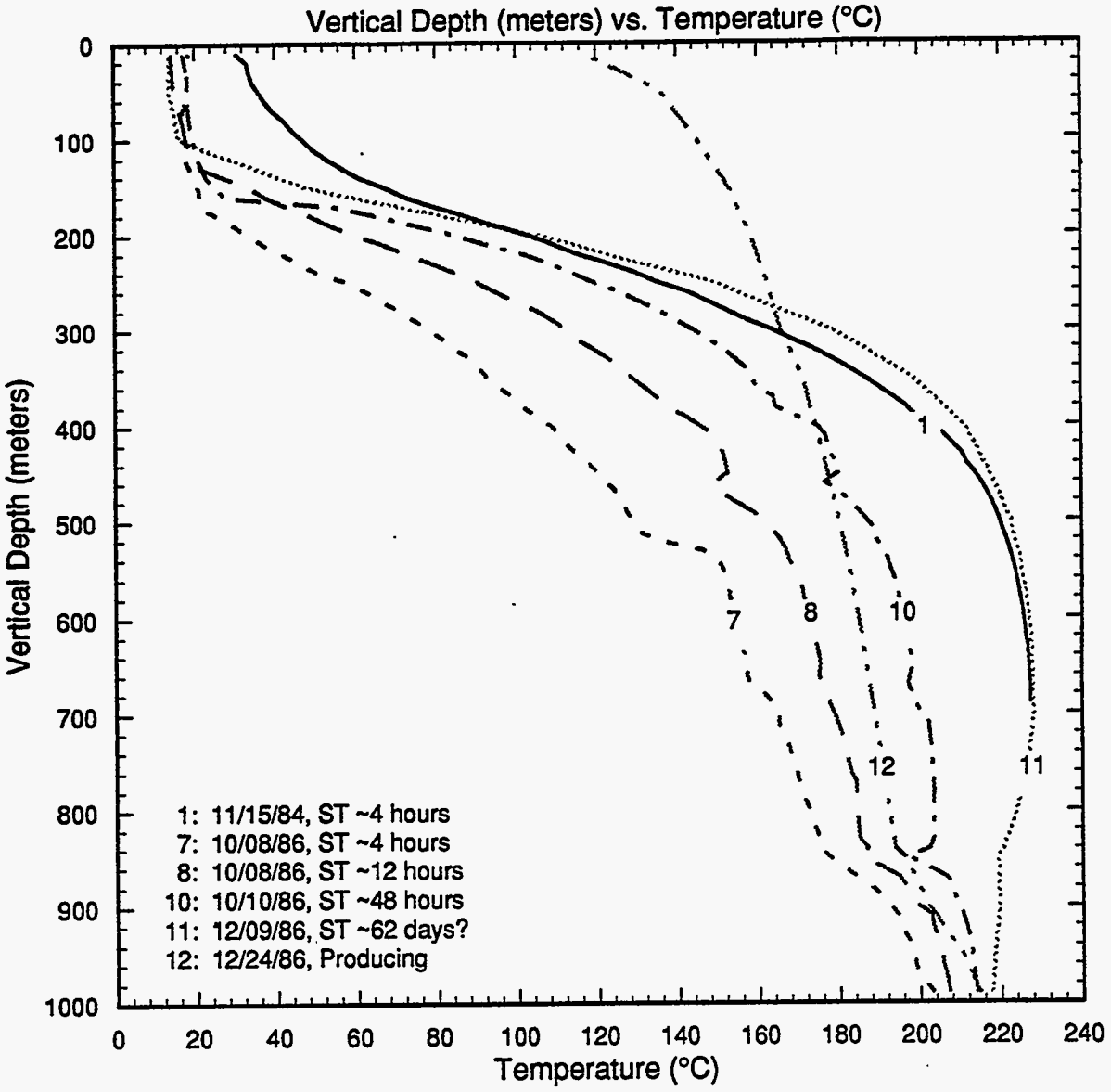

Figure 3.45. Selected temperature profiles for slim hole HH-2.

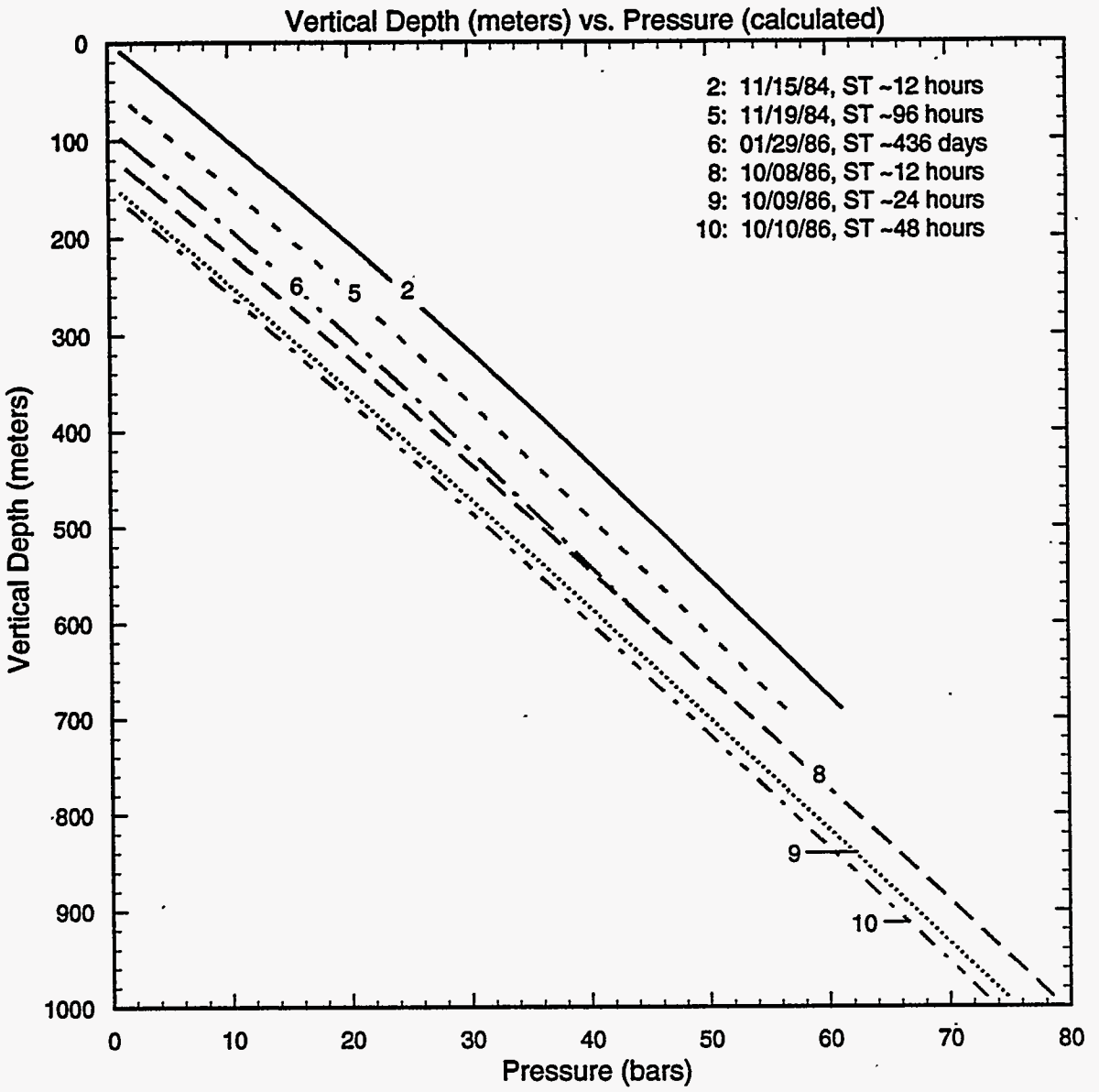

Figure 3.46. Pressure profiles, computed from water level and temperature data, for slim hole HH-2.

Heatup surveys 7, 8 and 10 in the deepened slim hole HH-2 show a persistent temperature depression at ~ 850 m TVD (Figure 3.45); a major circulation loss zone was encountered at about this depth. Temperature and pressure surveys (profile 12, Figure 3.45 and profile 2, Figure 3.47), taken during a production test, show the presence of two-phase fluid in the slim hole above ~ 850 m TVD; the fluid is single-phase (liquid) below ~ 880 m TVD. These production data imply that the major feedzone for slim hole HH-2 is located at about ~ 850 m TVD. Temperature profile 11 (Figure 3.45), taken after nearly two months of shutin, shows a temperature inversion in HH-2. The maximum temperature (~ 228°C) occurs at about 700 m TVD.

The water level (and hence computed pressures) in the deepened slim hole continued to decline during the 48-hour shutin period (profiles 8, 9, and 10; Figure 3.46); these data imply that the pressure at 850 m TVD (≈10 m ASL) is less than 61.5 bars. A downhole pressure survey taken after nearly two months of shutin (profile 1, Figure 3.47) gave a pressure of ~ 60.5 bars at 850 m TVD.

3.17 Well IH-1

Heatup surveys for well IH-1 (Figure 3.48) show a persistent temperature depression centered at about 590 m TVD. A circulation loss zone was encountered near the latter depth. It is therefore, likely that the major feedzone for IH-1 is located at ~ 590 m TVD.

Pressure profiles, computed from water level and temperature data are shown in Figure 3.49. The stable feedpoint (590 m TVD ≈ 163 m ASL) pressure is estimated (profiles 3 and 4, Figure 3.49) to be ~ 42.5 bars.

In an attempt to increase injectivity, the casing in well IH-1 was gun perforated (June 1988–February 1989) at 313 m MD (311.5 m TVD). During a downhole survey on December 11, 1991, it was found impossible to lower the Kuster gauge below 495 m MD. It is likely that the principal feedzone for the recompleted IH-1 is at some depth (311.5 m TVD?) other than 590 m TVD; the available data are, however, insufficient for determining the new feedzone depth.

3.18 Well IH-2

Heatup surveys for well IH-2 show a rapid temperature recovery at ~ 550 m TVD (profiles 1 and 4, Figure 3.50); a total circulation loss was recorded nearby during drilling. Temperature survey recorded on March 2, 1990 (profile 6, Figure 3.50) during a production test shows an isothermal zone over the depth interval 500–550 m TVD. It appears that liquid water (temperature

Continued on page 3-59

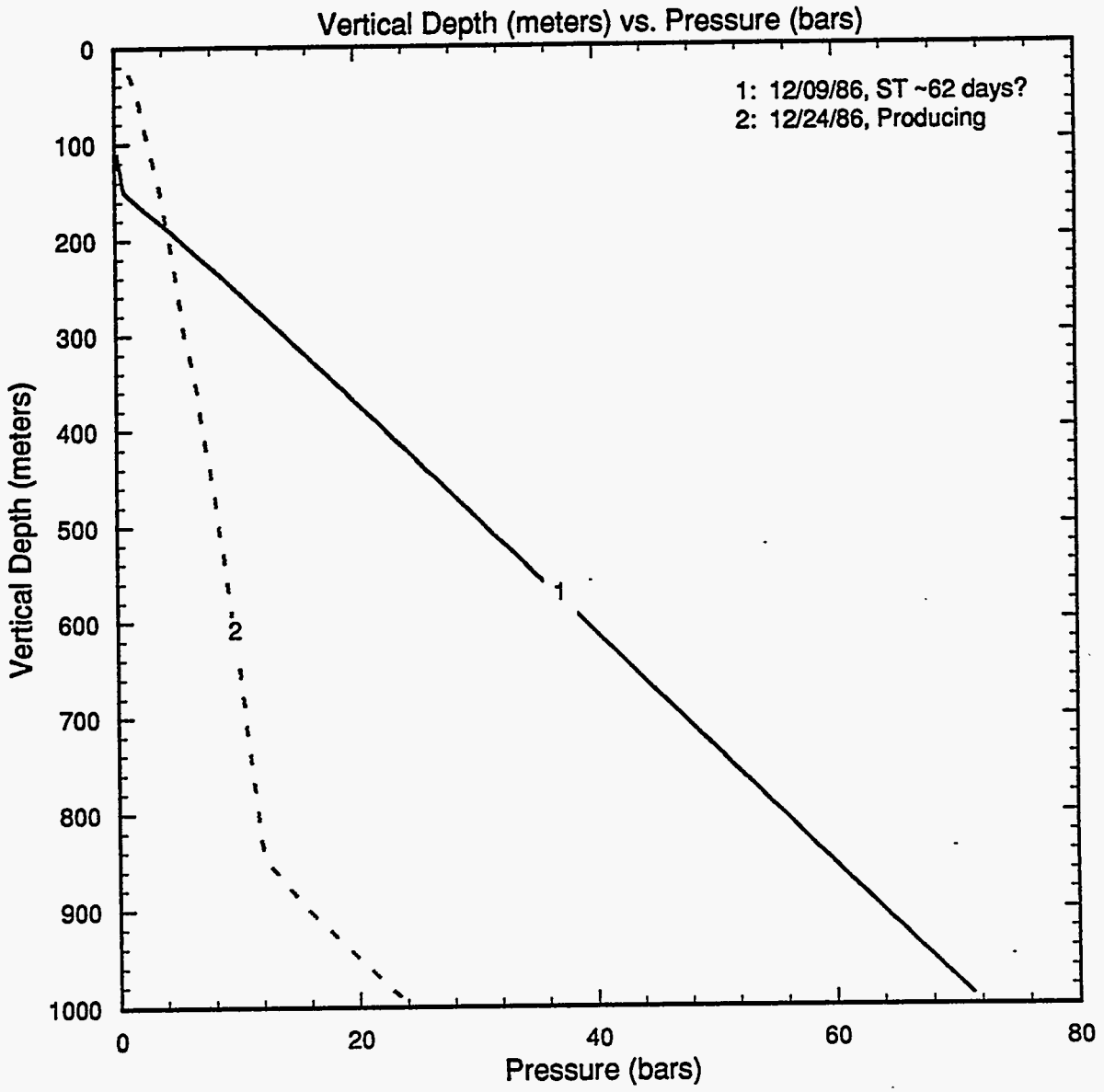

Figure 3.47. Selected measured pressure (bars, gauge) profiles for slim hole HH-2.

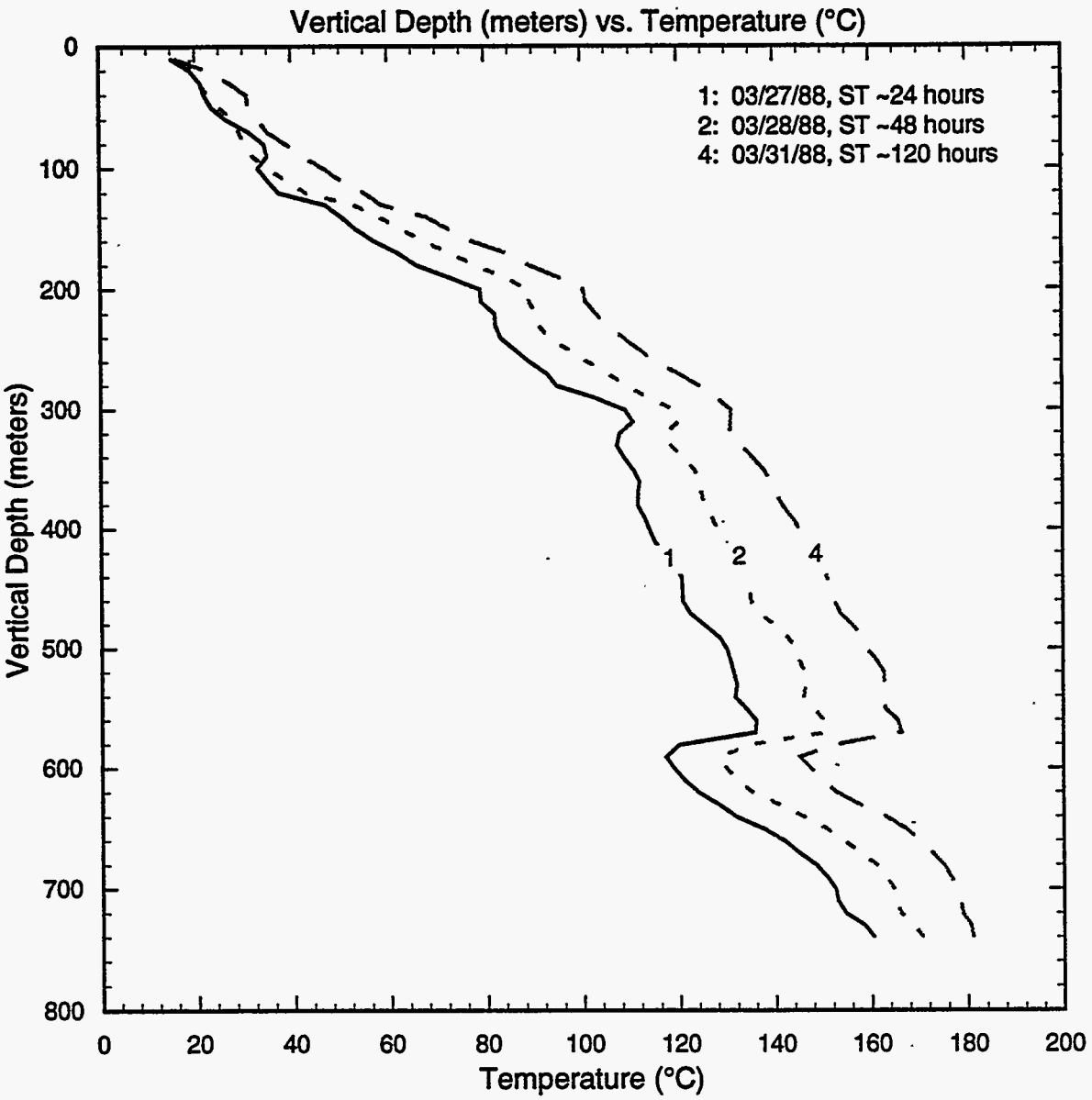

Figure 3.48. Selected heatup surveys for well IH-1.

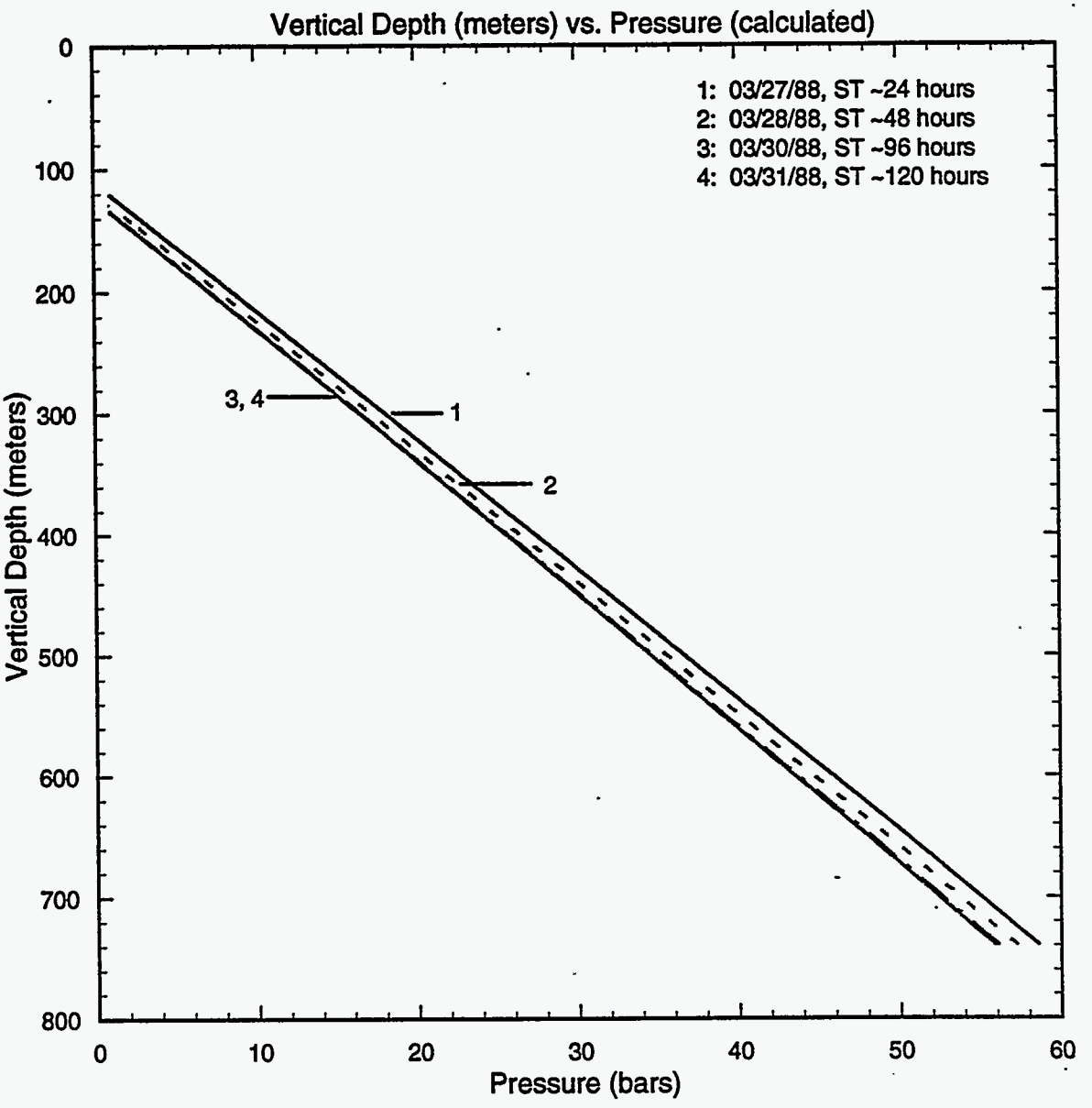

Figure 3.49. Pressures profiles, computed from water level and temperature data, for well IH-1.

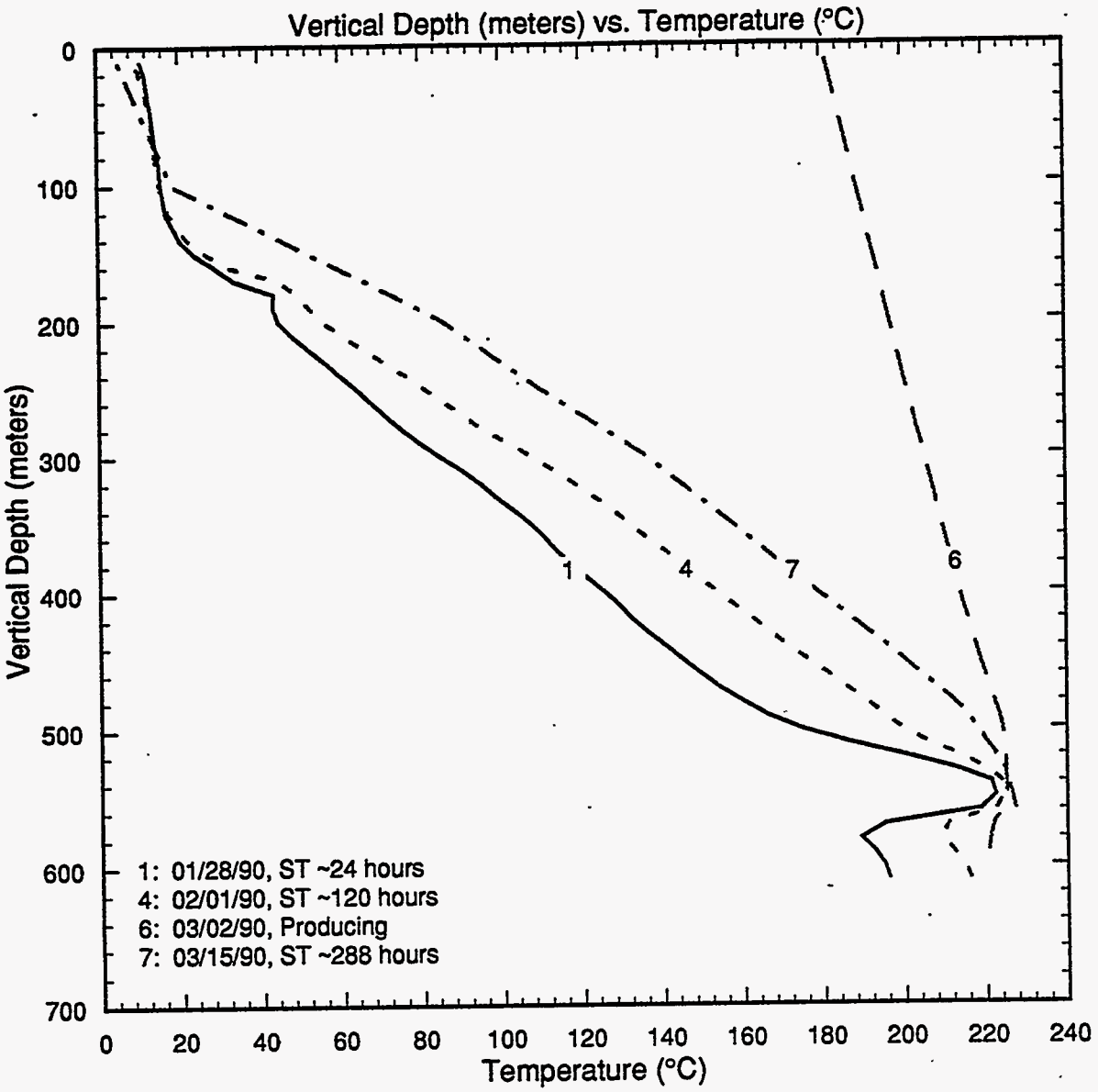

Figure 3.50. Selected temperature profiles for well IH-2.

(~ 226°C) enters the well at 550 m TVD and flows upwards in the well. The corresponding pressure profile (profile 2, Figure 3.51) implies that the flash point is located at ~ 500 m TVD.

Pressures computed from water level and temperature data are displayed in Figure 3.52; the pressure at 550 m TVD (≈ 235 m ASL) is approximately 35.5 bars. The latter pressure value is significantly higher than the one (~ 32 bars) recorded by a downhole pressure survey (profile 3, Figure 3.51). The discrepancy between the measured and the computed pressure values is most likely the result of an error in gauge calibration.

3.19 Slim Hole N2-KW-1

Heatup surveys 1–3 (Figure 3.53) indicate rapid temperature recovery at 680–740 m TVD and below a depth of ~ 860 m TVD. Temperature survey 4, recorded during an injection test, shows evidence of fluid loss at ~ 680 m TVD and at ~ 860 m TVD; the fluid loss at ~ 680 m TVD is, however, not confirmed by injection survey 5 (Figure 3.53). We will, therefore, tentatively assume that the major feedzone for slim hole N2-KW-1 is at 860 m TVD.

Pressure profiles, computed from water level and temperature data, are shown in Figure 3.54; the pressure at 860 m TVD (–39 m ASL) is ~ 57.5 bars. The latter pressure value is somewhat higher than that (56 bars) recorded by a downhole gauge on February 7, 1991 (Figure 3.55); we suggest that a gauge error (or calibration) is responsible for this discrepancy.

3.20 Slim Hole N2-KW-2

Temperature surveys 1 and 2 (Figure 3.56) recorded during an injection test show abrupt changes in temperature gradient at 810 m TVD and at 910 m TVD. Comparison of injection pressures at 810 m TVD and 910 m TVD (Figure 3.57) with shutin pressures at these depths (Figure 3.58) implies that the injected fluid is lost at both the depths. Heatup surveys 4 and 6 (Figure 3.56) show a temperature depression at 910 m TVD; this confirms the existence of a fluid entry at this depth. The available data are, however, insufficient to determine the principal feedzone for slim hole N2-KW-2.

Pressure profiles, computed from water level and temperature, are displayed in Figure 3.58; the pressure at 860 m TVD (–80 m ASL; middle of two feedzones) is about 61.5 bars.

Continued on page 3-68

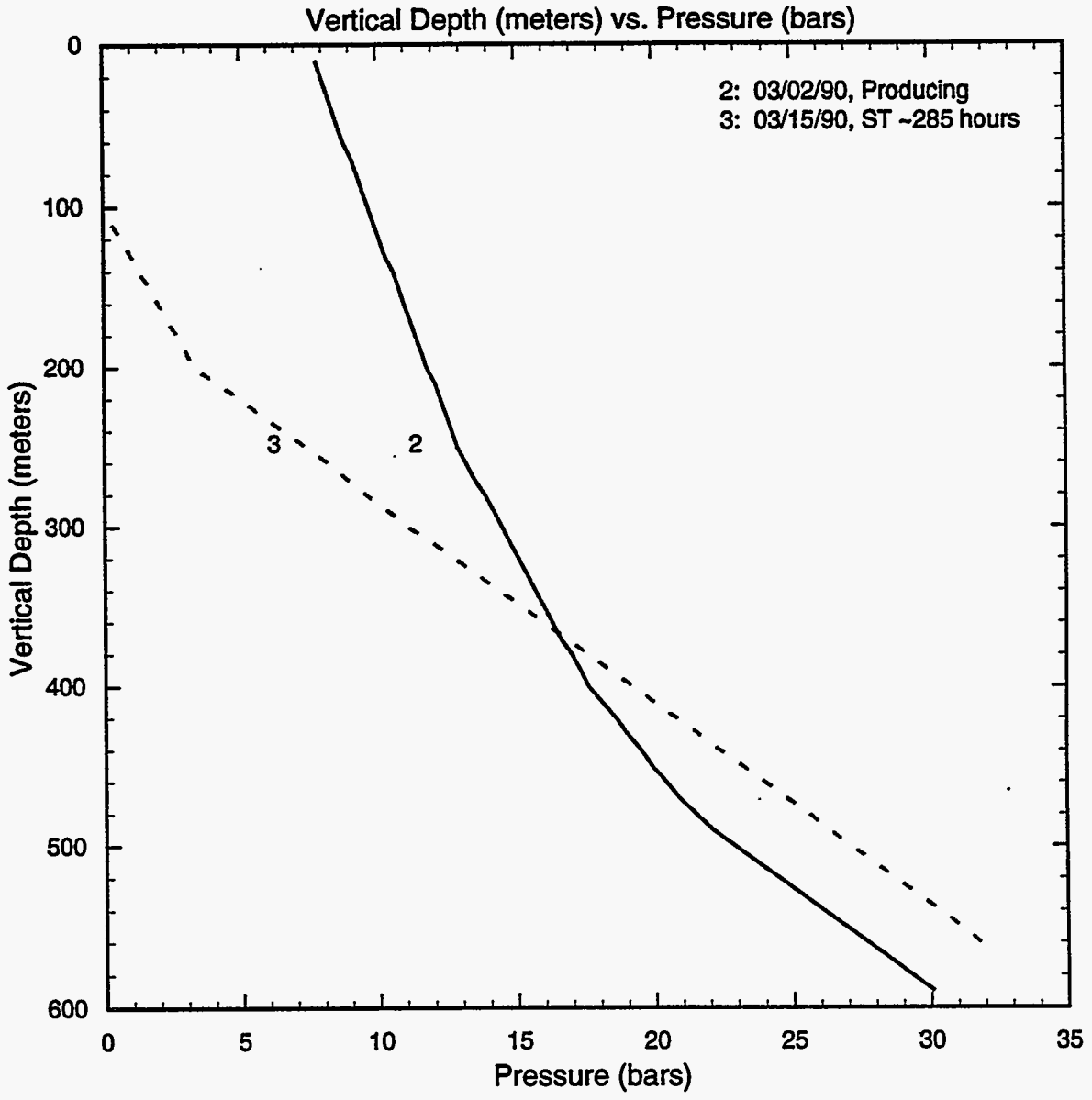

Figure 3.51. Measured pressure (bars, gauge) profiles in well IH-2.

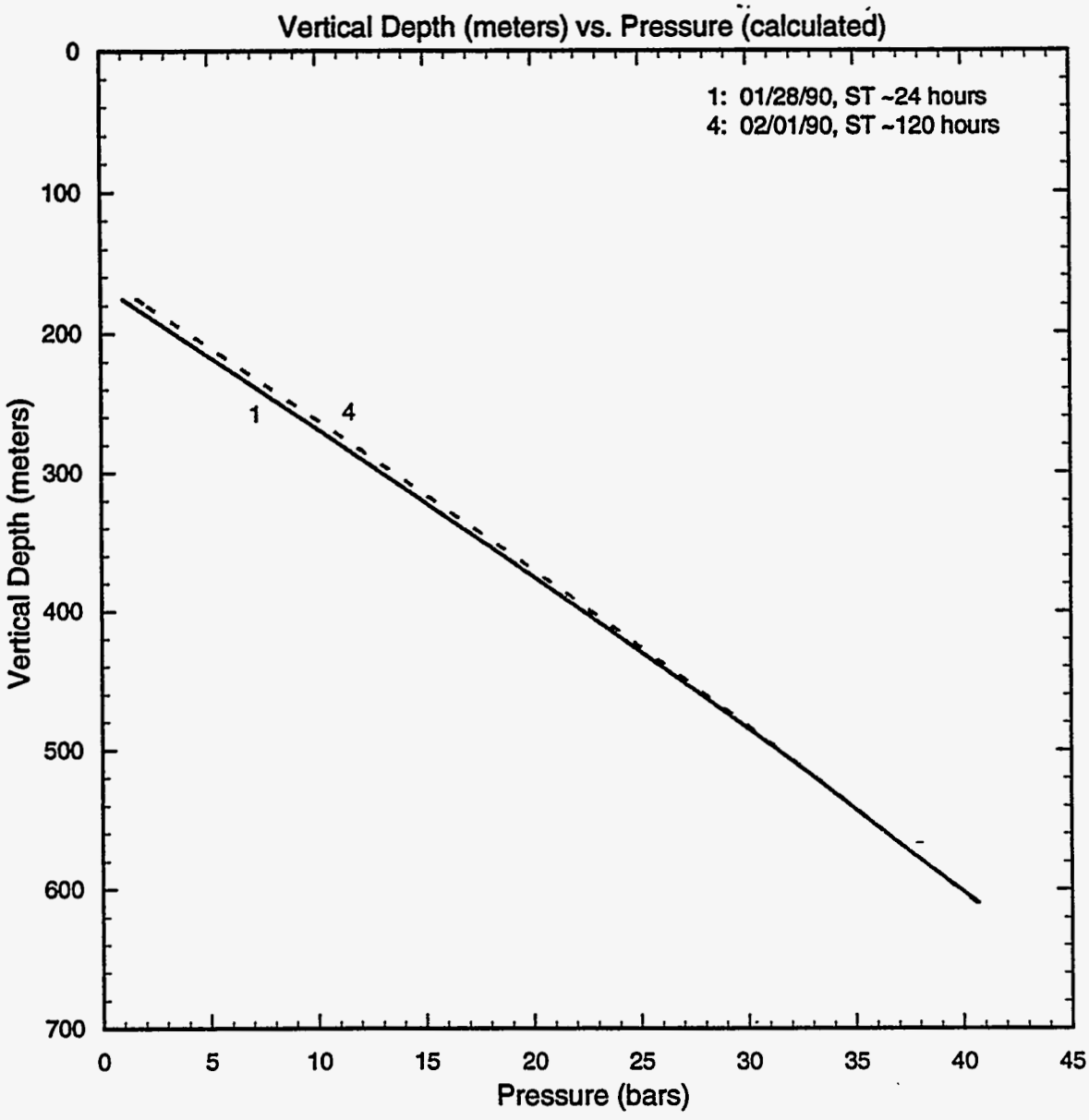

Figure 3.52. Pressure profiles, computed from water level and temperature data, for well IH-2.

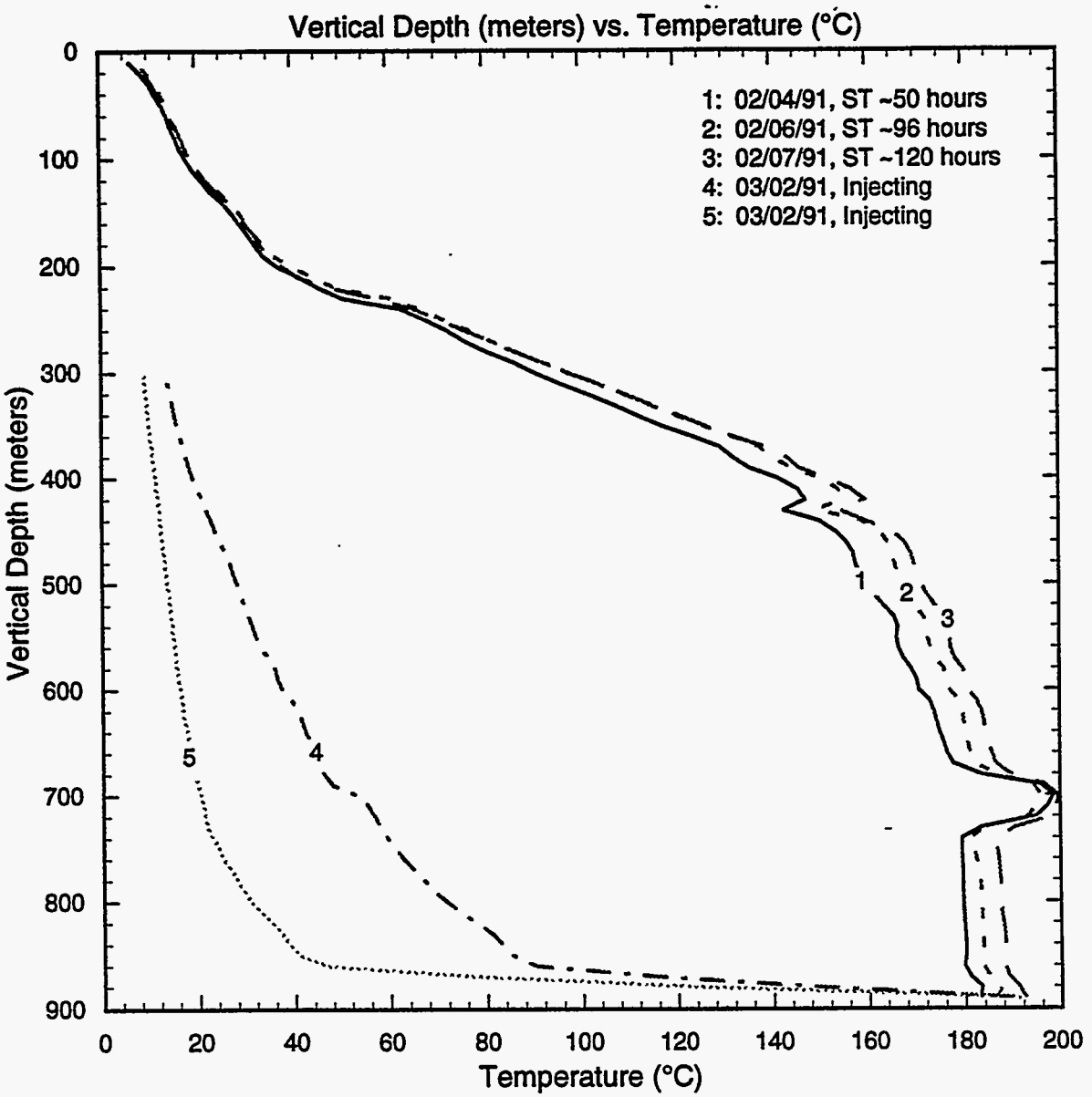

Figure 3.53. Available temperature surveys for slim hole N2-KW-1.

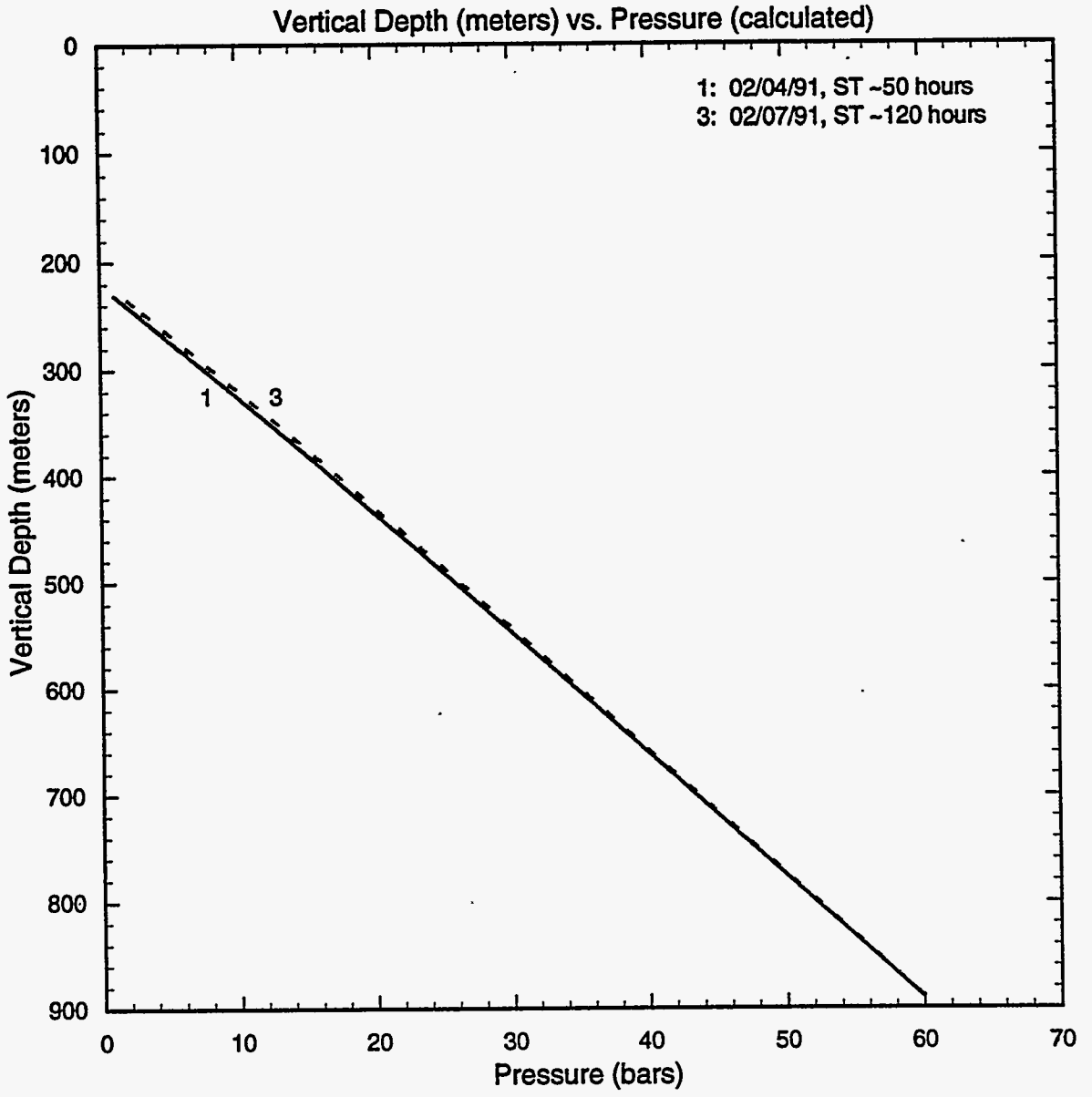

Figure 3.54. Pressure profiles, computed from water level and temperature data, for slim hole N2-KW-1.

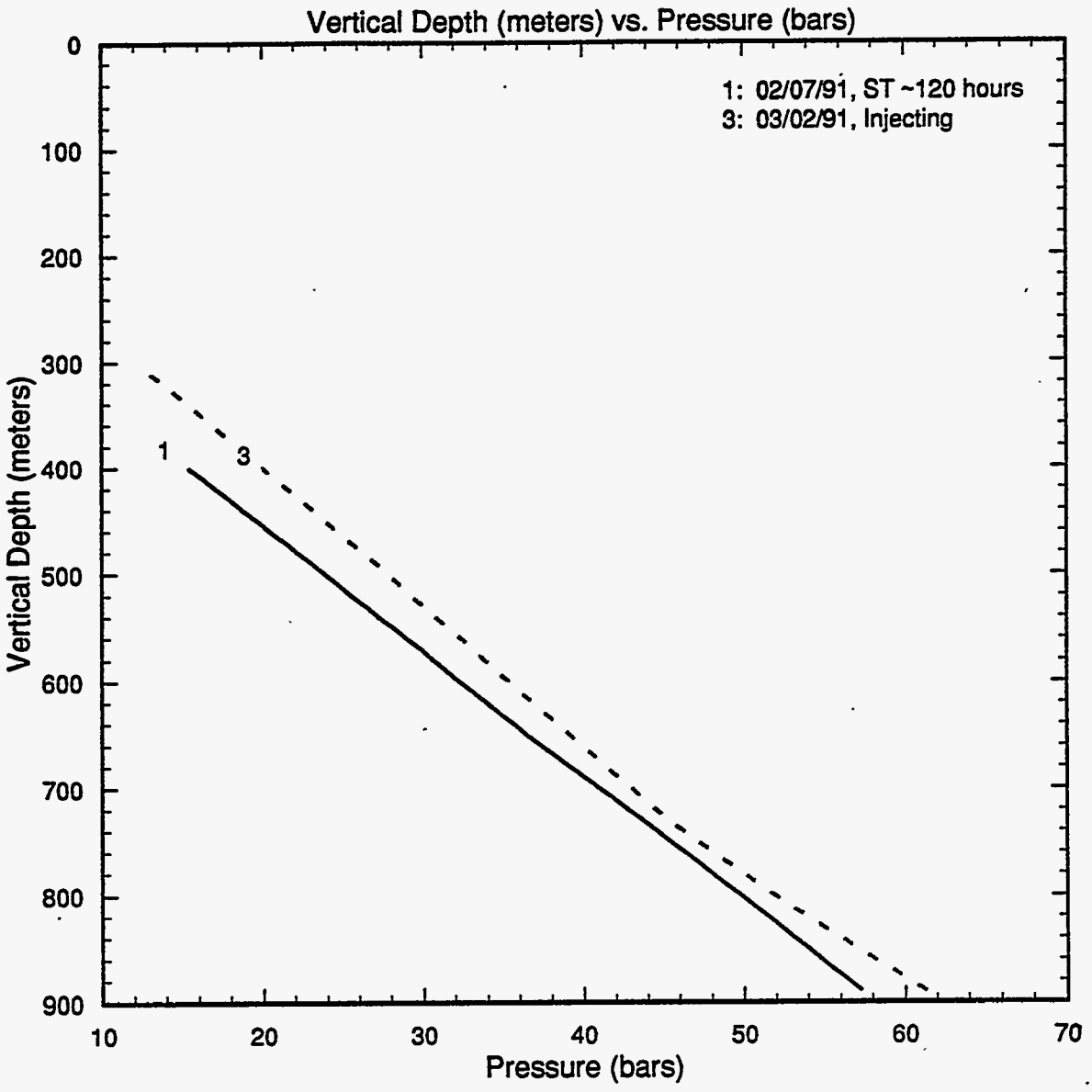

Figure 3.55. Measured pressure (bars, gauge) profiles in slim hole N2-KW-1.

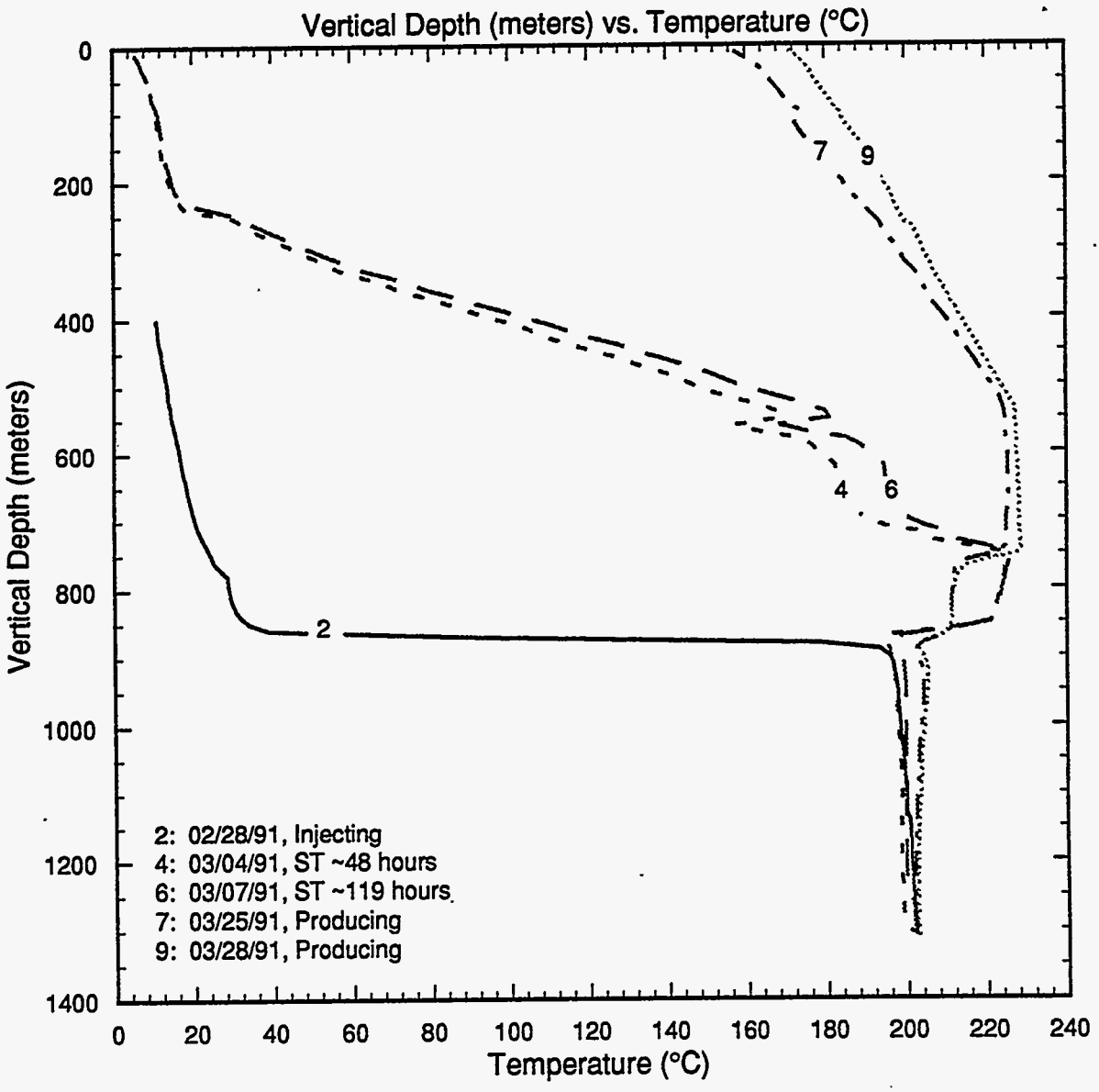

Figure 3.56. Selected temperature surveys recorded in slim hole N2-KW-2.

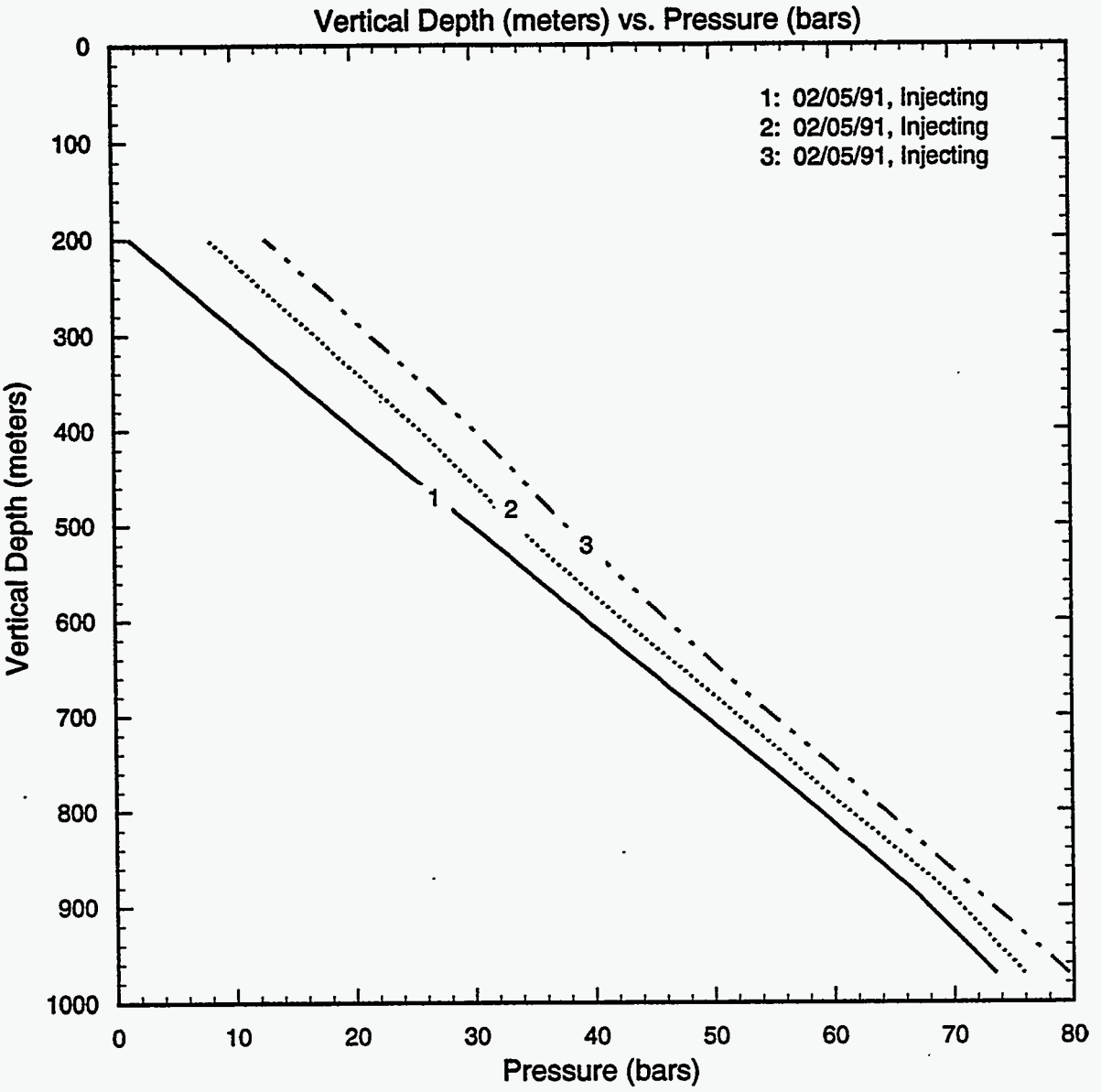

Figure 3.57. Pressure (bars, gauge) profiles recorded during an injection test in slim hole N2-KW-2.

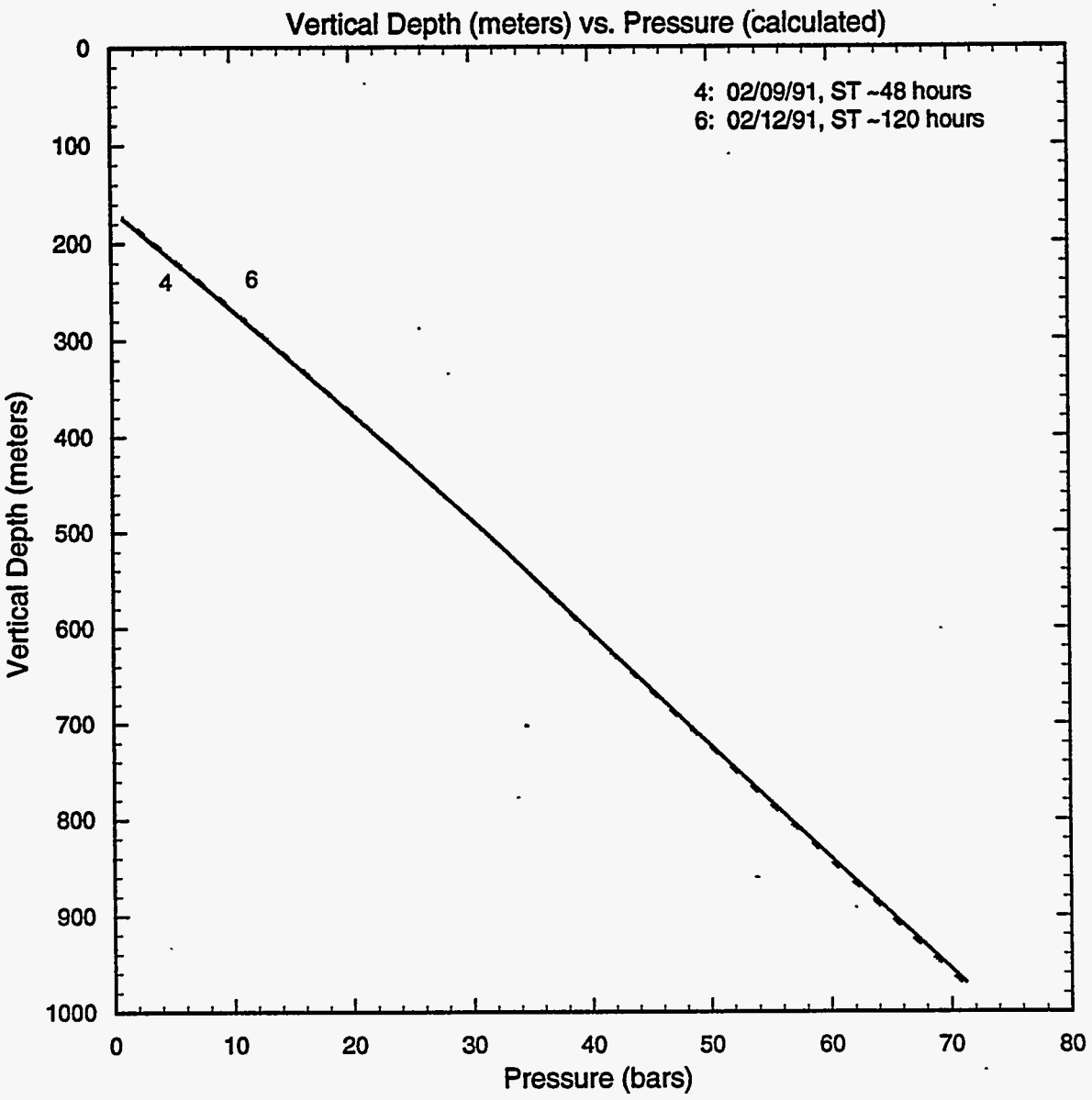

Figure 3.58. Pressure profiles, computed from water level and temperature data, for slim hole N2-KW-2.

3.21 Slim Hole N2-KW-3

Heatup surveys 4 and 6 (Figure 3.59) in slim hole N2-KW-3 display an isothermal temperature profile from ~ 750 m TVD to ~ 850 m TVD; an isothermal temperature profile implies permeable zones at both its end points. Profile 2, taken during an injection test, indicates that most of the fluid is lost at about 860–870 m TVD. Temperature and pressure surveys (profiles 7 and 9, Figure 3.59; profiles 3 and 5, Figure 3.60) recorded during a production test, show clear evidence of liquid entries at 860–870 m TVD and at 750–770 m TVD. The temperature of the lower feedzone is ~ 211°C; the upper feedzone temperature exceeds 227°C. These feedzone temperatures imply the existence of a temperature inversion in the vicinity of slim hole N2-KW-3.

Pressure profiles, computed from water level and temperature data, are shown in Figure 3.61; the pressure at 810 m TVD (= 158 m ASL, middle of two feedzones) is 52 bars. The latter pressure value is slightly higher than that (51 bars) recorded by a downhole gauge on February 24, 1991 (Figure 3.60). This discrepancy between measured and computed pressures is most likely due to an error in gauge calibration. (Note that measured feedzone pressures during the production test exceed the shutin pressures recorded on February 24, 1991!)

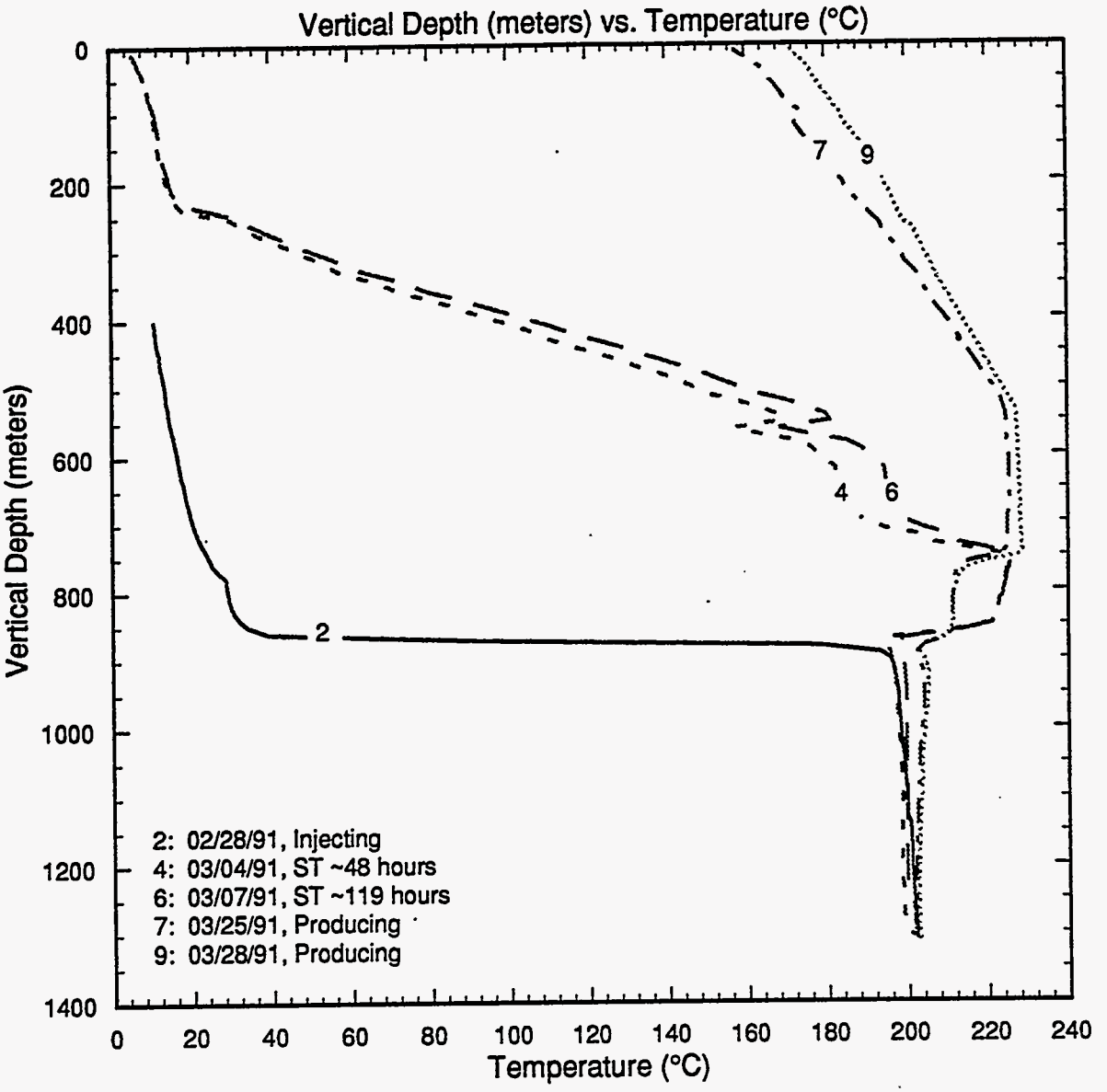

Figure 3.59. Selected temperature surveys for slim hole N2-KW-3.

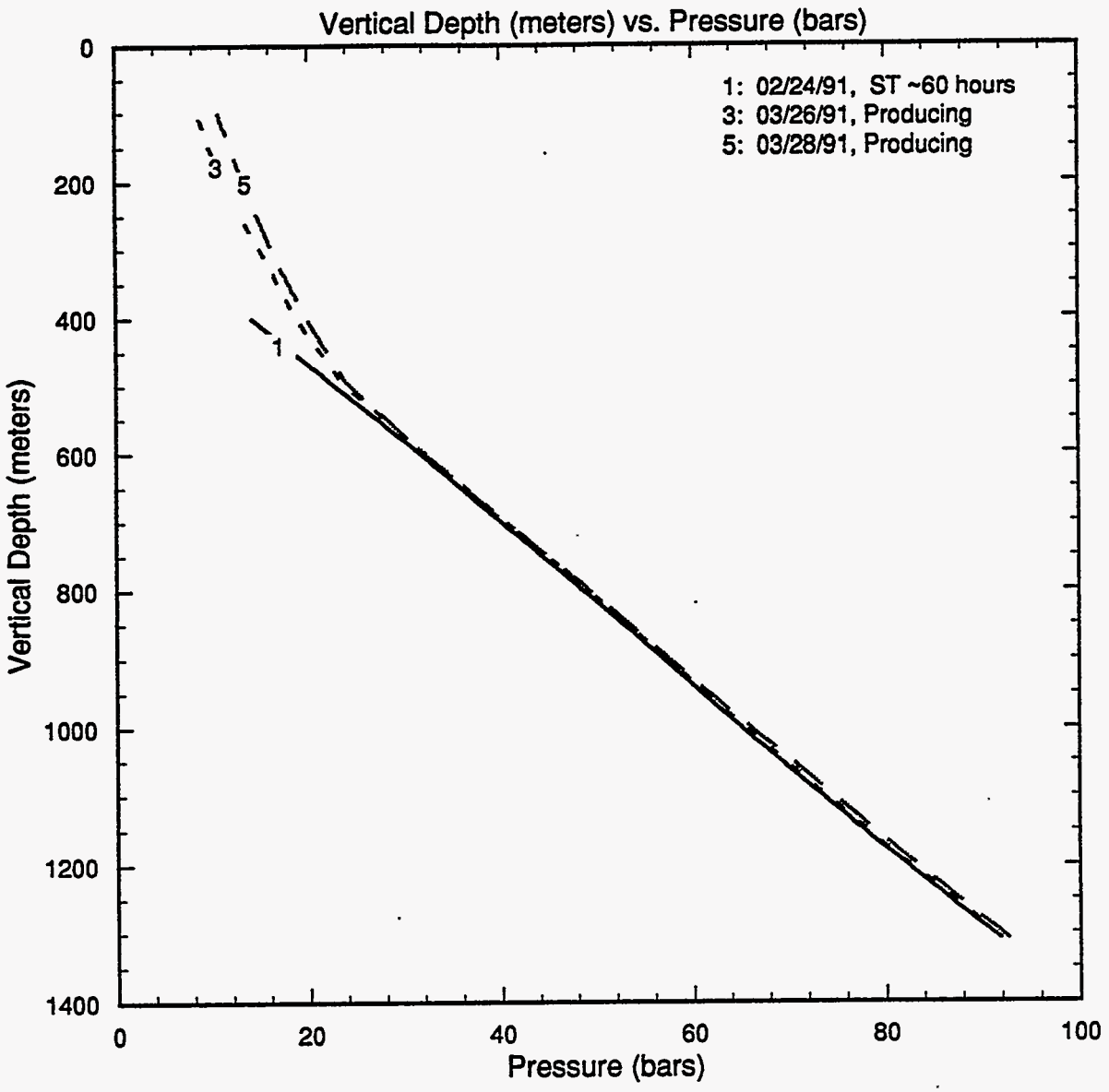

Figure 3.60. Measured pressures (bars, gauge) in slim hole N2-KW-3.

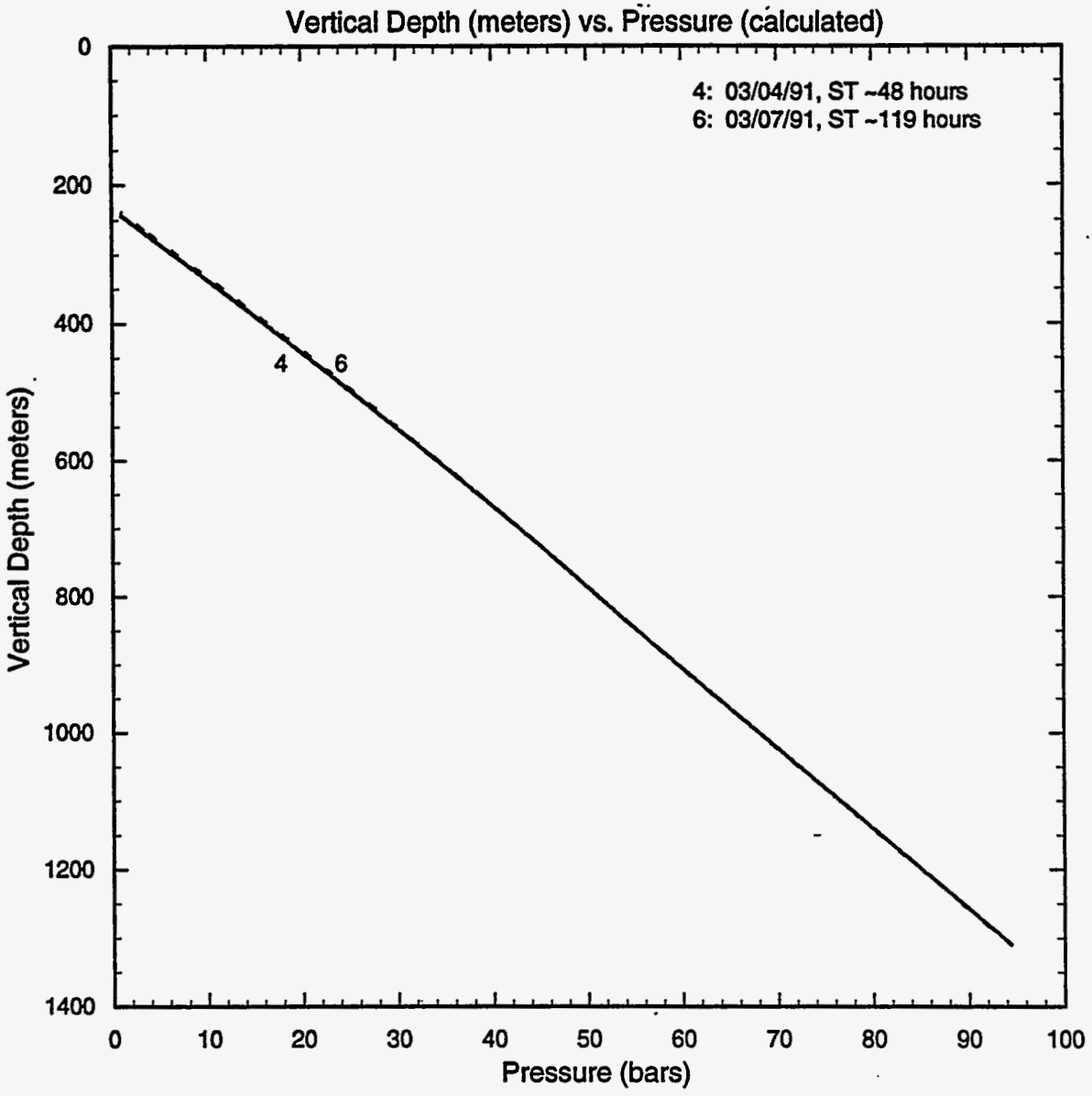

Figure 3.61. Pressure profiles, computed from water level and temperature data, for slim hole N2-KW-3.

SECTION 4

Injection Tests

It is common practice at Oguni to conduct a short term (a few hours) injection test soon after the drilling and completion of a borehole. The injection test consists of injecting cold water into the borehole and simultaneously recording pressure and temperature downhole. Measurements taken during the injection tests of Oguni boreholes are shown in Figures 4.1 to 4.15. In a few cases (see *e.g.*, Figure 4.1 for slim hole GH-8 and Figure 4.3 for well GH-10), the pressure/temperature tool was placed substantially above the feedzone; these pressure measurements are dominated by thermal effects and are not useful for inferring formation properties. However, the pressure and temperature tool in most of the injection tests was placed either near or beneath the principal feedzone; measurements made during the injection test of well GH-11 (Figure 4.4) are typical of downhole pressure/temperature data. After start of injection in well GH-11 (Figure 4.4), the pressure at first rapidly rises and then slowly falls. As soon as injection is terminated, the pressure begins to decline very rapidly. The rapid fall-off at shutin is not unusual, but the rise and subsequent fall in pressure which accompany injection in well GH-11 (*e.g.*, Figure 4.4) need to be explained. Since most of the Oguni injection tests were performed right after borehole completion, it is likely that fractures were still laden with cuttings and/or drilling mud at the time of the injection tests. Injection tests presumably washed these cuttings/mud away from the borehole, and thus improved the near wellbore permeability. Strictly speaking, injection does not cause borehole stimulation in the usual sense (*i.e.*, by fracturing the formation); it merely accomplishes an effective washing of the borehole. Based on this interpretation, the three pressure fall-offs for GH-11 in Figure 4.4 represent the real response to changes in injection rate; the pressure records during the injection phase for GH-11 (as well as most other Oguni boreholes) merely reflect the washing of the wellbore. The fall-off data from injection tests may be analyzed to obtain formation transmissivity (*i.e.*, permeability × effective formation thickness).

Although pressure data recorded during the injection phase are not generally useful for determining formation transmissivity, these data are required for evaluating the injectivity index (II). II is defined as follows:

$$II = \frac{M}{P_f - P_i}$$

where M is the mass rate of injection, P_f is the flowing pressure and P_i is the initial (or static) pressure. It was noted earlier that the flowing pressure P_f was observed to fall in many of the Oguni injection tests; in such cases, the computed injectivity index represents a lower limit.

Analyses of injection data for individual Oguni boreholes are discussed in the following subsections.

Continued on page 4-24

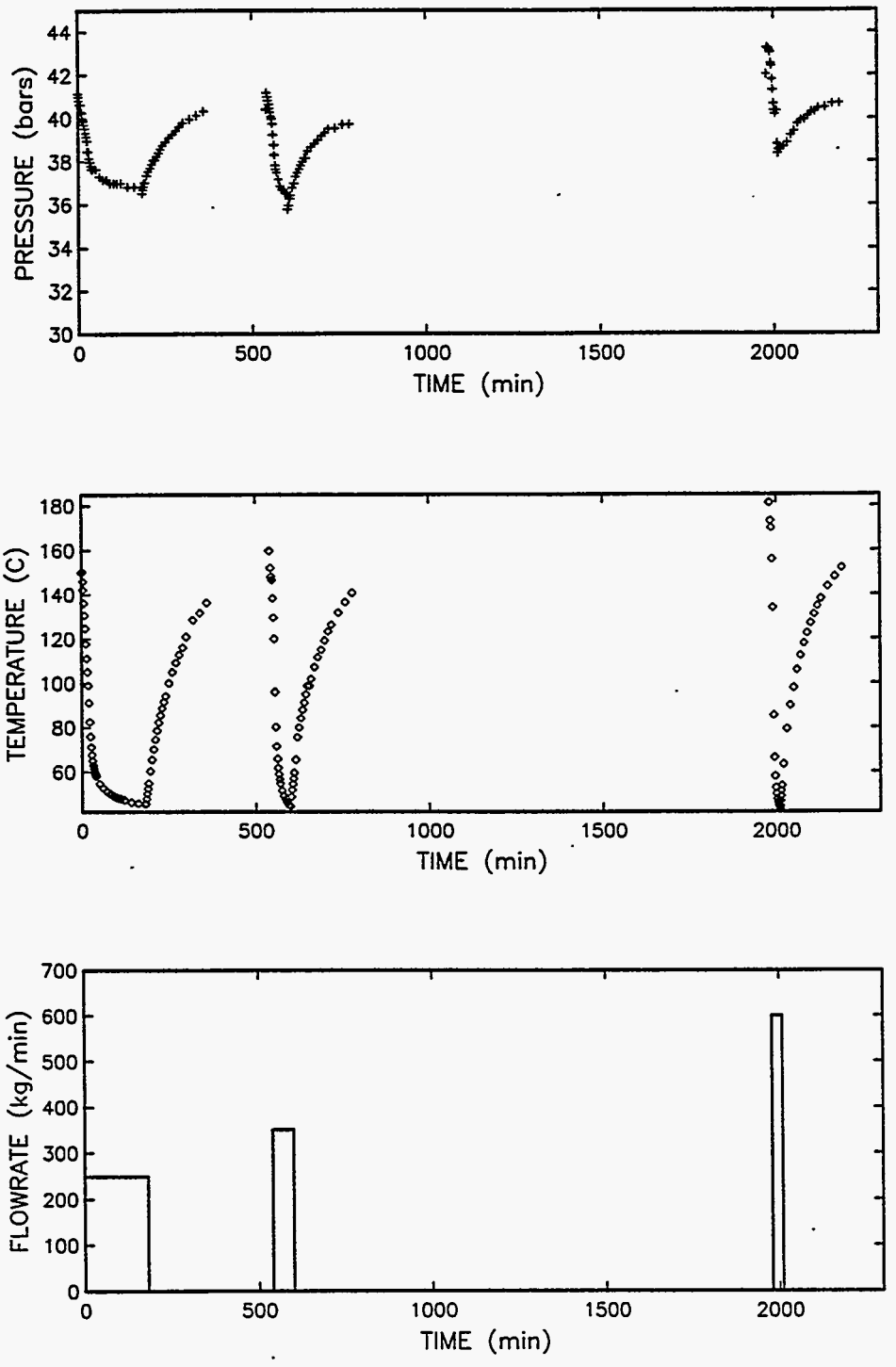

Figure 4.1. Downhole pressure and temperature (gauge depth = ?; feedzone depth = 1220 m TVD) recorded during the injection test of slim hole GH-8 in March 1987.

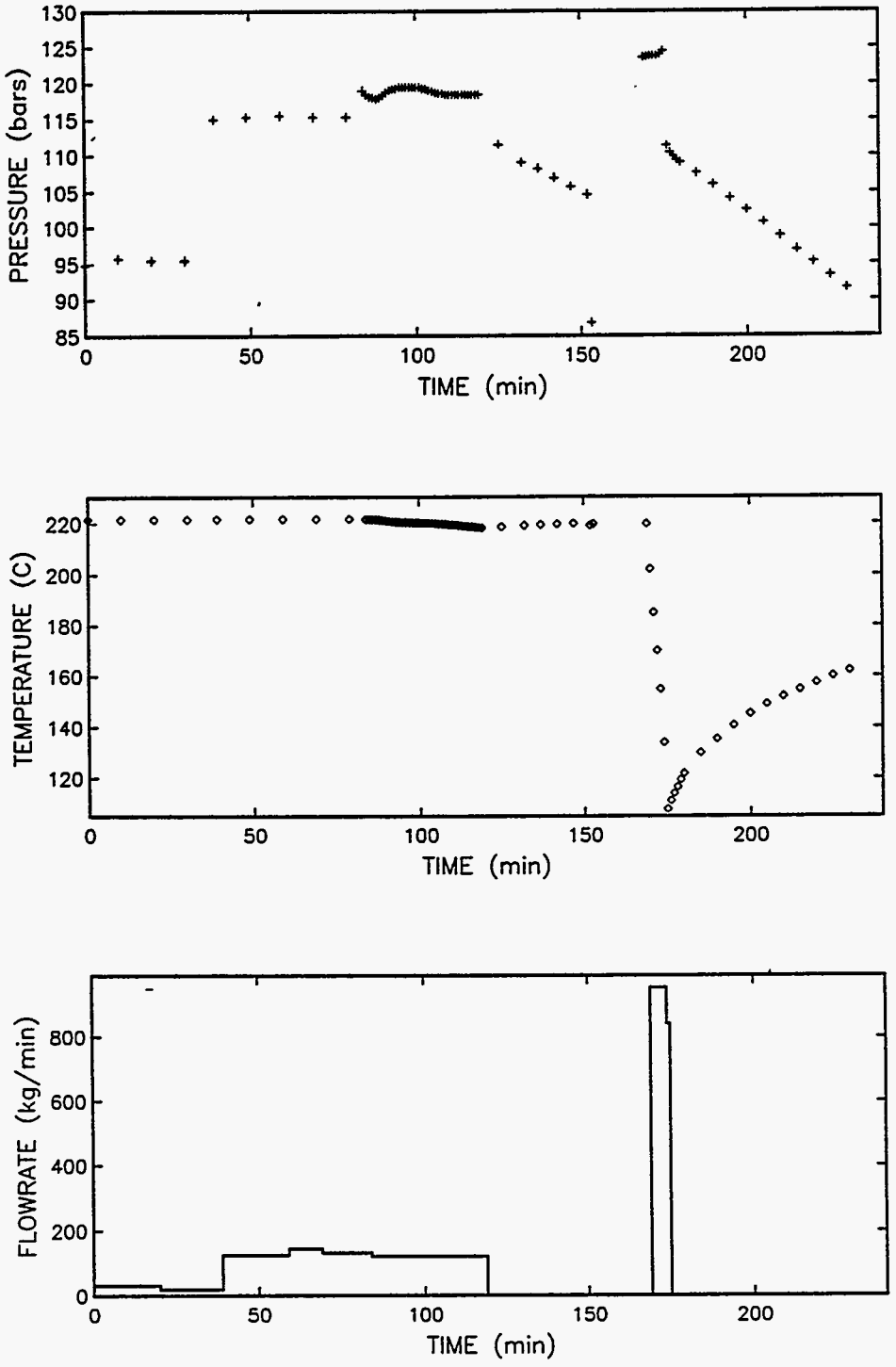

Figure 4.2. Downhole pressure and temperature (gauge depth = 950 m TVD; feedzone depth = ?) recorded during the injection test of slim hole GH-9 on March 22, 1987.

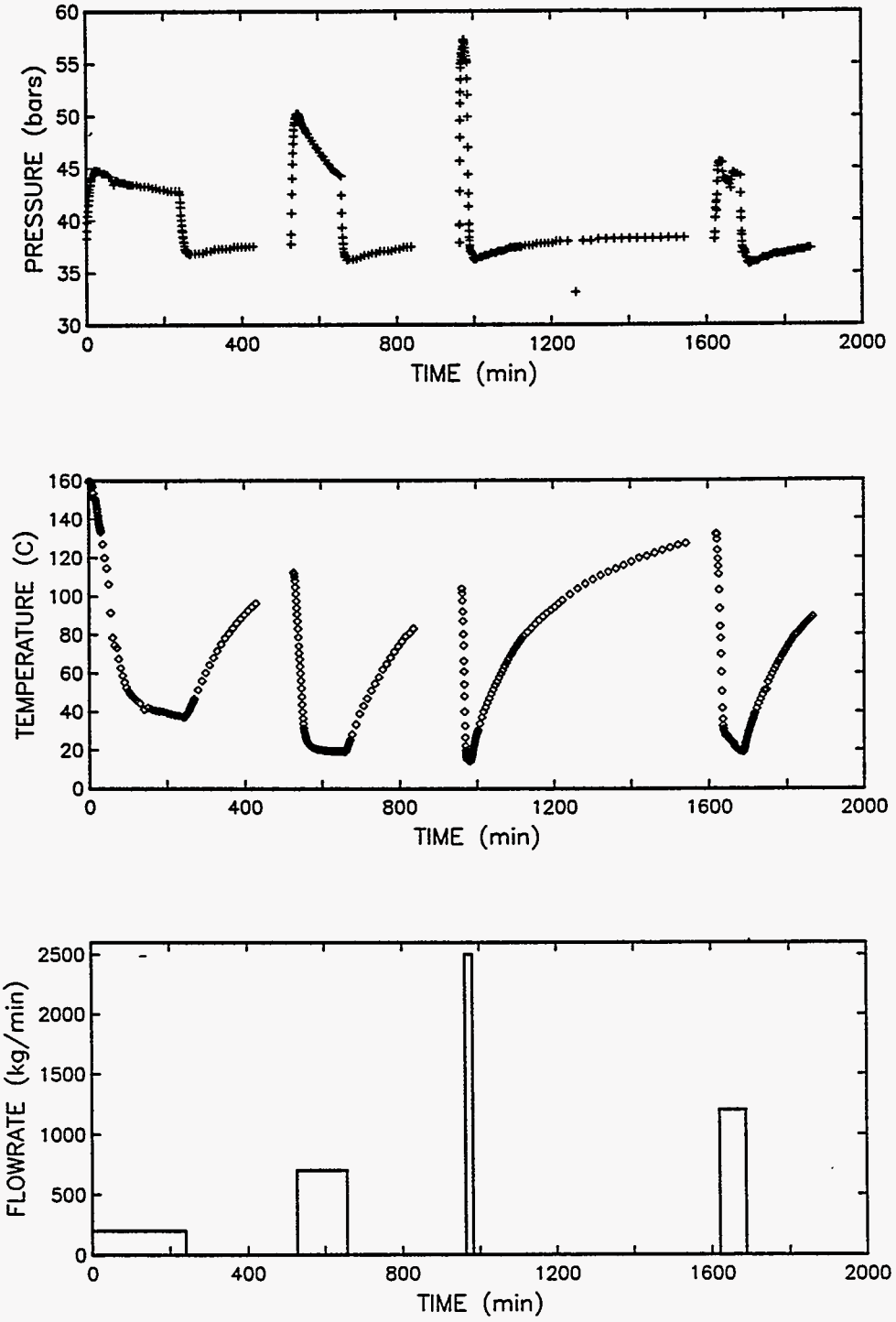

Figure 4.3. Downhole pressure and temperature (gauge depth = 689 m TVD; feedzone depth = 1010 m TVD) recorded during the injection test of well GH-10 in March 1987.

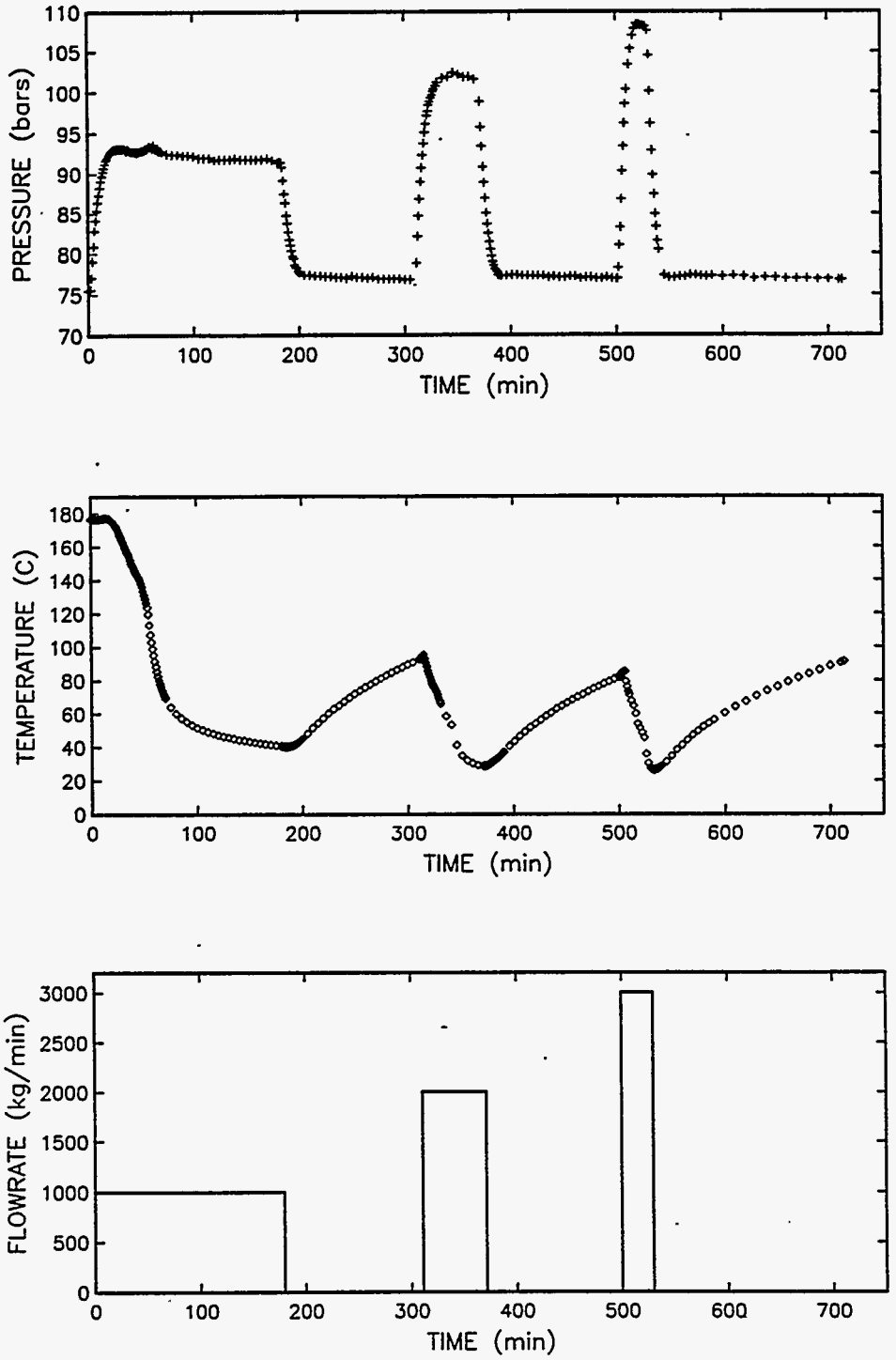

Figure 4.4. Downhole pressure and temperature (gauge depth = 1121 m TVD; feedzone depth = 1140 m TVD) recorded during the injection test of well GH-11 on March 30, 1988.

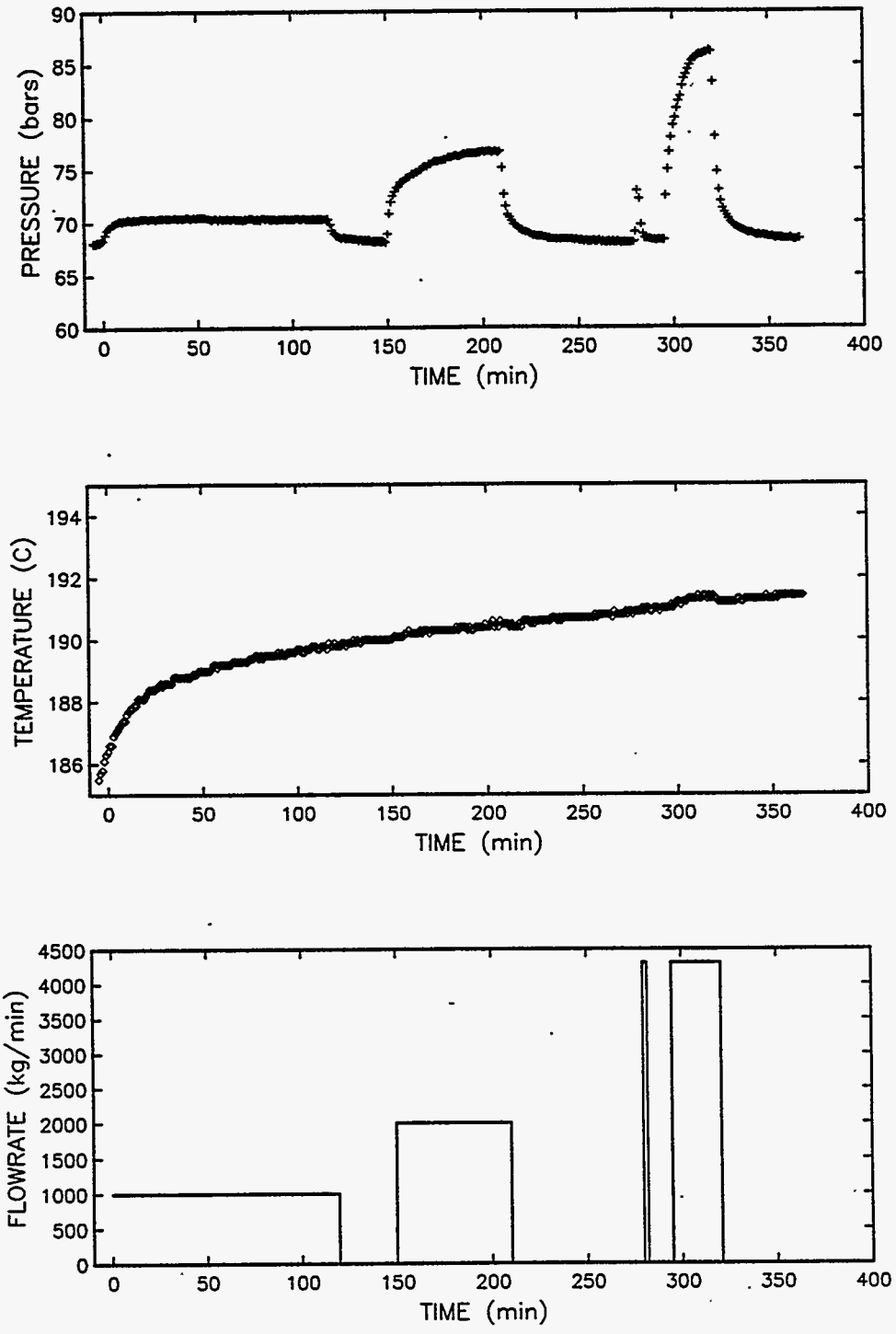

Figure 4.5. Downhole pressure and temperature (gauge depth = 990 m TVD; feedzone depth = 750 m TVD) recorded during the injection test of well GH-12 on February 14, 1989.

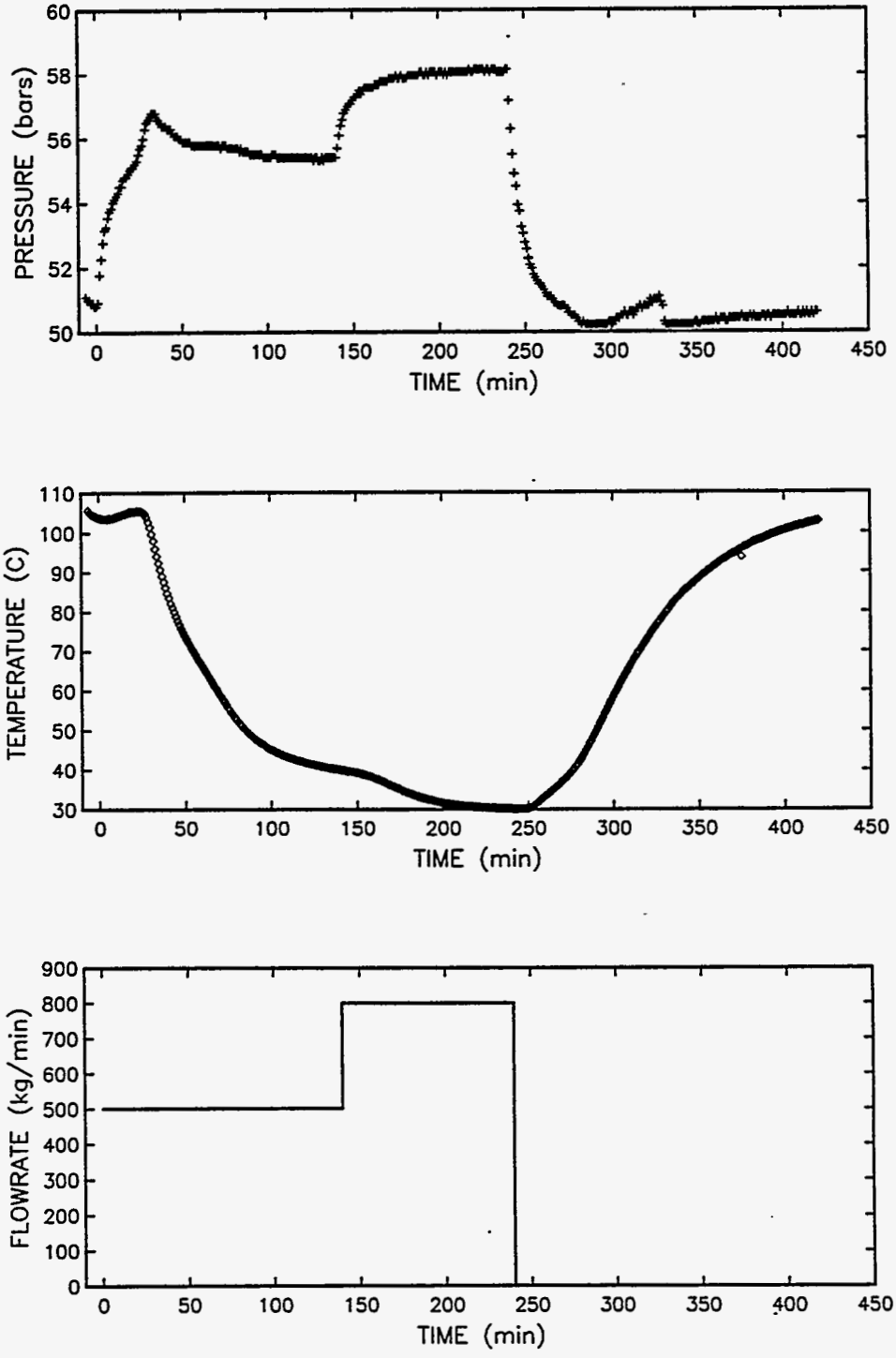

Figure 4.6a. Downhole pressure and temperature (gauge depth = 678 m TVD; feedzone depth = 680 m TVD) recorded during Injection Test No. 1 of well GH-15 on October 12, 1990.

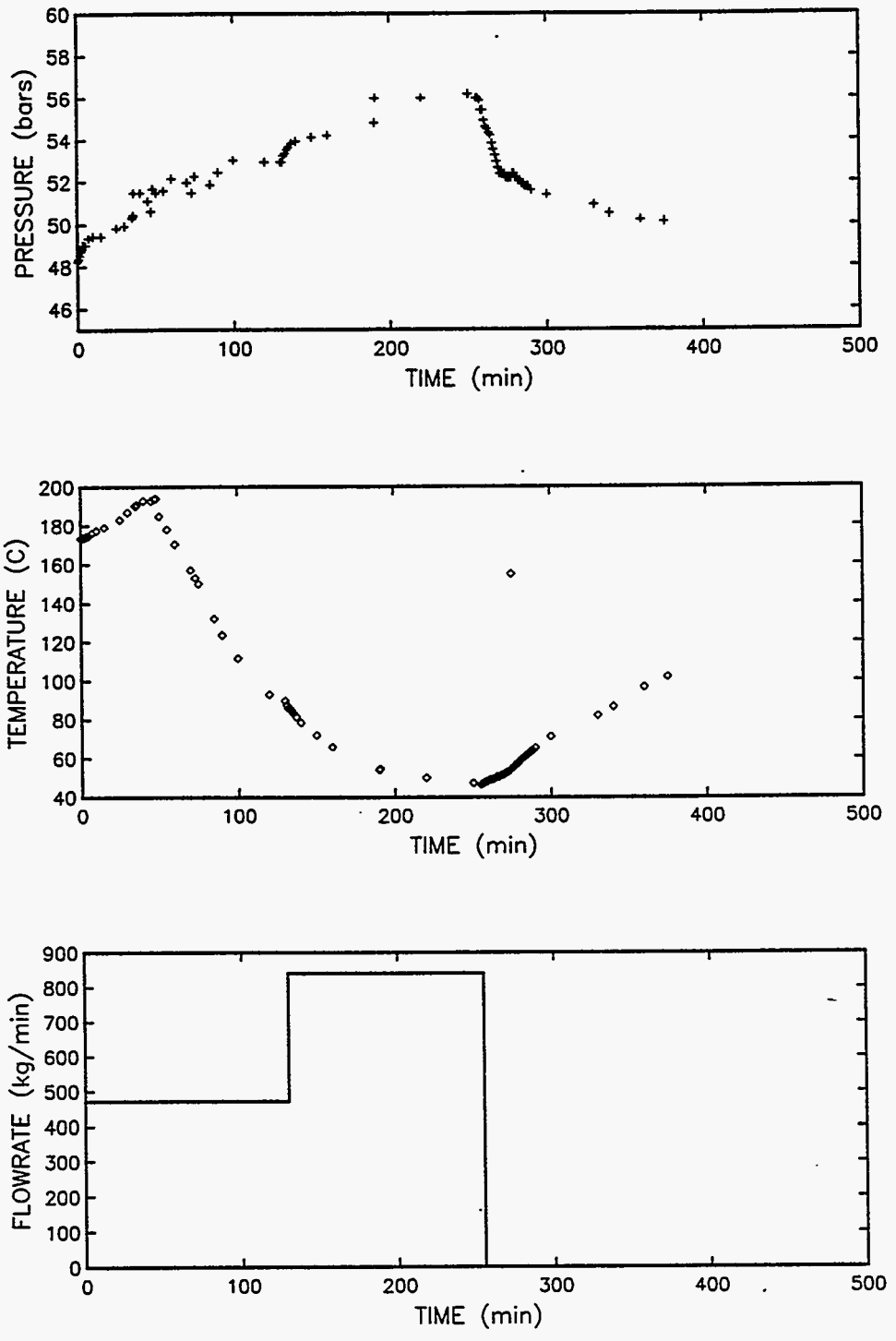

Figure 4.6b. Downhole pressure and temperature (gauge depth = 686 m TVD; feedzone depth = 680 m TVD) recorded during Injection Test No. 2 of well GH-15 on November 18, 1990.

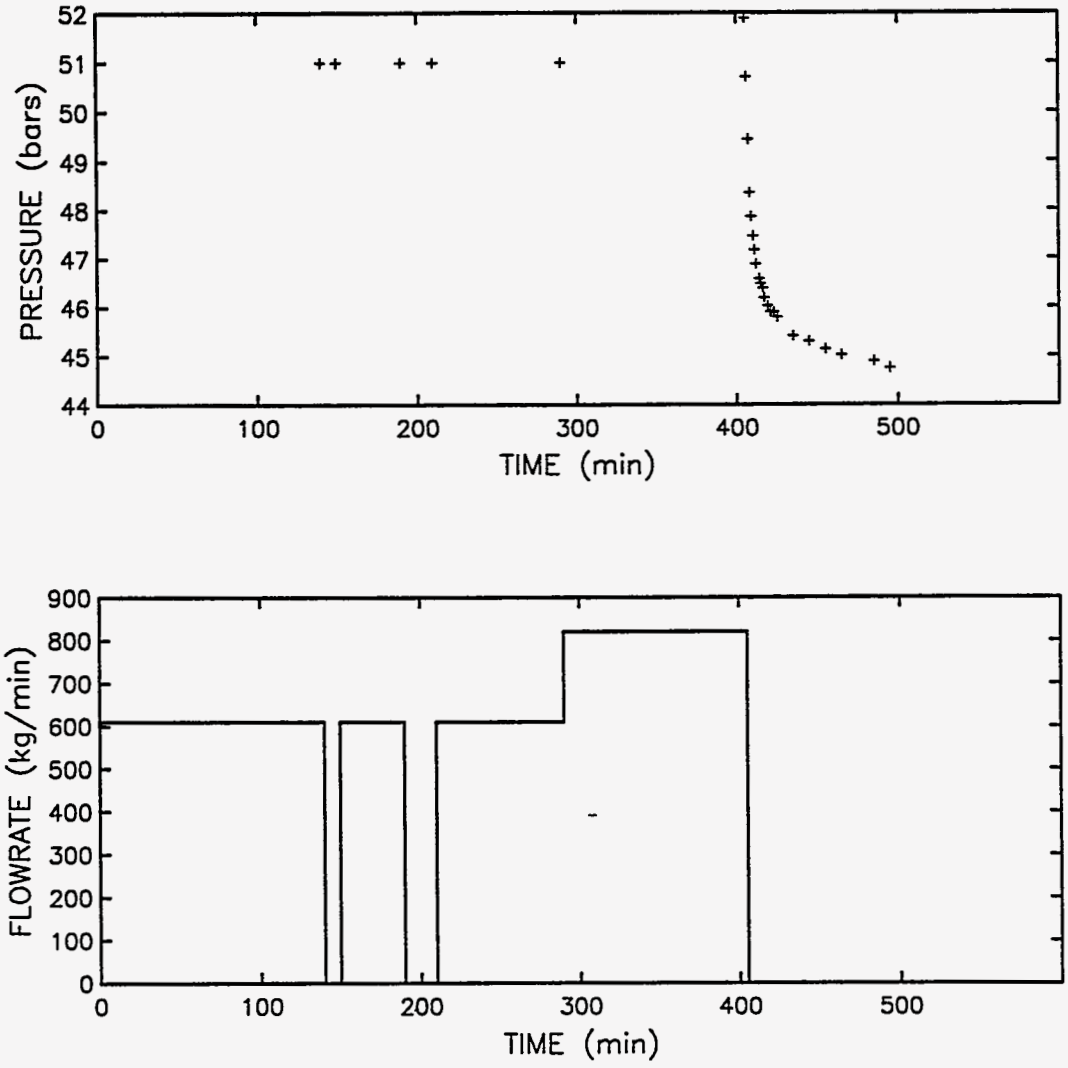

Figure 4.6c. Downhole pressure (gauge depth = 596 m TVD; feedzone depth = 680 m TVD) recorded in well GH-15 during Injection Test No. 3 on October 24, 1991.

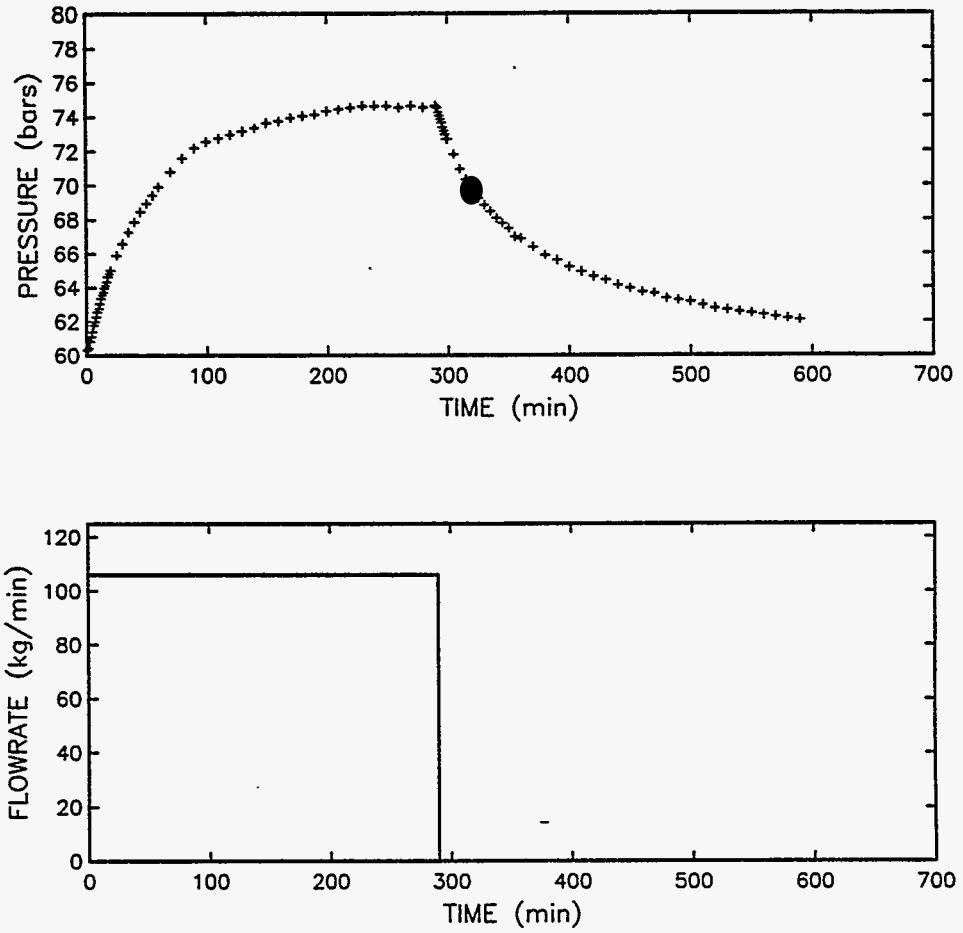

Figure 4.7a. Downhole pressure (gauge depth = 810 m TVD; feedzone depth = 760 m TVD) recorded during Injection Test No. 1 of well GH-17 on November 7, 1991.

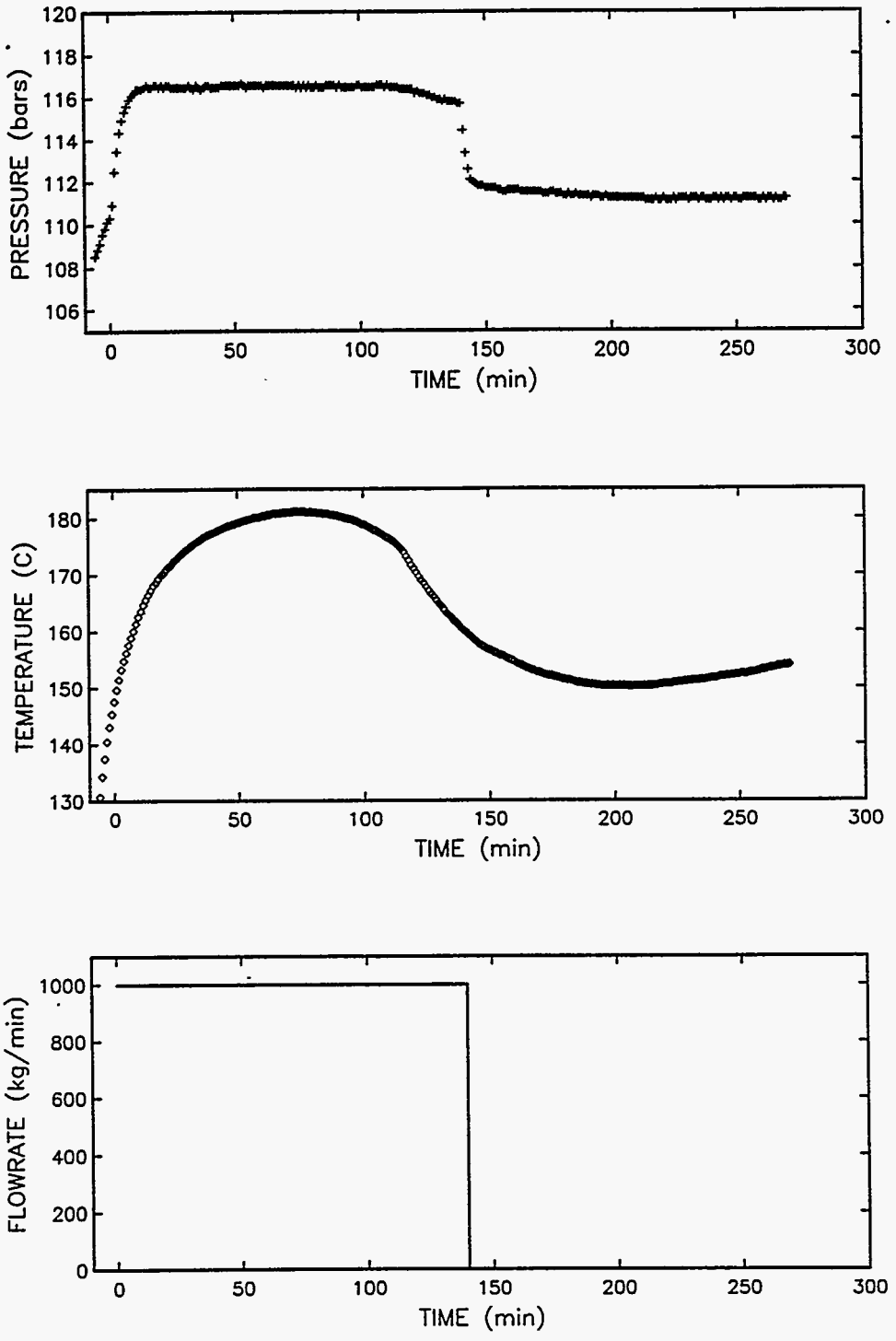

Figure 4.9a. Downhole pressure and temperature (gauge depth = 1550 m TVD; feedzone depth = 1560 m TVD) recorded during Injection Test No. 1 of well GH-20 on April 1, 1991.

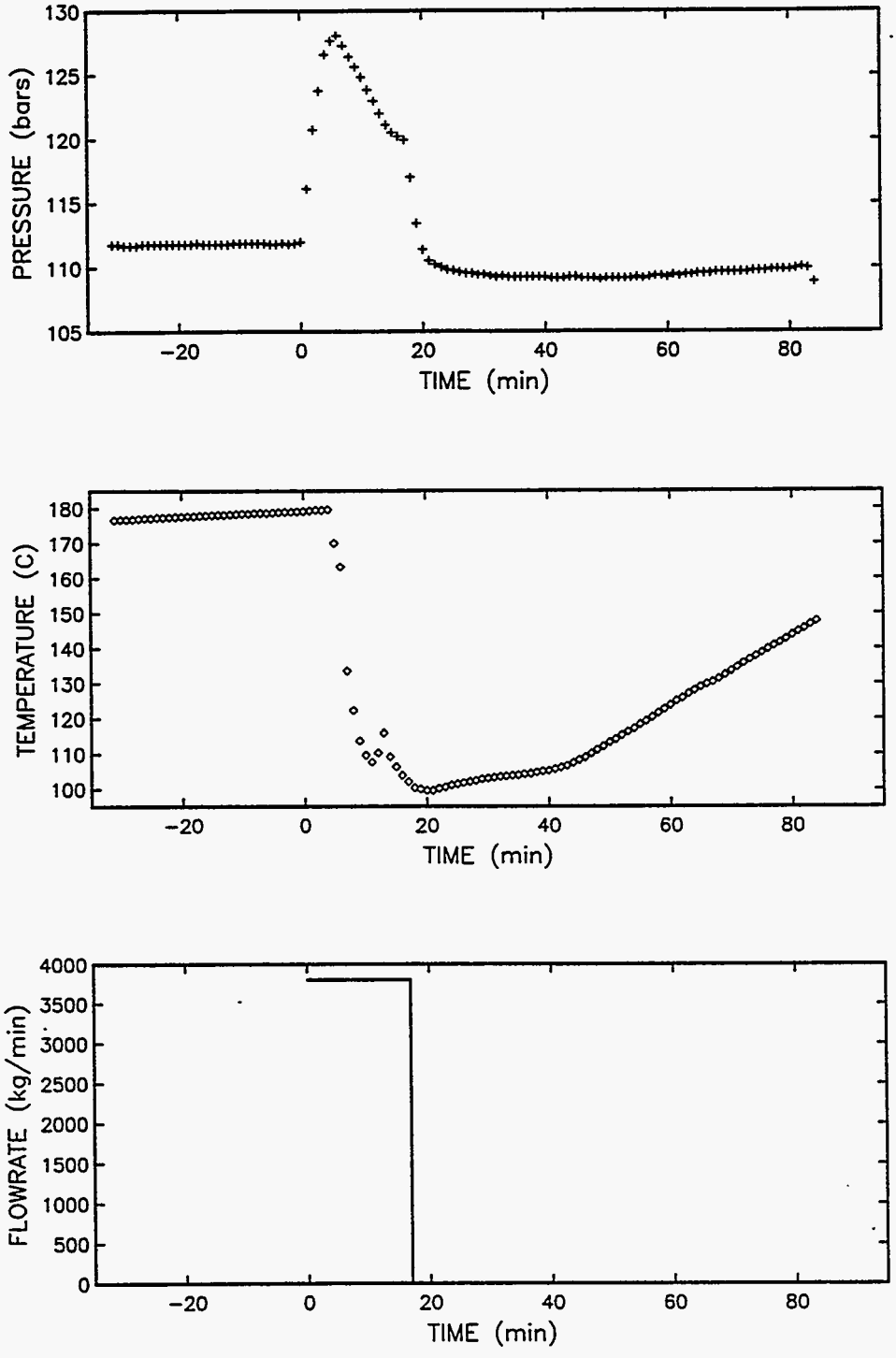

Figure 4.9b. Downhole pressure and temperature (gauge depth = 1550 m TVD; feedzone depth = 1560 m TVD) recorded during Injection Test No. 2 of well GH-20 on April 2, 1991.

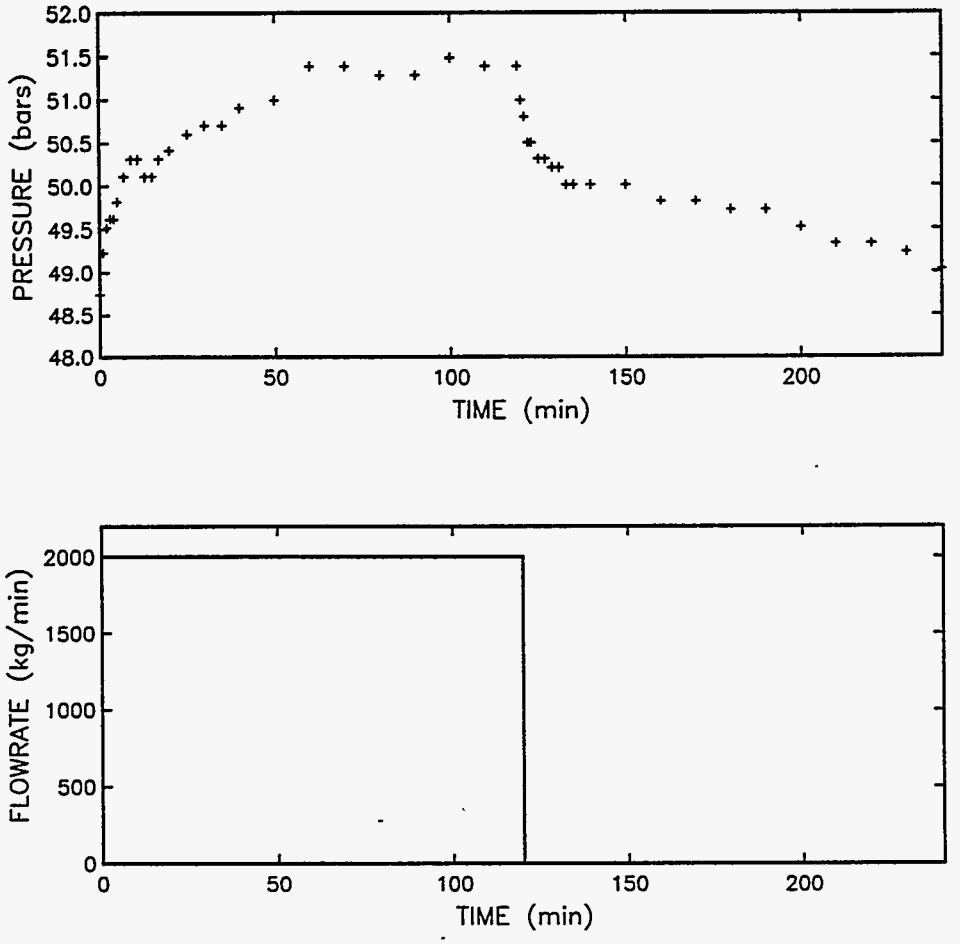

Figure 4.10a. Downhole pressure (gauge depth = 804 m TVD; feedzone depth = 650 m TVD) recorded in well GH-21 during Injection Test No. 1 on November 18, 1992.

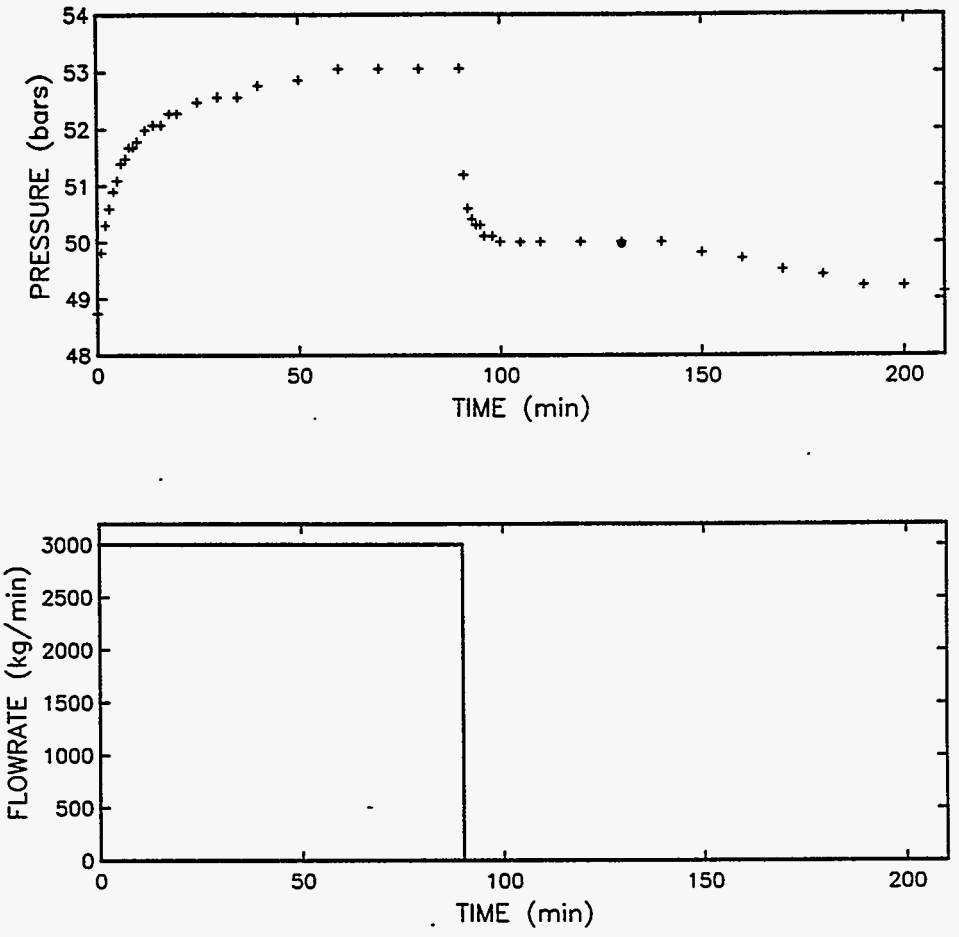

Figure 4.10b. Downhole pressure (gauge depth = 804 m TVD; feedzone depth = 650 m TVD) recorded in well GH-21 during Injection Test No. 2 on November 19, 1992.

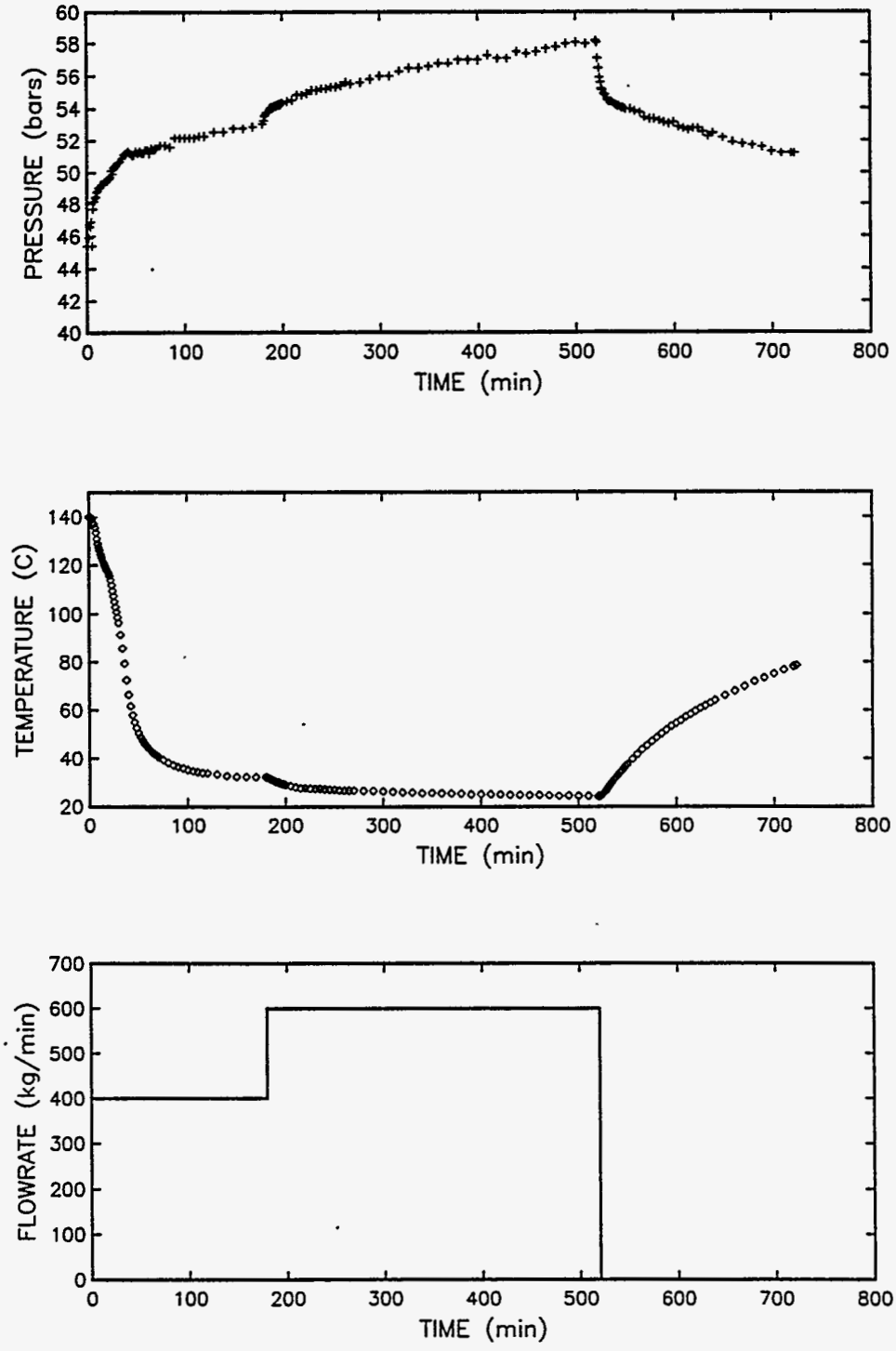

Figure 4.11. Downhole pressure and temperature (gauge depth = 563 m TVD; feedzone depth = 590 m TVD) recorded in well IH-1 during an injection test on March 25, 1988.

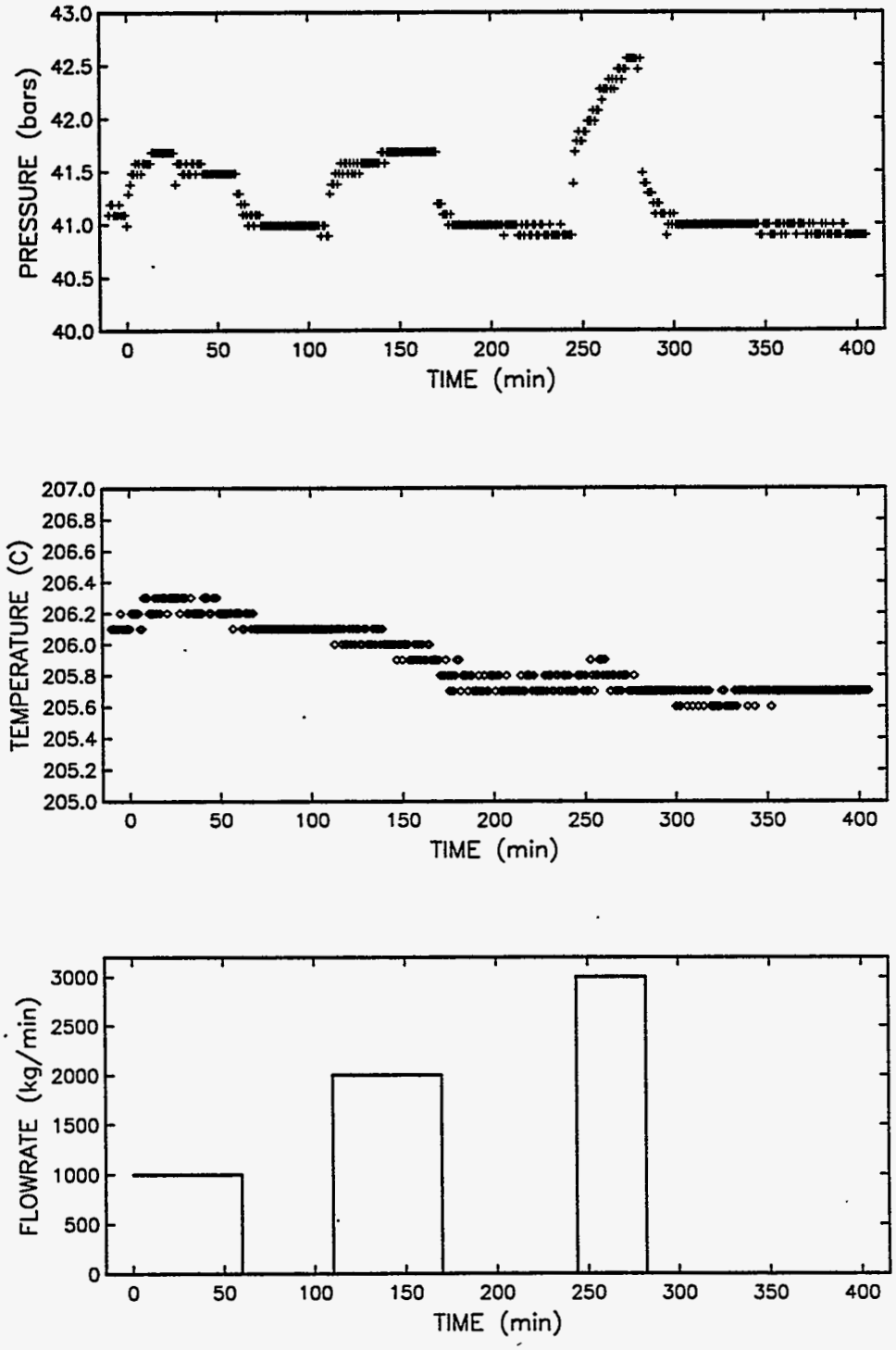

Figure 4.12. Downhole pressure and temperature (gauge depth = 581 m TVD; feedzone depth = 550 m TVD) recorded during an injection test of well IH-2 on January 26, 1990.

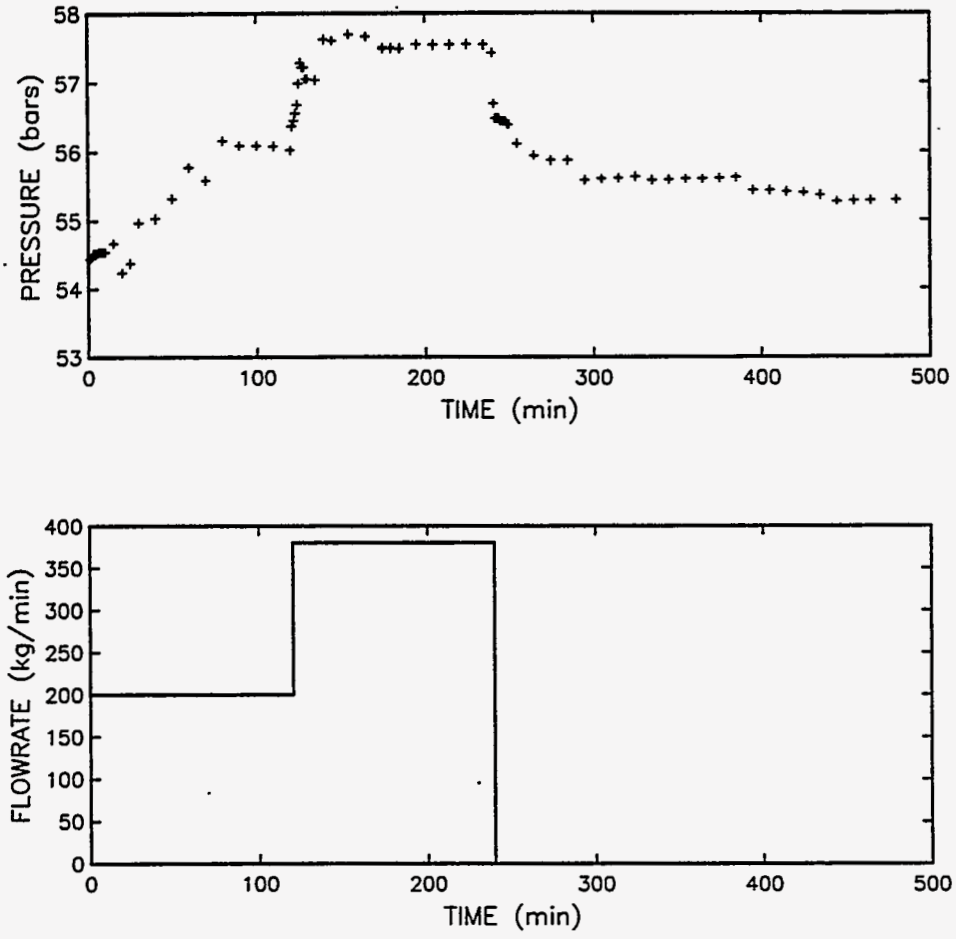

Figure 4.13a. Downhole pressure (gauge depth = 858 m TVD; feedzone depth = 860 m TVD) recorded in slim hole N2-KW-1 during Injection Test No. 2 on February 8, 1991.

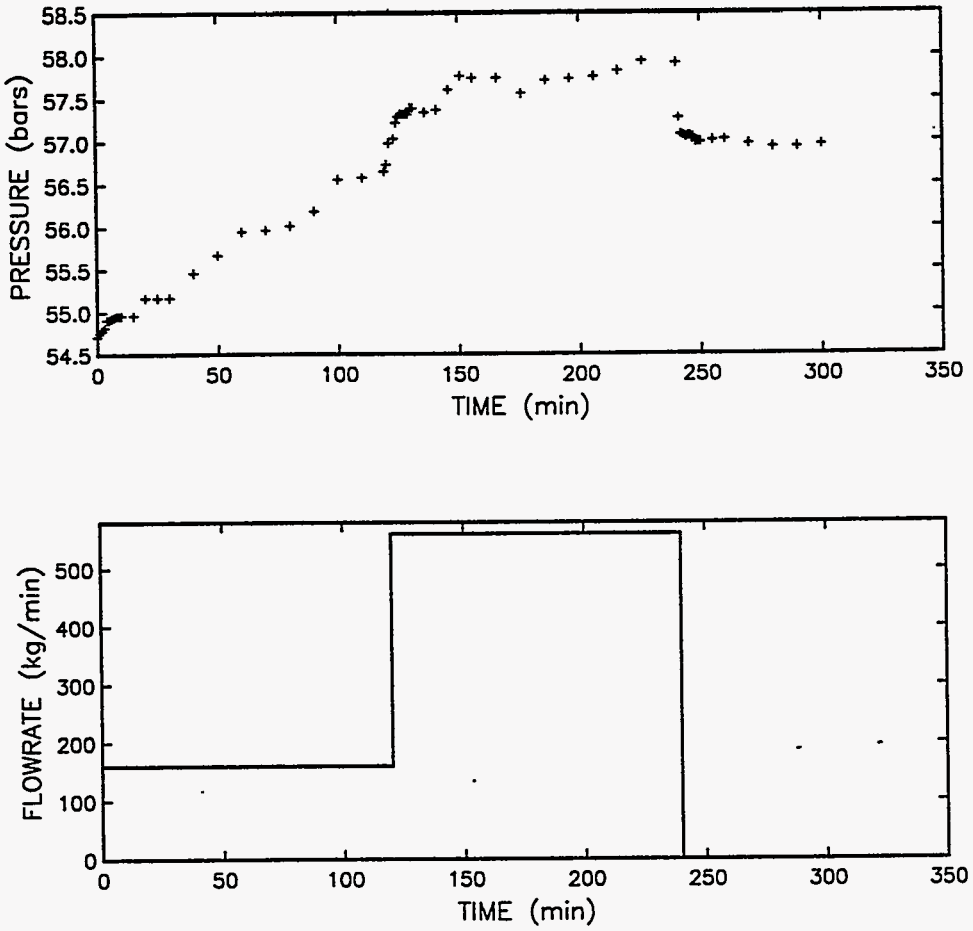

Figure 4.13b. Downhole pressure (gauge depth = 873 m TVD; feedzone depth = 860 m TVD) recorded in slim hole N2-KW-1 during Injection Test No. 3 on March 2, 1991.

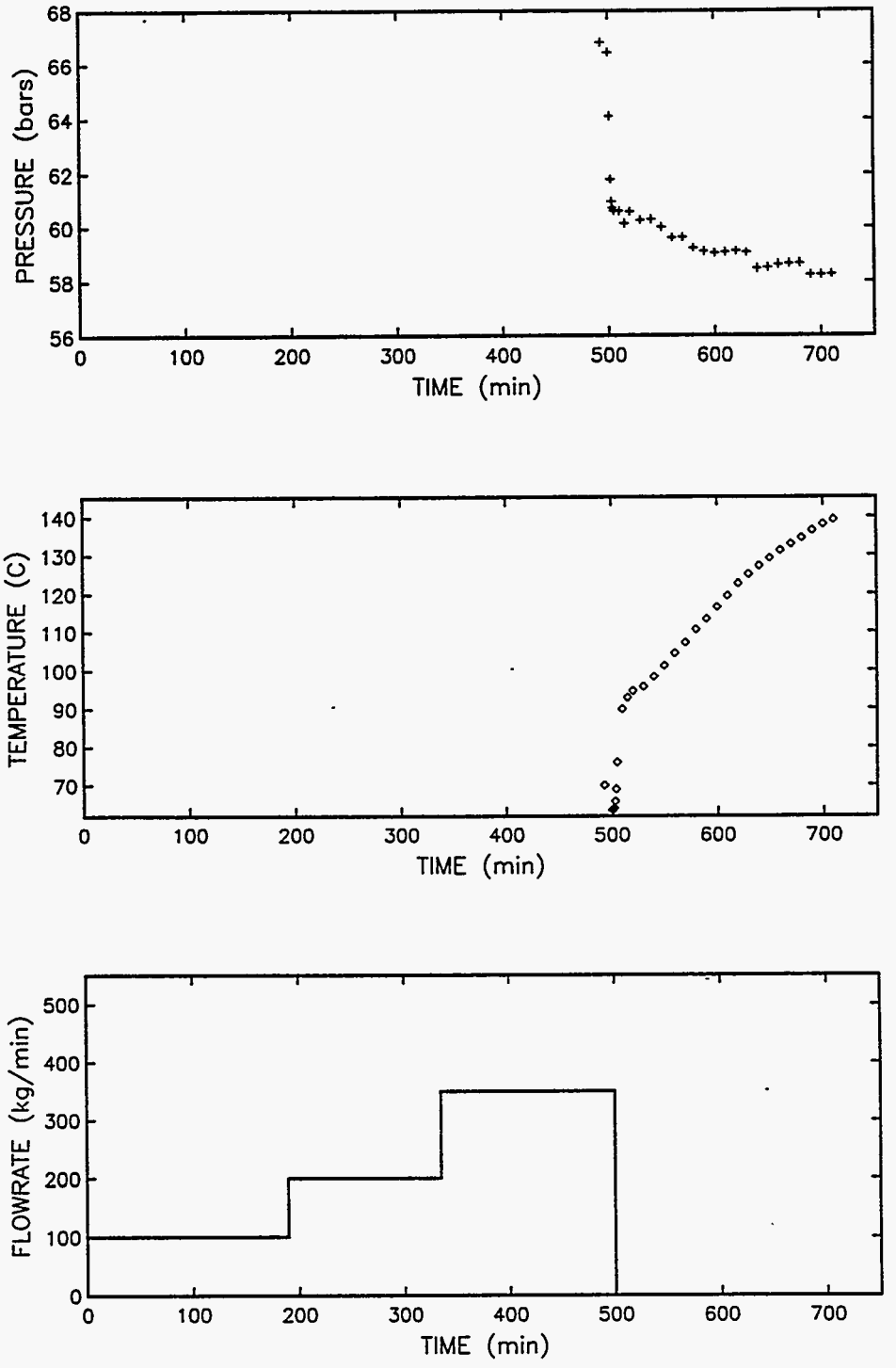

Figure 4.14a. Downhole pressure and temperature (gauge depth = 765 m TVD; feedzone depth = 860 m TVD) recorded during Injection Test No. 1 of slim hole N2-KW-2 on February 5, 1991.

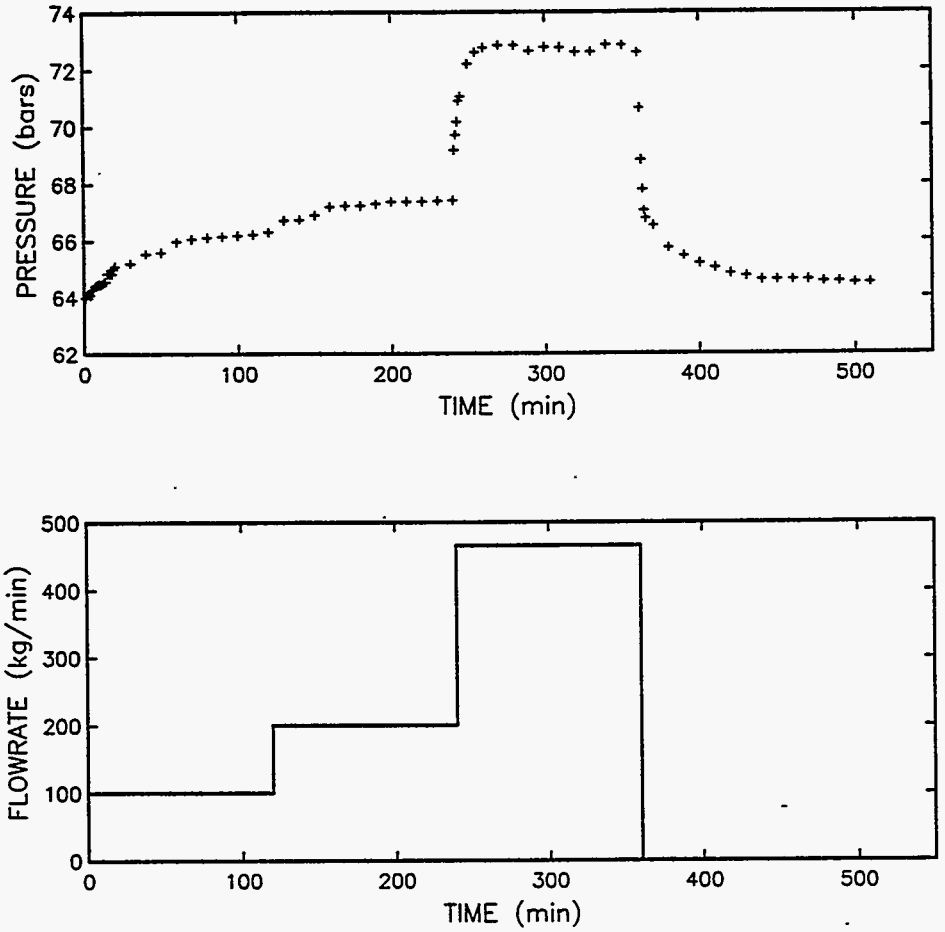

Figure 4.14b. Downhole pressure (gauge depth = 840 m TVD; feedzone depth = 860 m TVD) recorded during Injection Test No. 2 of slim hole N2-KW-2 on February 6, 1991.

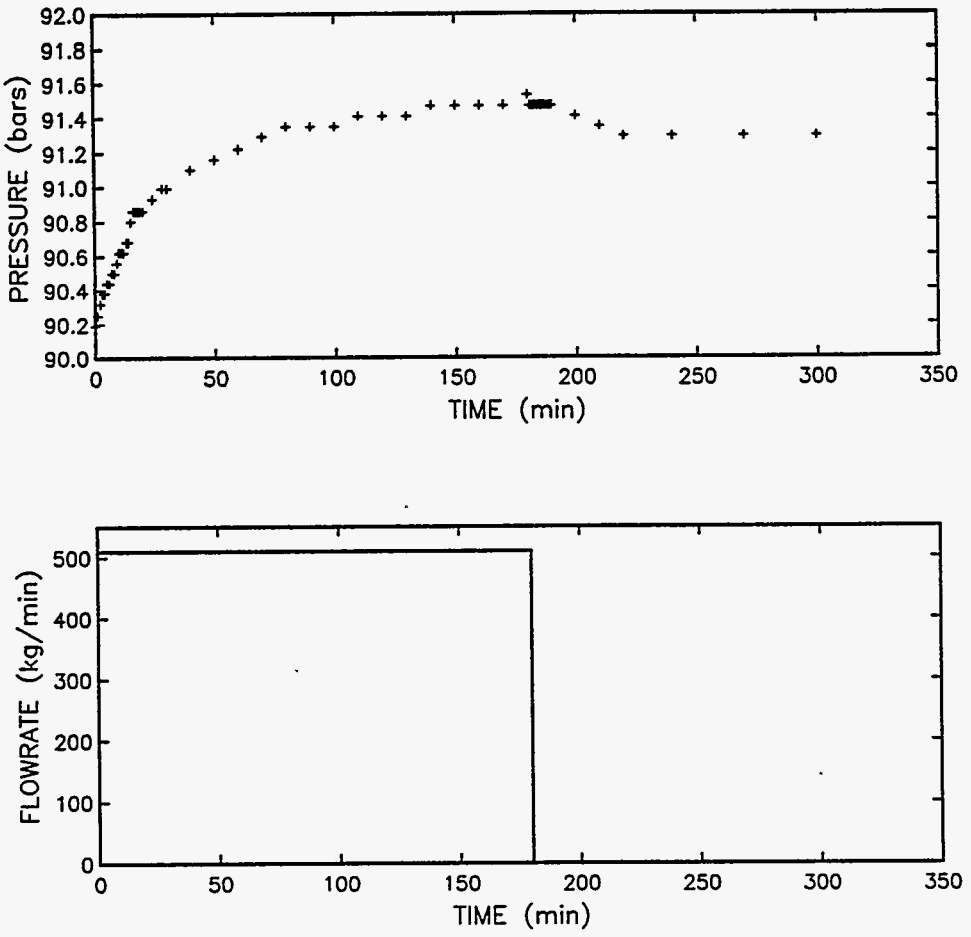

Figure 4.15. Downhole pressure (gauge depth = 1288 m TVD; feedzone depth = 810 m TVD) recorded during an injection test of slim hole N2-KW-3 on March 7, 1991.

4.1 Slim Hole GH-8

Slim hole GH-8 exhibits an anomalous pressure response. The pressures decline during injection and increase during fall-off phases (see Figure 4.1). This anomalous response is most likely the result of the pressure/temperature tool being located several hundred meters above the feedzone depth (The gauge depth is not known to the authors.). Because of wellbore cooling caused by cold water injection, pressures at shallow depths (depths << feedzone depth) can fall even while the feedzone pressure is increasing. Wellbore heating during the fall-off phase will result in an opposite effect (*i.e.*, an increase in shallow pressures even in the presence of declining feedzone pressures). The pressure data for GH-8 (Figure 4.1) are thus dominated by thermal effects, and are consequently useless for inferring formation transmissivity and injectivity index.

4.2 Slim Hole GH-9

The feedzone depth for slim hole GH-9 is not known, and the slim hole has poor permeability. A pressure of 95.8 bars(a) was recorded at gauge depth of 950 m TVD prior to the start of cold water injection on March 22, 1987. At the end of first injection period (duration = 119 minutes, injection rate ≤ 120 kg/min), the pressure at 950 m TVD was 119.4 bars(a). This yields an injectivity index of ~ 0.08 kg/s-bar. No significant temperature change (at gauge depth) was observed during the first injection and subsequent fall-off phases (Figure 4.2). After the fall-off phase (50 minutes), injection was resumed at a relatively high rate (952 kg/min → 840 kg/min). This time cold water injection was accompanied by a steep drop in temperature. The second injection test lasted for only five minutes. The brief duration of this test makes pressure data recorded during the injection phase of questionable value for evaluating the injectivity index.

The pressure transient analysis methods for multiple rate flow tests are discussed by Matthews and Russell (1967). A convenient technique is to plot shutin pressure p versus a reduced time (multi-rate Horner time).

$$\left[\frac{1}{M_n}\sum_{j=1}^{n}\left(M_j - M_{j+1}\right)\log\left(t-t_{j-1}\right)\right] - \log\left(t-t_n\right)$$

Here M_j denotes the constant mass flow rate during the j^{th} flow period ($t_{j-1} < t < t_j$), M_n is the final flow rate prior to shutin, and M_o and t_o are taken to be zero. Ideally, the plot should give a straight line with slope m such that

$$\frac{kh}{\nu} = \frac{1.15\,M_n}{2\pi m}$$

Here k is the average formation permeability, h is the effective formation thickness, and ν is the kinematic viscosity of the *in situ* (*i.e.*, reservoir) fluid (see also Garg and Pritchett, 1990).

The Horner plots of pressure fall-off data for slim hole GH-9 are displayed in Figures 4.16a and 4.16b. The late-time fall-off data can be approximated by straight lines with slopes of 18.7 bars/cycle (Figure 4.16a) and 113.2 bars/cycle (Figure 4.16b). Assuming a kinematic viscosity ν of 1.44×10^{-7} m^2/s (corresponding to liquid water at a temperature of 225°C), the formation transmissivity (kh) is estimated as follows:

Fall-Off Test 1: $kh = 0.03$ darcy-m
Fall-Off Test 2: $kh = 0.03$ darcy-m

These low kh values are in conformity with heatup and circulation loss data which indicated little or no permeability in slim hole GH-9.

4.3 Well GH-10

The pressure response during fall-off in well GH-10 is anomalous (Figure 4.3). The rise in downhole pressure during fall-off is most likely due to heating of the water column between the gauge depth (689 m TVD) and the feedzone depth. The fall-off data cannot be used to infer formation transmissivity (kh).

During each of the injection phases, the pressure at first increased abruptly, and then declined slowly. This fall in pressure may be due to (1) cooling of liquid in the interval between the pressure gauge and the feedzone, and (2) hole cleanup. With an initial pressure of 39.3 bars(a) at gauge depth and using the last flowing pressure for each injection interval, we obtain the following estimates for the injectivity index:

$$\text{Injection Test 1: } II = \frac{200}{60(43.8-39.3)} = 0.74 \text{ kg/s-bar}$$

$$\text{Injection Test 2: } II = \frac{700}{60(45.2-39.3)} = 1.98 \text{ kg/s-bar}$$

$$\text{Injection Test 3: } II = \frac{2500}{60(56.3-39.3)} = 2.45 \text{ kg/s-bar}$$

$$\text{Injection Test 4: } II = \frac{1200}{60(45.2-39.3)} = 3.39 \text{ kg/s-bar}$$

Apparently, the injectivity index increases with each injection episode; this indicates a progressive hole cleaning. The injectivity index for GH-10 is, therefore, estimated to be at least 3.39 kg/s-bar.

Continued on page 4-28

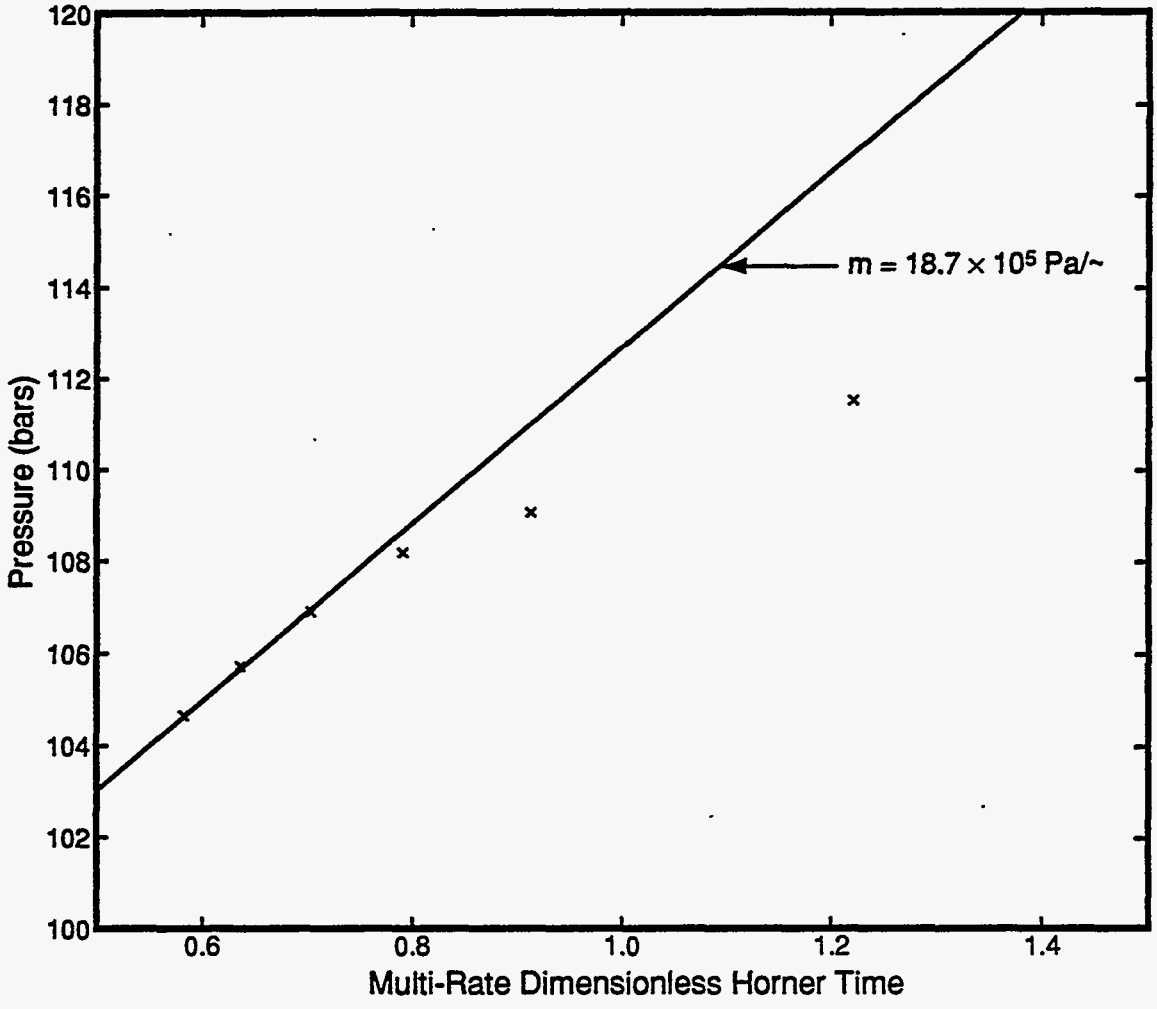

Figure 4.16a. Horner plot of pressure fall-off data no. 1 for slim hole GH-9 (March 22, 1987). The flow rate prior to shutin was 120 kg/min. The gauge depth is 950 m TVD. The feedzone depth for slim hole GH-9 is unknown.

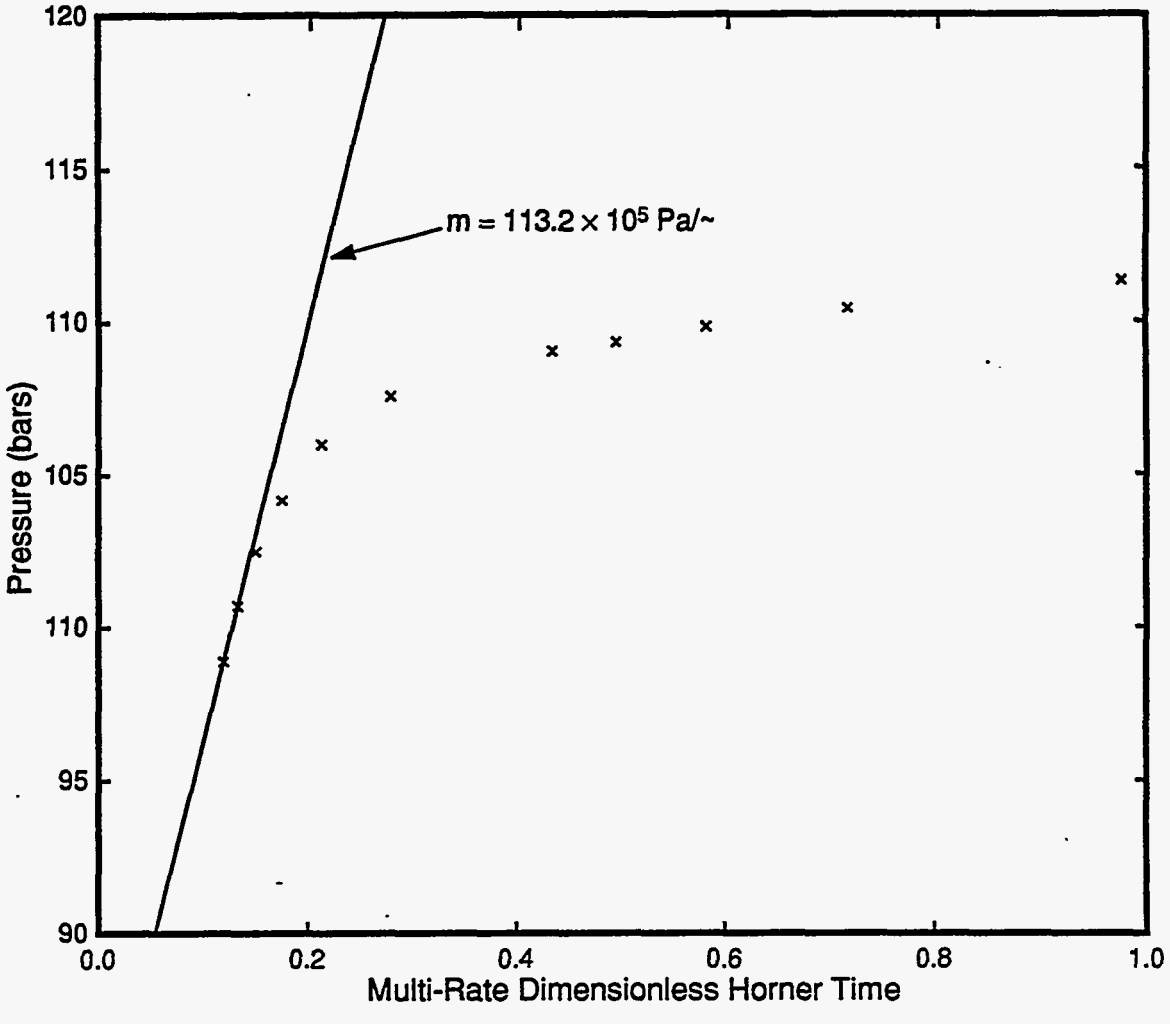

Figure 4.16b. Horner plot of pressure fall-off data no. 2 for slim hole GH-9 (March 22, 1987). The flow rate prior to shutin was 840 kg/min. The gauge depth is 950 m TVD. The feedzone depth for slim hole GH-9 is unknown.

4.4 Well GH-11

During injection testing of well GH-11, the pressure gauge was located within 20 meters of the principal feedzone; the pressure drop in the injection phases is very likely due to hole cleanup. A pressure of 76.5 bars was recorded at the gauge depth prior to the start of cold water injection (Figure 4.4). The pressure measurements taken at the end of each injection interval were used to compute the injectivity index.

$$\text{Injection Test 1: } II = \frac{1000}{60(92.7-76.5)} = 1.03 \text{ kg/s-bar}$$

$$\text{Injection Test 2: } II = \frac{2000}{60(102.6-76.5)} = 1.28 \text{ kg/s-bar}$$

$$\text{Injection Test 3: } II = \frac{3000}{60(109.2-76.5)} = 1.53 \text{ kg/s-bar}$$

The injectivity index increases with each increase in the injection rate. The best estimate for II is 1.53 kg/s-bar.

The pressure fall-off data recorded after each of the three injection tests are displayed in Figures 4.17(a)–(c). At small shutin times ($\Delta t < 15$ minutes), the pressure falls rather rapidly; after a shutin time of about 15 minutes, the pressure fall-off slows down considerably. The late shutin time ($\Delta t \geq 15$ minutes) fall-off data are replotted in Figures 4.17(d)–(f). These late-time fall-off data can be approximated by straight lines (Figure 4.17 d–f). Because of insufficient gauge resolution (Figures 4.17 d–f), there is considerable uncertainty associated with the slope m of each of these straight line fits. With a kinematic viscosity ν of 1.44×10^{-7} m^2/s (corresponding to liquid water at a temperature of 225°C), we obtain the following estimates for formation transmissivity:

Fall-Off No. 1: $kh = 3.7$ darcy-m
Fall-Off No. 2: $kh = 9.0$ darcy-m
Fall-Off No. 3: $kh = 8.1$ darcy-m

The average value of kh obtained from the three fall-off tests is thus 6.9 darcy-m.

4.5 Well GH-12

The pressure and temperature tool in well GH-12 was located about 240 meters below the main feedzone. The temperature at the gauge depth displays a slight increase (Figure 4.5) during the injection tests. These temperature data indicate that the injected fluid is being lost above the gauge depth. Prior to the start of cold water injection, the pressure at gauge depth was 69.1 bars(a). The pressure record for each of the three injection rates was used to compute the injectivity index.

Continued on page 4-35

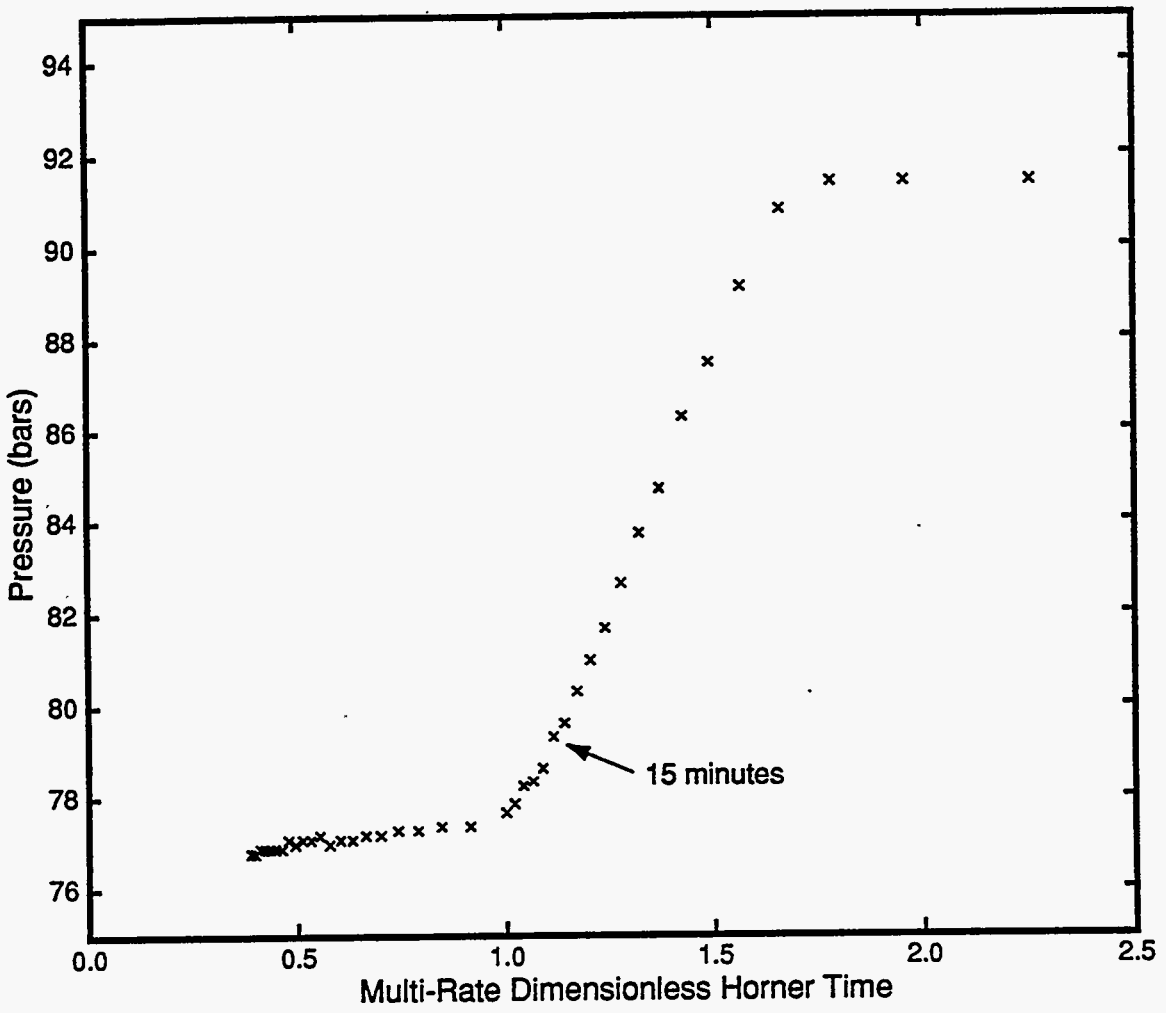

Figure 4.17a. Horner plot of pressure fall-off data no. 1 for well GH-11 (March 30, 1988).

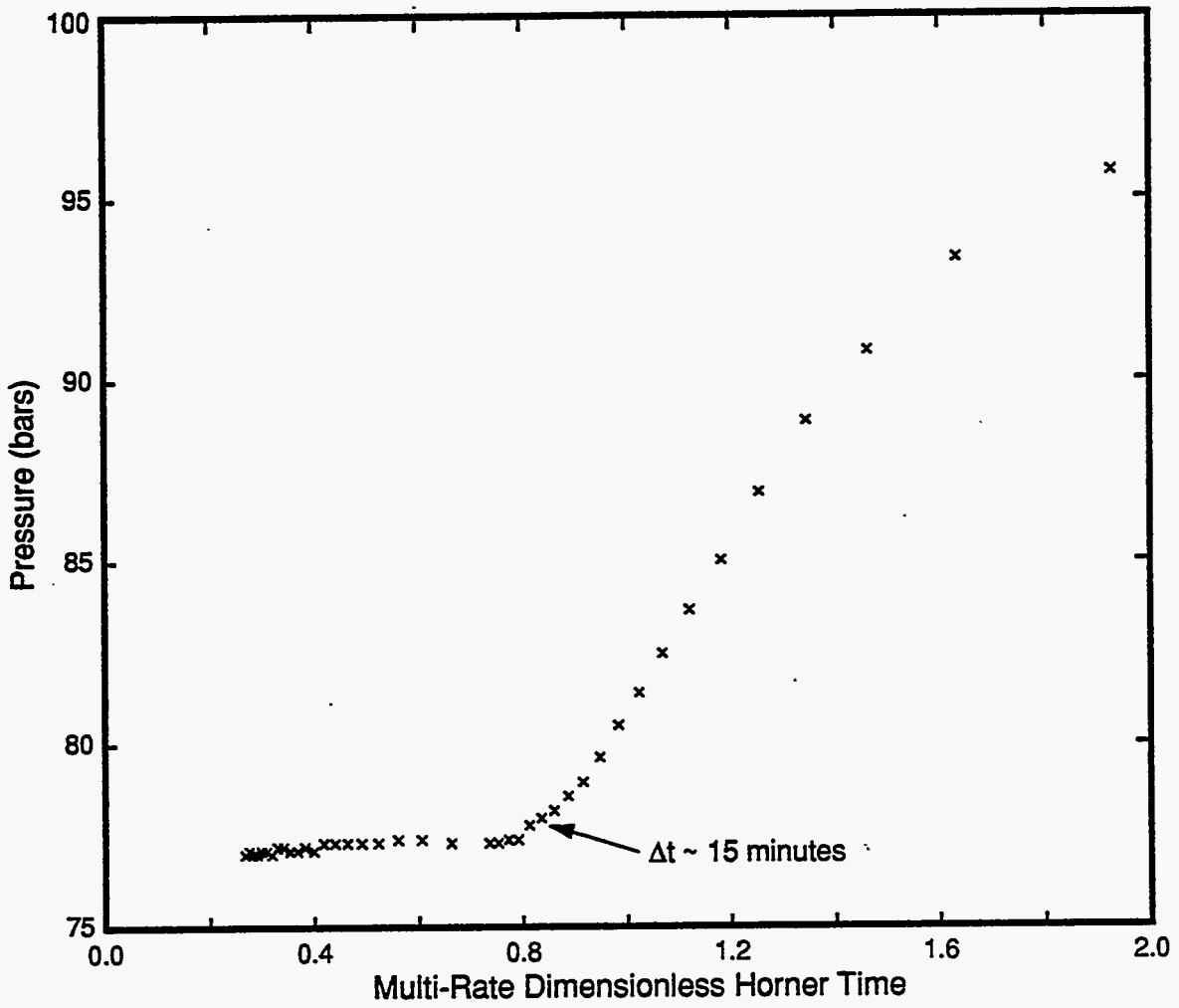

Figure 4.17b. Horner plot of pressure fall-off data no. 2 for well GH-11 (March 30, 1988).

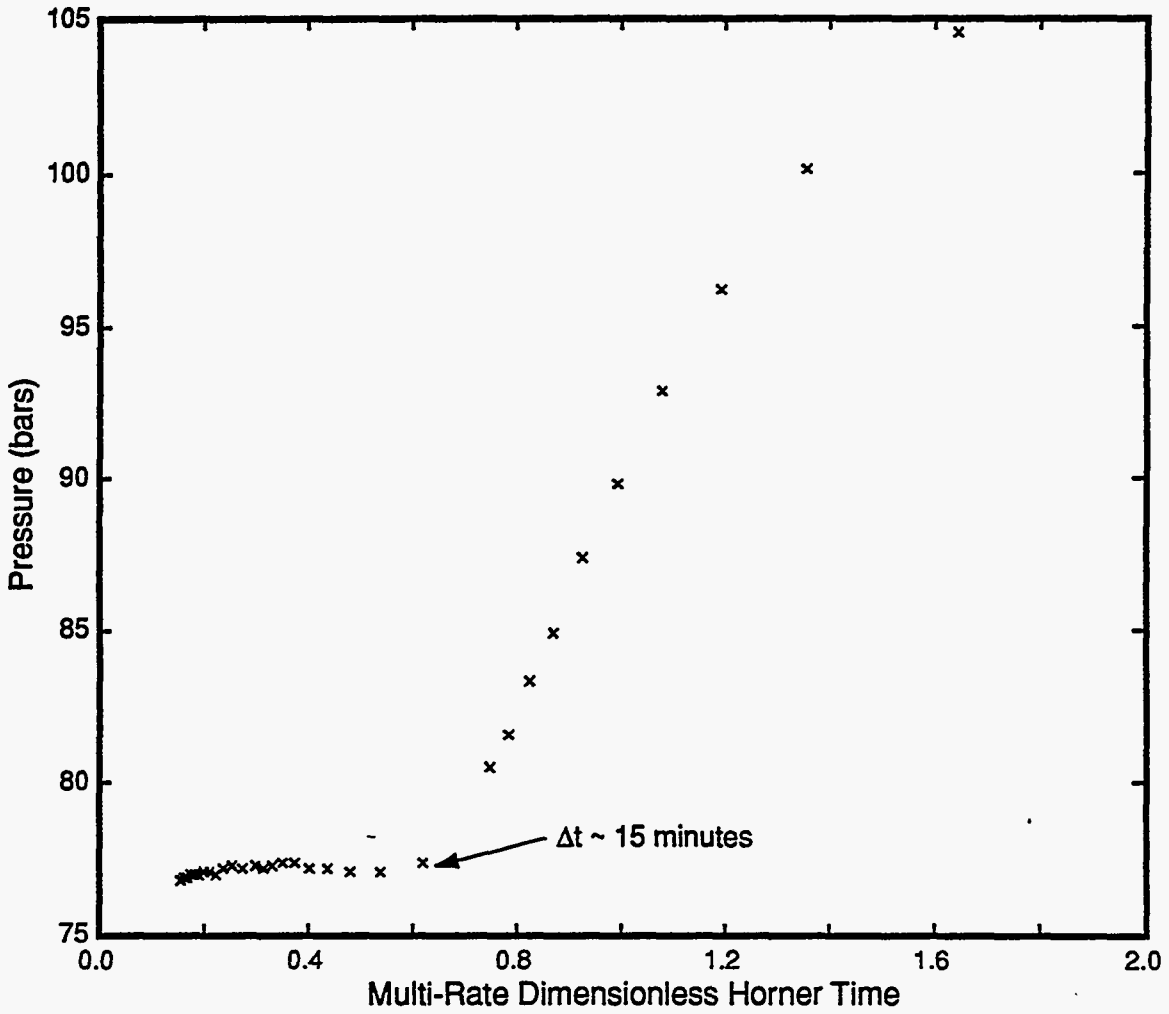

Figure 4.17c. Horner plot of pressure fall-off data no. 3 for well GH-11 (March 30, 1988).

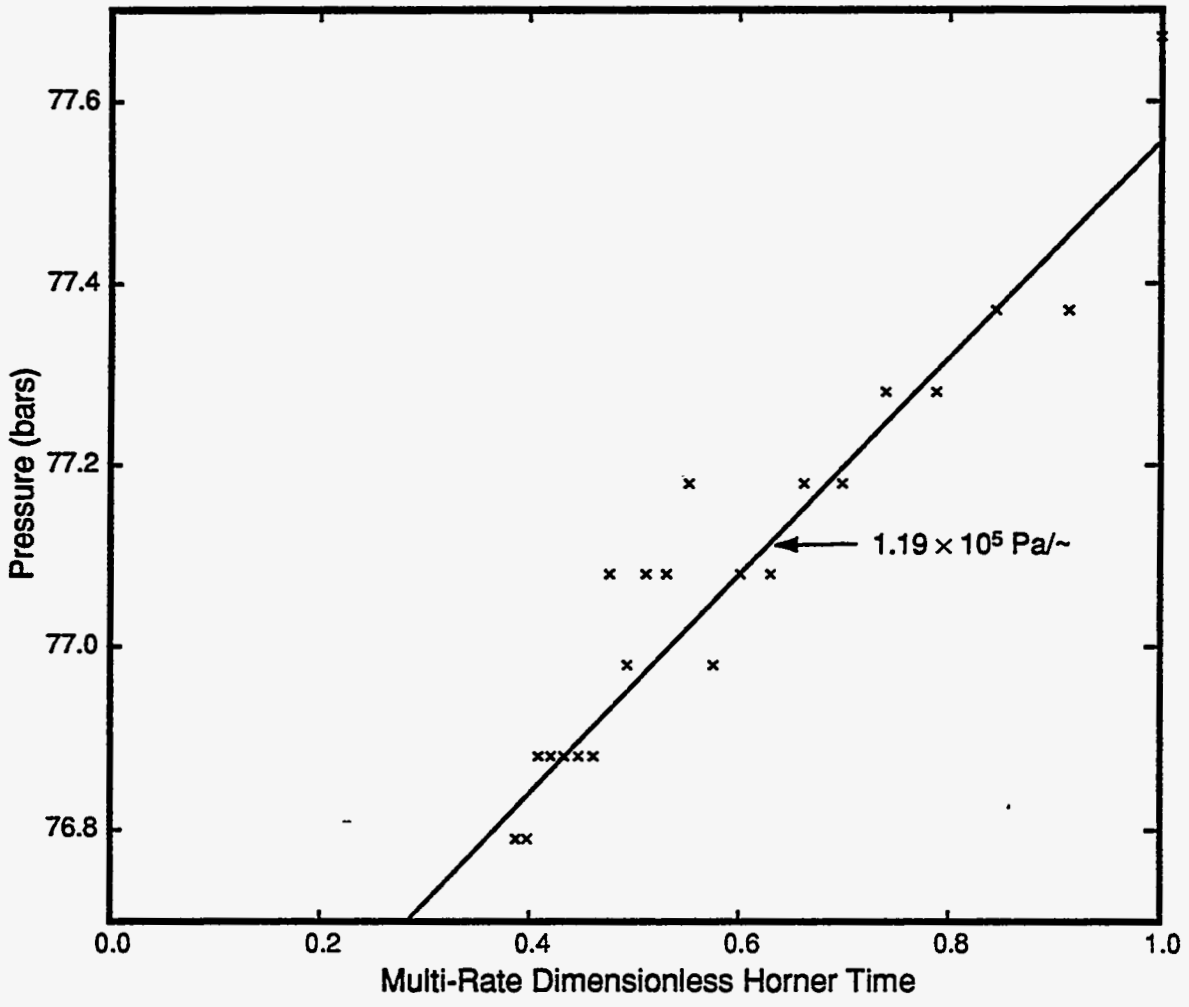

Figure 4.17d. Horner plot of pressure fall-off data no. 1 (late shutin time) for well GH-11 (March 30, 1988).

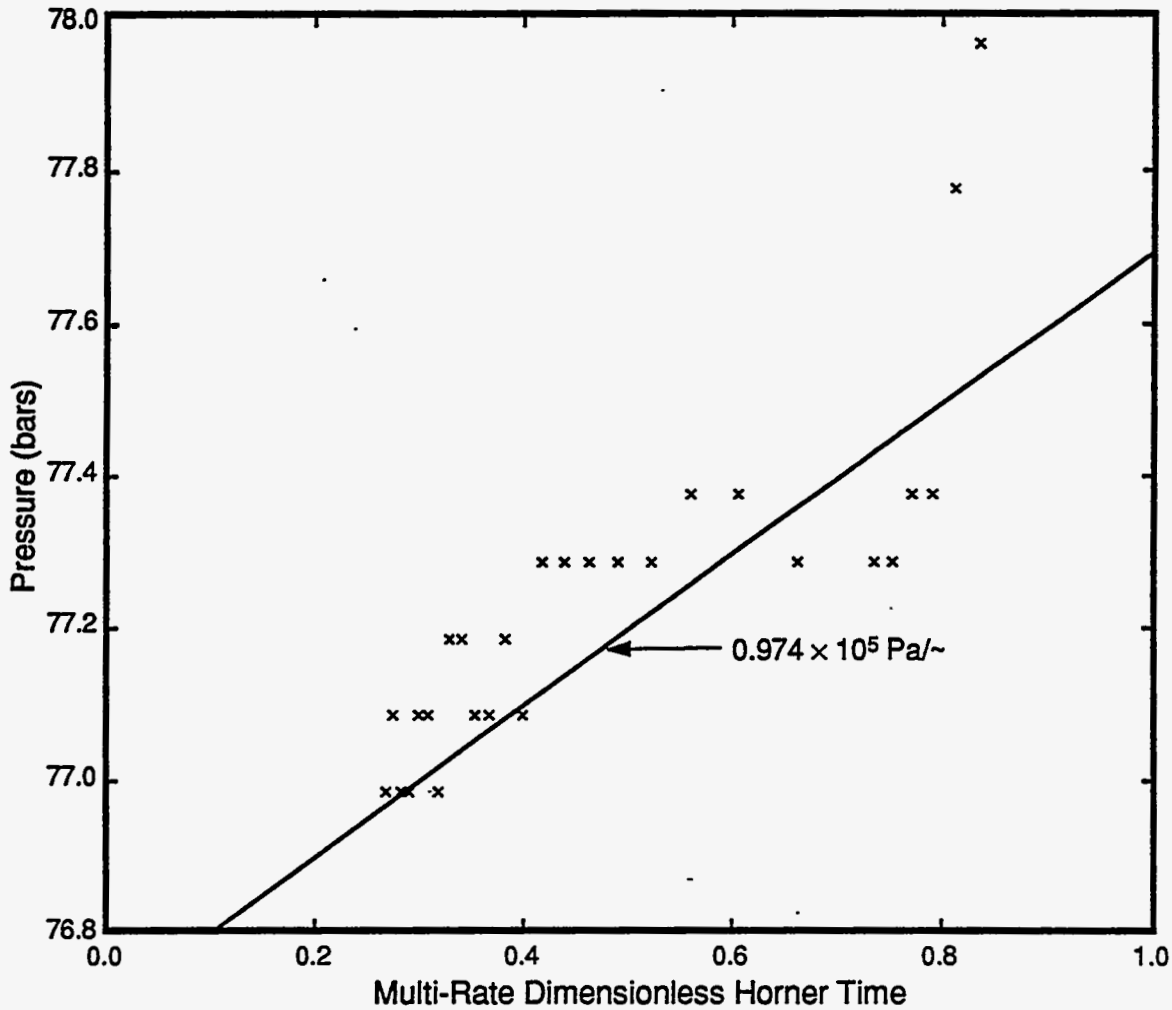

Figure 4.17e. Horner plot of pressure fall-off data no. 2 (late shutin time) for well GH-11 (March 30, 1988).

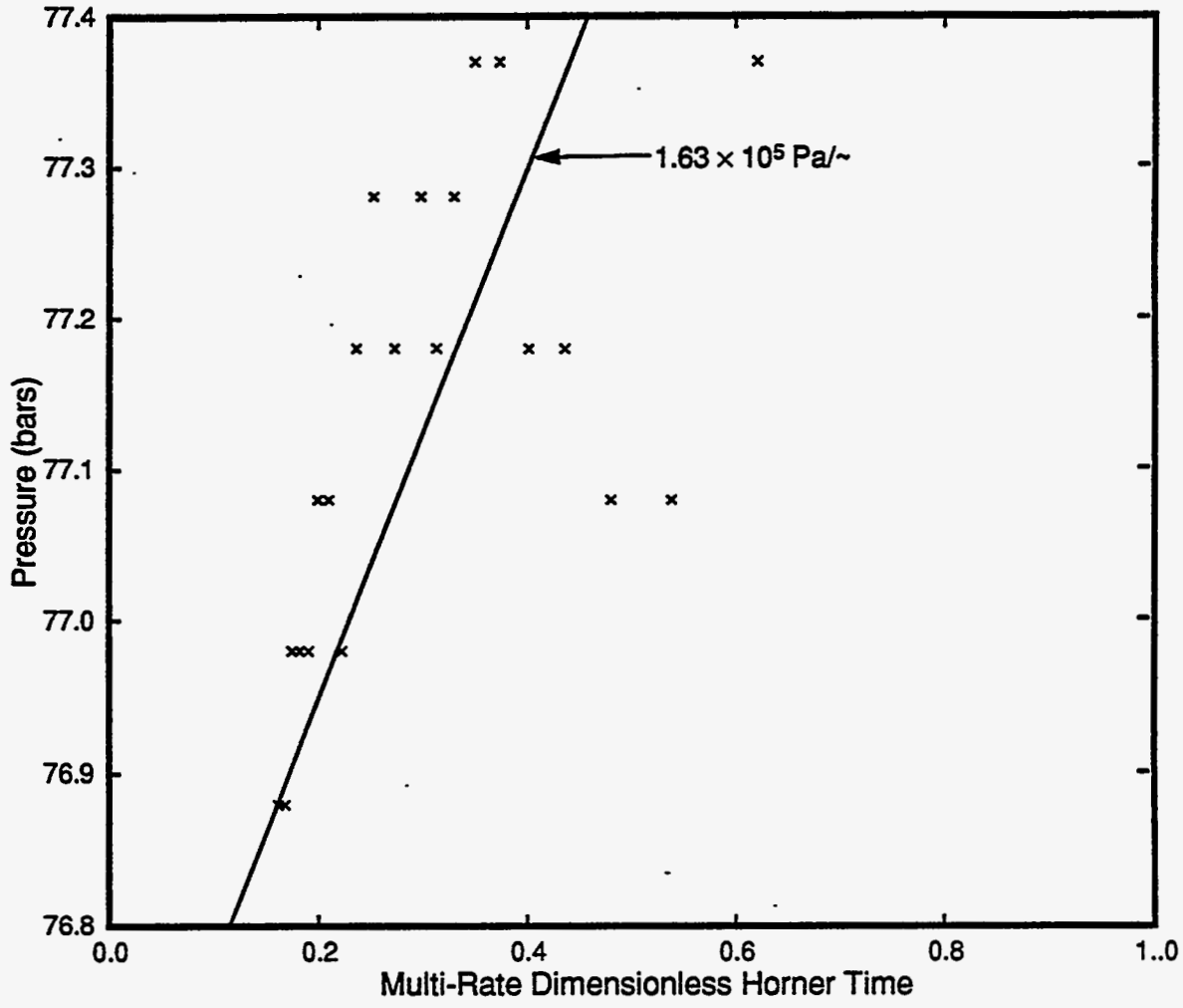

Figure 4.17f. Horner plot of pressure fall-off data no. 3 (late shutin time) for well GH-11 (March 30, 1988).

$$\text{Injection Test 1: } II = \frac{1000}{60(71.3-69.1)} = 7.58 \text{ kg/s-bar}$$

$$\text{Injection Test 2: } II = \frac{2000}{60(77.8-69.1)} = 3.83 \text{ kg/s-bar}$$

$$\text{Injection Test 3: } II = \frac{4300}{60(87.2-69.1)} = 3.96 \text{ kg/s-bar}$$

The average value of the injectivity index is 5.12 kg/s-bar.

The Horner plots of pressure fall-off data for the three injection tests are displayed in Figures 4.18(a)–(c). In each case, the late shutin time fall-off data can be approximated by a straight line. Assuming that kinematic viscosity ν is 1.44×10^{-7} m²/s (liquid water at a temperature of 225°C), we obtain the following estimates for formation kh.

Fall-Off Test 1: $kh = 5.4$ darcy-m
Fall-Off Test 2: $kh = 4.8$ darcy-m
Fall-Off Test 3: $kh = 5.1$ darcy-m

The average value of formation transmissivity is 5.1 darcy-m.

4.6 Well GH-15

Well GH-15 was injection tested on three separate occasions in October 1990, November 1990, and October 1991. In the October 1990 and November 1990 injection tests, the pressure/temperature tool was placed within a few meters of the principal feedzone for Well GH-15 (see Figures 4.6a and 4.6b). Using the pressures recorded both prior to and during these injection tests, we obtain the following estimates for formation injectivity:

Injection Test No. 1 (October 12, 1990)

$$M = 500 \text{ kg/min}, \; II = \frac{500}{60(56.4-51.8)} = 1.81 \text{ kg/s-bar}$$

$$M = 800 \text{ kg/min}, \; II = \frac{800}{60(59.2-51.8)} = 1.80 \text{ kg/s-bar}$$

Injection Test No. 2 (November 18, 1990)

$$M = 470 \text{ kg/min}, \; II = \frac{470}{60(54.0-49.2)} = 1.63 \text{ kg/s-bar}$$

$$M = 840 \text{ kg/min}, \; II = \frac{840}{60(57.1-49.2)} = 1.77 \text{ kg/s-bar}$$

Continued on page 4-39

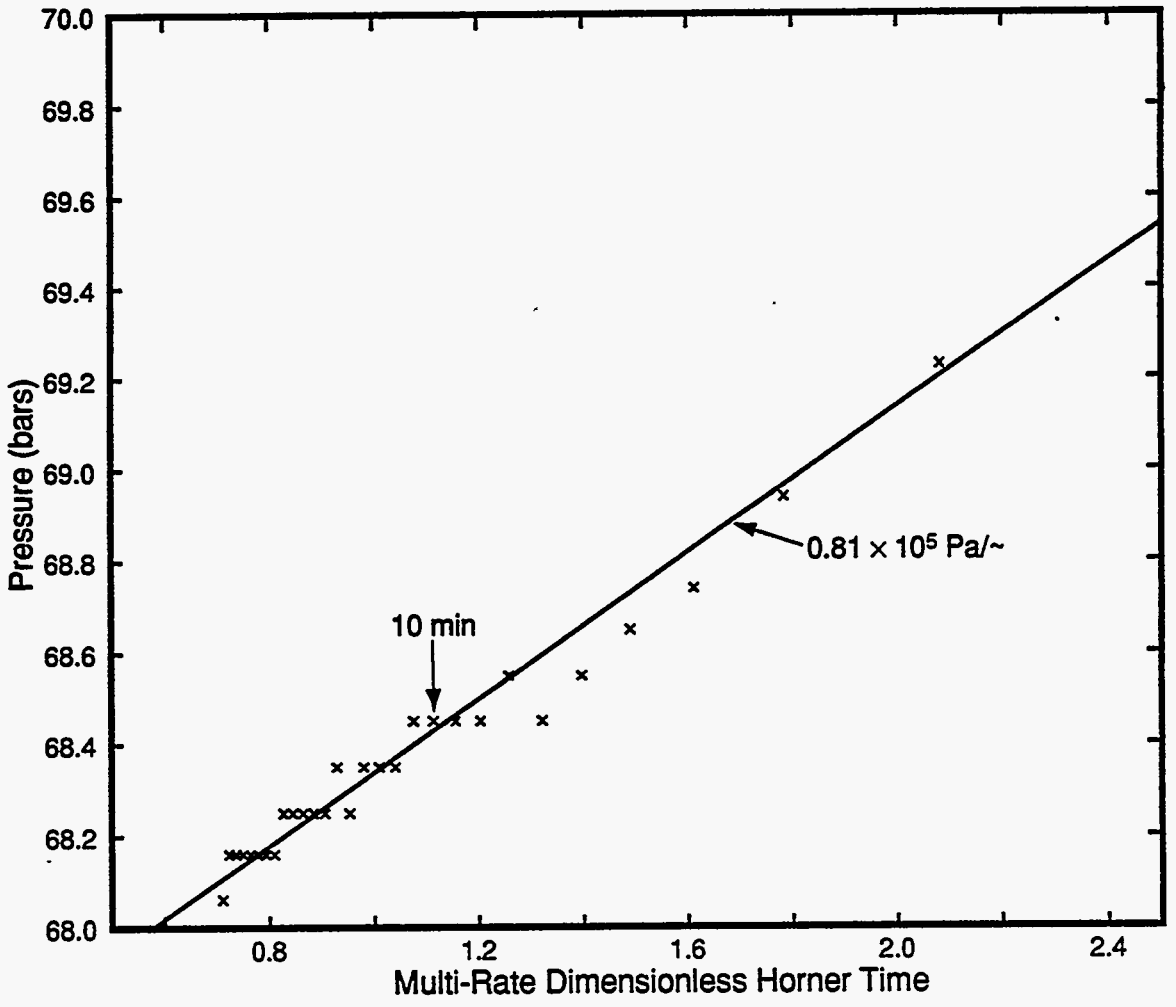

Figure 4.18a. Horner plot of pressure fall-off data no. 1 for well GH-12 (February 14, 1989).

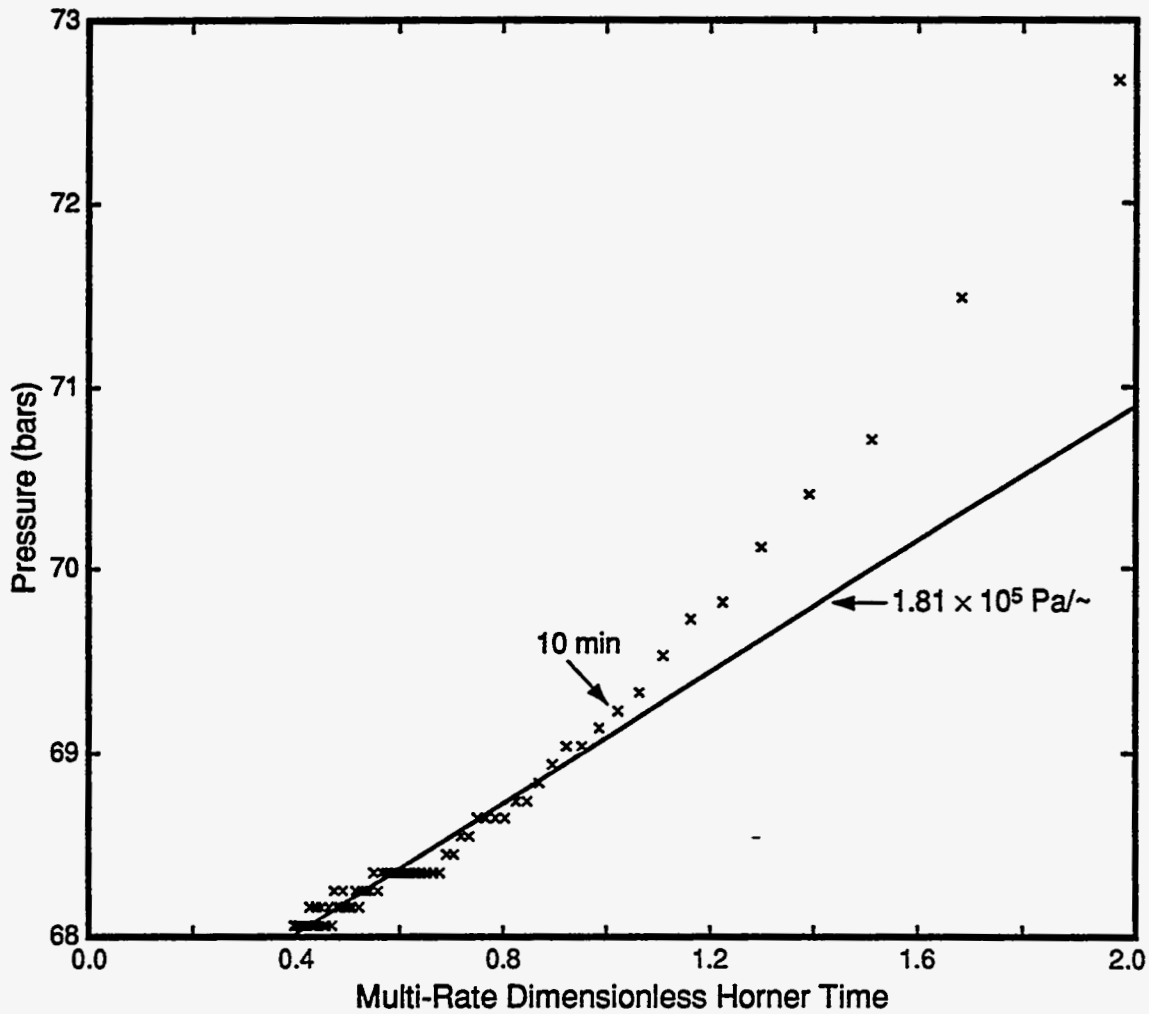

Figure 4.18b. Horner plot of pressure fall-off data no. 2 for well GH-12 (February 14, 1989).

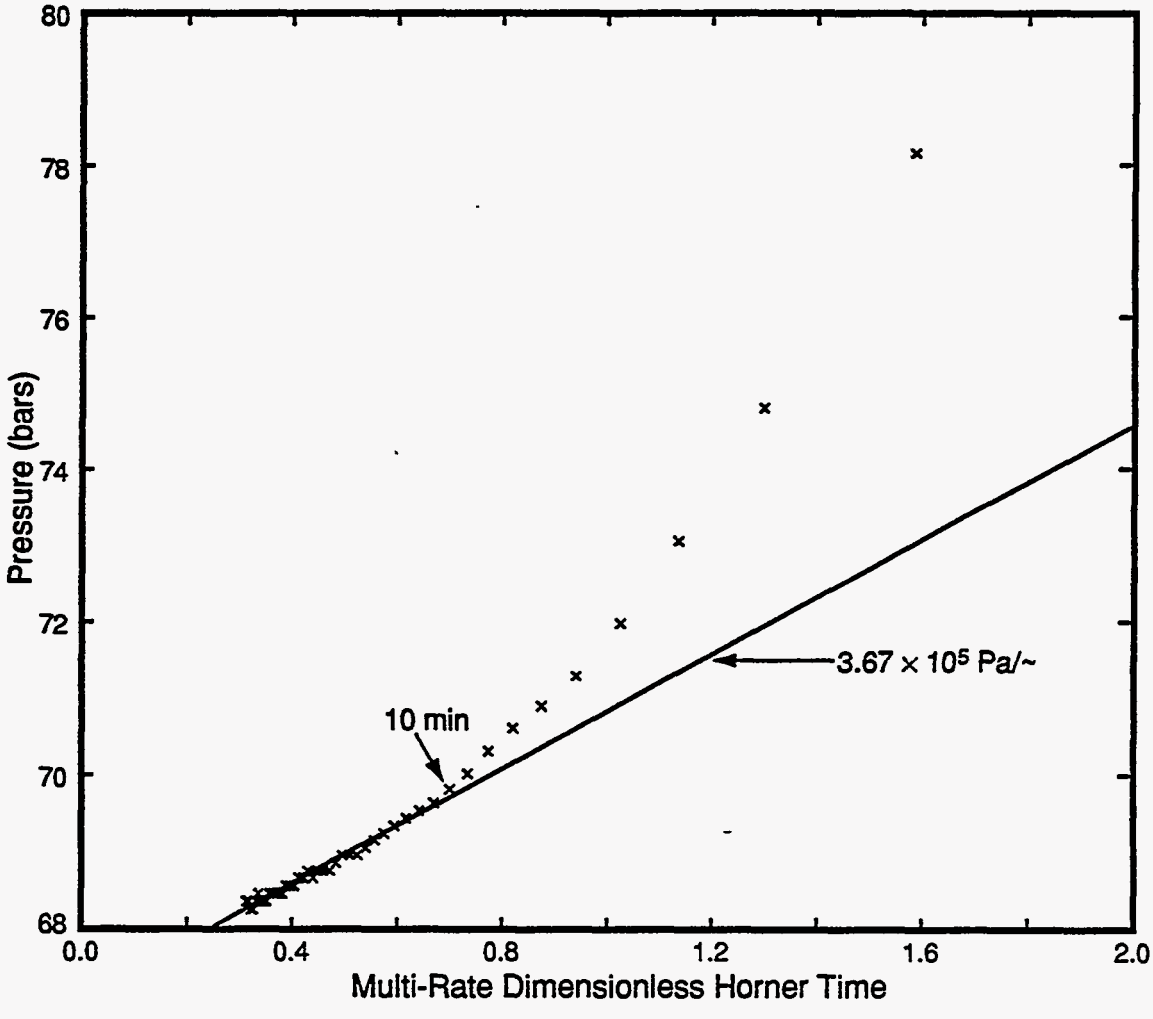

Figure 4.18c. Horner plot of pressure fall-off data no. 3 for well GH-12 (February 14, 1989).

In the October 1991 injection test, no continuous pressure recording was made during the injection phase; instead, a pressure/temperature/spinner tool was used to make two separate downhole runs. Since no downhole pressure recordings were made prior to this injection test, the pressure prior to the injection test was assumed equal to the stable feedzone pressure (50.5 bars). Using the pressures recorded by the PTS tool, the injectivity index is estimated as follows:

$$M = 610 \text{ kg/min}, \; II = \frac{610}{60(57.9 - 50.5)} = 1.38 \text{ kg/s-bar}$$

$$M = 820 \text{ kg/min}, \; II = \frac{820}{60(60.1 - 50.5)} = 1.42 \text{ kg/s-bar}$$

Since the initial pressure (*i.e.*, pressure prior to the injection test) was not recorded during the October 1991 test, the above estimates for the injectivity index are not as reliable as those obtained from the two 1990 tests. The average value of the injectivity index from the two 1990 tests is 1.75 kg/s-bar.

After the October 1991 injection test, the pressure fall-off data were monitored by a downhole gauge placed at 596 m TVD (*i.e.*, approximately 84 meters above the main feedzone). Because of the heatup of the fluid column in the depth interval from 596 m TVD to 680 m TVD, the pressure fall-off at the gauge depth is likely to be slower than at the feedzone depth. Horner plots of pressure fall-off data for the three injection tests are shown in Figures 4.19 (a-c). In each case, a straight line can be fit to the fall-off data. With a kinematic viscosity ν of 1.44×10^{-7} m^2/s (liquid water at a temperature of 225°C), the following estimates for *kh* are obtained:

Fall-Off Test No. 1: $kh = 0.93$ darcy-m
Fall-Off Test No. 2: $kh = 0.91$ darcy-m
Fall-Off Test No. 3: $kh = 1.9$ darcy-m

Because of the gauge location in the October 1991 test, the *kh* value from this test (Fall-Off Test No. 3) is not considered to be reliable. The best estimate for *kh* (0.92 darcy-m) is obtained by averaging *kh* values from the first two fall-off tests.

4.7 Well GH-17

No downhole temperature data are available for the two injection tests of well GH-17. The pressure tool was placed (at ~ 810 m TVD) about 50 meters below the principal feedzone at 760 m TVD during the injection test of November 7, 1991. Using $P_i = 61.2$ bars(a) and $P_f = 75.6$ bars(a), the injectivity index is given by

$$II = \frac{106}{60(75.6 - 61.2)} = 0.12 \text{ kg/s-bar}$$

Continued on page 4-43

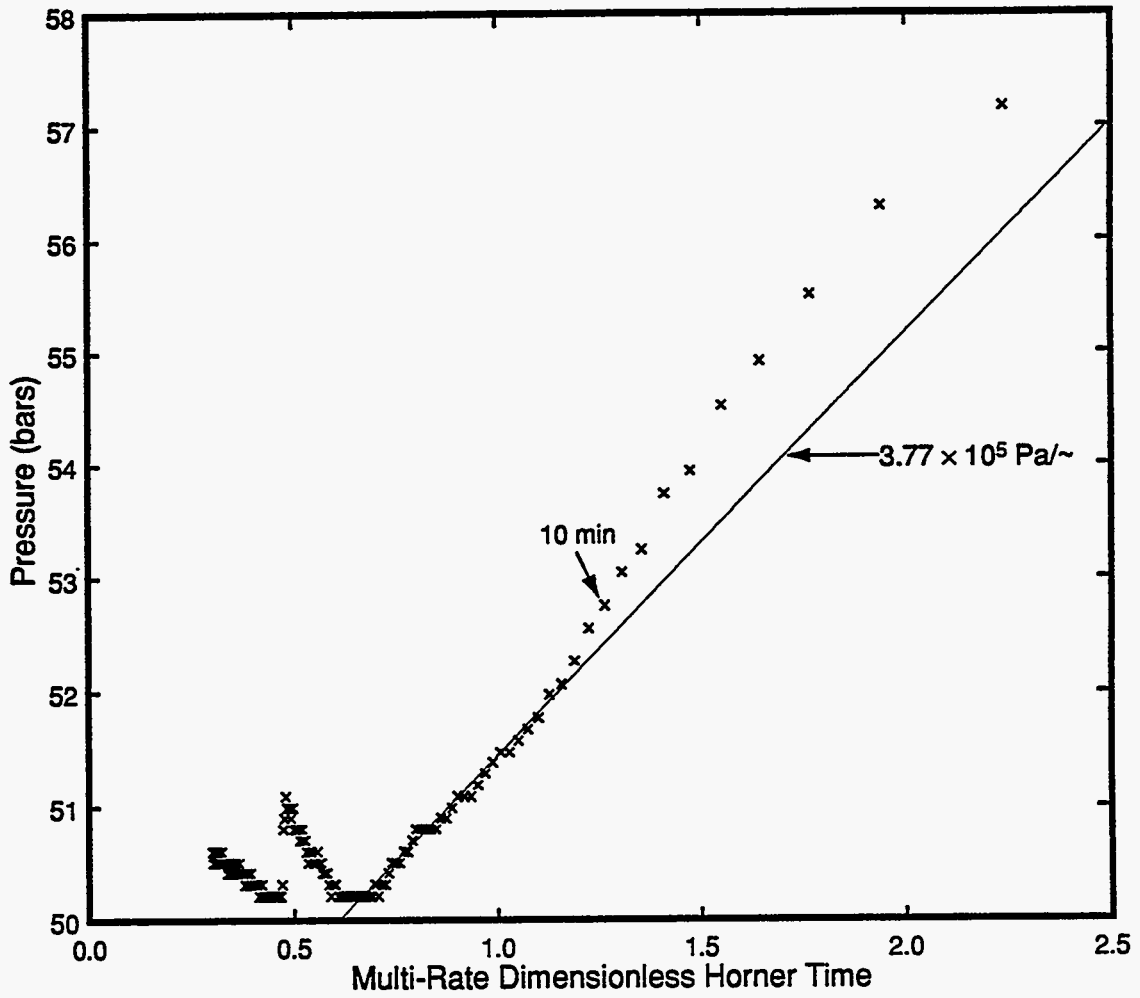

Figure 4.19a. Horner plot of pressure fall-off data no. 1 for well GH-15 (October 12, 1990).

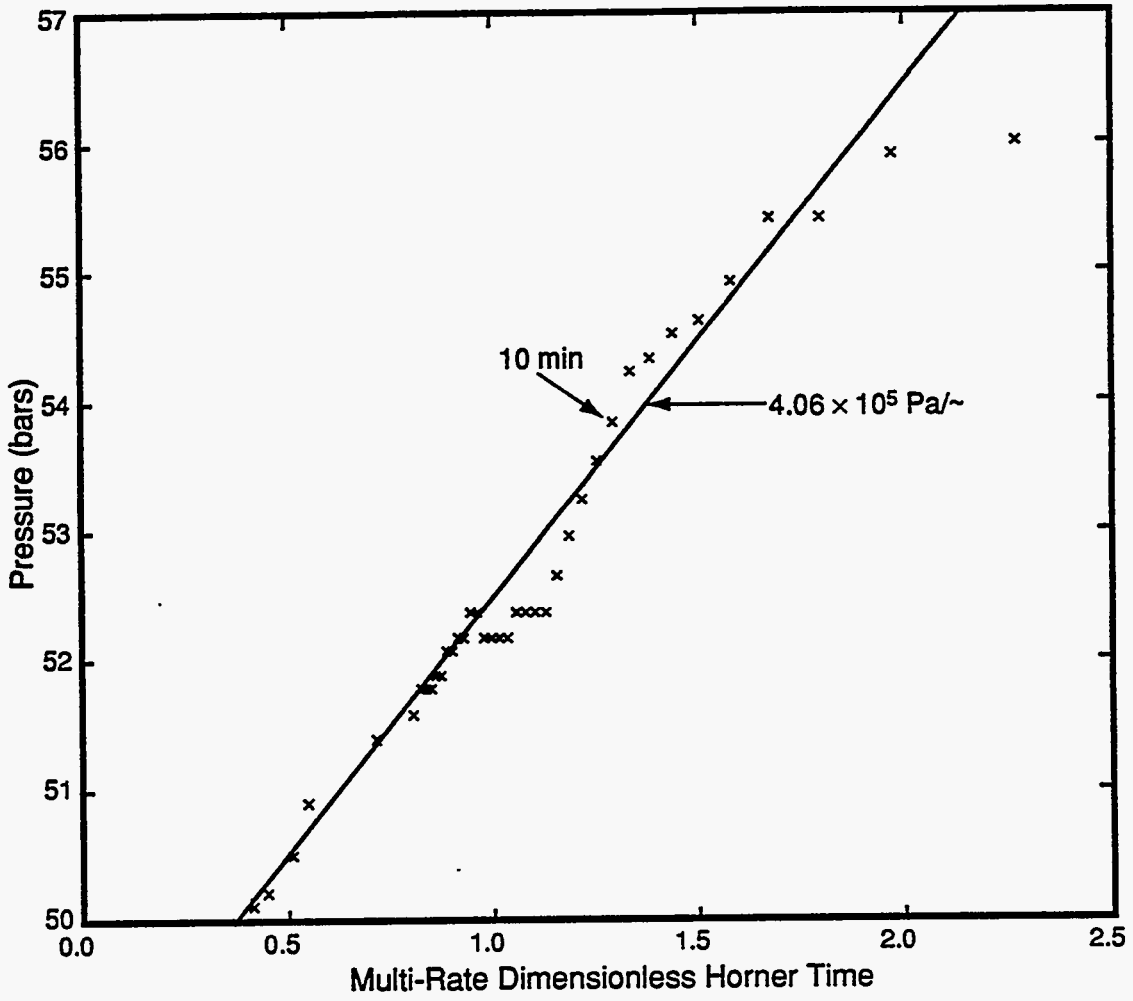

Figure 4.19b. Horner plot of pressure fall-off data no. 2 for well GH-15 (November 18, 1990).

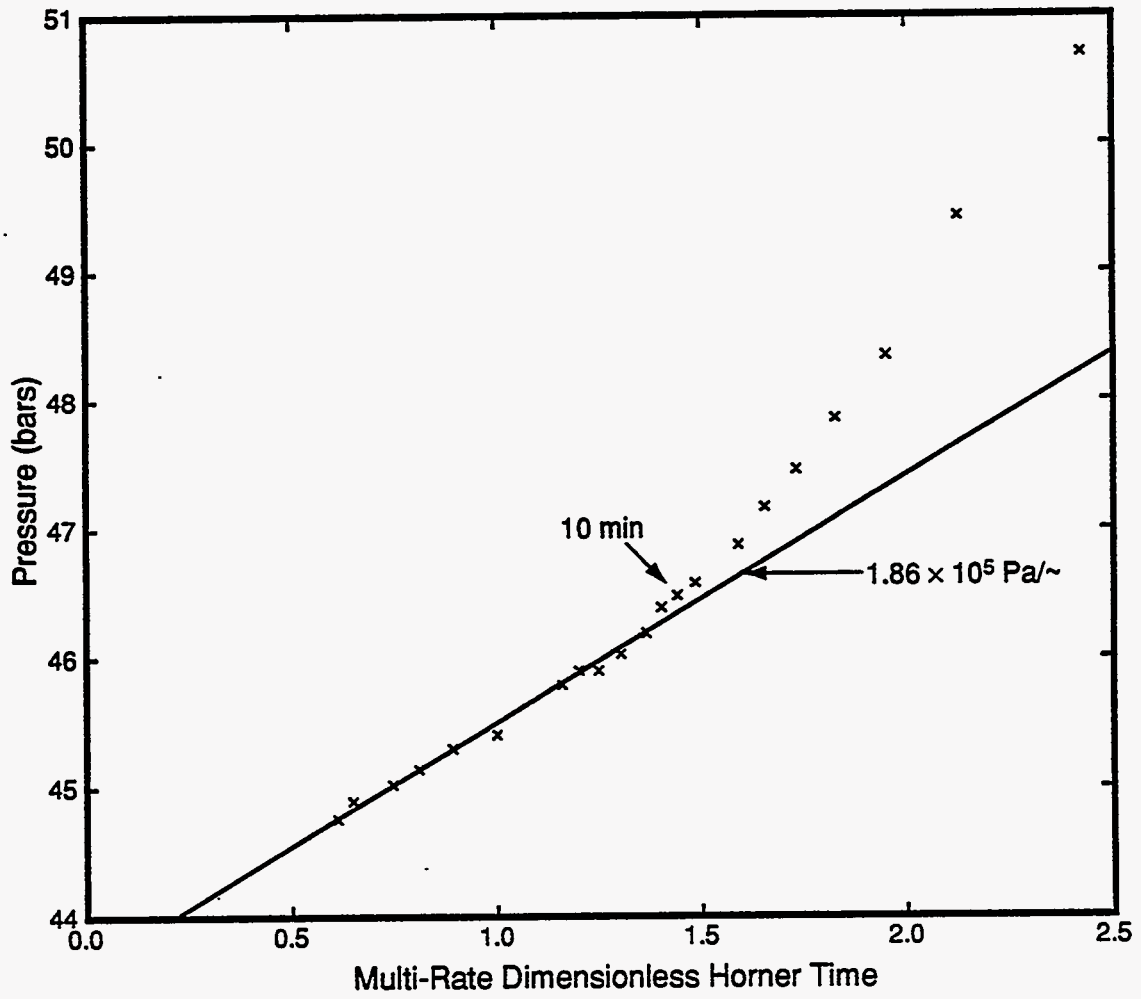

Figure 4.19c. Horner plot of pressure fall-off data no. 3 for well GH-15 (October 24, 1991).

The gauge depth for the injection test of November 22, 1991 is not known. Judging from the measured pre-injection pressures (61.2 bars on November 7, 1991 versus 68.0 bars on November 22, 1991), it would appear that the gauge depth for the November 22, 1991 test is deeper than 880 m TVD (*i.e.*, more than 120 meters below the principal feedzone for GH-17). The injectivity index for the second injection test is

$$II = \frac{113}{60(72.1 - 68.0)} = 0.46 \text{ kg/s-bar}$$

The above results imply that the injectivity index increased substantially during the two injection tests. The best estimate for the injectivity index is given by the second injection test ($II = 0.46$ kg/s-bar).

Horner plots of pressure fall-off data from the two injection tests of well GH-17 are shown in Figures 4.20 (a) and (b); the late shutin time fall-off data do asymptote to straight lines. Using a kinematic viscosity of $1.44 \times 10^{-7} m^2/s$, we obtain for kh:

Fall-Off Test 1: $kh = 0.04$ darcy-m
Fall-Off Test 2: $kh = 0.14$ darcy-m

Like the injectivity index, the formation transmissivity appears to have improved considerably between the two tests. This increase in kh is most likely associated with hole cleanup and a reduction in near wellbore formation damage. In any case, the formation transmissivity in the vicinity of well GH-17 is rather low.

4.8 Well GH-19

No continuous recordings of downhole pressure and temperature were made during the injection test of well GH-19 on December 26 and 27, 1991. A PTS tool was run in the hole once during each of the two constant rate injection periods shown in Figure 4.8. Prior to the start of injection test, a pressure of 52.22 bars(a) was measured on December 25, 1991 at 755 m TVD. Using the pressures measured with the PTS tool, the injectivity index is computed as follows:

$$M = 67 \text{ tons/hour}, \quad II = \frac{67000}{3600(53.02 - 52.22)} = 23.3 \text{ kg/s-bar}$$

$$M = 136 \text{ tons/hour}, \quad II = \frac{136000}{3600(53.56 - 52.22)} = 28.2 \text{ kg/s-bar}$$

The average value of the injectivity index is 25.7 kg/s-bar.

Continued on page 4-46

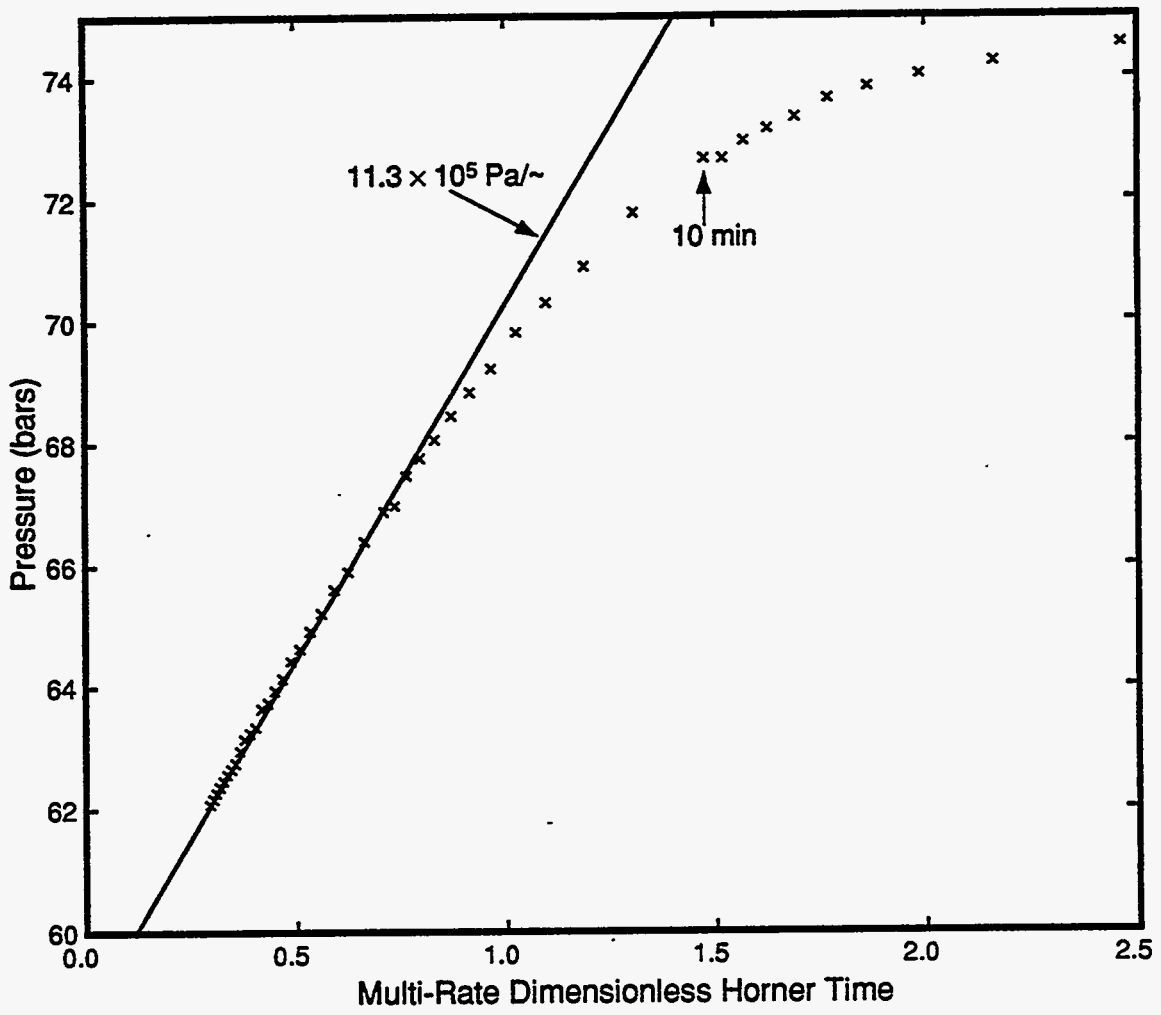

Figure 4.20a. Horner plot of pressure fall-off data no. 1 for well GH-17 (November 7, 1991).

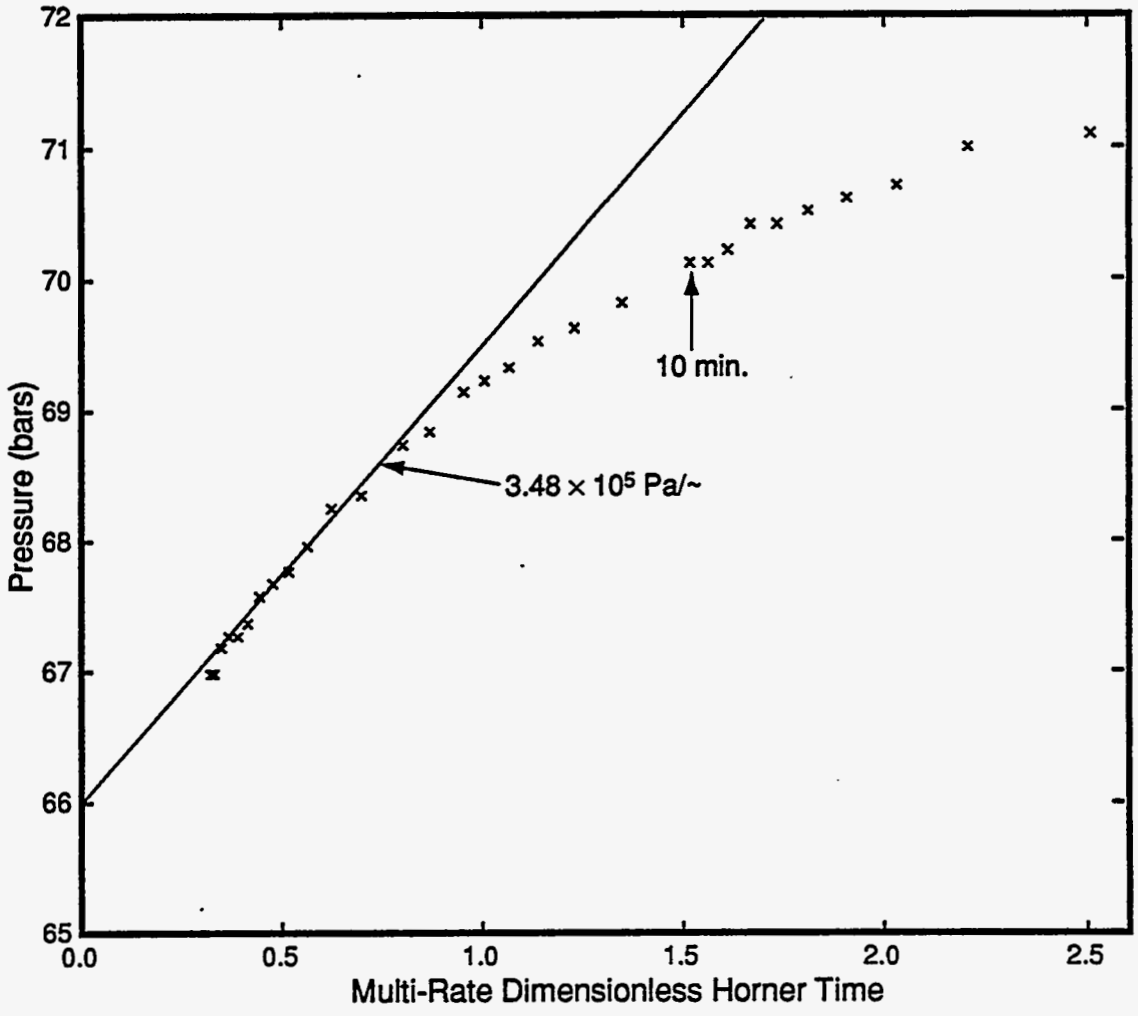

Figure 4.20b. Horner plot of pressure fall-off data no. 2 for well GH-17 (November 22, 1991).

Following cold fluid injection, the pressure fall-off response of GH-19 was recorded by placing a pressure tool at 755 m TVD (*i.e.*, within a few meters of the principal feedzone at 750 m TVD). A Horner plot of the pressure fall-off data is shown in Figure 4.21. For some unknown reason, the pressures fall below the pre-injection pressure (52.22 bars(a)) recorded at the gauge depth. We are unable to identify a straight line segment of sufficient duration (about 1 log cycle) on the Horner plot. Accordingly, we suggest that the pressure fall-off data cannot be interpreted to yield an estimate for formation transmissivity.

4.9 Well GH-20

The downhole pressures and temperatures recorded during the two injection tests of well GH-20 are displayed in Figure 4.9 (a) and (b). Prior to the low rate (1000 kg/min) injection test of April 1, 1991, a pressure of 111 bars(a) was recorded at 1550 m TVD (*i.e.*, ~ 10 meters above the feedzone); the pressure in well GH-20 was increasing slowly at this time. Towards the end of the injection period on April 1, 1991, the pressure was declining slowly (Figure 4.9a). Using P_f = 116.7 bars(a), a lower limit on the injectivity index is calculated as follows:

$$II = \frac{1000}{60(116.7-111.1)} = 2.98 \text{ kg/s-bar}$$

According to EPDC, the pressure readings taken during the second injection test on April 2, 1991 may be suspect. (The pressure tool employs a strain gauge type pressure transducer; the response of this tool depends on the rate of change of temperature. A large rate of change of temperature introduces an error of unknown magnitude in the pressure readings.) A pressure of 112.8 bars(a) was recorded at 1550 m TVD before the start of the second injection test. With a final flowing pressure value of 120.9 bars(a), the injectivity index is given by:

$$II = \frac{3800}{60(120.9-112.8)} = 7.82 \text{ kg/s-bar}$$

The improvement in injectivity index with an increase in injection rate is most likely due to a cleanup of the borehole. The best estimate for the injectivity index is 7.82 kg/s-bar.

Horner plots of pressure fall-off data from the two injection tests are displayed in Figures 4.22 (a) and (b). The pressure fall-off data in Figure 4.22 (b) exhibit an anomalous behavior (an increase in pressure) at very large shutin times; we suspect that a gauge malfunction is involved. Using the straight line approximations to fall-off data shown in Figures 4.22 (a) and (b) and

Continued on page 4-50

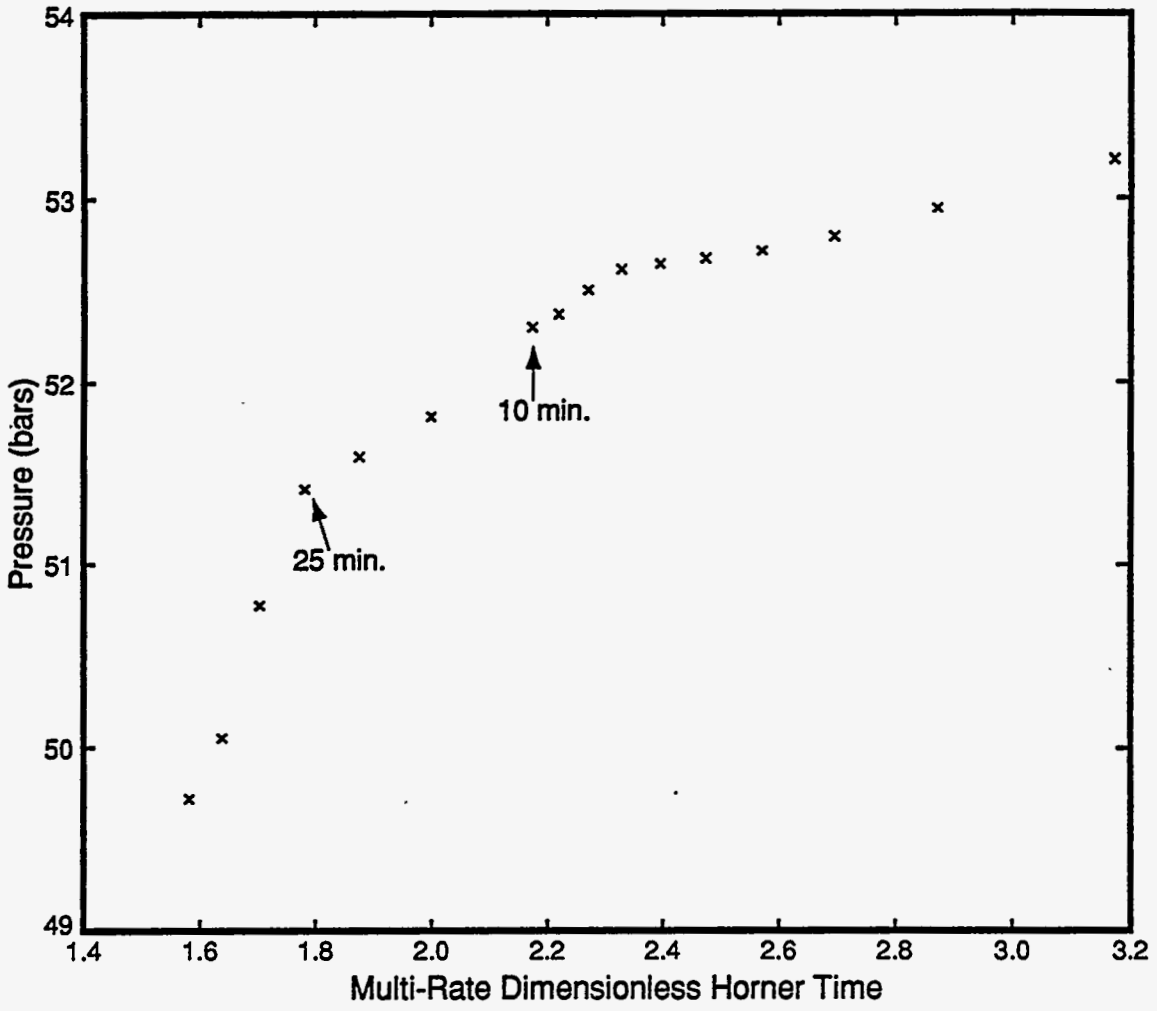

Figure 4.21. Horner plot of pressure fall-off data for well GH-19 (December 27, 1991).

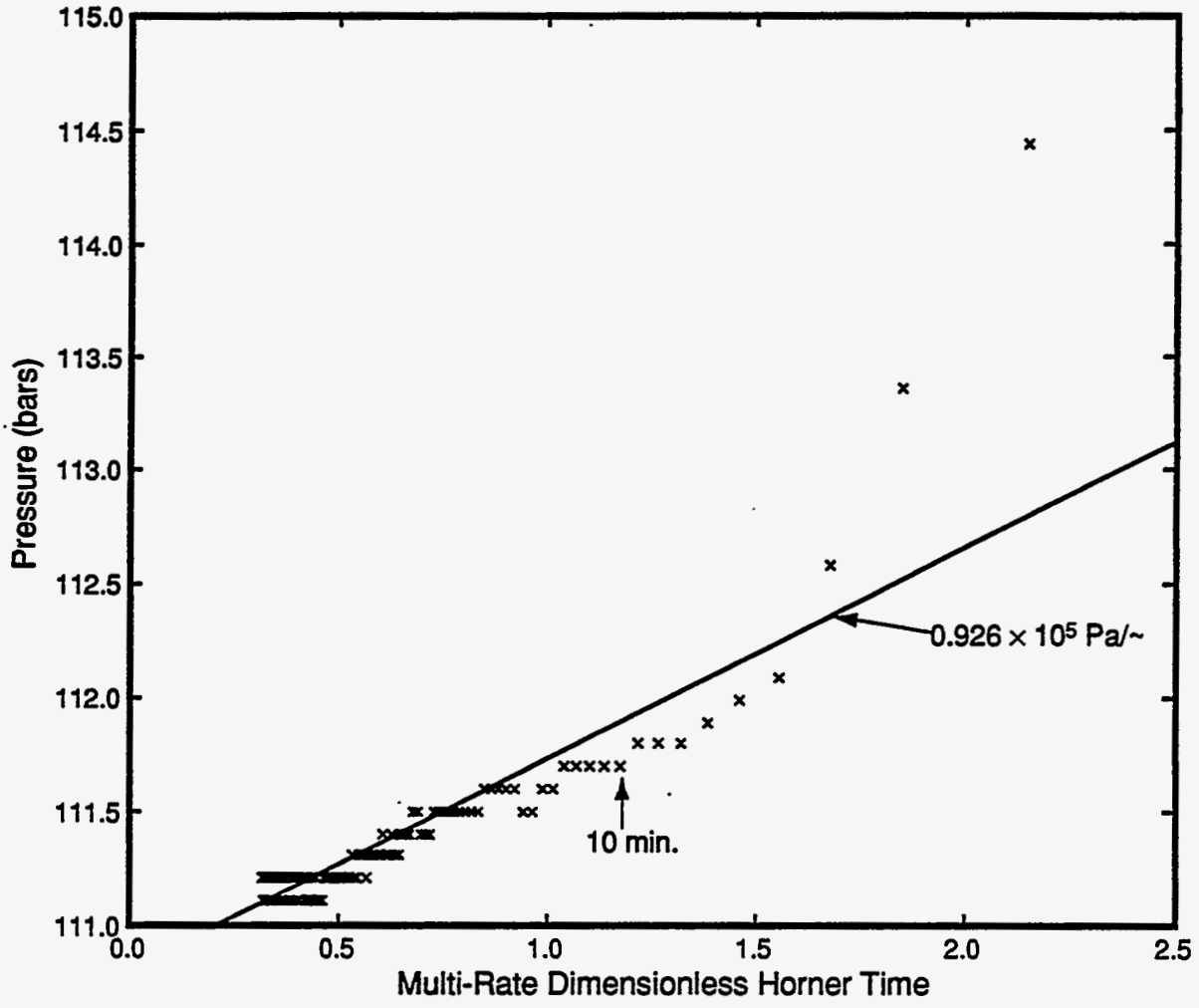

Figure 4.22a. Horner plot of pressure fall-off data no. 1 for well GH-20 (April 1, 1991).

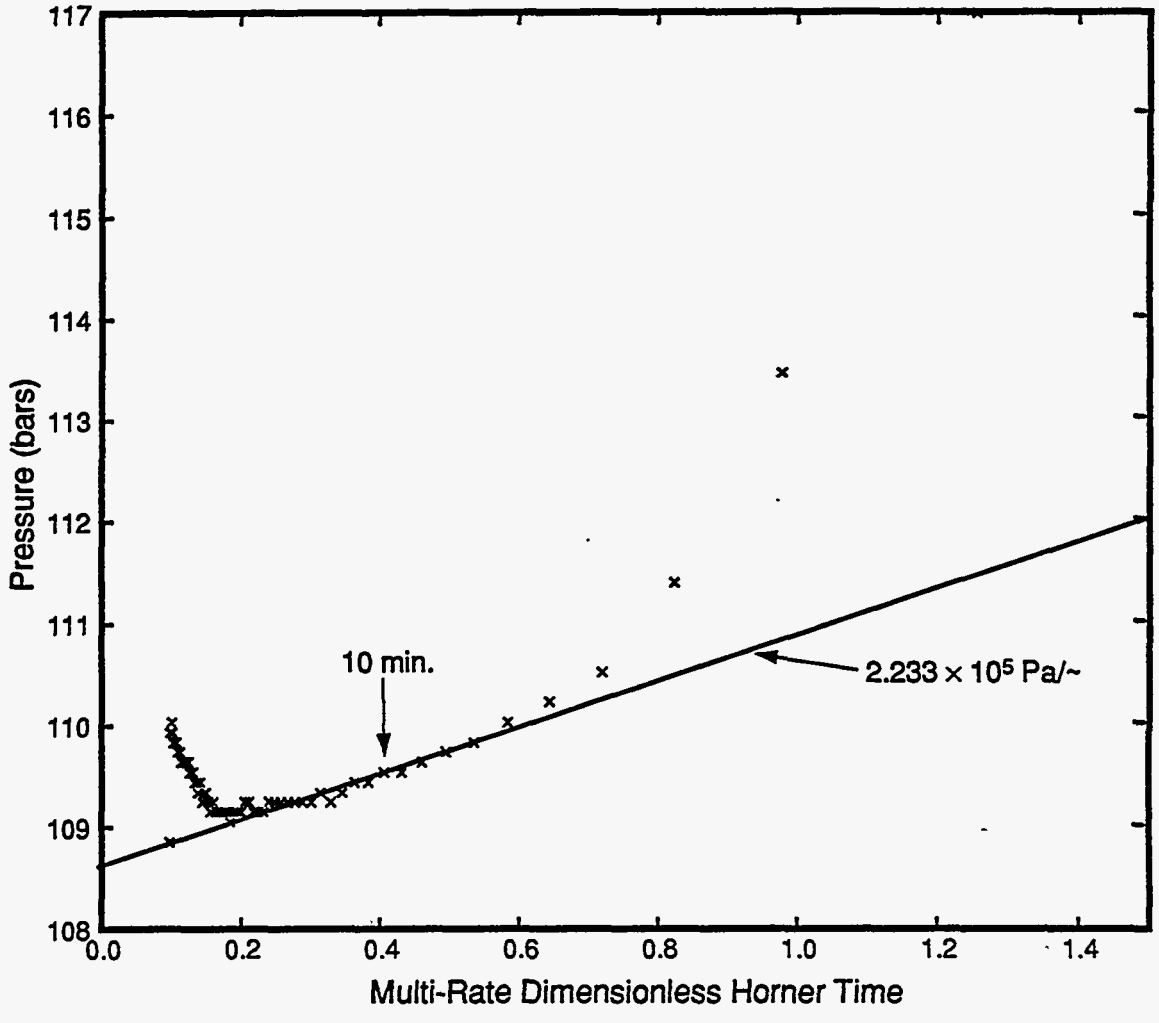

Figure 4.22b. Horner plot of pressure fall-off data no. 2 for well GH-20 (April 2, 1991).

putting kinematic viscosity $\nu = 1.44 \times 10^{-7}$ m²/s, formation transmissivity is given by:

Fall-Off Test 1: $kh = 4.7$ darcy-m
Fall-Off Test 2: $kh = 7.5$ darcy-m

The average value for kh is 6.1 darcy-m.

4.10 Well GH-21

No downhole temperature measurements are available for the two injection tests of well GH-21 (Figure 4.10). The pressure gauge during the injection tests was located at 804 m TVD (*i.e.*, ~ 150 meters below the principal feedzone at 650 m TVD). A pressure of 48.74 bars(a) was recorded at the gauge depth prior to the start of cold water injection on November 18, 1992. Using the last flowing pressures during the injection phases, the injectivity indices are:

$$\text{Injection Test 1:} \quad II = \frac{2000}{60(51.39 - 48.74)} = 12.6 \text{ kg/s-bar}$$

$$\text{Injection Test 2:} \quad II = \frac{3000}{60(53.05 - 48.74)} = 11.6 \text{ kg/s-bar}$$

The average value for the injectivity index is 12.1 kg/s-bar.

The Horner plots of pressure fall-off data are shown in Figures 4.23 (a) and (b). The pressures do not appear to asymptote to the pre-injection pressure (48.74 bars). Furthermore, the pressure fall-off rate increases sharply at late times. The apparent increase in pressure fall-off rate and the failure of pressure to return to its pre-injection value is most likely caused by interzonal flow between the principal feedzone at 650 m TVD and the secondary feedzone at 780 m TVD (see Section 3.15). Using the straight line approximations shown in Figures 4.23 (a–b) and $\nu = 1.44 \times 10^{-7}$ m²/s, the formation transmissivity is given by:

Fall-Off Test 1: $kh = 13.6$ darcy-m
Fall-Off Test 2: $kh = 14.4$ darcy-m

The average value of *kh* is thus 14 darcy-m.

4.11 Well IH-1

During the injection testing of well IH-1 on March 25, 1988, the pressure/temperature tool was placed about 27 meters above the main feedzone at 590 m TVD. Before the start of cold water injection, a pressure of 46.4 bars(a)

Continued on page 4-53

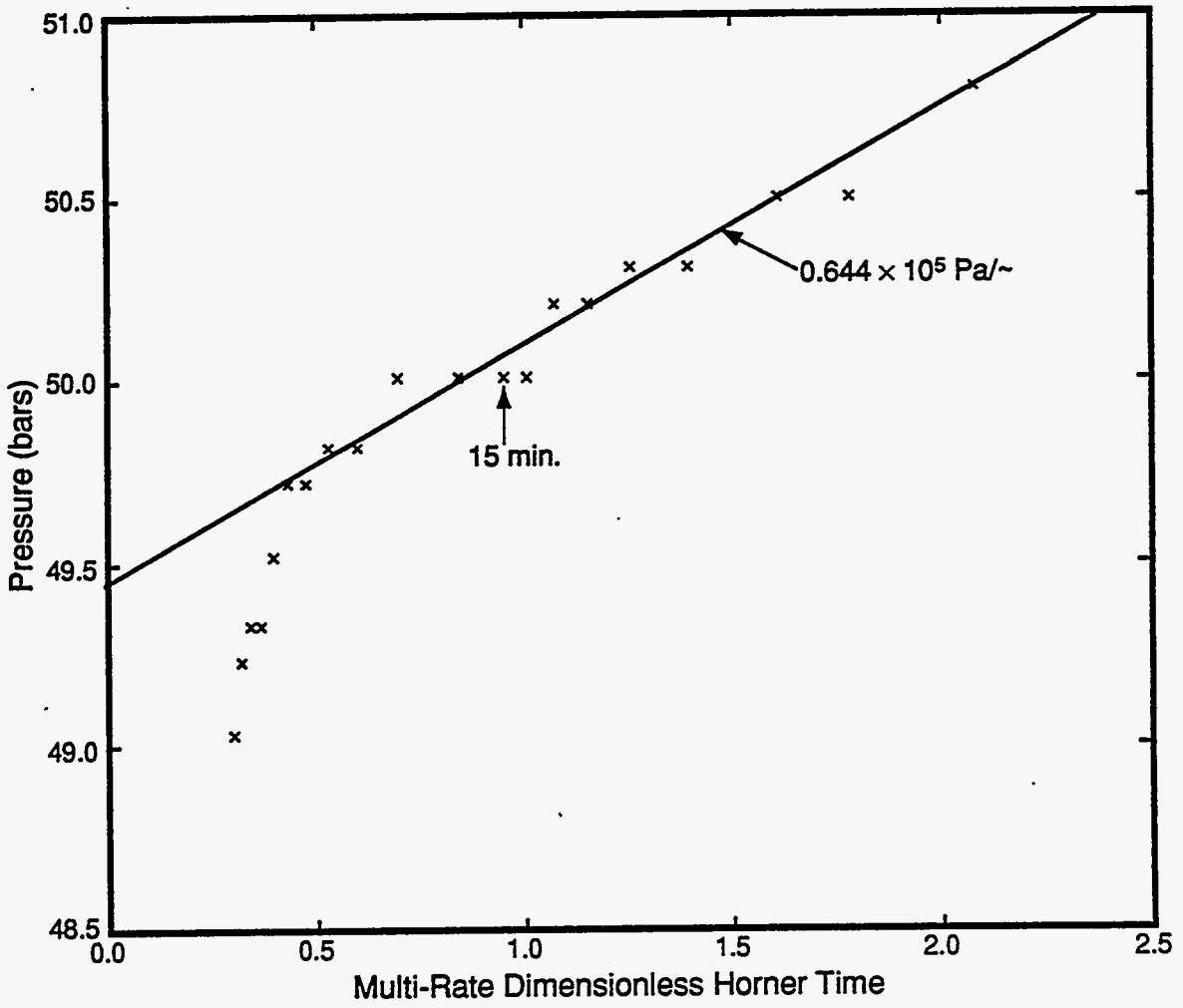

Figure 4.23a. Horner plot of pressure fall-off data no. 1 for well GH-21 (November 18, 1992).

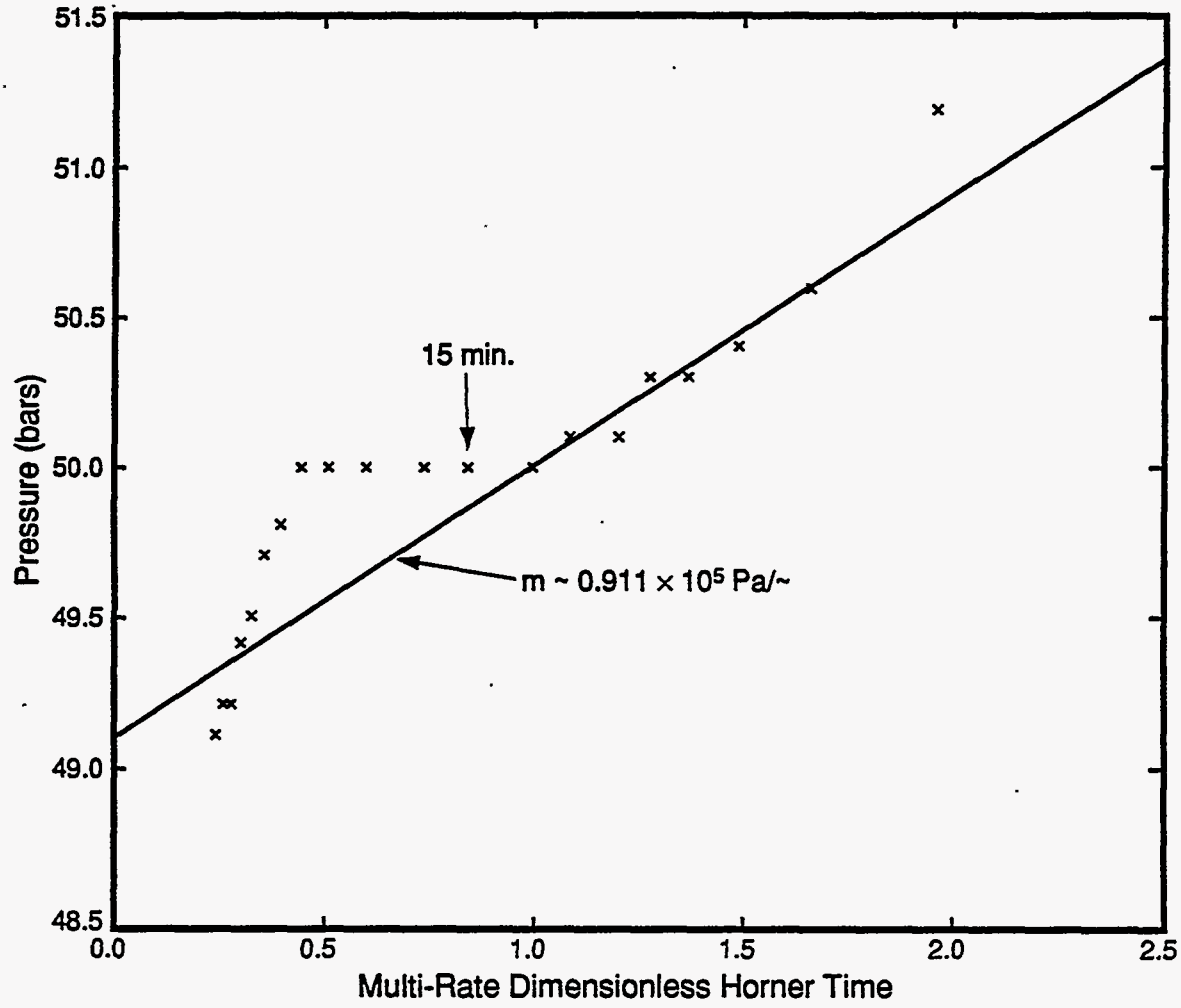

Figure 4.23b. Horner plot of pressure fall-off data no. 2 for well GH-21 (November 19, 1992).

was measured at the gauge depth. Using the final flowing pressures recorded for the two injection rates (Figure 4.11), the injectivity index is given by:

$$M = 400 \text{ kg/min} \quad II = \frac{400}{60(53.9-46.4)} = 0.89 \text{ kg/s-bar}$$

$$M = 600 \text{ kg/min} \quad II = \frac{600}{60(59.1-46.4)} = 0.79 \text{ kg/s-bar}$$

The average value for the injectivity index is 0.84 kg/s-bar.

The Horner plot of pressure fall-off data (Figure 4.24) suggests a classical double-porosity behavior (two parallel straight lines separated by a transition line with a lower slope). The slope of the late-time fall-off data can be used to determine the formation transmissivity. With kinematic viscosity $\nu = 1.44 \times 10^{-7}$ m^2/s (liquid water at a temperature of 225°C), we obtain a formation transmissivity of 0.73 darcy-m.

4.12 Well IH-2

During the injection testing of well IH-2 on January 26, 1990, the pressure/temperature tool was placed about 30 meters beneath the main feedzone at 550 m TVD. The rather small temperature drop at the gauge depth (Figure 4.12) implies that practically all of the injected fluid enters the formation at some place above the gauge depth. A pressure of 42.1 bars(a) was measured at the gauge depth prior to the start of the injection test. Using the final flowing pressures during the three constant rate injection periods, we obtain the following values for the injectivity index:

$$M = 1000 \text{ kg/min} \quad II = \frac{1000}{60(42.5-42.1)} = 42 \text{ kg/s-bar}$$

$$M = 2000 \text{ kg/min} \quad II = \frac{2000}{60(42.7-42.1)} = 56 \text{ kg/s-bar}$$

$$M = 3000 \text{ kg/min} \quad II = \frac{3000}{60(43.6-42.1)} = 33 \text{ kg/s-bar}$$

Because of the extremely small changes in pressure associated with the first two injection tests, the values of injectivity index obtained from these tests may not be reliable. The best estimate for the injectivity index is 33 kg/s-bar.

The Horner plots of pressure fall-off data for the three injection periods are shown in Figures 4.25 (a)–(c); it is apparent from these figures that gauge resolution is insufficient for resolving details of the fall-off behavior of IH-2. In any event, the fall-off data (Figures 4.25 a–c) can be approximated by straight lines. The slopes of these straight lines together with $\nu = 1.44 \times 10^{-7}$ m^2/s

Continued on page 4-58

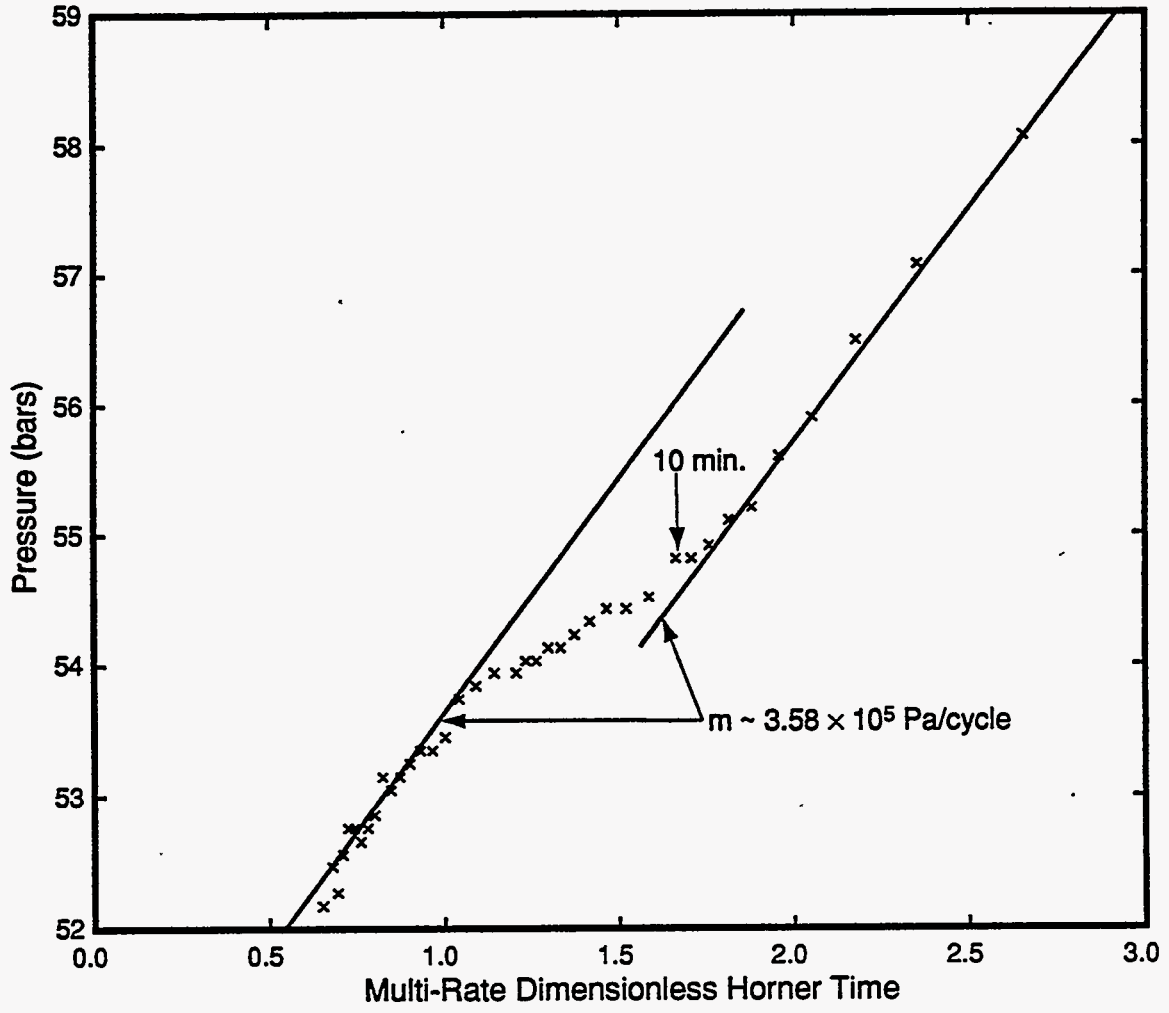

Figure 4.24. Horner plot of pressure fall-off data for well IH-1 (March 25, 1988).

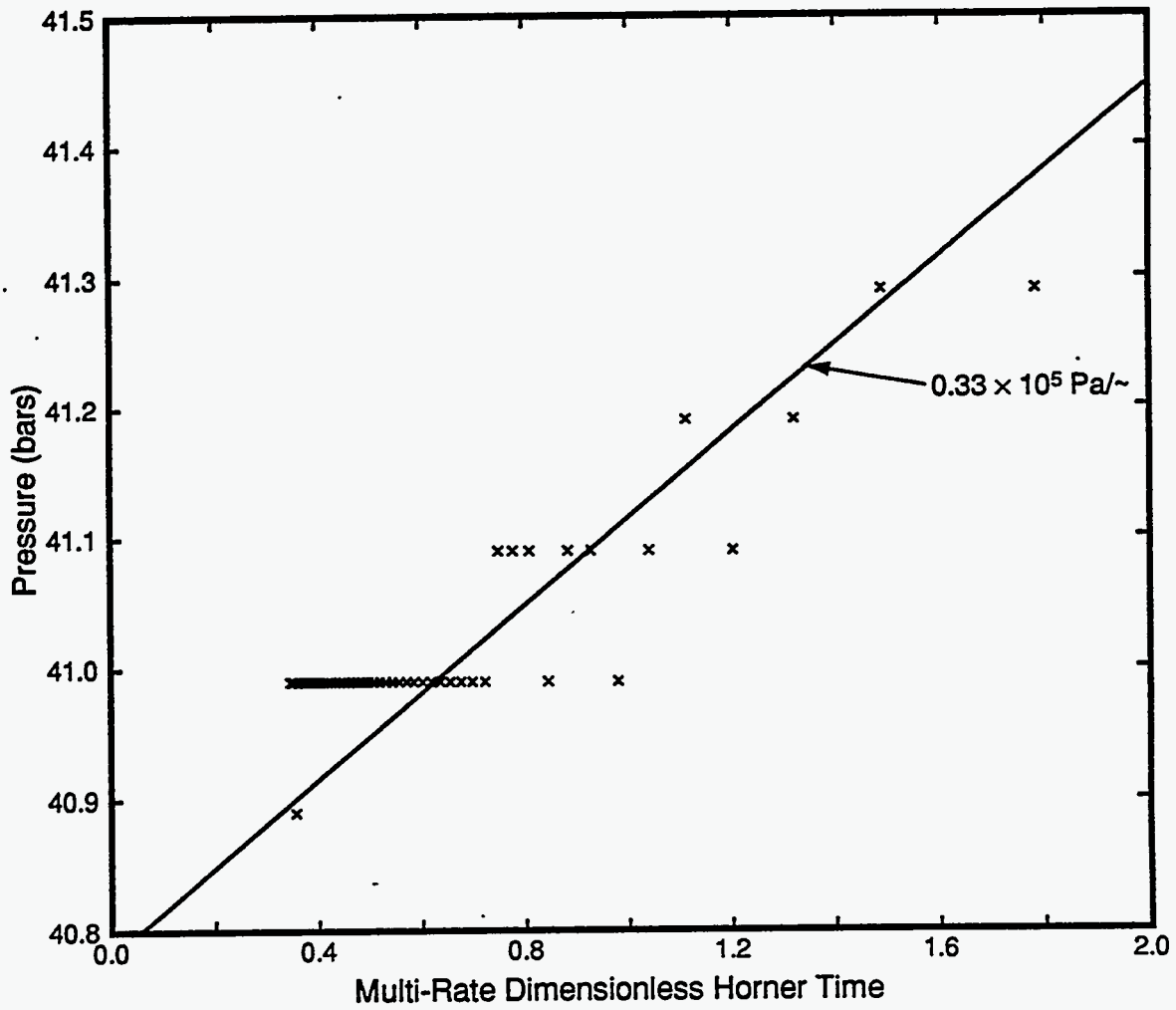

Figure 4.25a. Horner plot of pressure fall-off data no. 1 for well IH-2 (January 26, 1990).

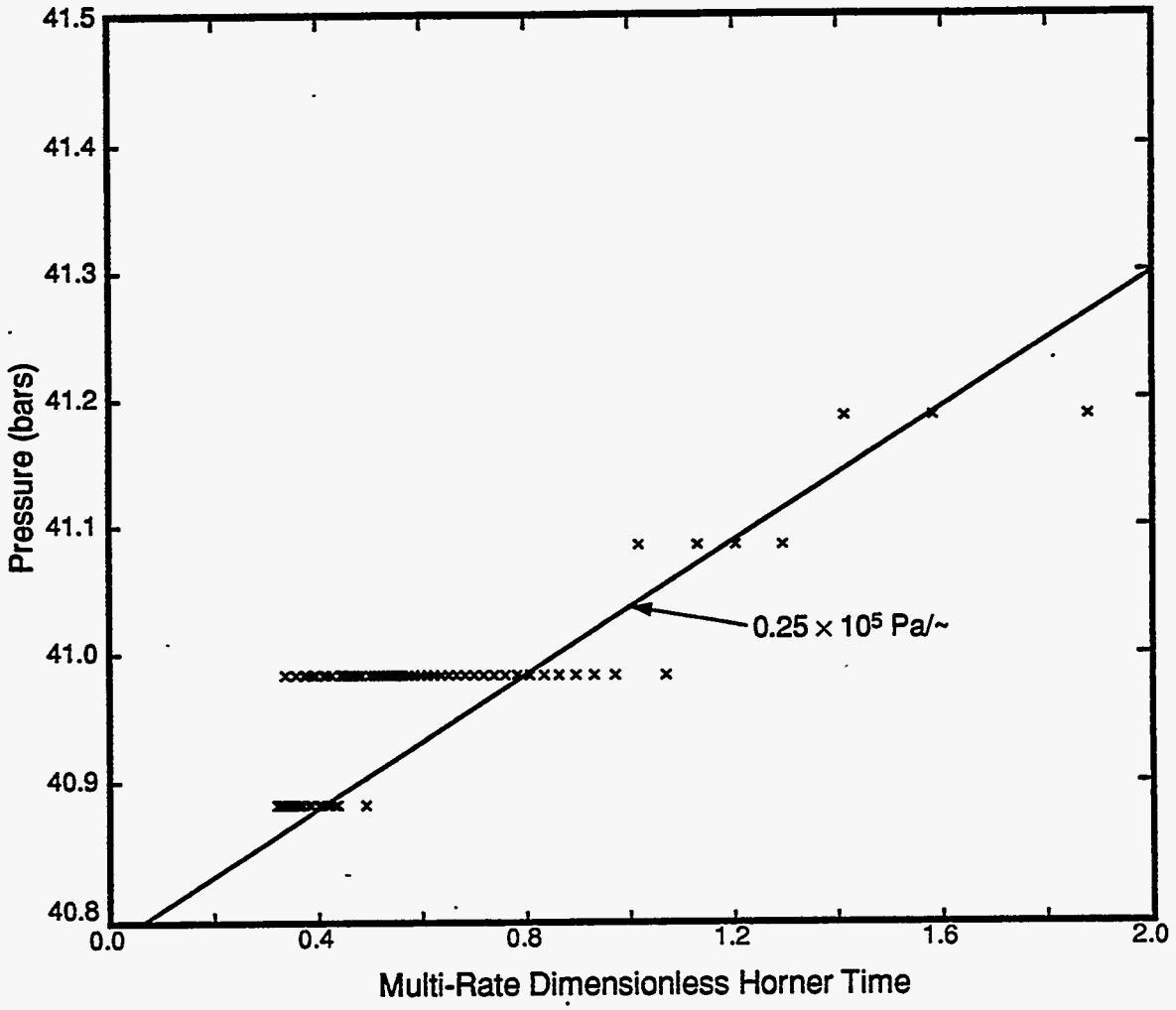

Figure 4.25b. Horner plot of pressure fall-off data no. 2 for well IH-2 (January 26, 1990).

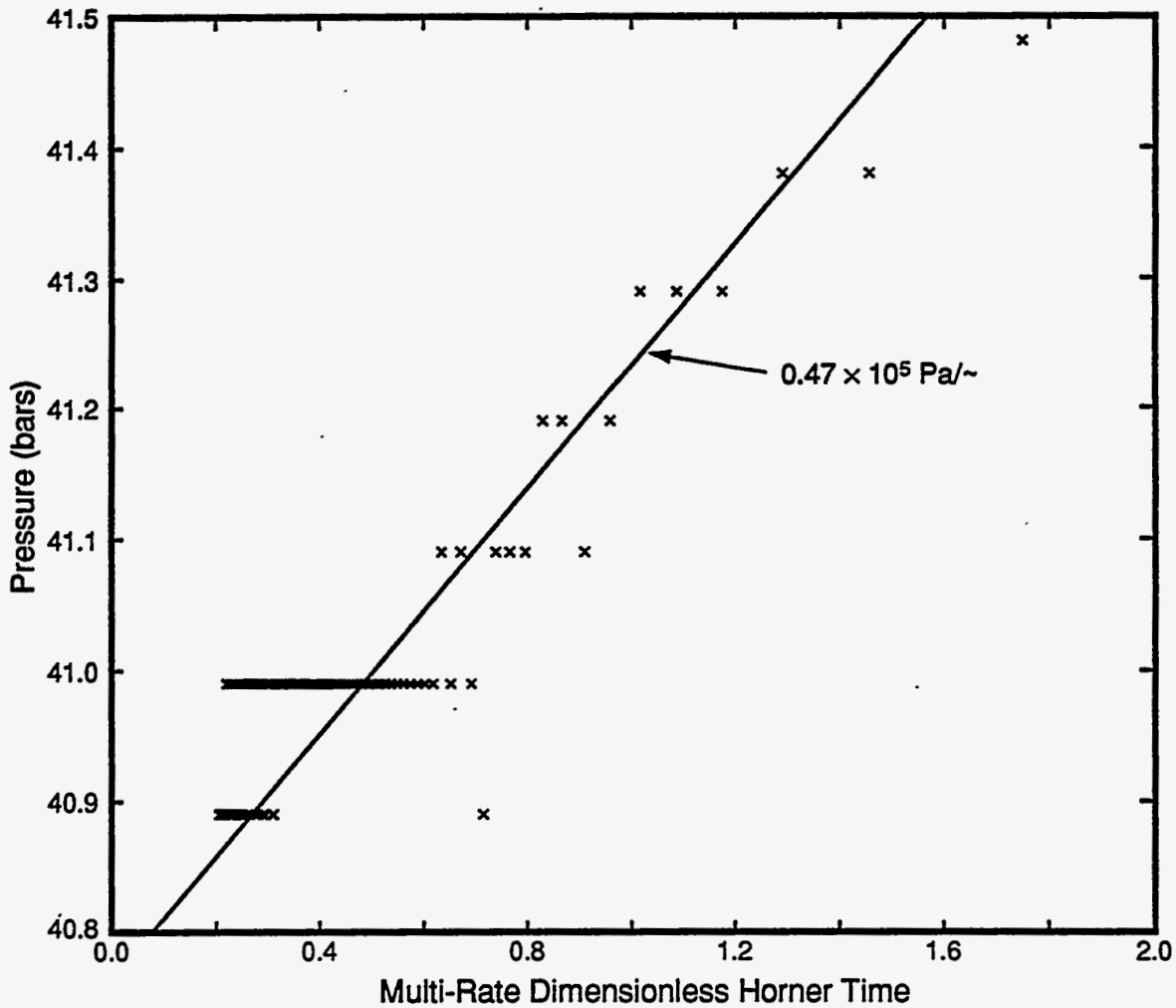

Figure 4.25c. Horner plot of pressure fall-off data no. 3 for well IH-2 (January 26, 1990).

(liquid water at a temperature of 225°C) were used to compute the following values for formation transmissivity:

Fall-Off Test 1: $kh = 13$ darcy-m
Fall-Off Test 2: $kh = 35$ darcy-m
Fall-Off Test 3: $kh = 28$ darcy-m

The average vale of kh is 25 darcy-m.

4.14 Slim Hole N2-KW-1

No downhole data are available for this study for the first injection test of slim hole N2-KW-1 on January 31, 1991. In the injection test run on February 8, 1991 (Injection Test 2), the pressure/temperature tool was placed at 858 m TVD (*i.e.*, within 2 meters of the feedzone at 860 m TVD); the pre-injection pressure was 55.44 bars(a). For the third injection test conducted on March 2, 1991, the pressure/temperature tool was located at 873 m TVD; a pressure of 55.71 bars was recorded before the injection test. Using the pressures measured during the injection phases, the following values for injectivity index are obtained:

Injection Test 2:

$$M = 200 \text{ kg/min} \quad II = \frac{200}{60(57.02 - 55.44)} = 2.11 \text{ kg/s-bar}$$

$$M = 380 \text{ kg/min} \quad II = \frac{380}{60(58.43 - 55.44)} = 2.12 \text{ kg/s-bar}$$

Injection Test 3:

$$M = 160 \text{ kg/min} \quad II = \frac{160}{60(57.73 - 55.71)} = 1.32 \text{ kg/s-bar}$$

$$M = 560 \text{ kg/min} \quad II = \frac{560}{60(58.93 - 55.71)} = 2.90 \text{ kg/s-bar}$$

The average value for the injectivity index is 2.11 kg/s-bar.

The Horner plots of pressure fall-off data from injection tests 2 and 3 are shown in Figures 4.26 (a) and (b). Poor gauge resolution makes these fall-off data less than ideal for inferring formation properties. With a kinematic viscosity of $\nu = 1.44 \times 10^{-7}$ m^2/s, we obtain the following values for kh:

Fall-Off Test 2: $kh = 1.7$ darcy-m
Fall-Off Test 3: $kh = 16.9$ darcy-m

The two estimates of kh differ by an order of magnitude! The average kh value is 9.3 darcy-m.

Continued on page 4-61

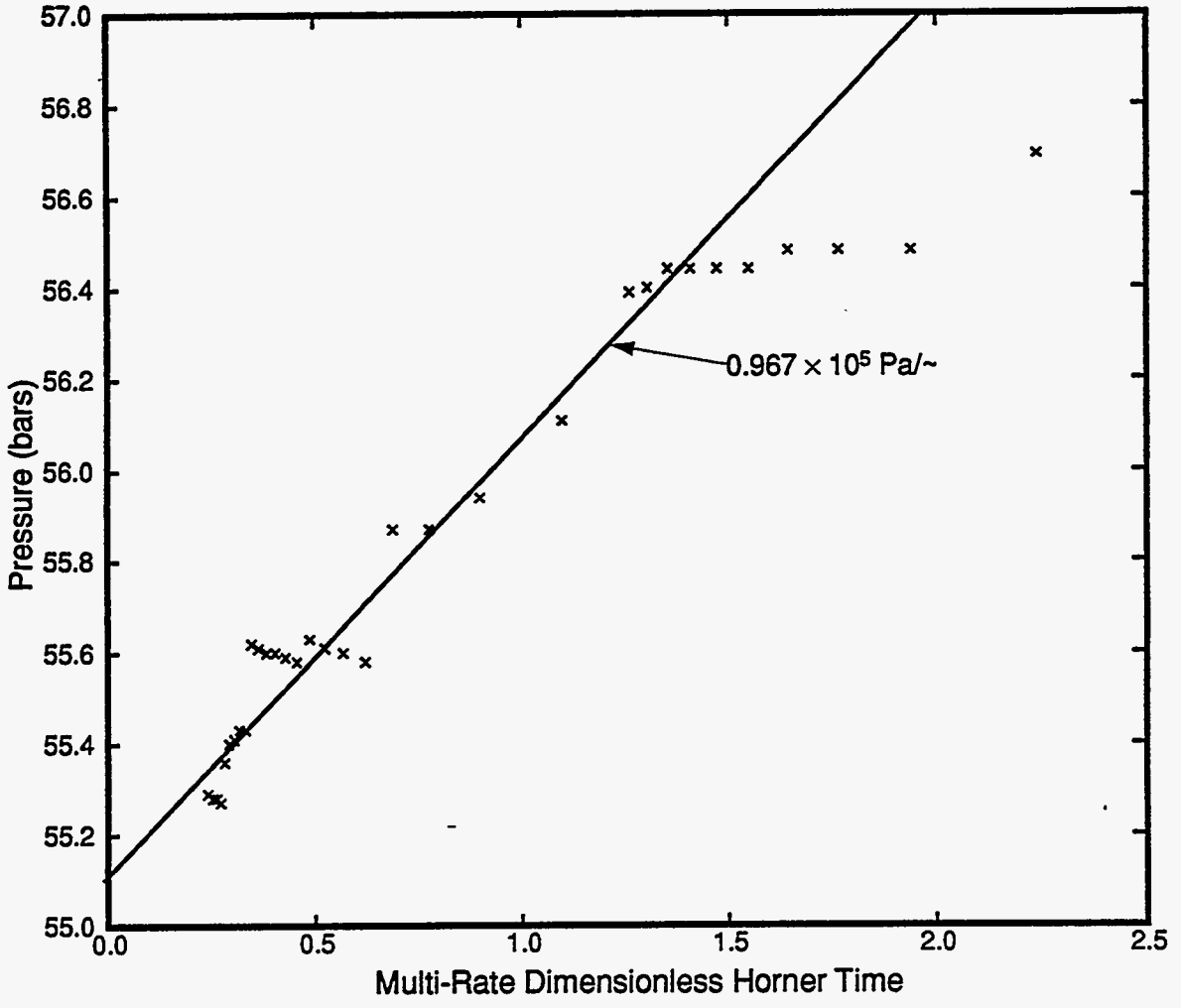

Figure 4.26a. Horner plot of pressure fall-off test no. 2 for slim hole N2-KW-1 (February 8, 1991).

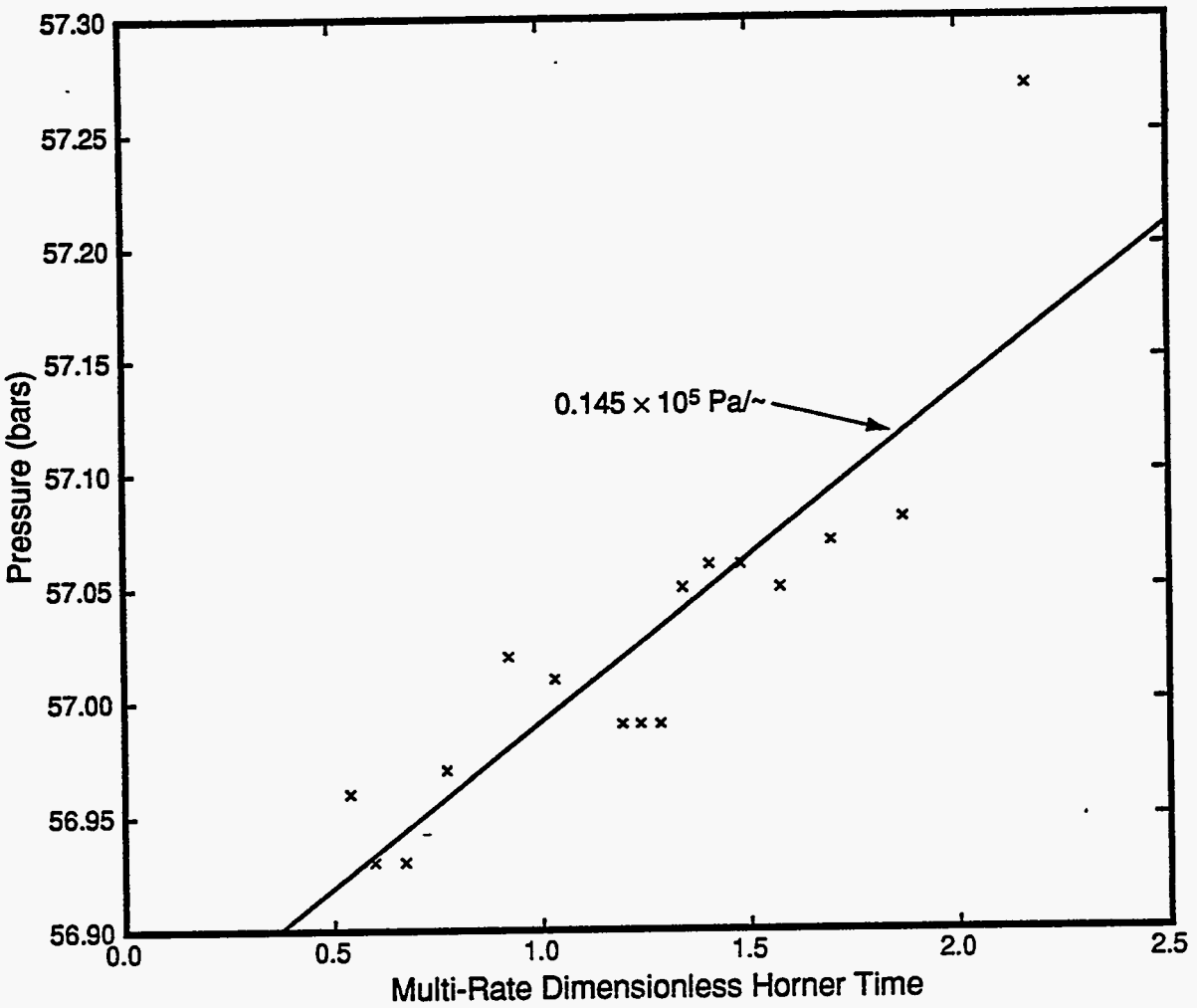

Figure 4.26b. Horner plot of pressure fall-off test no. 3 for slim hole N2-KW-1 (March 2, 1991).

4.14 Slim Hole N2-KW-2

During the first injection test of slim hole N2-KW-2 on February 5, 1991, no downhole pressure measurements were made. After cold water injection, fall-off response was recorded by lowering a pressure/temperature tool to a depth of 765 m TVD (*i.e.*, about 95 meters above the nominal feedzone depth of 800 m TVD). In the second injection test run on February 6, 1991, the pressure gauge was located at 840 m TVD; the pre-injection pressure was 64.99 bars. Using the pressures recorded during the three constant rate injection periods (see Figure 4.14b), we obtain the following estimates for the injectivity index.

$$M = 100 \text{ kg/min} \quad II = \frac{100}{60(67.32 - 64.99)} = 0.72 \text{ kg/s-bar}$$

$$M = 200 \text{ kg/min} \quad II = \frac{200}{60(68.41 - 64.99)} = 0.97 \text{ kg/s-bar}$$

$$M = 466 \text{ kg/min} \quad II = \frac{466}{60(73.77 - 64.99)} = 0.88 \text{ kg/s-bar}$$

The average value for the injectivity index is 0.86 kg/s-bar.

The Horner plots of pressure fall-off data are displayed in Figures 4.27 (a) and (b). With $\nu = 1.44 \times 10^{-7}$ m²/s (kinematic viscosity for liquid water at a temperature of 225°C) and using the straight line approximations shown in Figures 4.27 (a) and (b), we have the following estimates for kh:

Fall-Off Data No. 1: $kh = 0.36$ darcy-m
Fall-Off Data No. 2: $kh = 0.79$ darcy-m

The average value of kh is 0.58 darcy-m.

4.15 Slim Hole N2-KW-3

During the injection test of slim hole N2-KW-3 on March 7, 1991, the pressure gauge was located at 1288 m TVD (*i.e.*, about 480 meters below the main feedzone at 810 m TVD). The pre-injection pressure at 1288 m TVD was 91.19 bars(a). With a final flowing pressure of 92.50 bars(a), the injectivity index becomes:

$$II = \frac{510}{60(92.50 - 91.19)} = 6.49 \text{ kg/s-bar}$$

On February 28, 1991, a pressure/temperature survey was run while injecting cold water at a rate of 500 kg/min; a pressure of 52.1 bars(a) was measured at 810 m TVD. A static pressure of 50.5 bars was recorded at 810 m TVD in

Continued on page 4-64

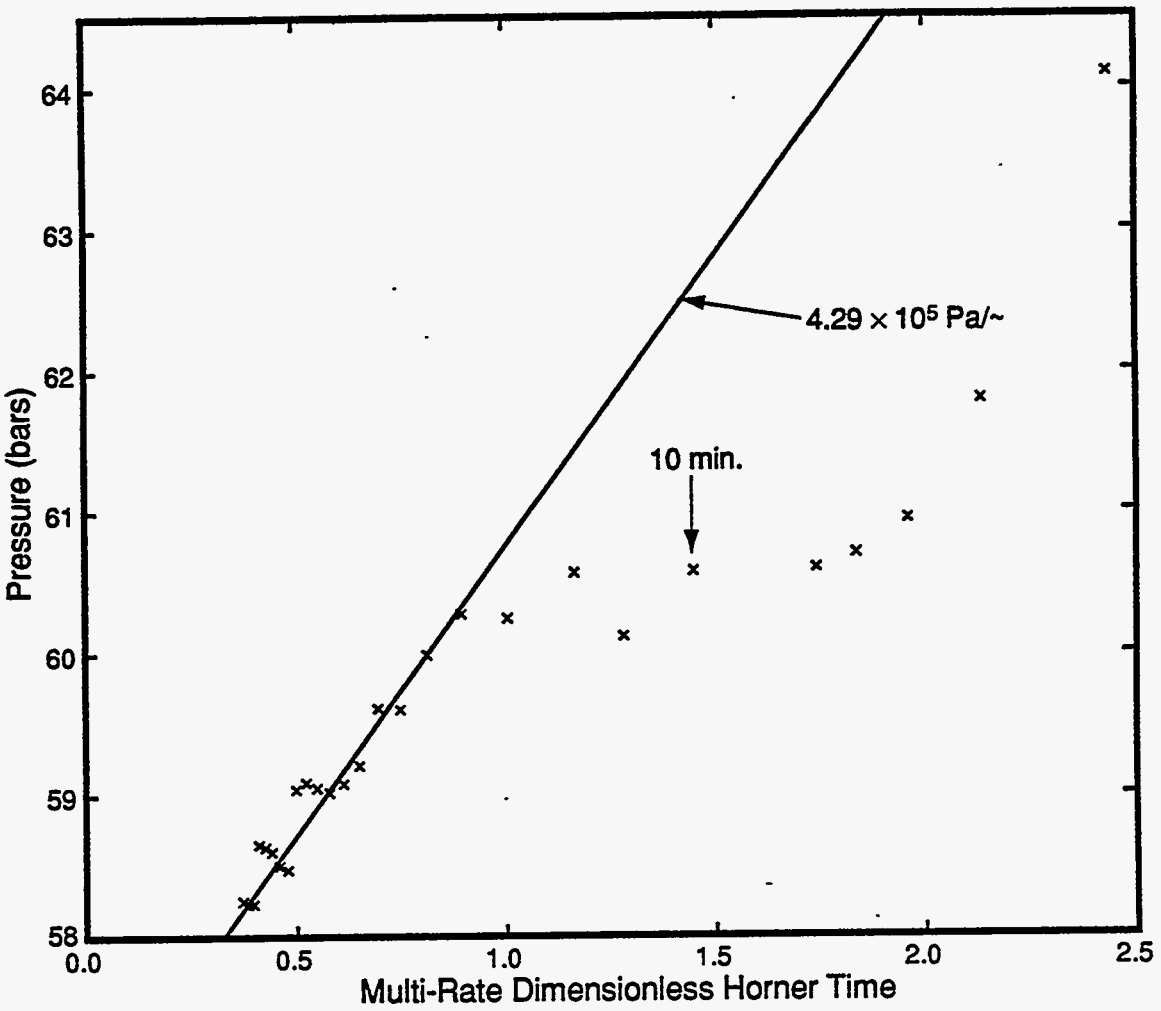

Figure 4.27a. Horner plot of pressure fall-off data no. 1 for slim hole N2-KW-2 (February 5, 1991).

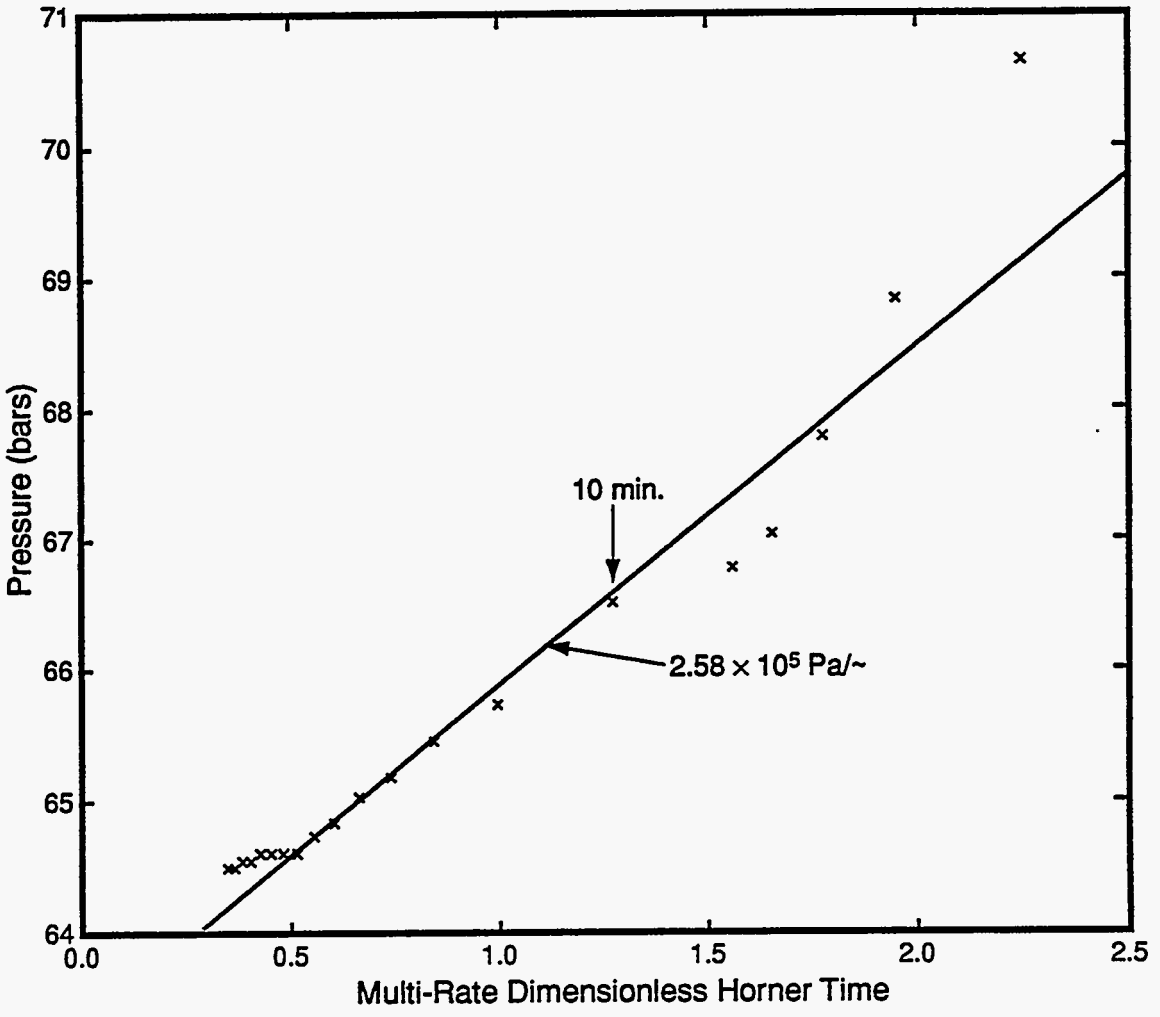

Figure 4.27b. Horner plot of pressure fall-off data no. 2 for slim hole N2-KW-2 (February 6, 1991).

another pressure survey made on February 24, 1991. These pressure/flow measurements yield the following value for the injectivity index:

$$II = \frac{500}{60(52.1-50.5)} = 5.21 \text{ kg/s-bar}$$

The above two determinations for the injectivity index yield an average value of 5.85 kg/s-bar.

The fall-off response recorded after the March 7, 1991 index test is shown in Figures 4.15 and 4.28. The pressure fall-off data (Figure 4.28) lack sufficient resolution for evaluating formation transmissivity. An examination of Figure 4.15 indicates that at the end of the fall-off period, the pressure does not return to its pre-injection value. We suggest that a cooling of the fluid column between the gauge and feedzone depths is responsible for the observed pressure behavior.

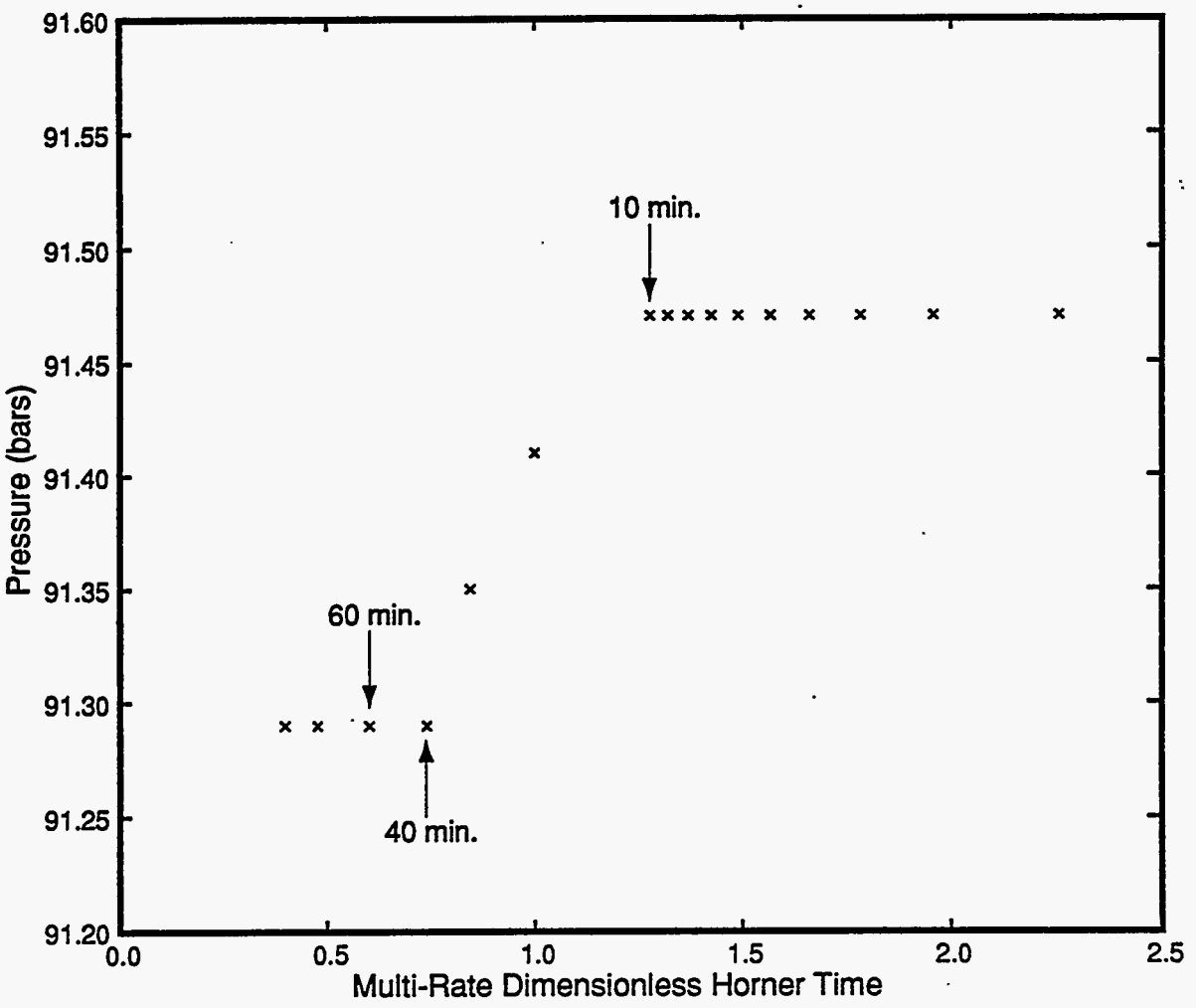

Figure 4.28. Horner plot of pressure fall-off data for slim hole N2-KW-3 (March 7, 1991).

SECTION 5

Discharge Tests

5.1 Characteristic Tests

A borehole must be discharged to ascertain its productive capacity. A total of eight slim holes and six large-diameter Oguni wells have been discharged at one time or another. With the exception of two boreholes in the high pressure reservoir (boreholes HH-2 and GH-15), all-liquid conditions prevail at the feedzone depth in Oguni boreholes under discharge conditions. The feedzone temperatures for Oguni boreholes producing from liquid feedzones are given in Table 3.1. As part of the discharge tests of Oguni boreholes, the characteristic output curves (*i.e.*, mass and enthalpy versus wellhead pressure) were also obtained. An oddity of the "Well Characteristic" data set from Oguni boreholes is that the "measured wellhead enthalpies" often exceed downhole enthalpies computed from downhole (feedzone) temperatures. Because there is no evidence for a two-phase or a steam feed in most Oguni boreholes, it would appear that the "measured enthalpies" may be in error. The "measured enthalpies" are computed from measured water and steam flow rates at the surface. It is, therefore, likely that there is a systematic error in water-flow (underestimate?) or steam-flow (overestimate?). As far as the total discharge rate is concerned, the errors in water and steam flow rates would tend to cancel each other out. The mass output curves for the various Oguni boreholes are shown in Figures 5.1 through 5.14. It is apparent from Figures 5.1 through 5.14 that the wellhead pressure corresponding to the maximum discharge rate varies from borehole-to-borehole. The maximum discharge rates for the various Oguni boreholes are given in Table 5.1.

During all of the discharge tests, pressure and temperature (or pressure, temperature and spinner) surveys were run. The pressure and temperature data from these surveys are tabulated in Appendix C. These pressure/temperature surveys are used to calculate the productivity indices for the Oguni boreholes in Subsection 5.2. Following the discharge tests (varying in duration from a few days to several months) pressure buildup was recorded by lowering a gauge (usually Kuster) into the borehole. The pressure buildup data are analyzed in Subsection 5.3.

5.2 Productivity Indices

Productivity index, PI, is defined as follows:

$$PI = \frac{M}{P_{ns} - P_{fp}}$$

Continued on page 5-16

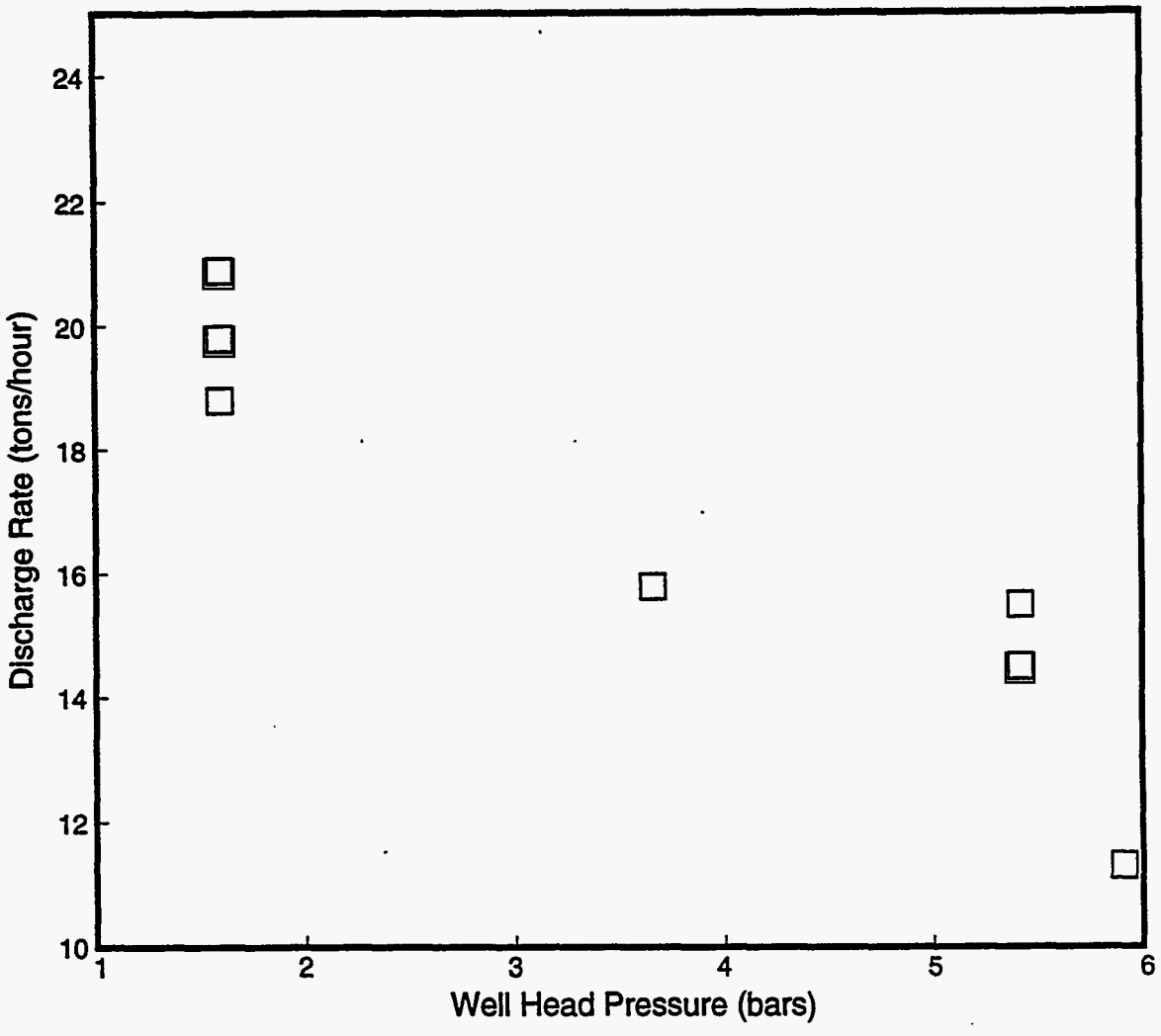

Figure 5.1. Discharge rate versus wellhead pressure for slim hole GH-3 (February 1987).

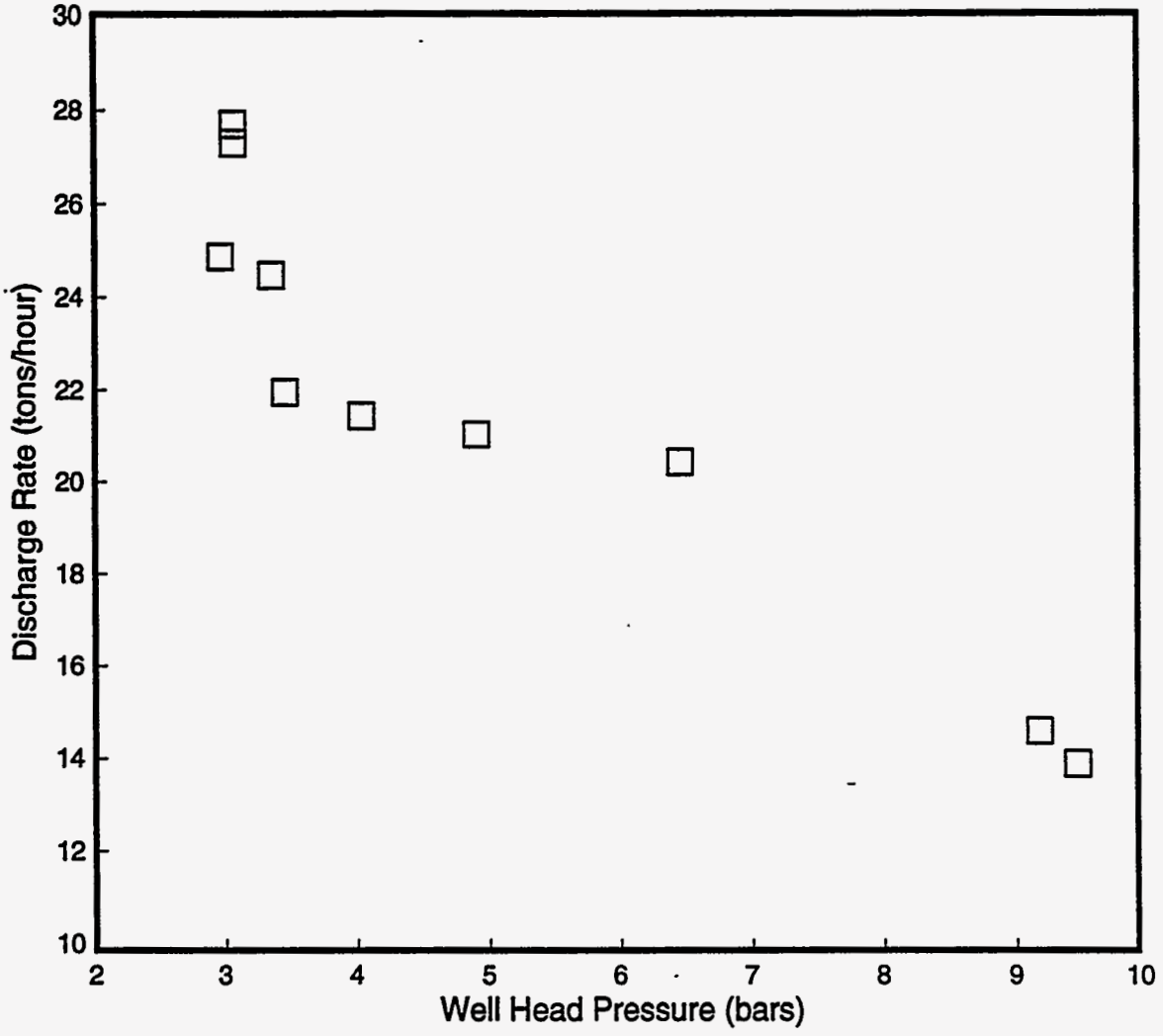

Figure 5.2. Discharge rate versus wellhead pressure for slim hole GH-4 (February and March 1986).

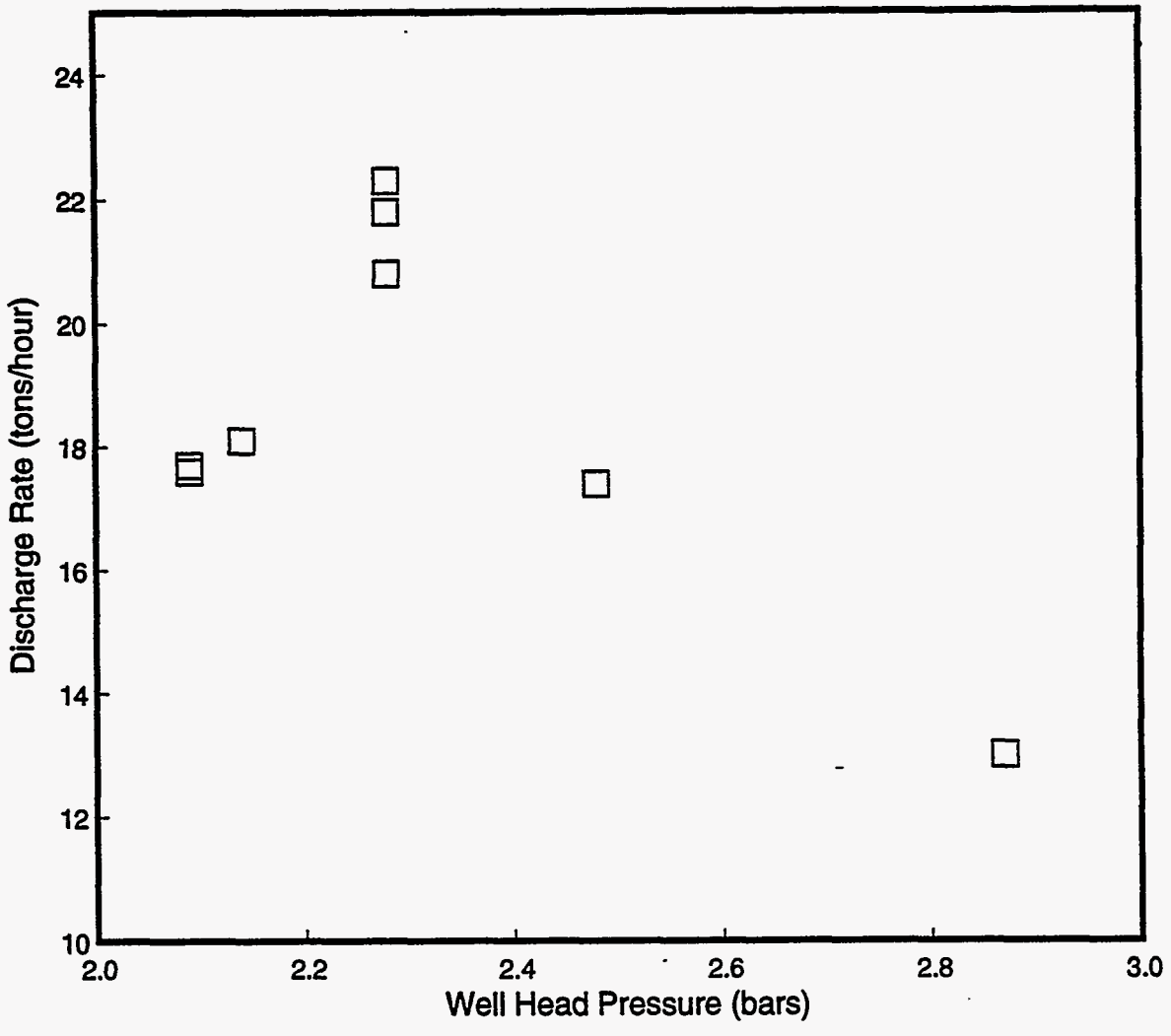

Figure 5.3. Discharge rate versus wellhead pressure for slim hole GH-5 (February and March 1986).

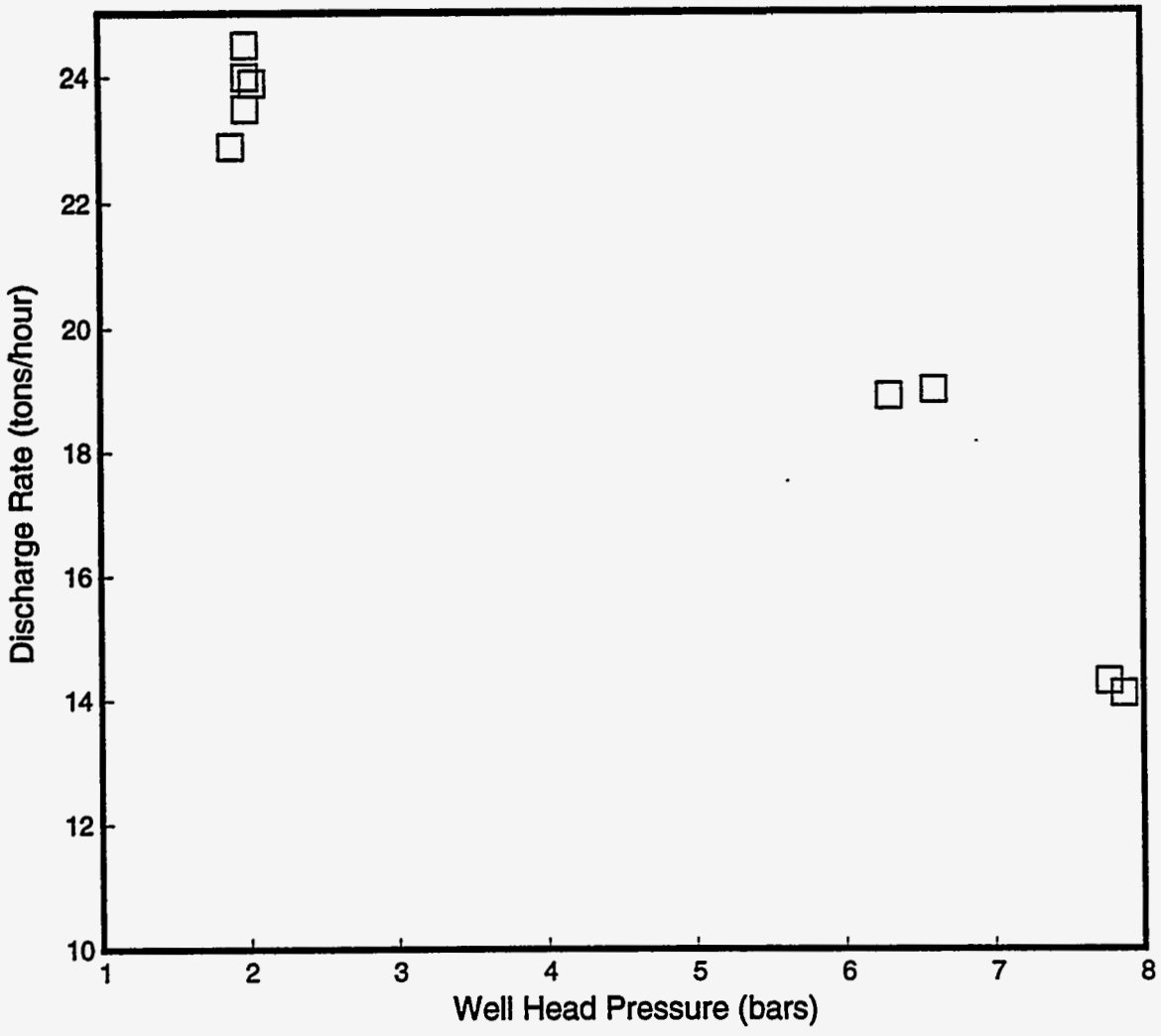

Figure 5.4. Discharge rate versus wellhead pressure for slim hole GH-6 (March 1986).

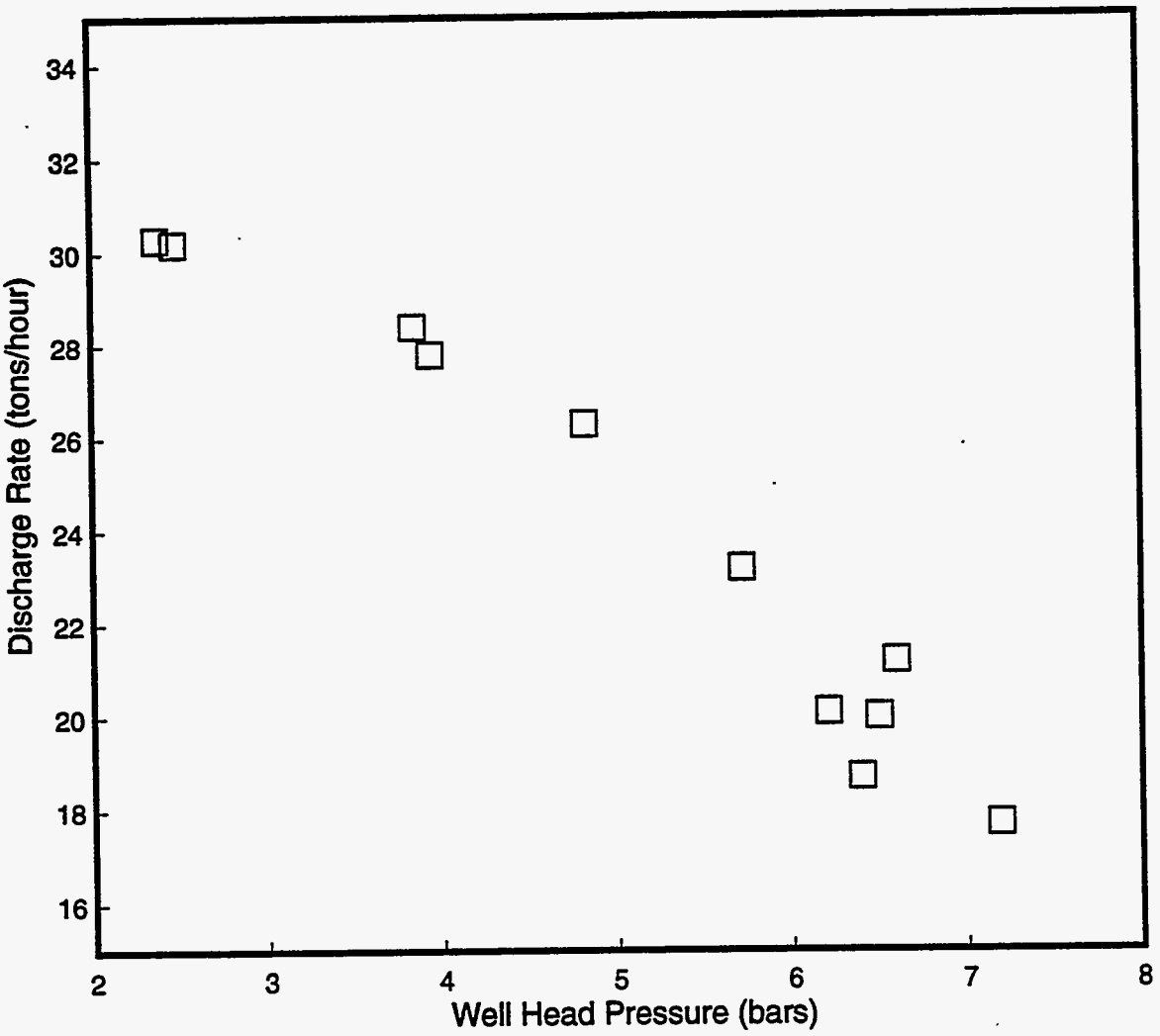

Figure 5.5. Discharge rate versus wellhead pressure for slim hole GH-7 (January 1987).

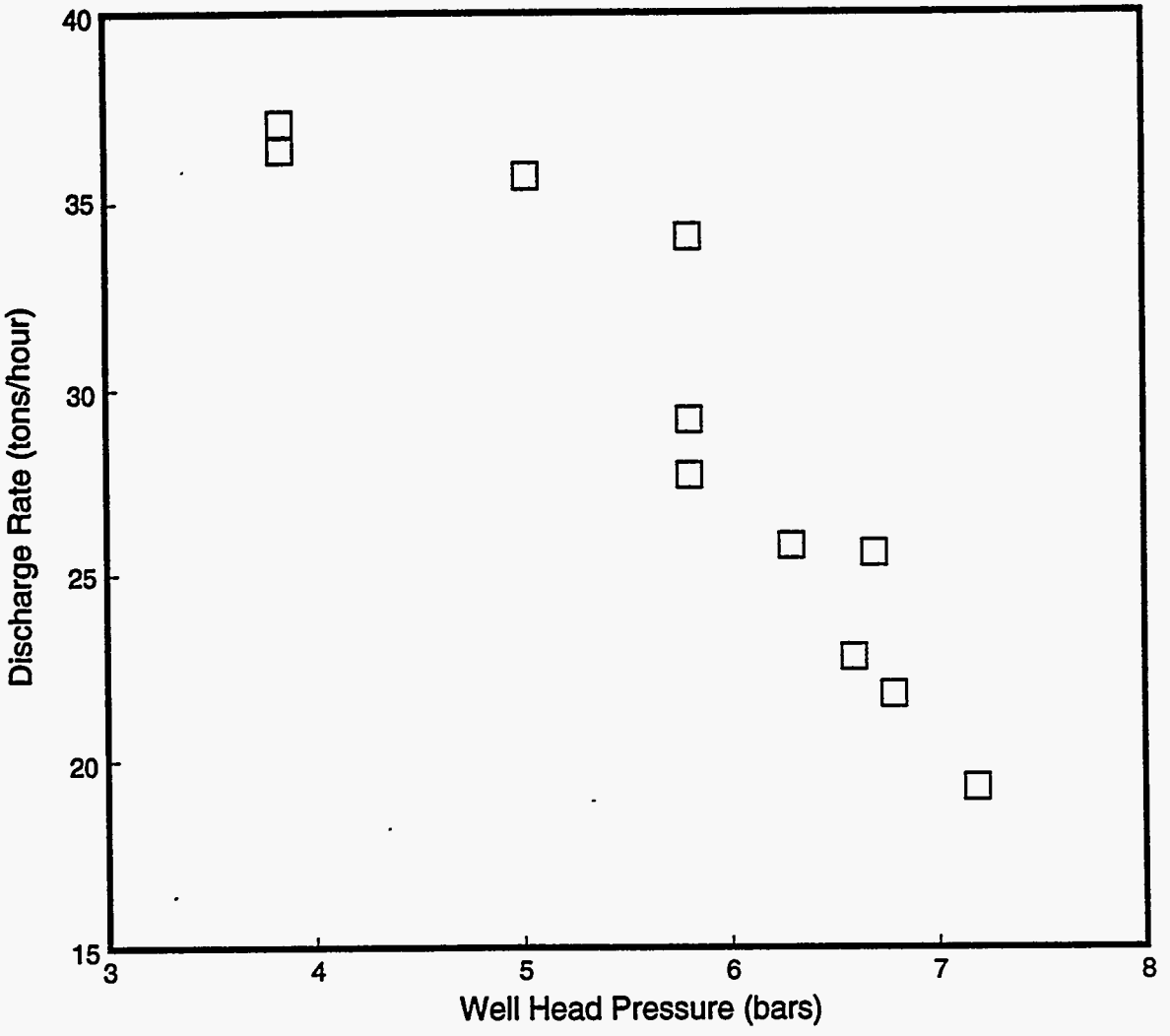

Figure 5.6. Discharge rate versus wellhead pressure for slim hole GH-8 (September 1987).

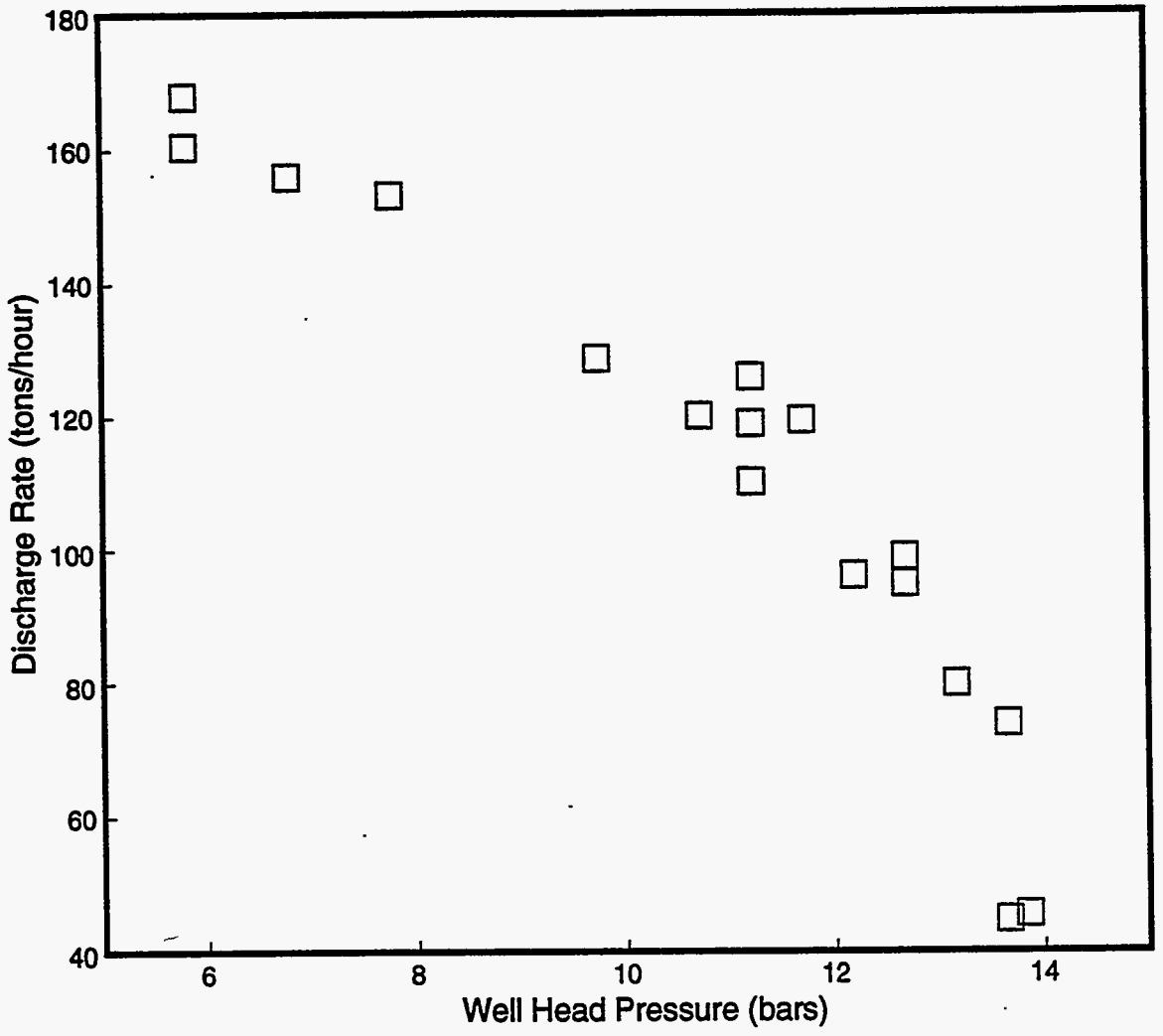

Figure 5.7. Discharge rate versus wellhead pressure for well GH-10 (July and August 1987).

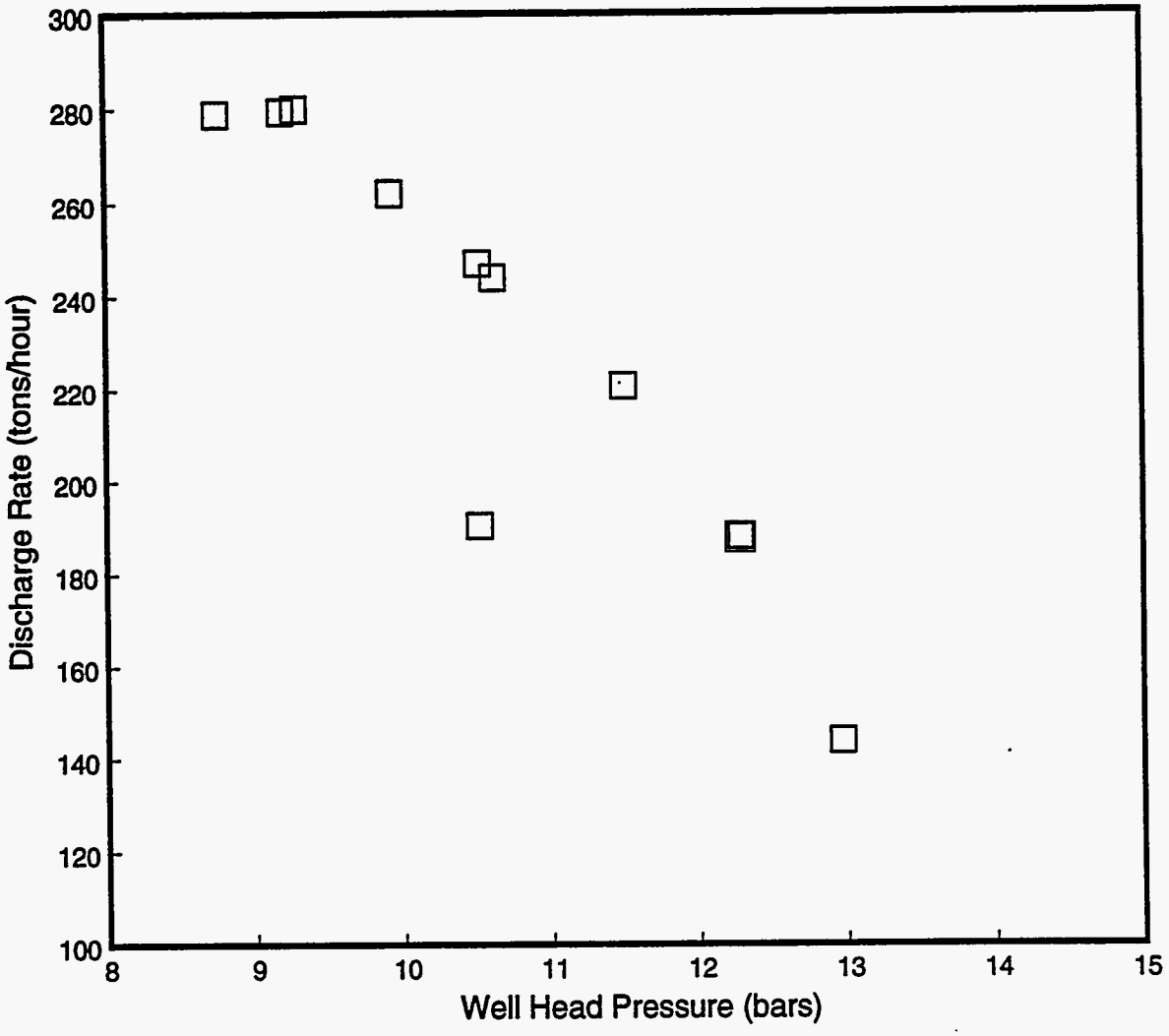

Figure 5.8. Discharge rate versus wellhead pressure for well GH-11 (June and July 1991).

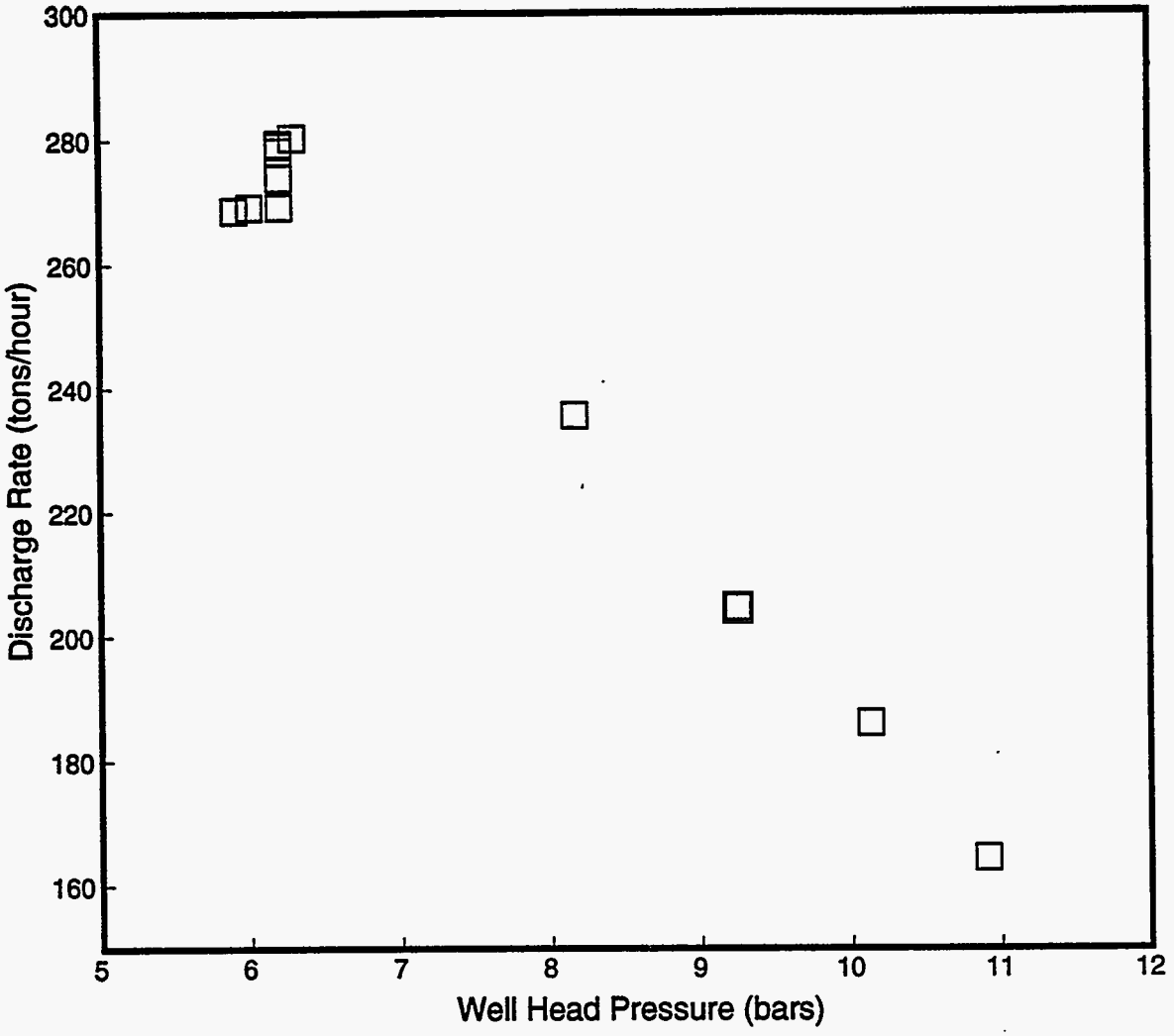

Figure 5.9. Discharge rate versus wellhead pressure for well GH-12 (September and October 1991).

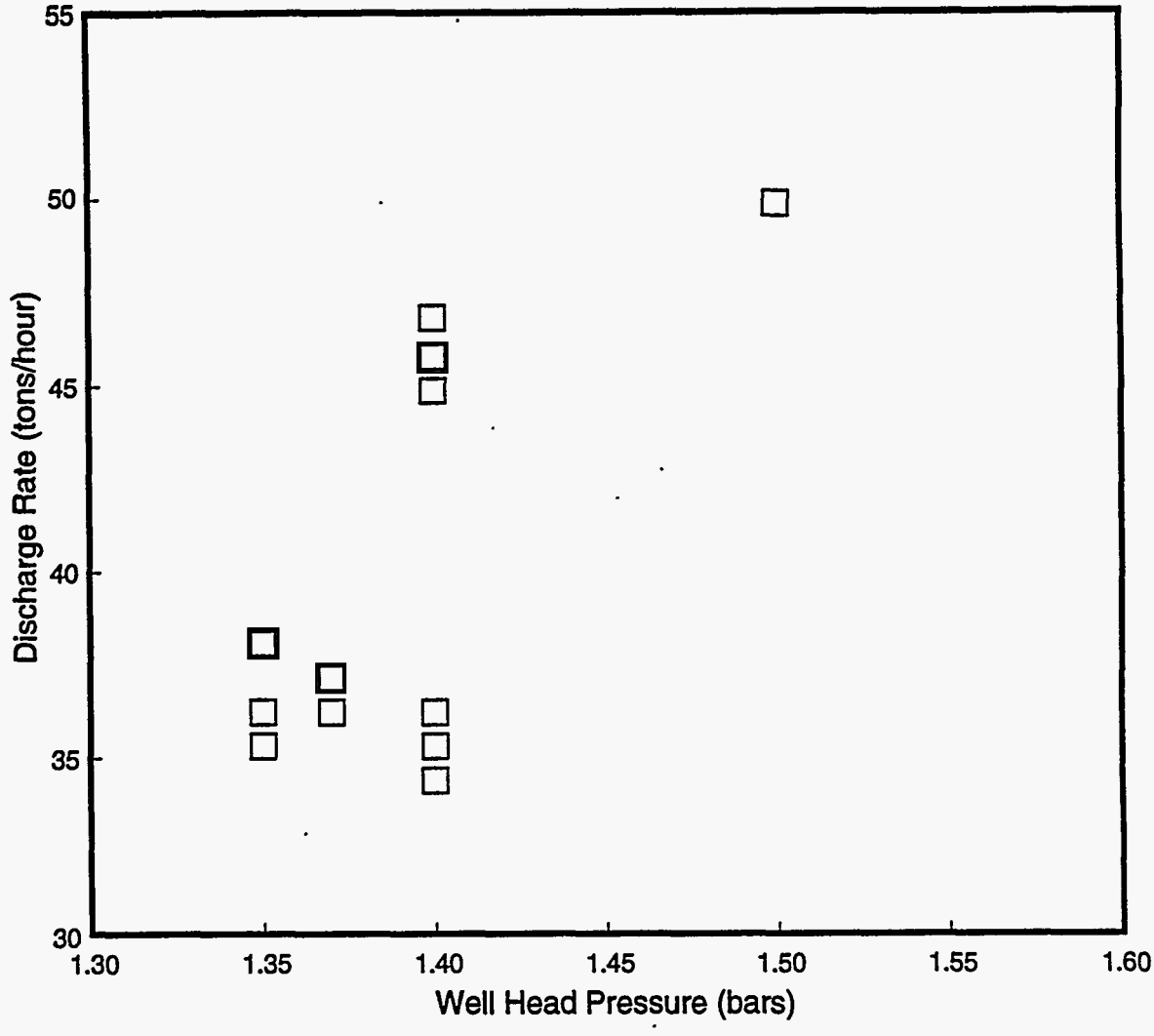

Figure 5.10. Discharge rate versus wellhead pressure for well GH-15 (October and November 1990).

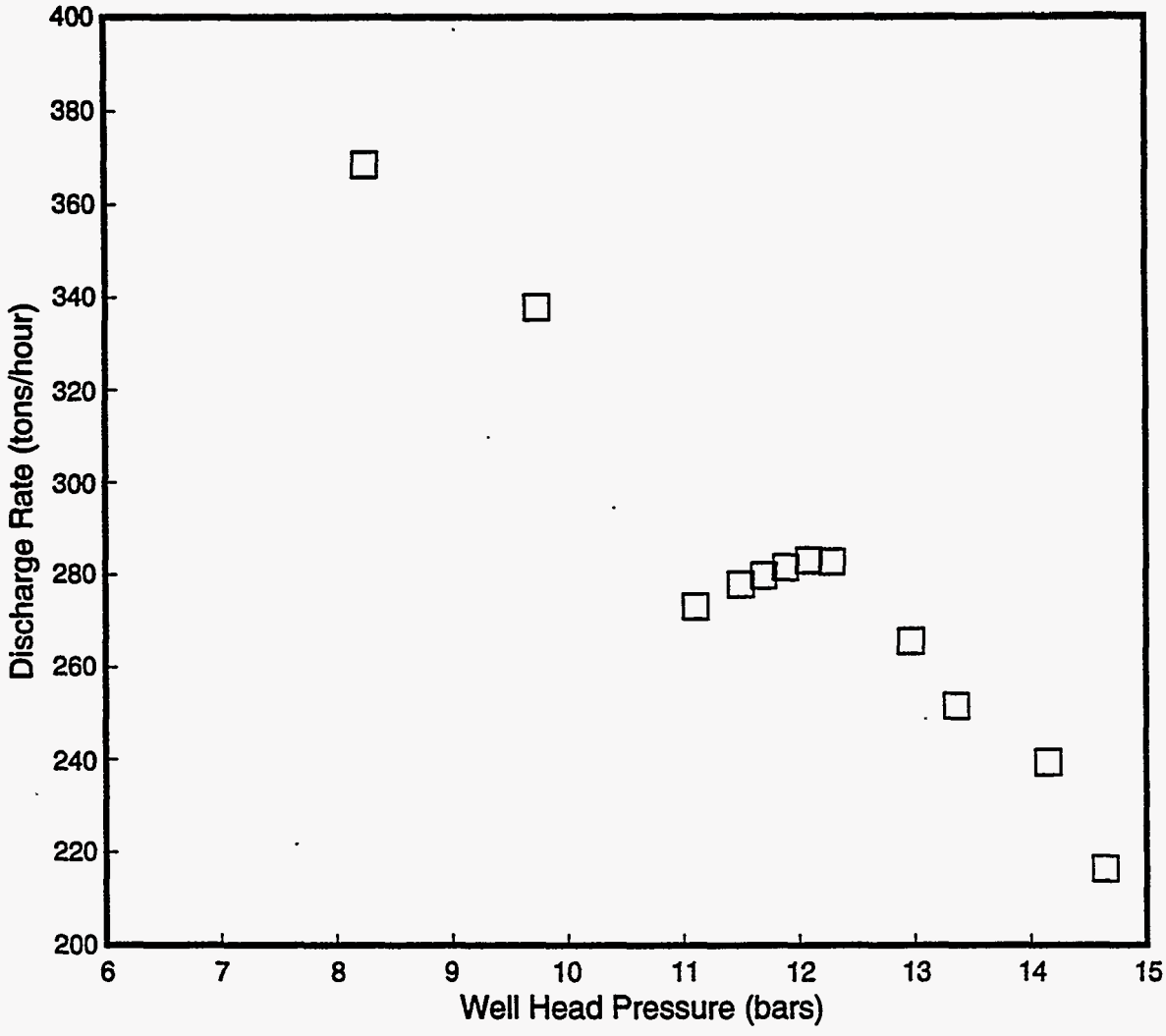

Figure 5.11. Discharge rate versus wellhead pressure for well GH-20 (April 1991).

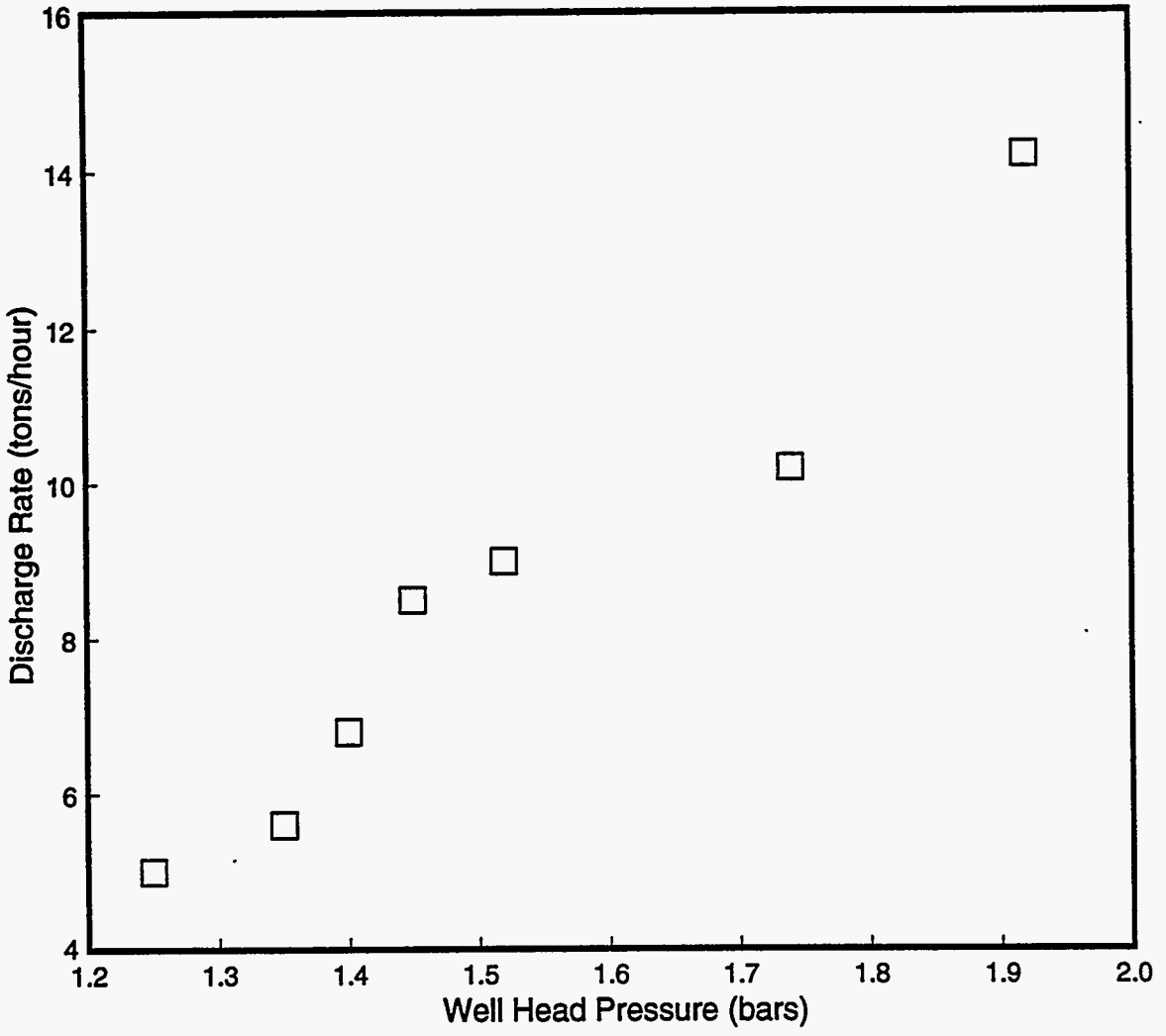

Figure 5.12. Discharge rate versus wellhead pressure for slim hole HH-2 (December 1986).

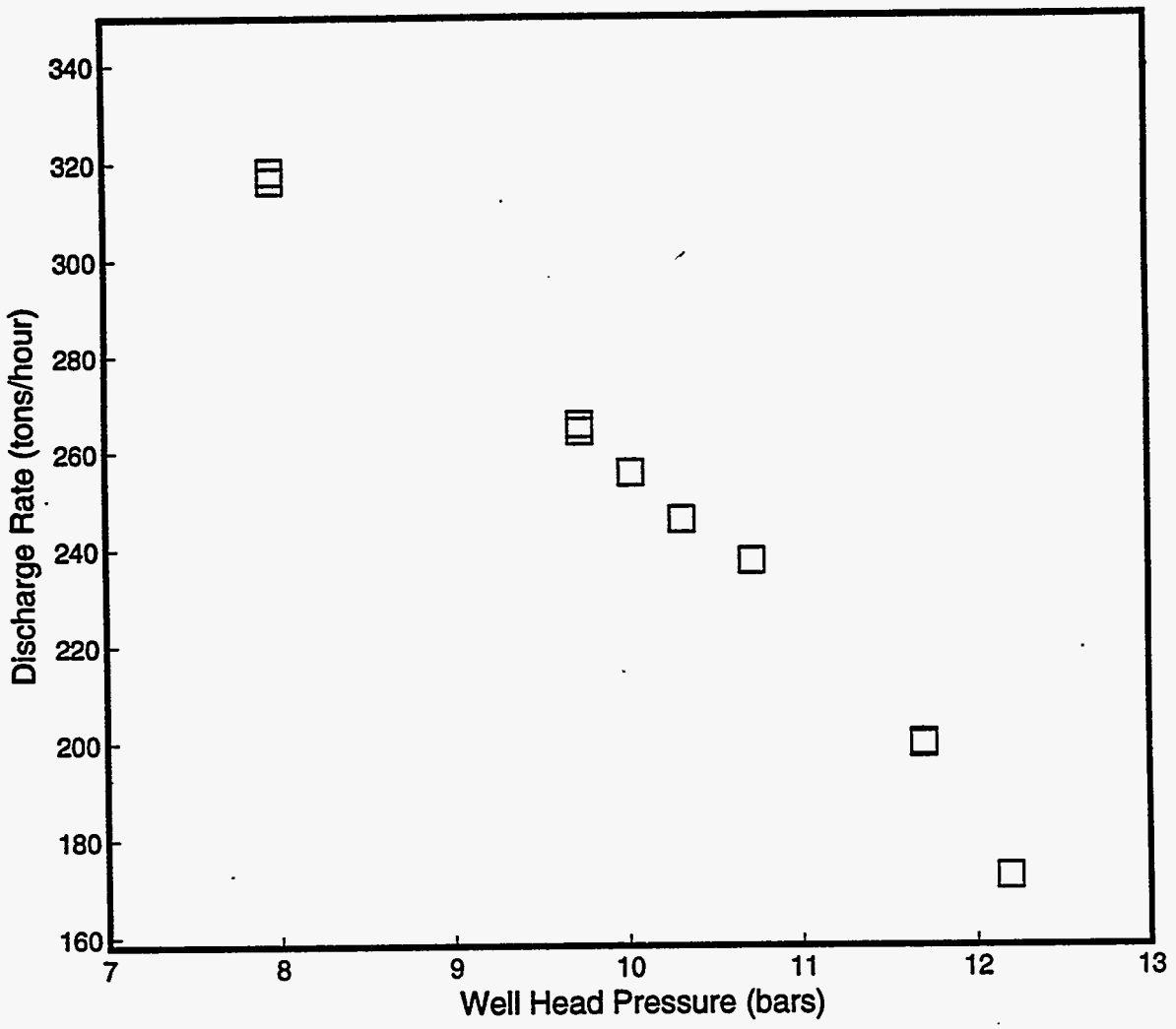

Figure 5.13. Discharge rate versus wellhead pressure for well IH-2 (February and March 1990).

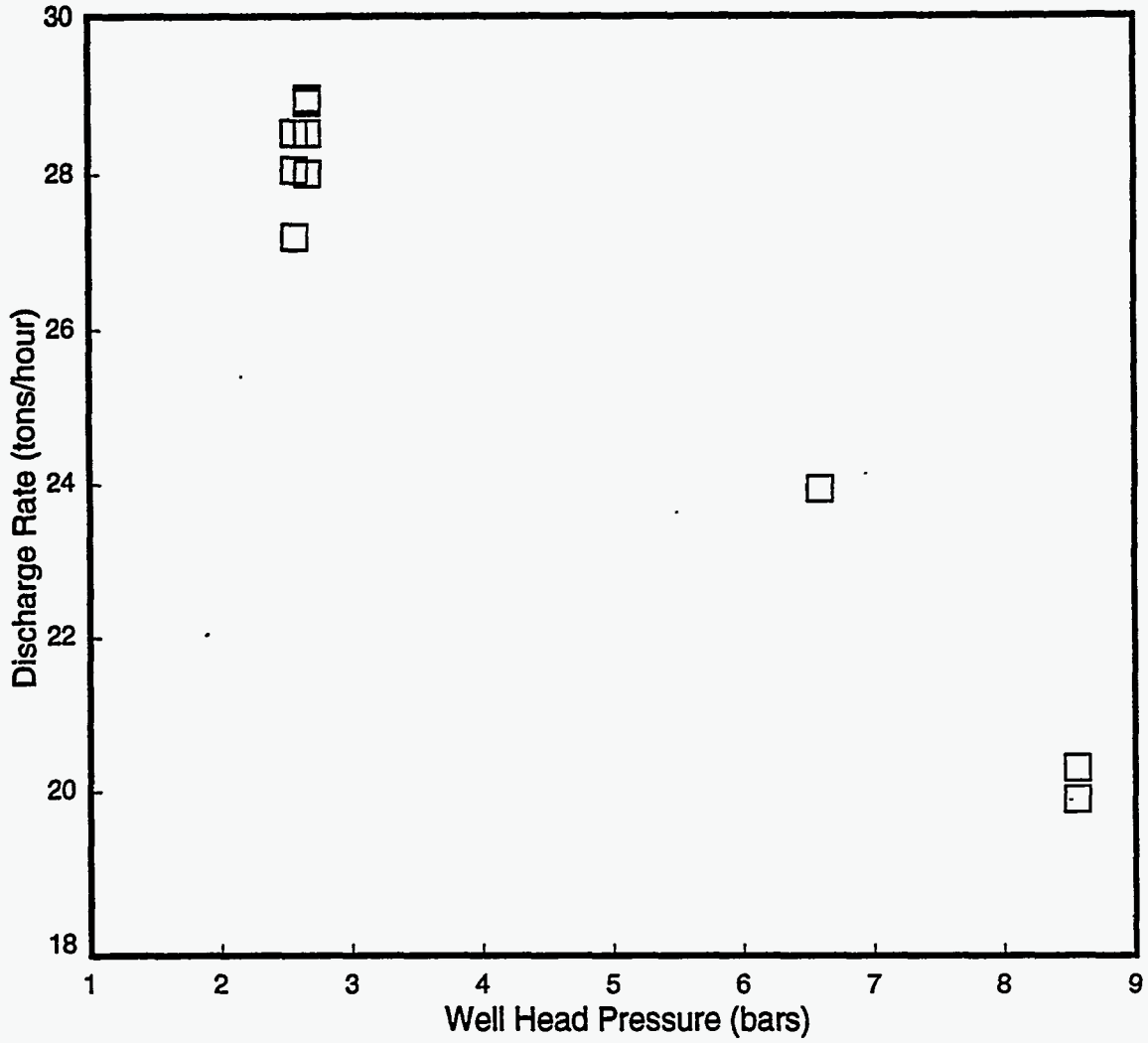

Figure 5.14. Discharge rate versus wellhead pressure for slim hole N2-KW-3 (March 1991).

Table 5.1. Measured maximum discharge rates for Oguni boreholes.

Borehole Name	Final Diameter (mm)	Measured Discharge (tons/hr)
A. Low-Pressure Reservoir		
GH-3	79	20
GH-4	76	27
GH-5	76	22
GH-7	98	30
GH-8	78	36
GH-10	159	164
GH-11	216	279
GH-12	216	279
GH-20	216	369
IH-2	216	316
B. High-Pressure Reservoir		
GH-6	76	24
GH-15	216	36*
HH-2	76	5*
N2-KW-3	76	28

* Two-Phase Flow

where M is the discharge (*i.e.*, mass production) rate, P_{ns} is the stable (static) feedzone (or gage depth) pressure, and P_{fp} is the flowing feedzone (or gauge depth) pressure. As remarked earlier, downhole pressure and temperature (under discharge conditions) are available for all the Oguni boreholes that have been discharged. These pressure surveys can be used for estimating flowing feedzone pressures.

A comparison of the measured pressure and temperature values in the two-phase zone of the borehole with the corresponding steam table values revealed significant discrepancies for most of the boreholes (pressure/temperature data for wells GH-11, 12 and 20 are the only exceptions). The measured pressures are compared with saturation pressures (for the measured temperature) in Appendix C. It has been our experience that the pressure gauges are often out of calibration. Accordingly, measured pressure values were corrected using the measured temperatures (in the two-phase zone) and the corresponding saturation pressures. In the single-phase liquid zone of the wellbore, a constant value—determined from measurements in the two-phase zone—was added to (or subtracted from) the measured pressure values. The stable feedzone pressure P_{ns} was calculated using the pressure correlation for low-pressure reservoir boreholes. For high pressure reservoir boreholes, measured values for P_{ns} were used.

The computed productivity indices for the various Oguni boreholes are listed in Table 5.2.

Table 5.2. Productivity indices for Oguni boreholes.

Borehole Name and Final Diameter (mm)	Feedzone Depth (m TVD)	Static Feedzone Pressure (bars)	Survey Date	Production Rate (tons/h)	Flowing Feedzone Pressure (bars)	*PI* (kg/s-bar)	Comments
			Low Pressure Reservoir				
GH-3 79	1030	75.0 (Pressure Correlation)	02-18-87 02-19-87 02-20-87	18.7 15.7 11.3	65.4 66.2 69.2	0.54 0.50 0.54	Add 0.8 bars to measured flowing pressures. Add 1.0 bars to measured flowing pressures. Add 1.0 bars to measured flowing pressures. (*PI*) avg ≈ 0.53 kg/s-bar.
GH-4 76	900	59.0 (Pressure Correlation)	02-27-86 02-28-86 03-01-86	14.0 20.5 21.4	56.9 54.8 53.6	1.85 1.36 1.10	Subtract 1.5 bars from measured flowing pressures. Add 1.4 bars to measured flowing pressures. Add 1.5 bars to measured flowing pressures. (*PI*) avg ≈ 1.44 kg/s-bar.
GH-5 76	1100	74.5 (Pressure Correlation)	02-17-87 02-18-87 02-19-87	20.6 17.0 12.7	69.9 70.2 71.6	1.24 1.10 1.22	Add 1.2 bars to measured flowing pressure. Add 1.0 bars to measured flowing pressure. Add 1.0 bars to measured flowing pressure. (*PI*) avg ≈ 1.19 kg/s-bar.
GH-7 98	980 (Shallow Feedzone)	64.5 (Pressure Correlation)	01-21-87 01-22-87 01-23-87	30.7 23.2 18.7	55.75 58.25 59.95	0.97 1.03 1.14	Add 0.65 bars to measured flowing pressure. Add 0.75 bars to measured flowing pressure. Add 0.75 bars to measured flowing pressure. (*PI*) avg ≈ 1.05 kg/s-bar.
GH-8 78	1220	89.5 (Pressure Correlation)	09-11-87 09-12-87 09-17-87	23.8 29.9 24.8	80.7 81.8 83.7	0.75 1.08 1.19	No correction applied to flowing pressures. Measured temperatures in the two-phase zone imply that the pressures may be in substantial error. (*PI*) avg ≈ 1.01kg/s-bar.
GH-10 159	1010	68.5 (Pressure Correlation)	08-06-87 08-13-87 08-15-87	126 150 167.9	60.1 58.4 54.5	4.17 4.13 3.33	1.4 bars added to measured flowing pressure. 2.4 bars added to measured flowing pressure. 2.0 bars added to measured flowing pressure. (*PI*) avg ≈ 3.88 kg/s-bar

Table 5.2. Productivity indices for Oguni boreholes (con't).

Borehole Name and Final Diameter (mm)	Feedzone Depth (m TVD)	Static Feedzone Pressure (bars)	Survey Date	Production Rate (tons/h)	Flowing Feedzone Pressure (bars)	*PI* (kg/s-bar)	Comments
Low Pressure Reservoir (con't)							
GH-11 216	1140	80.0 (Pressure Correlation)	07-19-91 07-20-91	188.8 244	71.4 67.0	6.10 5.21	(*PI*) avg ≈ 5.65 kg/s-bar
GH-12 216	720	44.0 (Pressure Correlation)	10-19-91 10-20-91	236 269	33.1 30.5	6.01 5.53	(*PI*) avg ≈ 5.77 kg/s-bar
GH-20 216	1560	114.0 (Pressure Correlation)	04-24-91 04-25-91 04-26-91	216.4 251.6 282.9	110.3 109.3 108.6	16.25 14.87 14.55	(*PI*) avg ≈ 15.2 kg/s-bar.
IH-2 216	550	35.5 (Pressure Correlation)	03-01-90 03-02-90	164.1 232.4	31.8 29.9	12.32 11.33	1.1 bar added to measured flowing pressure. 1.9 bar added to measured flowing pressure. (*PI*) avg ≈ 11.8 kg/s-bar
High Pressure Reservoir							
GH-6 76	770	53.5 (Measured)	03-13-86 03-14-86 03-15-86	14.0 18.9 23.4	52.7 52.4 52.3	4.86 4.77 5.42	(*PI*) avg ≈ 5.02 kg/s-bar.
GH-15 216	680	50.5 (Measured)	11-12-90 11-13-90	36.9 38.4	7.3 7.4	0.24 0.25	Two-phase flow. Subtracted 0.4 bars from measured flowing pressures.
HH-2 76	850	61.0 (Measured)	12-24-86 12-25-86	5.1 4.4	14.0 14.2	0.03 0.03	Two-phase flow. 0.6 bars added to measured flowing pressures.
N2-KW-3 76	810	52.0 (Measured)	03-25-91 03-26-91 03-28-91	27.4 23.8 19.8	50.0 49.9 50.8	3.81 3.15 4.58	Subtract 1.0 bars from measured flowing pressures. Subtract 2.9 bars from measured flowing pressures. Subtract 0.3 bars from measured flowing pressures. (*PI*) avg ≈ 3.85 kg/s-bar.

5.3 Pressure Buildup Tests

Pressure buildup data are available for all of the Oguni boreholes that have been discharged. In all cases, the pressure buildup responses were recorded by lowering a mechanical pressure gauge (usually a Kuster tool) into the borehole, either just before or right after, the completion of the discharge test. Because of instrument limitations, it was in several cases necessary to pull (and reinsert) the gauge out of the hole after a few hours; this resulted in a gap in the pressure buildup record. The relevant discharge/pressure buildup data are summarized in Table 5.3.

Multi-rate Horner plots of pressure buildup data for thirteen Oguni boreholes are shown in Figures 5.15 through 5.27. For slim holes GH-4, GH-6 and N2-KW-3, the relatively small change in pressure make the buildup data unsuitable for inferring formation properties. No pressure buildup data are available for this study for slim hole GH-8; the *kh* value for GH-8 listed in Table 5.3 is from an EPDC document.

Pressure buildup data for slim holes GH-3, GH-5, GH-7, and wells GH-10, GH-11, GH-12, GH-20 and IH-2 can be approximated by straight lines on the multi-rate Horner plots (see Figures 5.15–5.27). The slope m of the straight line can be used to estimate the formation transmissivity from the following relationship:

$$kh = \frac{1.15Mv}{2\pi m}$$

where M is the last flow rate prior to shutin and v is the kinematic viscosity of the reservoir liquid. The *kh* values obtained from the Horner plots are given in Table 5.3. Pressure buildup data for slim hole GH-7 recorded prior to and after the gap in pressure data (90 to 238 minutes) yield different slopes on the Horner plot. Possibility of interzonal flow between the two feedzones of slim hole GH-7 (980 m TVD and 1400 m TVD) during shutin cannot be ruled out. Therefore, the listed *kh* value for GH-7 may not be reliable.

Production from boreholes GH-15 and HH-2 was accompanied by *in situ* boiling. In the case of well GH-15, the wellbore (at feedzone depth) returned to single-phase liquid conditions within a few minutes after the well was shutin. The late-time pressure buildup data from well GH-15 were, therefore, analyzed using conventional single-phase analysis methods (*e.g.*, see analysis above for other Oguni boreholes). Slim hole HH-2, however, did not return to single-phase conditions within the pressure observation period (0 to 507 minutes). The pressure buildup data for slim hole HH-2 were accordingly interpreted using two-phase analysis methods (see, *e.g.*, Garg, 1980; Grant, 1978). The total kinematic mobility (permeability.k × thickness h / total kinematic viscosity v_t) for slim hole HH-2 is given in Table 5.3; note that no estimate of *kh* is available for HH-2.

Table 5.3. Summary of pressure buildup data for Oguni boreholes.

Borehole	Feedzone Depth (m TVD)	Feedzone Pressure and Temperature	Discharge Interval	Sensor Depth	Pressure Buildup Interval	Comments
GH-3	1030	75 bars 214°C	02/02/87 13:55→ 02/22/87 10:12	1000 m MD	0–140 min 253–528 min	Single-phase liquid flow. Using T = 215°C, kh = 0.44 darcy-m.
GH-4	900	59 bars 234°C	02/12/86 15:40→ 03/02/86 12:26	850 m MD	0–240 min 326–596 min	Data lack sufficient resolution for analysis.
GH-5	1100	74.5 bars 187°C	02/10/86 12:00→ 03/03/86 11:11	1150 m MD (1097 m TVD)	0–240 min 330–569 min	Single-phase liquid flow. Using T =187°C, kh = 4.5 darcy-m.
GH-6	770	53.5 bars 215°C	03/08/86 10:14→ 03/20/86 10:58	750 m MD	0–196 min 320–561 min	Data lack sufficient resolution for analysis.
GH-7	980 and 1400	64.5/100.5 bars < 219°C/230°C	01/06/87 17:18→ 01/24/87 10:05	1500 m MD (1400 m TVD)	0–90 min 238–458 min	Single-phase liquid flow. Using T = 220°C, kh = 1.3 darcy-m. (See text.)
GH-8	1220	89.5 bars 212°C	09/01/87 11:30→ 09/22/87 10:26	?	?	Single-phase liquid flow. Using T = 215°C, kh = 28.6 darcy-m. (Analysis by EPDC).
GH-10	1010	68.5 bars 241°C	07/08/87 17:05→ 08/18/87 10:40	1000 m MD (968 m TVD)	0–146 min 371–540 min	Single-phase liquid flow. Using T = 241°C, kh = 92 darcy-m.
GH-11	1140	80 bars 236°C	06/05/91 17:30→ 07/21/91 11:43	1377 m MD (1140 m TVD)	0–240 min	Using T = 236°C, kh = 83 darcy-m.
GH-12	750	45.5 bars 232°C	09/05/91 13:00→ 10/20/91 10:44	765 m MD (746 m TVD)	0–300 min	Using T = 232°C kh = 32 darcy-m.
GH-15	680	50.5 bars 230°C	10/31/90 13:50→ 11/15/90 10:00	800 m MD (727 m TVD)	0–300 min 360–600 min	Two-phase flow. kh = 0.47 darcy-m. (See text.)
GH-20	1560	114.5 bars 241°C	04/15/91 15:05→ 04/27/91 11:04	1750 m MD (1542 m TVD)	0–256 min	Using T = 241°C kh = 55 darcy-m.
HH-2	850	61 bars 219°C	12/10/86 14:16→ 12/26/86 10:56	835 m MD	0–150 min 237–507 min	Two-phase flow. $kh/v_t = 3.4 \times 10^{-6}$ m-s. (See text.)
IH-2	550	35.5 bars 226°C	02/21/90 11:30→ 03/03/90 13:31	570 m MD (546 m TVD)	0–309 min .	Using T = 226°C, kh = 44 darcy-m.
N2-KW-3	810	52 bars 227°C	03/18/91 09:46→ 03/29/91 11:00	910 m MD (886 mTVD)	0–255 min	Pressure data lack sufficient resolution for analysis.

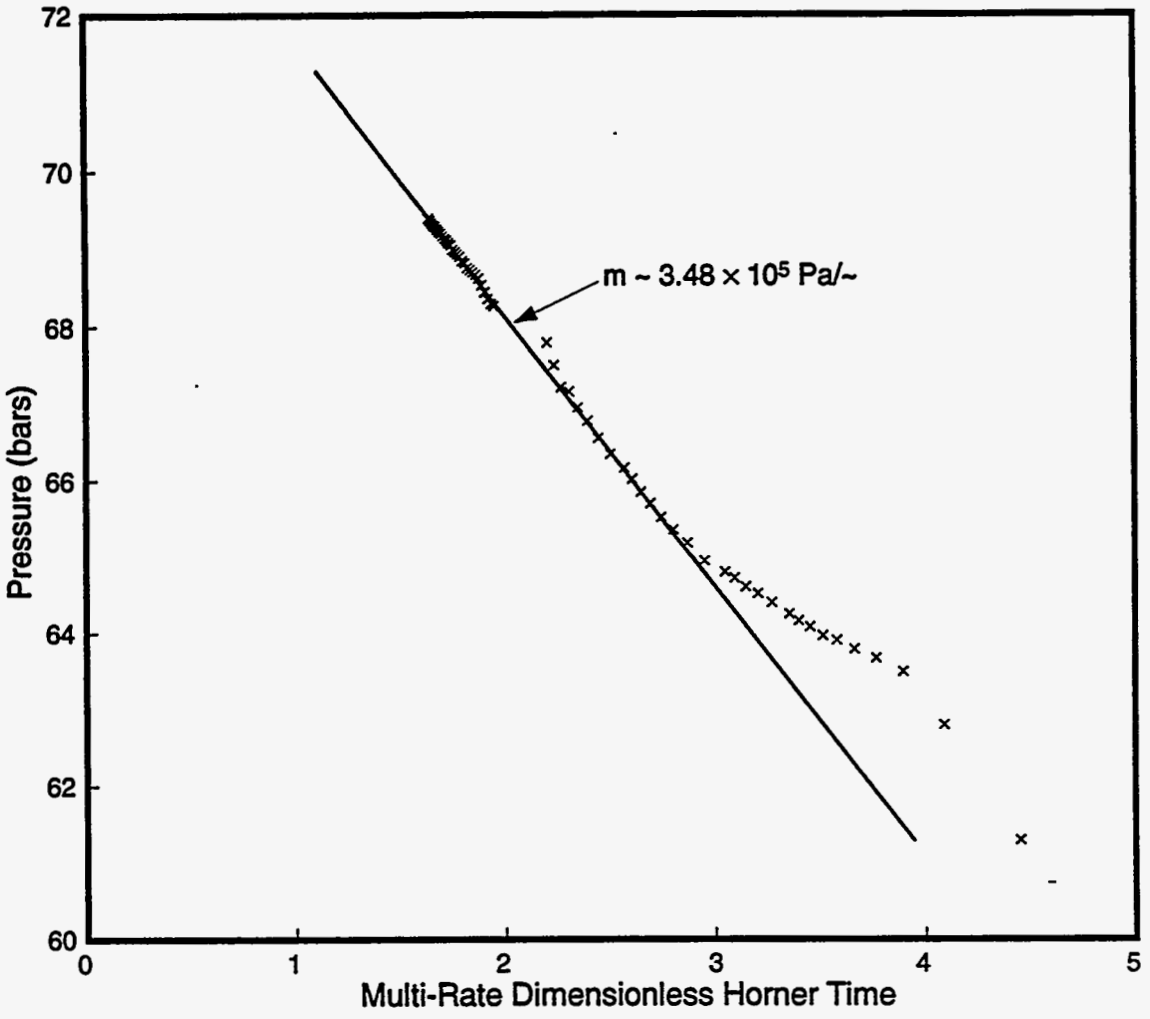

Figure 5.15. Multi-rate Horner plot of pressure buildup data for slim hole GH-3. Pressures were recorded at 1000 m MD from $\Delta t = 0$ minutes to $\Delta t = 140$ minutes, and from $\Delta t = 253$ minutes to $\Delta t = 528$ minutes. To remove an offset in the pressure data, 0.69 bars were subtracted from late time ($\Delta t = 253$ to 528 minutes) pressure data.

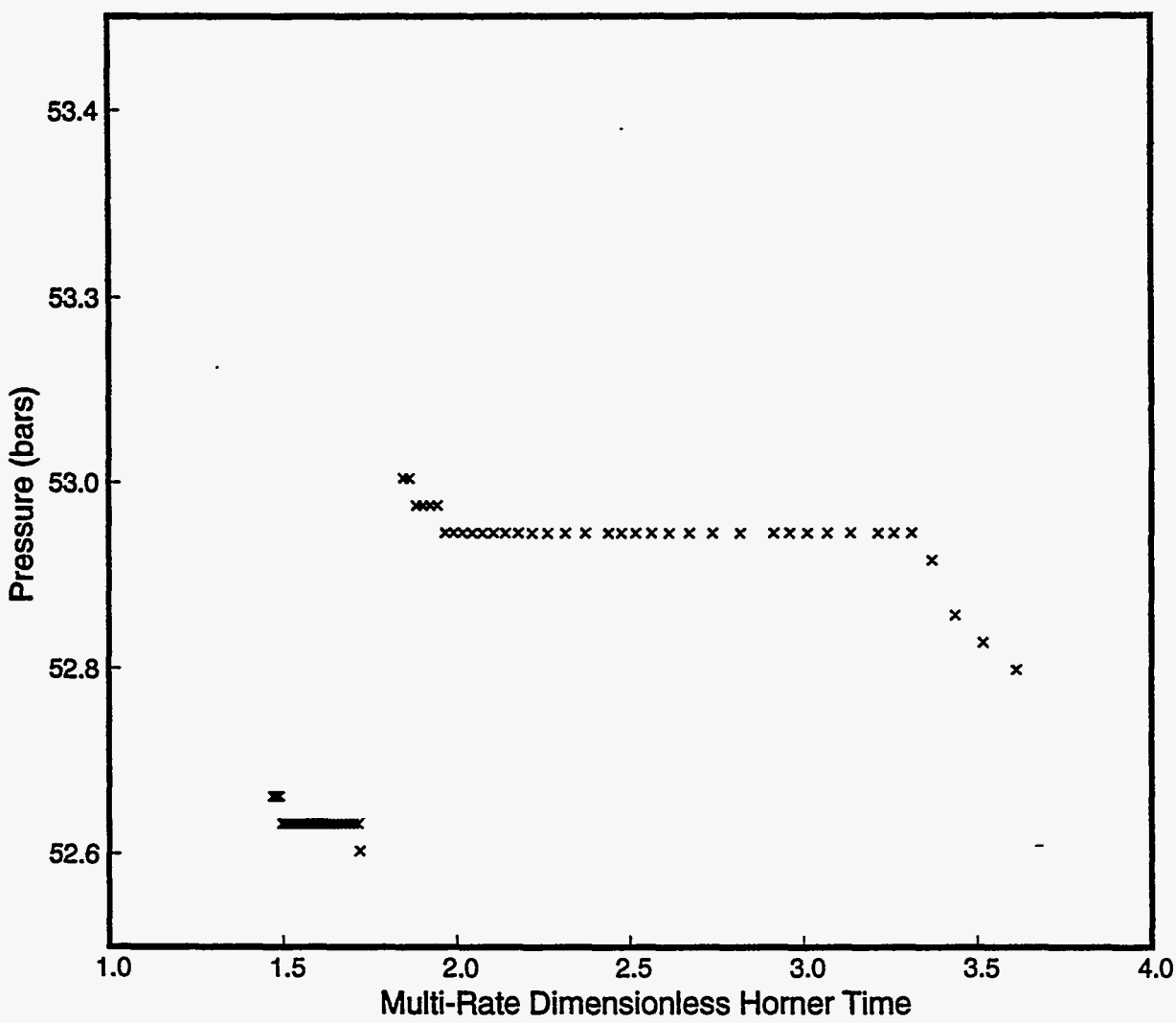

Figure 5.16. Multi-rate Horner plot of pressure buildup data for slim hole GH-4. The pressure data lack sufficient resolution to identify the appropriate straight line.

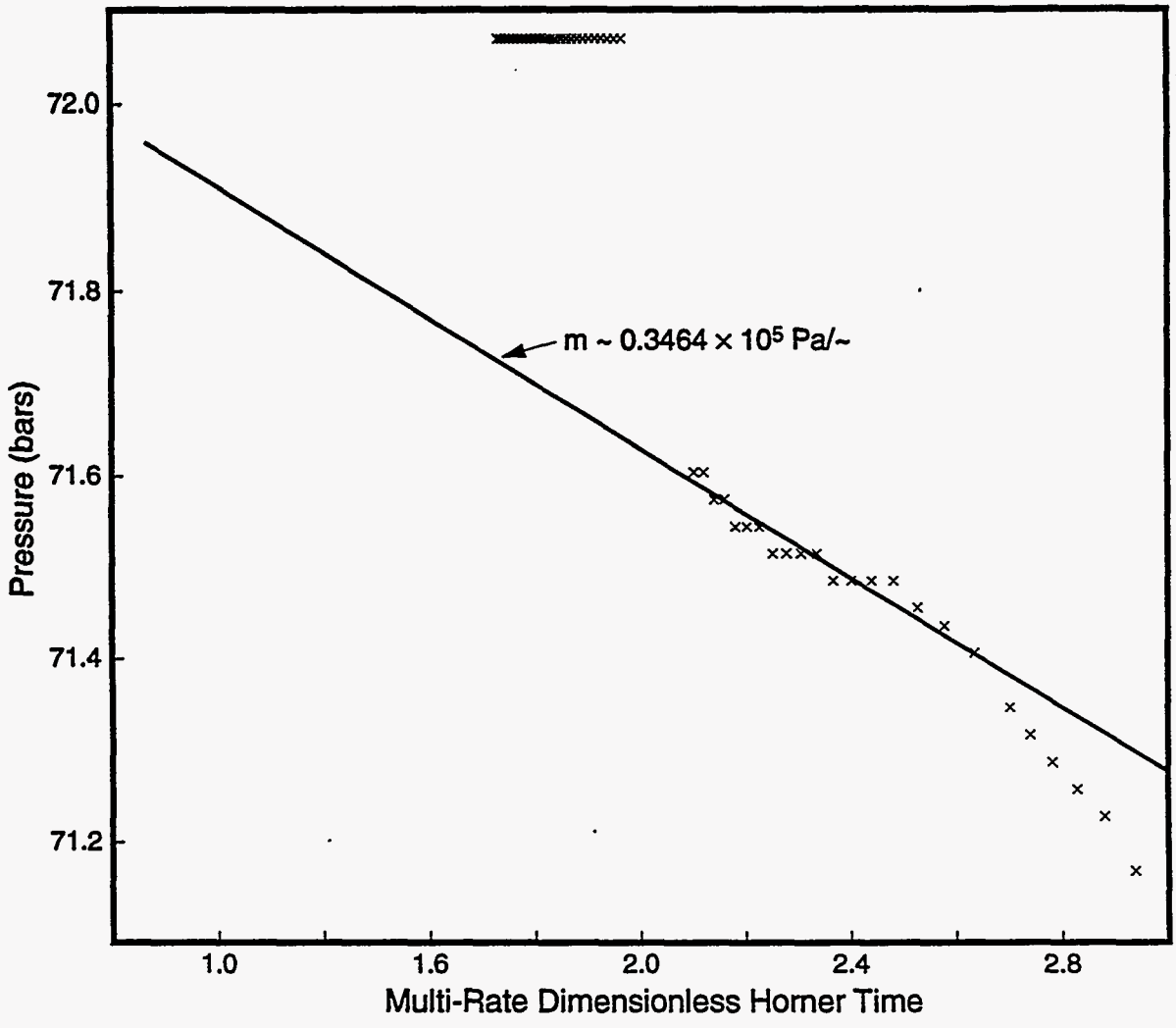

Figure 5.17. Multi-rate Horner plot of pressure buildup data for slim hole GH-5. Pressures were recorded at 1150 m MD (1097 m TVD) from $\Delta t = 0$ minutes to $\Delta t = 240$ minutes, and from $\Delta t = 330$ minutes to $\Delta t = 569$ minutes. Note the offset between the early-time ($\Delta t = 0$ to 240 min) and late-time ($\Delta t = 330$ to 569 minutes) pressure data. The straight line used for computing *kh* extends over less than one log-cycle; hence, the estimate for *kh* may not be too reliable.

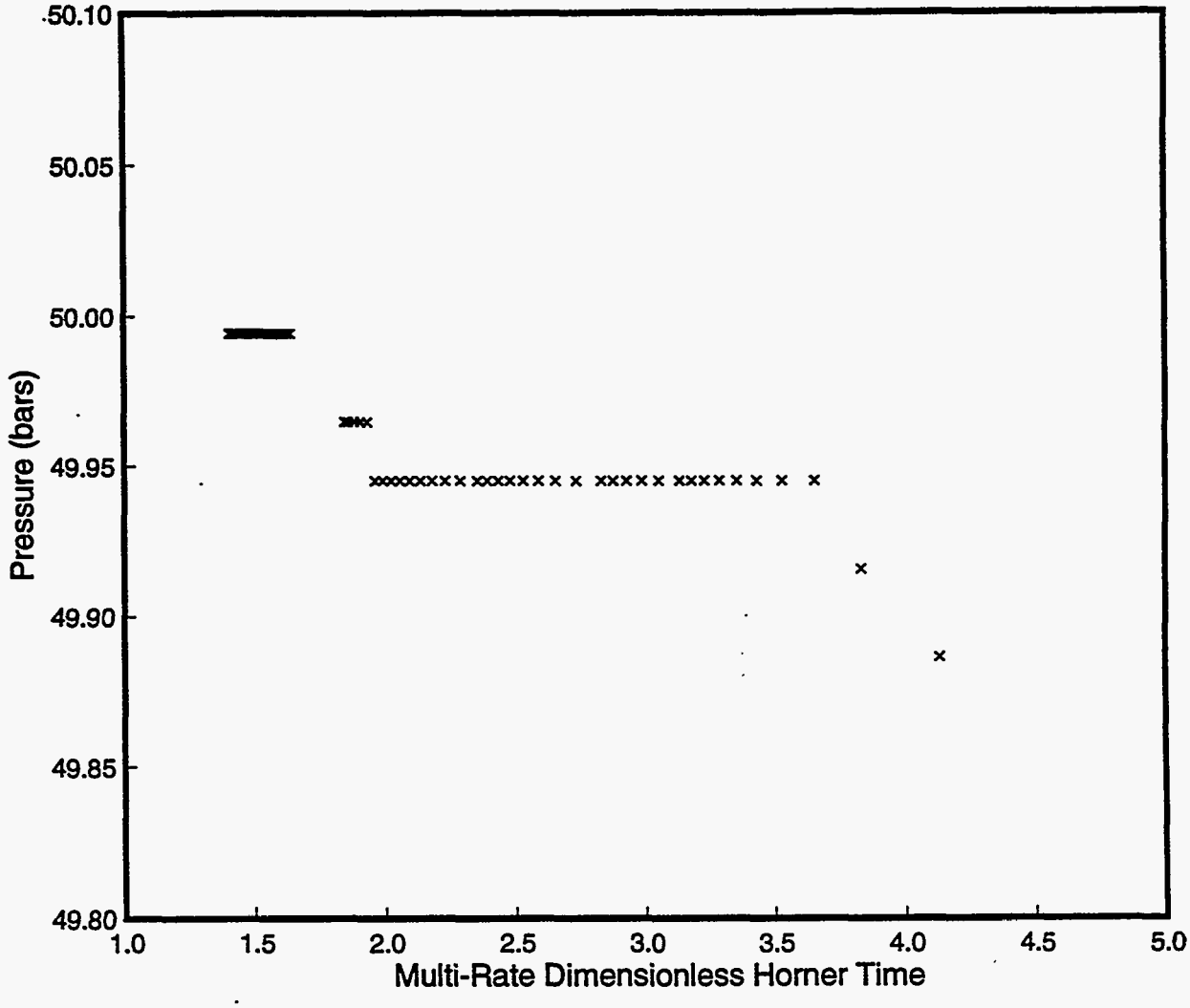

Figure 5.18. Multi-rate Horner plot of pressure buildup data for slim hole GH-6. The pressure data lack sufficient resolution to identify the proper straight line.

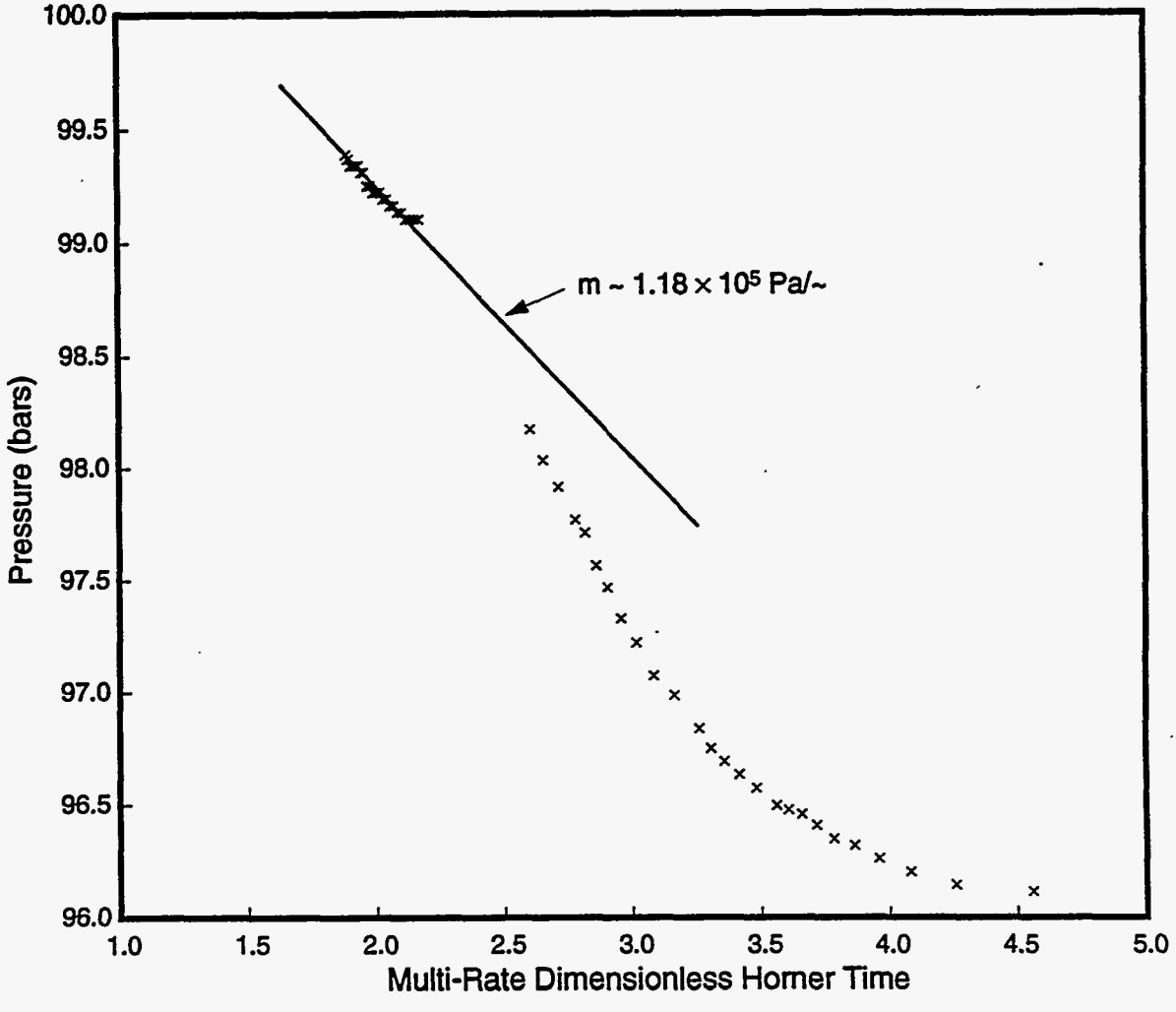

Figure 5.19. Multi-rate Horner plot of pressure buildup data for slim hole GH-7. Pressures were recorded at 1500 m MD (1400 m TVD) from $\Delta t = 0$ to 90 minutes and from $\Delta t = 238$ to 458 minutes. Note that the pressure buildup data recorded prior to and after the gap (90 to 238 minutes) yield different slopes on the Horner plot.

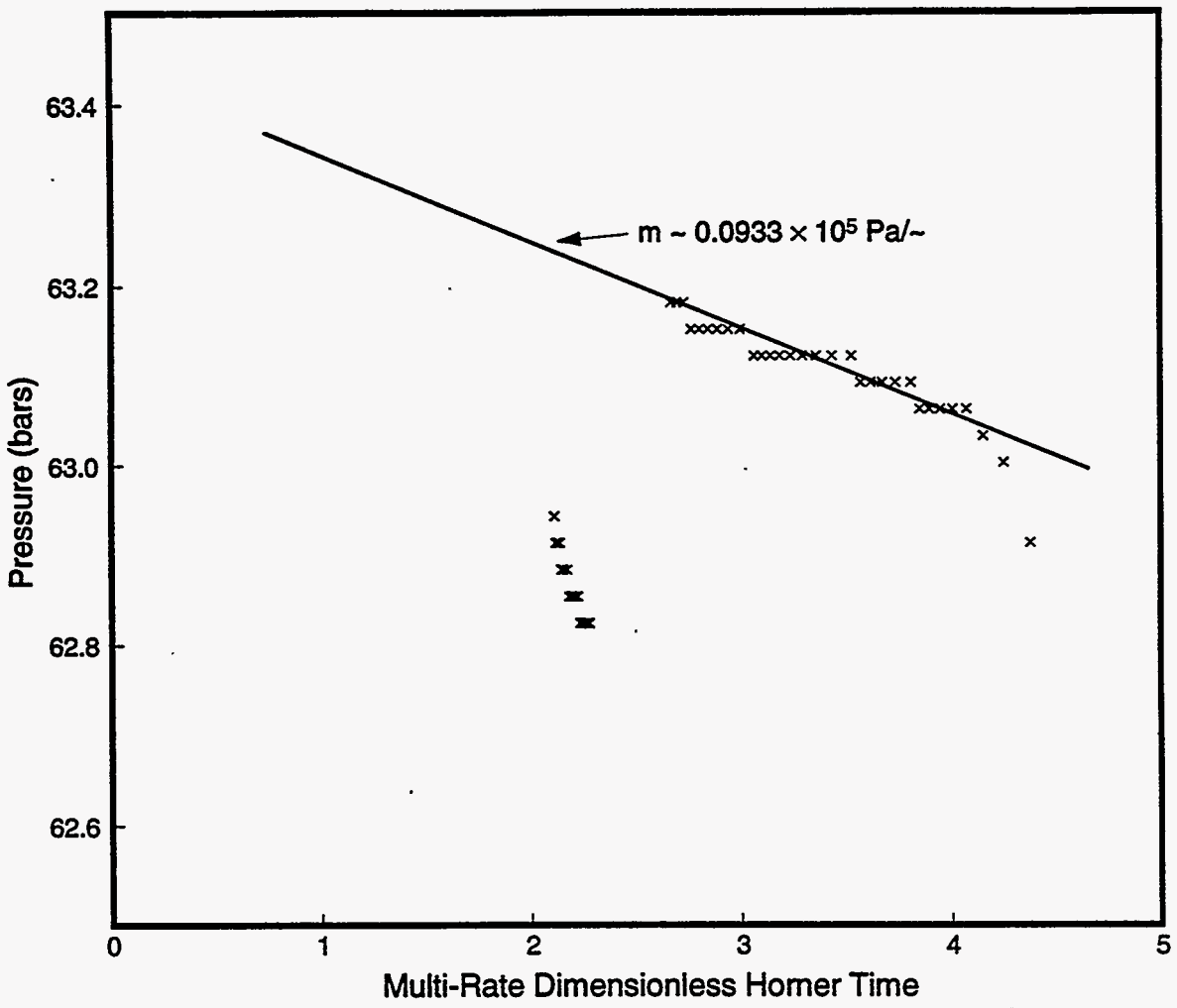

Figure 5.20. Multi-rate Horner plot of pressure buildup data for well GH-10. Pressures were recorded at 1000 m MD (968 m TVD) from $\Delta t = 0$ to 146 minutes and from $\Delta t = 371$ to 540 minutes.

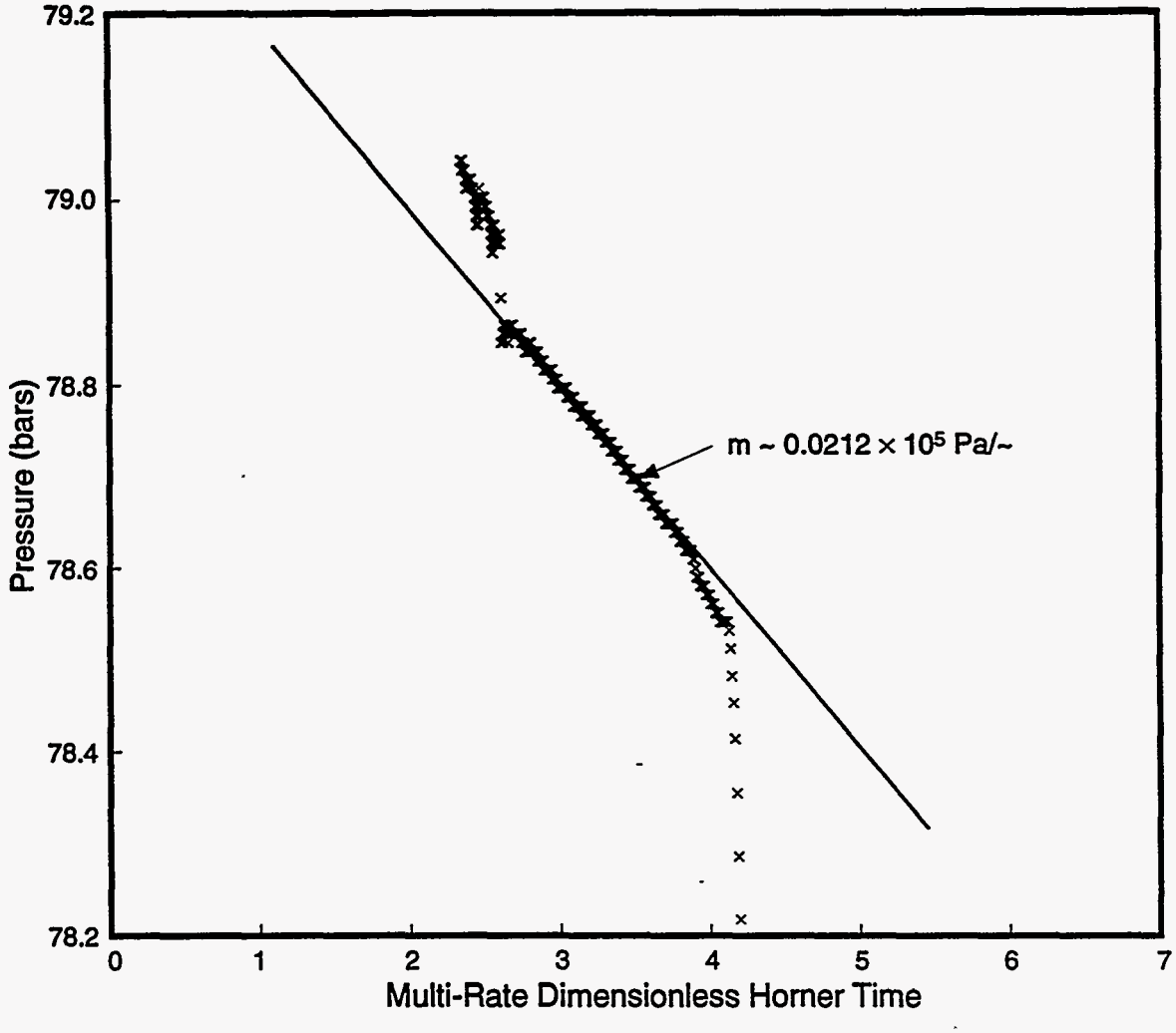

Figure 5.21. Multi-rate Horner plot of pressure buildup data for well GH-11. Pressures were recorded at 1377 m MD (1140 m TVD) for 240 minutes after shutin. The reasons for a sudden jump in pressure at about 128.5 minutes are unknown.

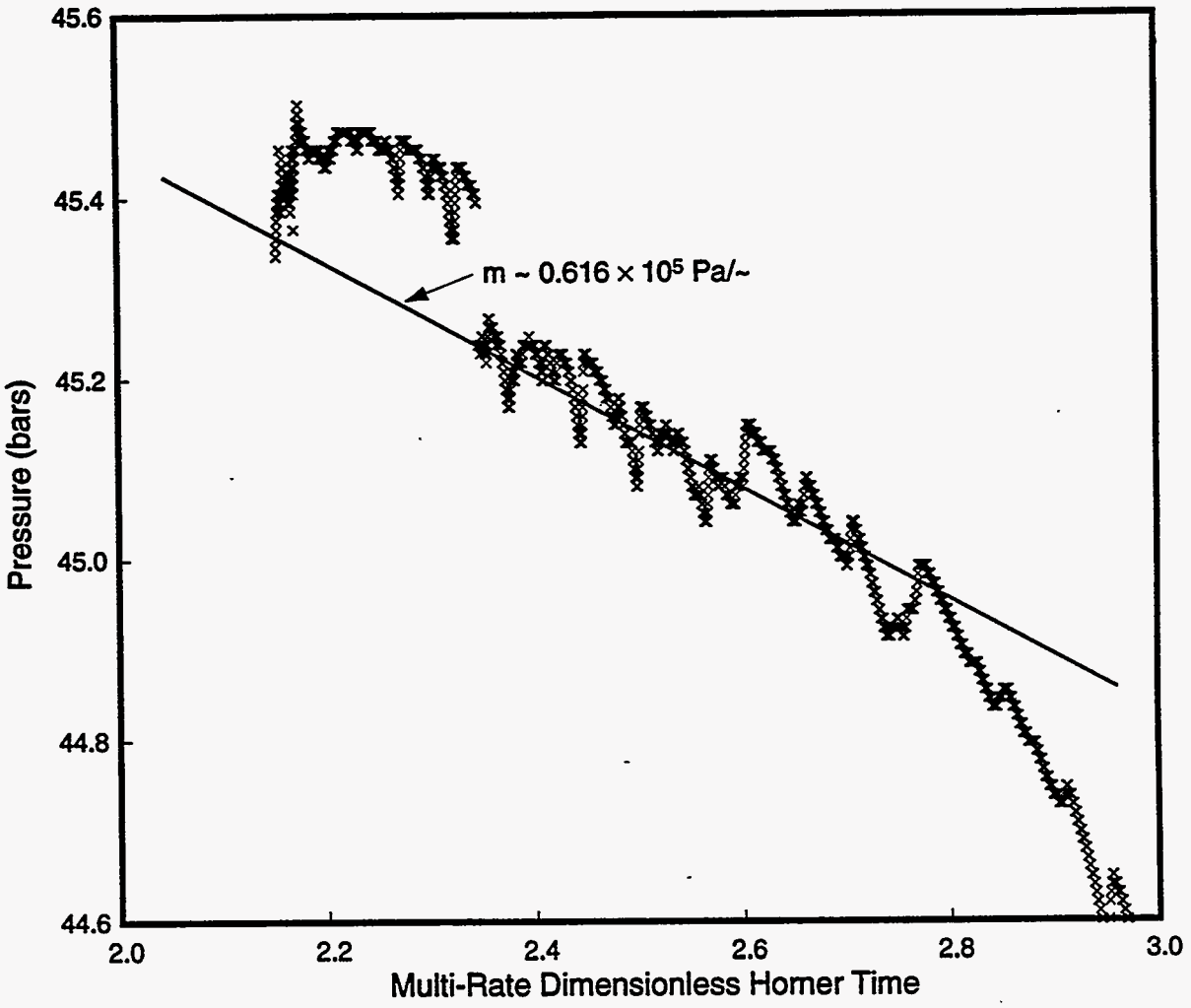

Figure 5.22. Multi-rate Horner plot of pressure buildup data for well GH-12. Pressures were recorded at 765 m MD (746 m TVD) for 300 minutes after shutin. The reasons for a sudden jump in pressure at about 169 minutes are unknown. Since the straight line extends over less than one log-cycle, the computed *kh* value (32 darcy-m) may not be reliable.

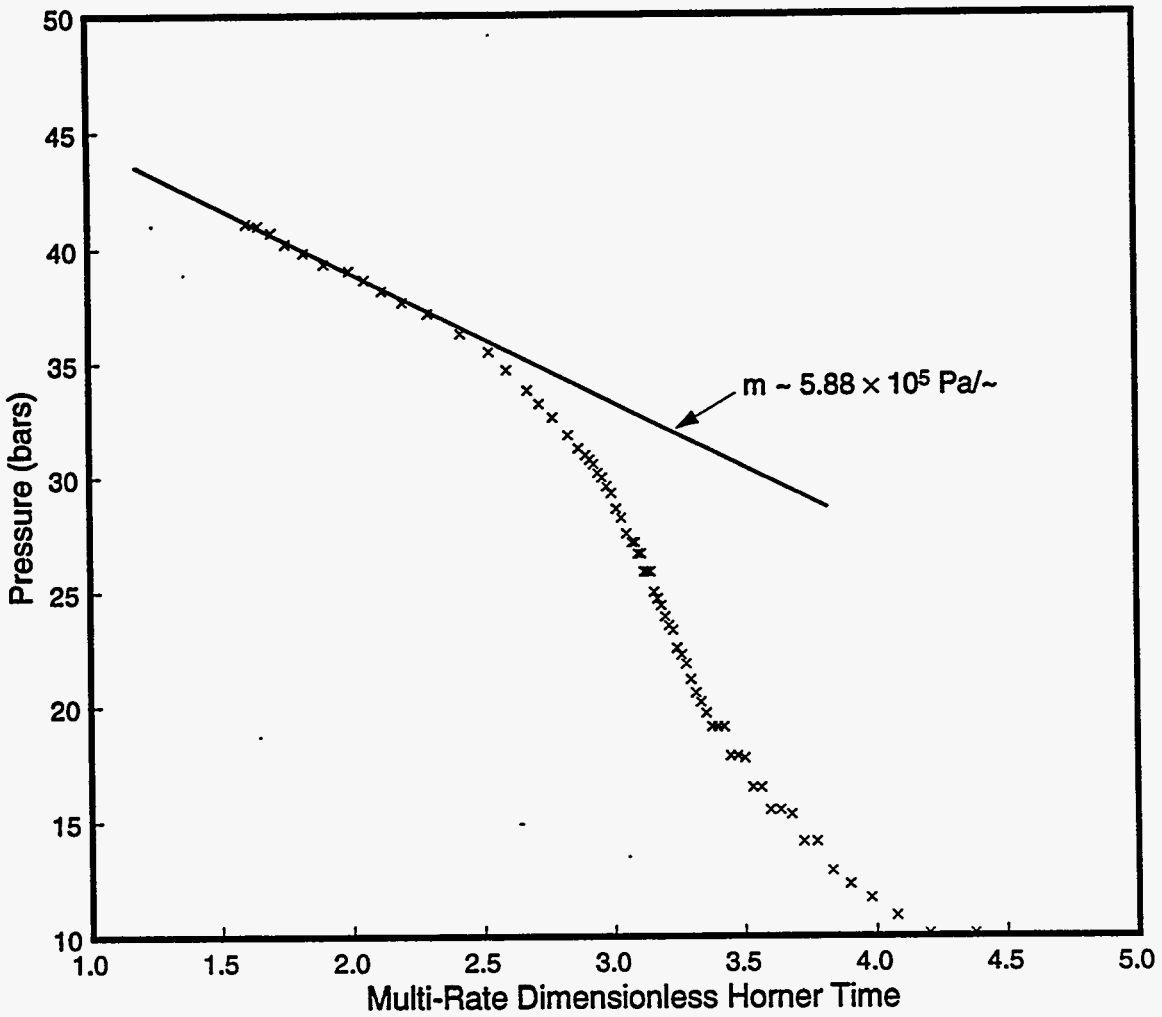

Figure 5.23. Multi-rate Horner plot of pressure buildup data for well GH-15. Pressures were recorded at 800 m MD (727 m TVD) from $\Delta t = 0$ to 300 minutes and from 360 to 600 minutes. To remove the offset in pressure data at 360 minutes, 1.6 bars were subtracted from all late-time ($\Delta t = 360$ to 600 minutes) buildup data.

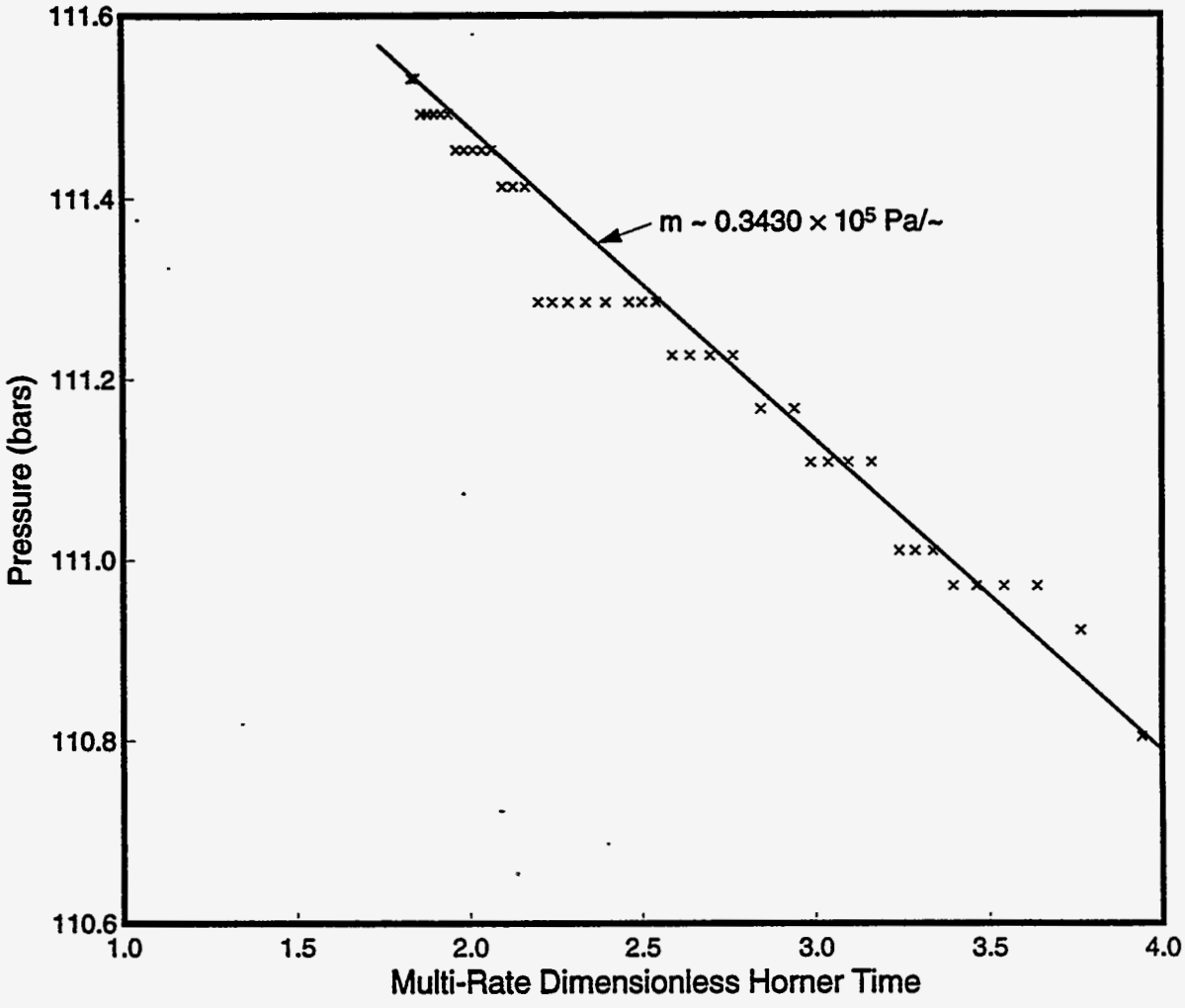

Figure 5.24. Multi-rate Horner plot of pressure buildup data for well GH-20. Pressures were recorded at 1750 m MD (1542 m TVD) for 256 minutes following well shutin.

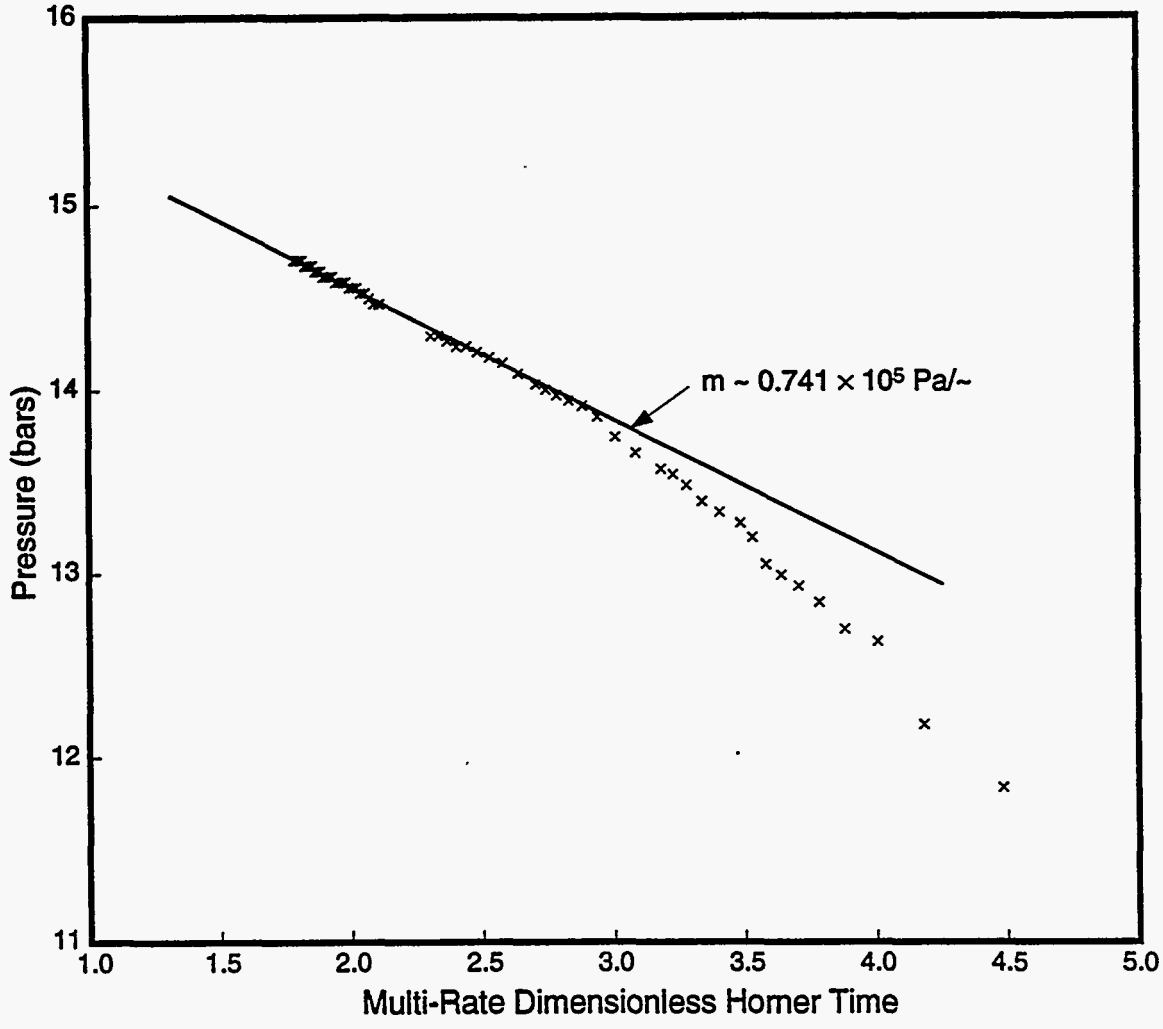

Figure 5.25. Multi-rate Horner plot of pressure buildup data for slim hole HH-2. Pressures were recorded at 835 m MD (835 m TVD) from $\Delta t = 0$ to 150 minutes and from 237 to 507 minutes. To remove the offset in pressure data at 237 minutes, 0.174 bars were subtracted from all late-time ($\Delta t = 237$ to 507 minutes) pressure data.

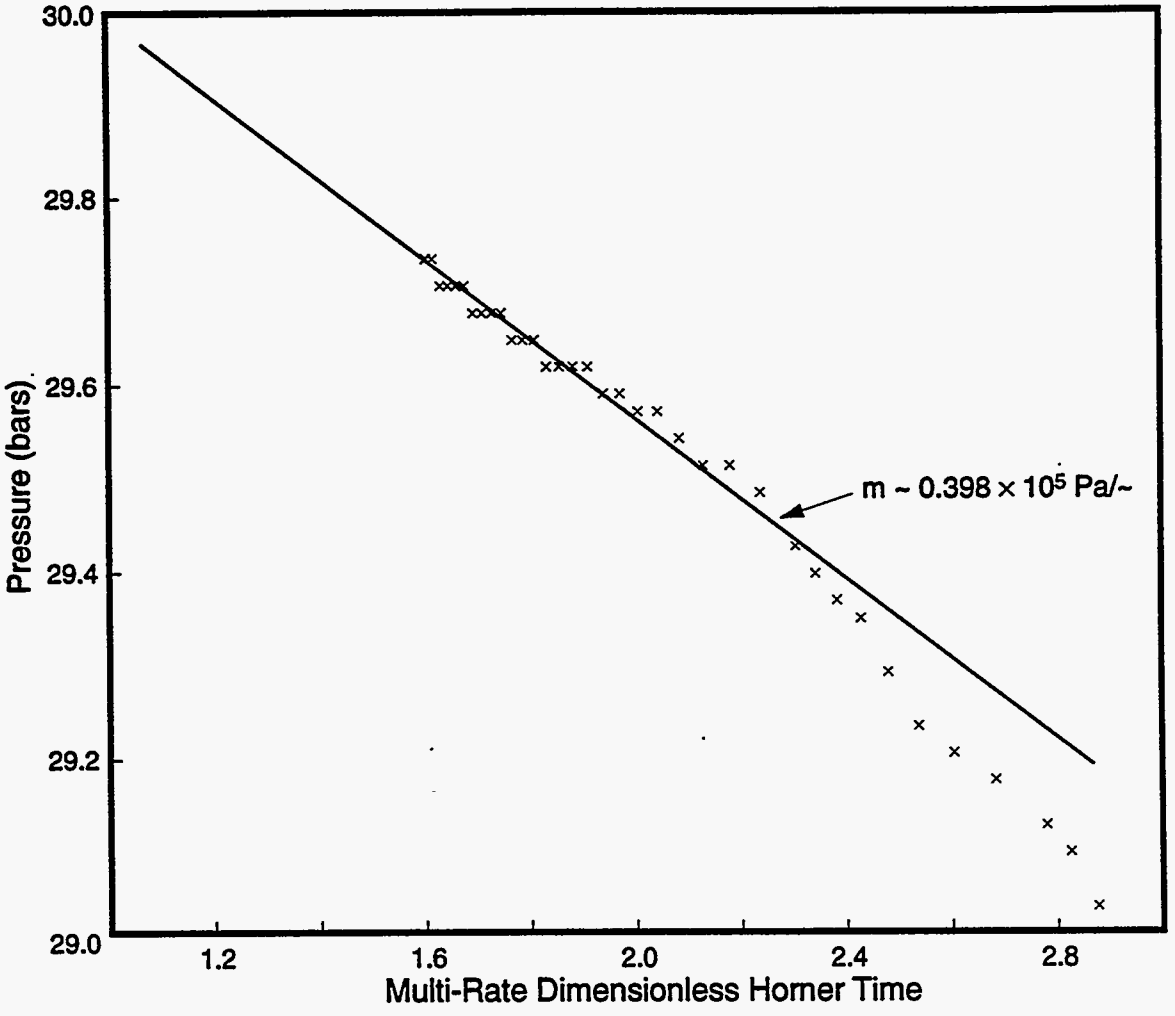

Figure 5.26. Multi-rate Horner plot of pressure buildup data for well IH-2. Pressures were recorded at 570 m MD (546 m TVD) for 309 minutes following well shutin.

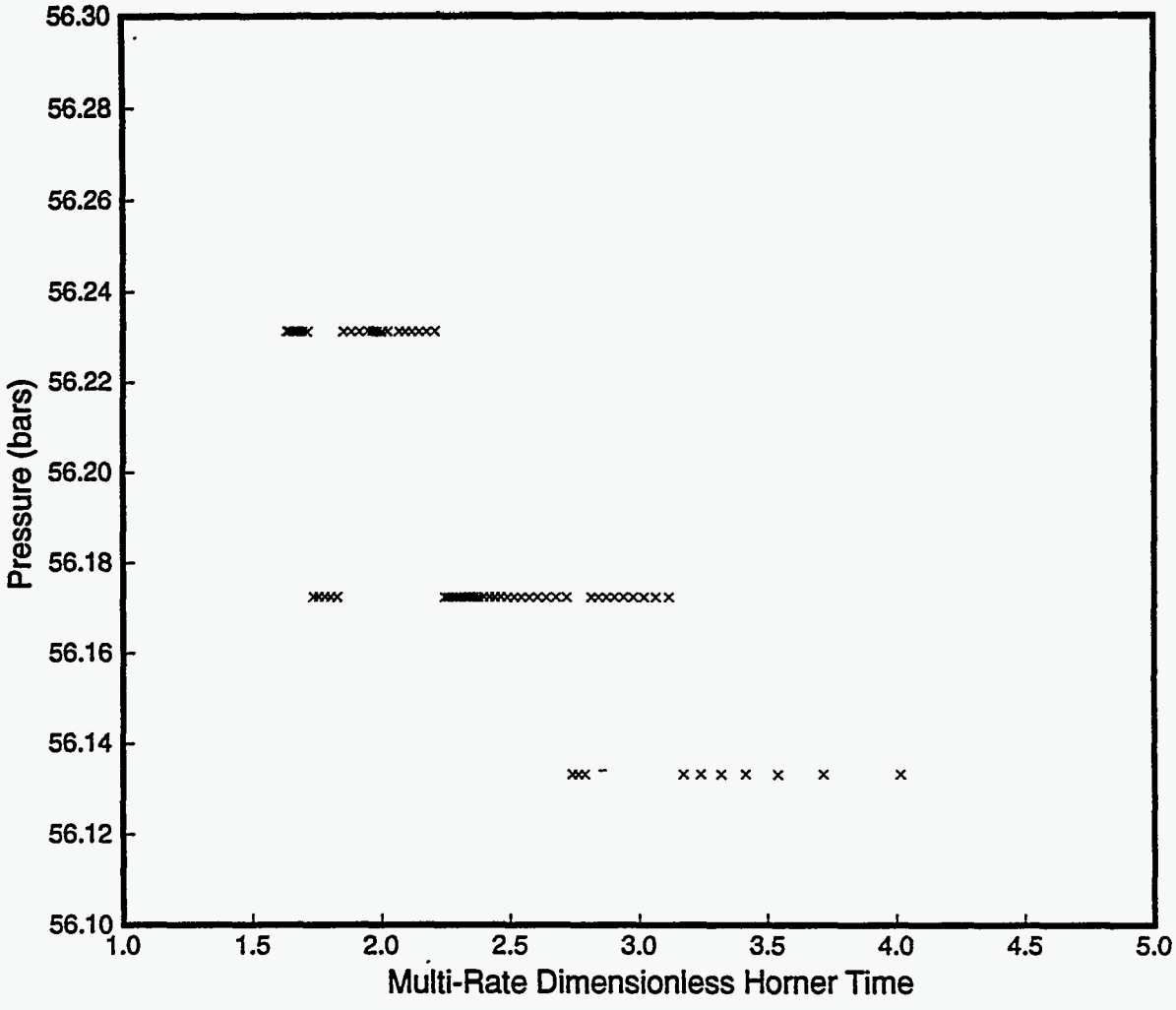

Figure 5.27. Multi-rate Horner plot of pressure buildup data for slim hole N2-KW-3. The pressure data lack sufficient resolution for analysis purposes.

SECTION 6

Discussion and Conclusions

6.1 Formation Transmissivity

EPDC has carried out a number of pressure interference tests on the boreholes in the Oguni Geothermal Field. Analyses of pressure interference data from the low-pressure reservoir boreholes indicate that the northern Hohi area has good permeability (kh = 100 to 250 darcy-meters); the transmissivity (kh) value for the high-pressure reservoir is of the order of 10 darcy-meters (Garg, *et al.*, 1993). Permeability-thickness values inferred from pressure fall-off (see Section 4) and pressure buildup data (Section 5) from individual Oguni boreholes are listed in Table 6.1. Pressure buildup data from individual "low-pressure reservoir" boreholes (Table 6.1) yield kh values in the range 0.4 to 92 darcy-meters; interestingly, smaller kh values are generally associated with small-diameter slim holes. For large-diameter wells, kh values inferred from buildup tests vary from 32 to 92 darcy-meters. The kh values obtained from short-term injection tests range from 0.1 and 25 darcy-meters for all the low-pressure zone boreholes; the kh values for large-diameter wells (excluding well GH-17) vary from 5 to 25 darcy-meters.

Table 6.1. Permeability-thickness (kh) inferred from pressure fall-off (injection tests) and pressure buildup (discharge tests) data for Oguni boreholes.

Borehole Name	Final Diameter (mm)	Production kh (darcy-m)	Injection* kh (darcy-m)
A. Low-Pressure Reservoir			
GH-3	79	0.44	—
GH-4	76.	—	—
GH-5	76.	4.5	—
GH-7	98.	1.3	—
GH-8	78.	29	—
GH-10	159.	92.	—
GH-11	216.	83.	6.9
GH-12	216.	32.	5.1
GH-17	216.	—	0.14
GH-20	216.	55.	6.1
GH-21	216.	—	14
IH-1	159.	—	0.73
IH-2	216.	44.	25
N2-KW-1	76.	—	9.3
N2-KW-2	76.	—	0.58
B. High-Pressure Reservoir			
GH-6	76.	—	—
GH-9	78.	—	0.03
GH-15	216.	0.47	0.92
GH-19	216.	—	—
HH-2	76.	—	—
N2-KW-3	76.	—	—

* Average value obtained from the various fall-off tests for a borehole.

Analyses of pressure transient data from the boreholes in the Oguni Geothermal Field indicate that (1) the *kh* values inferred from pressure interference and pressure buildup tests are significantly greater than those derived from pressure fall-off tests, and (2) the slim holes yield *kh* values which are smaller than those obtained from large-diameter wells..

In fractured geothermal reservoirs, interference tests commonly yield higher *kh* values than those given by pressure buildup (and pressure fall-off) tests. An individual borehole intersects at most a few major fractures. These major fractures join the fracture network at some distance from the borehole. The reservoir radius investigated during a borehole test is roughly proportional to the square root of time. A pressure buildup test generally samples a smaller region of the reservoir than that investigated by an interference test. The *kh* values obtained from pressure buildup tests (32 to 92 darcy-meters) for large-diameter wells at Oguni are smaller by a factor of about three from those given by pressure interference tests (100 to 250 darcy-meters). In contrast with longer term discharge tests (days to months in duration), short term injection tests (a few hours) sample only the near wellbore region. The pressure fall-off data yield *kh* values (5 to 25 darcy-meters for large-diameter wells) which are much smaller than those obtained from pressure buildup and pressure interference tests. These results suggest that short term injection tests are likely to yield a lower bound on reservoir transmissivity.

We speculate that the differences in *kh* values inferred for slim holes and large-diameter wells may be caused by the differences in drilling techniques (*i.e.*, core drilling versus rotary drilling). The core drilling is more likely to plug the near wellbore fractures with rock flour and/or mud than with rotary drilling. At Oguni, the formation permeability is mainly associated with a horizontal fracture zone located in the lower Hohi and upper Shishimuta formations. Many of the slim holes were drilled with a complete loss of circulation fluid (see Appendix B). The circulation fluid, in most cases, consisted of a dilute (mud density ~ 1.00 to 1.05 gm/cm^2) bentonite based mud. In contrast with slim holes, blind drilling was rarely used for rotary drilled large-diameter wells. It is thus possible that core drilling (at least in the case of Oguni Geothermal Field) causes greater formation plugging than that resulting from rotary drilling. Our speculation regarding formation plugging can only be verified by comparing "*kh*" values obtained from a large number of core- and rotary-drilled boreholes in several different geothermal fields.

6.2 Productivity and Injectivity Indices

Ignoring pressure transient effects, the flow resistance (*i.e.* pressure losses) of the reservoir rocks can be represented by the productivity (or injectivity) index. The productivity and injectivity indices (see Sections 4 and 5) for the various Oguni boreholes are listed in Table 6.2. Both the productivity and injectivity indices are available for seven of the Oguni boreholes (Table 6.2); these data are displayed in Figure 6.1. It appears from Figure 6.1 that to first order the productivity and injectivity indices for the Oguni boreholes are equal. The latter observation is at variance with the results of the

Table 6.2. Productivity/injectivity indices of Oguni boreholes.

Borehole Name	Final Diameter (mm)	Productivity Index (kg/s-bar)	Injectivity Index (kg/s-bar)
A. Low-Pressure Reservoir			
GH-3	79	0.53	—
GH-4	76.	1.44	—
GH-5	76.	1.19	—
GH-7	98.	1.05	—
GH-8	78.	1.01	—
GH-10	159.	3.88	3.39
GH-11	216.	5.65	1.53
GH-12	216.	5.77	5.12
GH-17	216.	—	0.46
GH-20	216.	15.2	7.82
GH-21	216.	—	12.1
IH-1	159.	—	0.84
IH-2	216.	11.9	33.
N2-KW-1	76.	—	2.11
N2-KW-2	76.	—	0.86
B. High-Pressure Reservoir			
GH-6	76.	5.02	—
GH-9	78.	—	0.08
GH-15	216.	0.25	1.75
GH-19	216.	—	25.7
HH-2	76.	0.03	—
N2-KW-3	76.	3.85	5.85

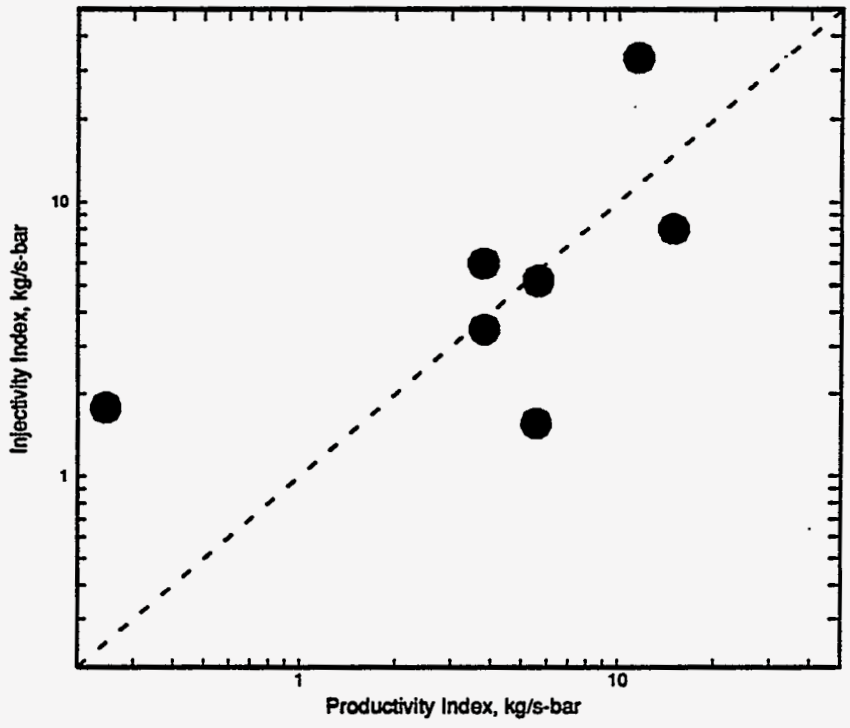

Figure 6.1. Productivity versus injectivity index for low-pressure reservoir Oguni boreholes.

classical porous-medium flow analyses (see *e.g.*, Garg and Pritchett, 1990) which suggest that the injectivity index should be a strong function of the sand face injection temperature. Grant *et al.* (1982), however, maintain that the classical analyses do not apply to geothermal systems which are mostly associated with fractured formations; and that injectivity is at least as great as productivity in discharge tests. The Oguni data are consistent with Grant, *et al.*'s viewpoint and imply that in the absence of productivity data, injectivity index may be used to characterize the flow resistance of the reservoir rocks.

Theoretical considerations (Pritchett, 1992 and Hadgu *et al.*, 1994) suggest that apart from any differences associated with differences in wellbore skin (*i.e.*, near borehole formation damage or stimulation), the productivity (or injectivity) index should exhibit only a weak dependence on borehole diameter. The available productivity/injectivity index data for low-pressure zone boreholes (see Table 6.2) are displayed in Figures 6.2a and 6.2b. Both the productivity and injectivity indices (and hence wellbore skin) display a strong dependence on borehole diameter. At present, the exact cause for the latter phenomenon remains unknown. We speculate that like the apparent dependence of formation transmissivity on borehole diameter (see Section 6.1), the apparent variation of productivity/injectivity indices with borehole diameter is caused by differences in drilling techniques (*i.e.*, rotary versus corehole

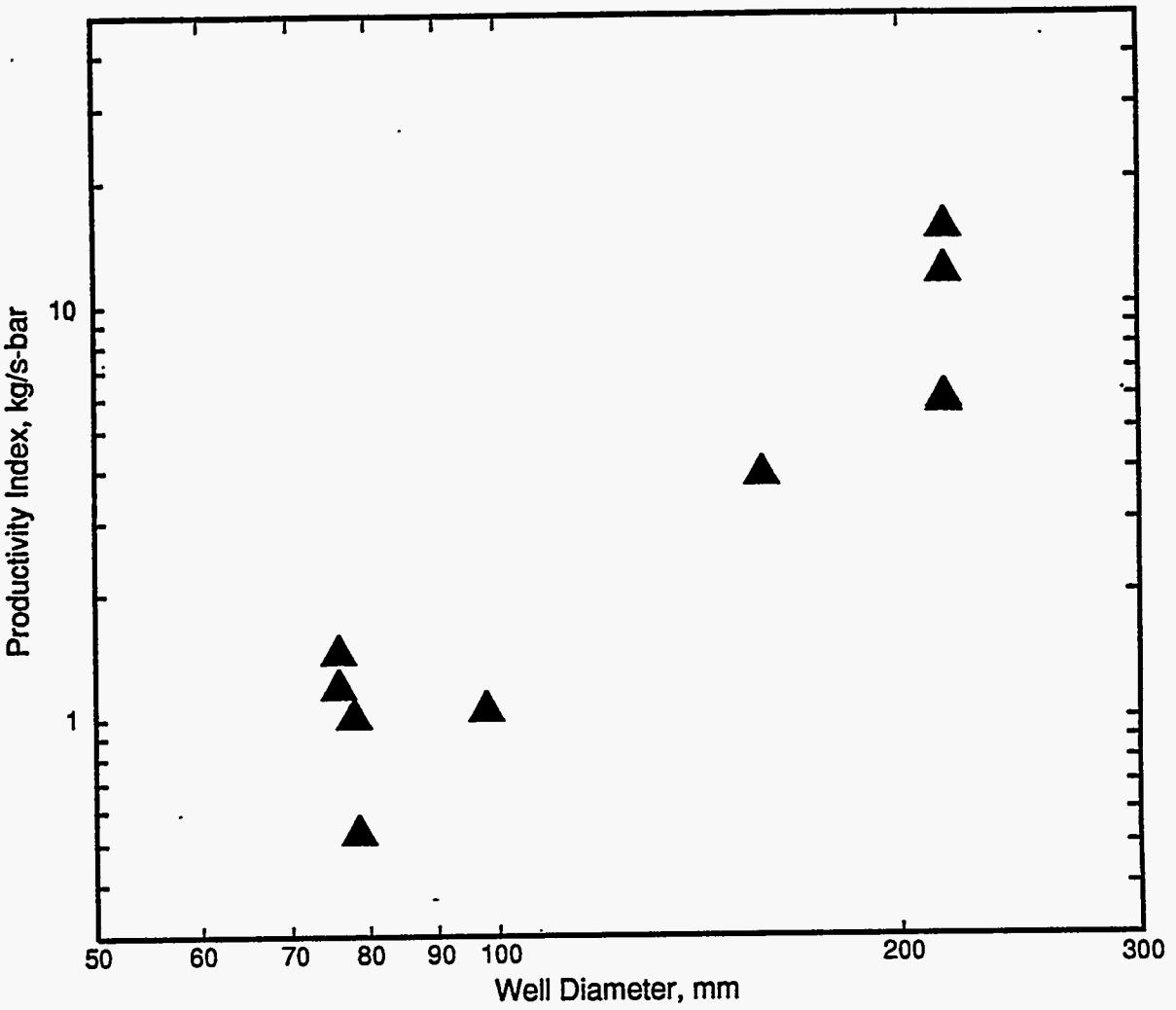

Figure 6.2a. Productivity index versus diameter for low-pressure reservoir Oguni boreholes.

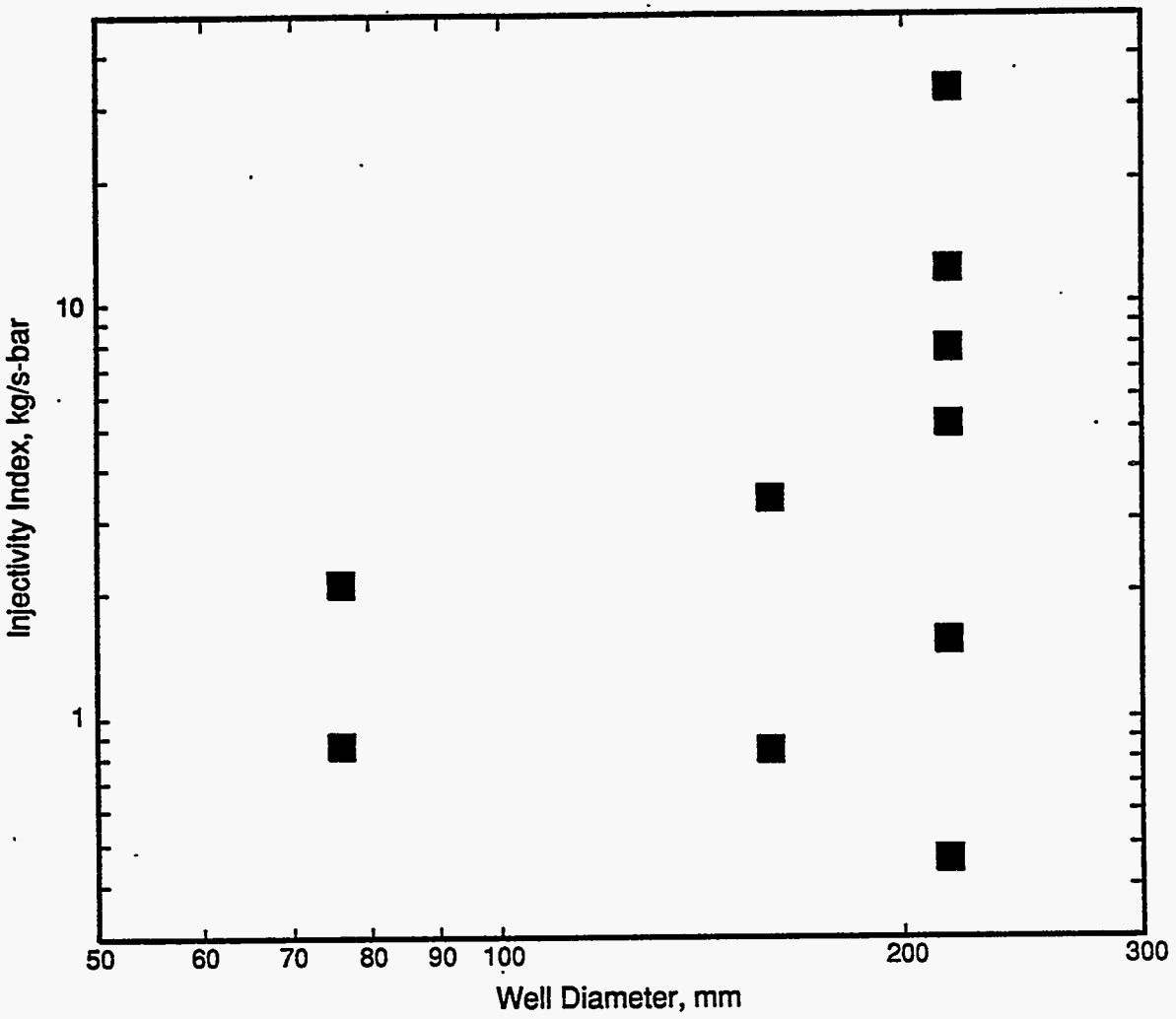

Figure 6.2b. Injectivity index versus diameter for low-pressure reservoir Oguni boreholes.

drilling). Clearly, there is a need to better quantify the formation damage (*i.e.*, fracture plugging) caused by core and rotary drilling techniques.

6.3 Effect of Borehole Diameter on Discharge Rate

Production characteristics of a geothermal borehole are in the main determined by (1) pipe friction and heat losses in the wellbore, and by (2) pressure losses associated with flow in the reservoir rocks. At Oguni, the formation permeability (and productivity indices) is sufficiently high such that the pressure losses in the reservoir are insignificant compared to pressure losses in the borehole. Stated somewhat differently, the discharge behavior of Oguni boreholes is principally determined by pipe friction and heat losses in the wellbore. As discussed by Pritchett (1992), both frictional pressure gradient and heat loss effects are more signficant for the small-diameter slim holes than for the large-diameter wells. The differences in heat loss effects is probably responsible, at least in some cases, for the difficulty encountered in inducing deep slim holes (depths >> 300 meters) to discharge.

To compare the fluid carrying capacity of boreholes of varying size, it is useful to introduce the "area-scaled discharge rate" M^* as follows:

$$M^* = M_o(d / d_o)^2$$

where M_o is the actual borehole discharge rate; and d and d_o are the internal borehole diameters (mm). Based on numerical simulation of fluid flow in boreholes of varying diameters, Pritchett (1992) suggests that the maximum discharge rate M_{max} will increase at a rate somewhat greater than the square of diameter.

$$M_{max} = M_o(d / d_o)^{2+n}, n \geq 0$$

The exact value of n will of course depend on the downhole conditions (*e.g.*, feedzone depth, flowing pressure and enthalpy, and gas content of the fluid). For the conditions assumed by Pritchett (feedzone depth = 1500 meters, feedzone pressure = 80 bars, feedzone temperature = 250°C, single-phase liquid-water at feedzone, uniform wellbore diameter), n is equal to 0.56. (Hadgu, *et al.* (1994) have considered single-phase (liquid) adiabatic flow (no heat loss) up a wellbore, and suggest that m equals 0.62. The importance of boiling in the borehole and of heat loss to the formation cannot be overstressed.) With the exception of two boreholes (GH-15 and HH-2) in the high pressure zone, all of the Oguni boreholes have single-phase liquid conditions at their principal feedzones. On average, the Oguni feedzones are shallower and the feedzone temperatures are somewhat lower than that assumed by Pritchett (1992) for his computations.

Both the "area-scaled" and "scaled maximum (n = 0.56)" discharge rates for the Oguni boreholes are presented in Table 6.3. For the low-pressure zone large-diameter (216 mm) wells (GH-11, GH-12, GH-20 and IH-2), the aver-

Table 6.3. Measured and predicted discharge rates for Oguni boreholes.

Borehole Name	Final Diameter (mm)	Measured Discharge (tons/hr)	Area Scaled Discharge† (tons/hr)	Scaled Maximum Discharge†† (tons/hr)
A. Low-Pressure Reservoir				
GH-3	79	20	151	266
GH-4	76	27	218	391
GH-5	76	22	178	319
GH-7	98	30	146	227
GH-8	78	36	276	488
Average (GH-3 to GH-8)			194	338
GH-10	159	164		
GH-11	216	279		
GH-12	216	279		
GH-20	216	369		
IH-2	216	316		
Average (GH-11 to IH-2)		311		
B. High-Pressure Reservoir				
GH-6	76	24	194	348
GH-15	216	36*		
HH-2	76	5*	40	72
N2-KW-3	76	28	226	406

† Area-Scaled Discharge Rate = Measured Discharge Rate × (216/well dia. in mm)^2

†† Scaled Maximum Discharge Rate = Measured Discharge Rate × (216/well dia. in mm)$^{2.56}$

* Two-Phase Flow

age measured maximum discharge rate (311 tons/hour) is bracketed by the averaged "area-scaled" (194 tons/hour) and averaged "scaled maximum" (338 tons/hour) discharge rates. Furthermore, using the slim hole data, the predicted M^* and M_{max} for GH-10 (159 mm diameter) are 105 tons/hour and 155 tons/hour, respectively. By comparison, the measured discharge rate for GH-10 is 164 tons/hour. Despite differences between the conditions assumed by Pritchett (1992) and the actual conditions existing in the Oguni boreholes, it would appear that the "scaled maximum discharge rate" provides a reasonable prediction of the discharge performance of large-diameter geothermal wells.

The above analyses of the Oguni borehole data are thus consistent with the premise that it should be possible to forecast the discharge performance of large-diameter production wells using production data from slim holes. This conclusion must, however, be tested with discharge data from a statistically significant collection of slim holes and production wells from a number of geothermal fields. Ideally, the set of geothermal fields should include both

large and moderate transmissivity geothermal fields; a wide range of reservoir permeabilities is needed to characterize the effect of pressure losses in the reservoir on the discharge characteristics of both slim holes and large-diameter production wells.

SECTION 7

References

Combs, J. and J. C. Dunn (1992), "Geothermal Exploration and Reservoir Assessment: The Need for a U.S. Department of Energy Slim-Hole Drilling R&D Program in the 1990s", *Geothermal Resources Council Bulletin, Vol. 21, No. 10*, pp. 329–337.

Finger, J. T., C. E. Hickox, R. R. Eaton, and R. D Jacobson (1994), "Slim-hole Exploration at Steamboat Hills Geothermal Field," *Geothermal Resources Council Bulletin, Vol. 23, No. 3*, pp. 97–104.

Garg, S. K. (1980), "Pressure Transient Analysis for Two-Phase (Water/Steam) Geothermal Reservoirs, "*Society of Petroleum Engineering Journal, Vol. 20*, pp. 206–214.

Garg, S. K. and J. Combs (1993), "Use of Slim Holes for Geothermal Exploration and Reservoir Assessment: A Preliminary Report on Japanese Experience", paper presented at *Eighteenth Workshop on Geothermal Reservoir Engineering*, Stanford University, Stanford, California, January 26–28.

Garg, S. K. and J. W. Pritchett (1990), "Cold Water Injection Into Single- and Two-Phase Geothermal Reservoirs", *Water Resources Research, Vol. 26*, pp. 331–338.

Garg, S. K., J. W. Pritchett, T. G. Barker, L.-A. Owusu, J. Haizlip and A. Truesdell (1993), "Reservoir Engineering Studies of the Oguni Geothermal Field (Phase 3)," S-Cubed, La Jolla, California, Report Number SSS-FR-92-13899.

Grant, M. A. (1978), "Two-Phase Linear Geothermal Pressure Transients: A Comparison With Single-Phase Transients," *New Zealand Journal of Science, Vol. 21*, pp. 355–364.

Grant, M. A. I. G. Donaldson and P. F. Bixley (1982), Geothermal Reservoir Engineering, *Academic Press, New York.*

Hadgu, T., R. W. Zimmermann and G. S. Bodvarsson (1994), "Comparison of Output from Slim Holes and Production-Size Wells," paper presented at *Nineteenth Workshop on Geothermal Reservoir Engineering*, Stanford University, Stanford, California, January 18–20.

Matthews, C. W. and D. G. Russell (1967), Pressure Buildup and Flow Tests in Wells, *Monograph Series, Vol. 1*, Society of Petroleum Engineers, Dallas, Texas.

Pritchett, J. W. (1992), "Preliminary Study of Discharge Characteristics of Slim Holes Compared to Production Wells in Liquid-Dominated Geothermal Reservoirs," Report Number SSS-TR-92-13133, S-Cubed, La Jolla, California, July, 48 pp.

Appendix A

EPDC's Approach to Geothermal Reservoir Assessment: Oguni Geothermal Field

Stage I

Scope of Survey	Survey Method	Survey and Evaluation Results
Verification of geothermal system model constructed on the basis of past survey data	Core drilling to define geological structure * GH-1 well (TD: 1950 m) was drilled to confirm a geothermal reservoir along the newly detected "Tsurumi-Miyanoharu line" fault zone. * GH-2 well (TD: 1800 m) was drilled in the low resistivity zone where "Excess Phase" was observed in an MT survey near the "Tsurumi-Miyanoharu" lineament.	* GH-1 was drilled to basement, but did not encounter either high temperature or lost circulation zones. * GH-2 was also drilled close to basement depth but did not encounter high temperature or lost circulation zones.
Construction of a new geothermal system model	Reevaluation of all available data and acquisition of additional geophysical survey data for a new prospect area.	It was found that the existing model was not appropriate and that it was necessary to construct a new model.
	Additional geophysical surveys	
	Mise-a-la-masse survey * Survey area: 3 km^2, 100 points using well K-7 as a current electrode	A new low resistivity area was confirmed in the deep portion beneath the western foot of Mt. Waita (i.e., the north-east side of Takenoyu hot spring area). Production of hot geothermal fluid from all wells drilled (e.g., K-6, K-7) in this area indicated the existence of an extensive geothermal reservoir in this area.
	Schlumberger resistivity survey * Survey area: 6 lines, 30 km, 102 points	
Confirmation of the existence of high temperature zone	Drilling of heat flow holes (slim holes) * HH-1, HH-2 and HH-3 wells (TD: 500–700 m)	Temperatures of 231°C in HH-2 and 210°C in HH-3 were measured.
	Geochemical survey * Soil gas (CO_2, Rn, Hg) and 1 m depth temperature * Survey area: 9 km^2, 661 points	Only lateral flow area was indicated.
	TDEM survey * 16 km^2, 48 points	No useful results were obtained.
		Existence of high temperature area adequate for conventional flash-steam power generation was confirmed.
		The survey allowed EPDC to estimate the extent of high temperature area.

Stage II

Scope of Survey	Survey Method	Survey and Evaluation Results
Verification of geothermal reservoir and estimation of reservoir extent	Slim hole (core) drilling to define geological structure	• Steam: 5 ton/hr, Hot water: 15 ton/hr was discharged. * GH-3 (TD: 1500 m, 76 mm dia)	* Steam: 6 ton/hr, Hot water: 18 ton/hr was discharged. * GH-4 (TD: 1000 m, 76 mm dia)	* Satisfactory discharge rates, flowing temperatures and productivity indices were obtained.
		Existence of a reservoir having enough capacity (temperature, permeability and size) for electric power generation was confirmed.
Additional detailed surveys	Mise-a-la-masse survey	
	* Survey area: 7 km^2, 120 points	Reservoir extent was estimated using GH-3 well.
	Minisosie seismic reflection survey	
	* Survey area: 6 lines, 15 km	Fault(s) contributing fluid production was(were) identified.
	Heat flow survey	Heat discharge rate was measured for purposes of estimating reservoir size.
		Estimation of reservoir extent, thickness, etc. Estimation of well production area.
	Calculation of reservoir capacity by volumetric method	
		It was confirmed that the reservoir extends over a large area in the Kumamoto and Oita prefectures and has enough capacity for a geothermal power plant. However, because of various constraints such as environmental protection of National Park area, developable capacity of the geothermal reservoir was not defined.

Stage III

Scope of Survey	Survey Method	Survey and Evaluation Results
Verification of reservoir extent by slim hole drilling	Slim hole drilling * GH-5 (TD: 1500 m, 76 mm dia) * GH-6 (TD: 1000 m, 76 mm dia) * GH-7 (TD: 1550 m, 98 mm dia) * GH-8 (TD: 1300 m, 78 mm dia) * GH-9 (TD: 1600 m, 80.5 mm dia)	* Steam: 2 ton/hr, Hot water: 17 ton/hr, Max. temp: 235°C * Steam: 8 ton/hr, Hot water: 28 ton/hr, Max. temp: 222 °C * Steam: 6 ton/hr, Hot water: 20 ton/hr, Max. temp: 230°C * Steam: 7 ton/hr, Hot water: 28 ton/hr, Max. temp: 223°C * Not discharged, Max. temp: 243°C The successful discharge of slim holes indicated that the exploration surveys were very effective. Production area was defined. Geological and thermal structure were clarified. Conceptual model of the geothermal system was refined. Production rate for a hypothetical large-diameter well was estimated by using a wellbore simulator.
	Fluid and heat flow simulation was carried out by a distributed parameter model	Satisfactory matching between measured and calculated temperature and pressure was obtained. It was confirmed that the area fulfilled requirements for geothermal development.
Large-diameter exploratory well drilling for defining reservoir characteristics	Large diameter well drilling * GH-10 (TD: 1060 m, 216 mm dia) * GH-11 (TD: 1380 m, 216 mm dia) * IH-1 (TD: 900 m, 159 mm dia) * GH-12 (TD: 1100 m, 216 mm dia) * IH-2 (TD: 650 m, 216 mm dia) * GH-15 (TD: 1190 m, 216 mm dia) * GH-20 (TD: 1790 m, 216 mm dia)	* Steam: 49 ton/hr, Hot water: 119 ton/hr, Max. temp: 239°C * Steam: 45 ton/hr, Hot water: 166 ton/hr, Max. temp: 235 °C * Injection capacity: 118 ton/hr, Max. temp: 181°C * Steam: 45 ton/hr, Hot water: 152 ton/hr, Max. temp: 230°C * Steam: 65 ton/hr, Hot water: 238 ton/hr, Max. temp: 216°C * Steam: 9 ton/hr, Hot water: 28 ton/hr, Max. temp: 232°C * Steam: 82 ton/hr, Hot water: 287 ton/hr, Max. temp: 248°C High productivity and high reservoir temperature were obtained as expected.
	Numerical simulation based on detailed data * The model was refined and calculations to forecast reservoir performance were carried out.	Information to define appropriate production/injection area and electric power generation capacity was obtained. Economic analysis was also carried out.

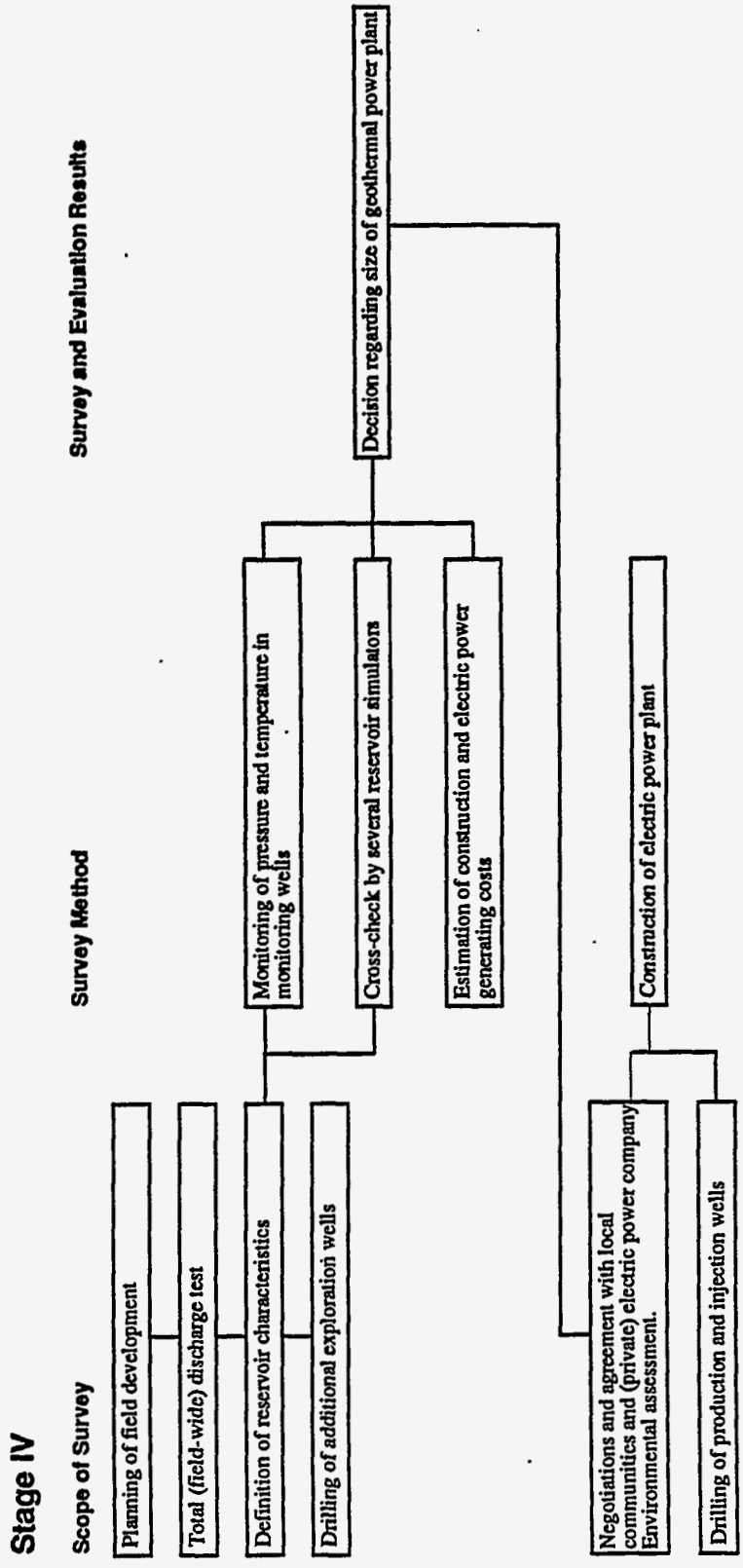
Stage IV
Scope of Survey
Survey Method
Survey and Evaluation Results
Planning of field development
Total (field-wide) discharge test
Definition of reservoir characteristics
Drilling of additional exploration wells
Monitoring of pressure and temperature in monitoring wells
Cross-check by several reservoir simulators
Estimation of construction and electric power generating costs
Decision regarding size of geothermal power plant
Negotiations and agreement with local communities and (private) electric power company
Environmental assessment.
Construction of electric power plant
Drilling of production and injection wells